

Zirconium- and phosphine-assisted C–F bond activation and functionalisation

Sara Bonfante

Doctor of Philosophy

University of York

Chemistry

January 2024

Abstract

Over the past two decades, the functionalisation of C–F bonds of perfluorinated compounds has attracted significant attention due to the numerous industrial applications of fluorinated organic compounds and the inherent challenges associated with these transformations, including the high strength of the C–F bond and the difficulty in the control of the reaction's selectivity. Furthermore, as fluorocarbons tend to be inert upon decomposition, they are persistent in the environment and the exploration of alternative methods for defluorination is of great interest.

This thesis presents novel protocols for the regioselective C–F bond functionalisation of polyfluorinated aromatics which are promoted by zirconium and catalysed by phosphines. Mechanistic investigations supported by experimental and, in selected examples, computational studies, complement the synthetic findings.

The reactivity of a zirconocene complex featuring a highly strained cyclohexyne ligand toward differently fluorinated pyridines was investigated. This complex, isolated by coordination of a PMe_3 ligand, exhibited different reactivity pathways depending on the fluorination pattern of the heteroaromatic. Remarkably, the reactive metal-alkyne bond could insert into the *ortho*-C–F bonds of 2,4,6-trifluoropyridine and 2,6-difluoropyridine, resulting in the net alkenylation of the polyfluorinated heterocycle. The reaction of the complex with 2,3,5,6-tetrafluoropyridine led instead to the 1,2-C–H addition over the $\text{Zr}(\eta^2\text{-C}\equiv\text{C})$. Conversely, the reaction with pentafluoropyridine mainly involved a parasitic $\text{S}_{\text{N}}\text{Ar}$ reaction of the dissociated PMe_3 ligand with the substrate, generating a series of difluorophosphoranes that triggered decomposition of the Zr complex.

These results led to the investigation into the stoichiometric reactivity between simple phosphines and pentafluoropyridine. Various trialkylphosphines exhibited the ability to activate the *para*-F of the heteroaromatic, leading to the formation of the products arising from hydrodefluorination or reductive homocoupling, along with methylenetetrafluoropyridyl-substituted or simple difluorophosphoranes, depending on the reaction conditions.

Because metal-free C–F bond activation is highly topical, these findings set the stage for the development of a metallomimetic catalytic system for the hydrodefluorination and aminodefluorination of polyfluorinated aromatics in the presence of silanes or silylamides. Remarkably, the catalyst employed for these transformations is the simple and readily available $\text{P}^{\text{n}}\text{Bu}_3$. It undergoes facile redox cycling between the P^{III} and P^{V} oxidation states, enabling oxidative addition of the substrate, pseudotransmetalation and reductive elimination of the product throughout the catalytic cycle – typical steps observed in classical transition-metal-catalysis.

List of Contents

Abstract.....	1
List of Contents.....	3
List of Figures.....	8
List of Schemes.....	12
List of Tables.....	21
Acknowledgments.....	22
Author's declaration.....	23
Summary of compounds.....	24
Chapter 1 – Introduction.....	27
1.1 Properties of fluorine.....	27
1.2 Origin of fluorine and applications of fluorinated organic molecules.....	28
1.3 Synthesis of fluorinated organic compounds.....	29
1.4 Aims and objectives.....	31
Chapter 2 – C–F bond functionalisation promoted by a zirconium-cyclohexyne complex.....	33
2.1 Introduction.....	33
2.1.1 Hydrodefluorination reaction.....	33
2.1.2 C–F bond functionalisation of perfluoro(hetero)arenes.....	35
2.1.3 Main-group metal-mediated C(sp ²)–C coupling reactions via C–F activation.....	36
2.1.4 LTM-mediated C(sp ²)–C coupling reactions via C–F activation.....	39
2.1.4.1 C(sp ²)–C bond formation at polyfluorinated benzene derivatives.....	39
2.1.4.2 C(sp ²)–C bond formation at polyfluorinated aromatics supported by a remote group	43
2.1.4.3 C(sp ²)–C bond formation at polyfluorinated pyridines.....	44
2.1.5 ETM-mediated C–F activation.....	49
2.1.5.1 C(sp ²)–F activation at polyfluorinated pyridines assisted by group 4 metals.....	50
2.1.5.1.1 C–F bond cleavage via oxidative addition mechanism.....	51

2.1.5.1.2	C–F bond cleavage via 1,n-C–F addition reaction	52
2.1.6	Zirconocene complexes of unsaturated organic molecules.....	54
2.2	Aims and objectives.....	56
2.3	Results and discussion	57
2.3.1	Synthesis of the zirconocene-cyclohexyne complex.....	57
2.3.2	Reactivity of the Zr-cyclohexyne complex with pentafluoropyridine	62
2.3.3	Reactivity of the zirconocene-cyclohexyne complex with Py-F ₄ , Py-F ₃ and Py-F ₂	68
2.4	Summary, conclusions and perspectives	76
Chapter 3 –	Stoichiometric reactivity between trialkylphosphines and Py-F ₅	78
3.1	Introduction.....	78
3.1.1	Synthesis of perfluoroaromatic compounds	78
3.1.2	S _N Ar reactions with polyfluoro(hetero)aromatic compounds	79
3.1.2.1	Mechanism and regioselectivity.....	79
3.1.2.2	Metal-free C(sp ²)–C bond forming reactions in polyfluoroaromatics.....	83
3.1.2.2.1	Neutral nucleophiles	83
3.1.2.2.2	Charged nucleophiles	86
3.1.3	C–F bond activation promoted by phosphorus-containing species.....	88
3.1.3.1	Phosphorus-containing Lewis bases.....	89
3.1.4	Synthesis of fluorophosphoranes.....	96
3.2	Aims and objectives.....	98
3.3	Results and discussion	99
3.3.1	Spectroscopic characterisation of the products	99
3.3.2	Analysis of experimental conditions	104
3.3.3	Mechanistic proposal	108
3.4	Summary, conclusions and perspectives	112
Chapter 4 –	P ⁿ Bu ₃ -catalysed hydro- and aminodefluorination of polyfluoroaromatics.....	114
4.1	Introduction.....	114
4.1.1	Main-group-mediated HDF reactions.....	115
4.1.1.1	Fluoride abstraction by Lewis acids.....	115
4.1.1.1.1	Si-based electrophiles	116
4.1.1.1.2	Other electrophiles	120
4.1.2	Photoinduced HDF.....	121

4.1.3	HDF via nucleophilic substitution	122
4.1.4	Reversible two-electron redox catalytic HDF	125
4.2	Aims and objectives	130
4.3	Results and discussion	130
4.3.1	Reaction optimisation.....	131
4.3.2	Substrate scope	135
4.3.3	Catalytic aminodefluorination reaction.....	140
4.3.4	Mechanistic studies	150
4.4	Summary, conclusions and perspectives.....	162
Chapter 5 – Experimental Section.....		164
5.1	General considerations.....	164
5.2	Chapter 2 – C–F bond functionalisation promoted by a zirconium-cyclohexyne complex 165	
5.2.1	Synthesis of 1-bromocyclohexene (1)	165
5.2.2	Synthesis of methylzirconocene chloride (2)	166
5.2.2.1	Via reaction between zirconocene dichloride and 1 equivalent of MeLi:.....	166
5.2.2.2	Via reaction between zirconocene dichloride and 2 equivalents of MeLi:	166
5.2.2.3	Via [(Cp ₂ ZrCl) ₂ (μ-O)]:.....	167
5.2.2.3.1	First step: synthesis of [(Cp ₂ ZrCl) ₂ (μ-O)]	167
5.2.2.3.2	Second step: synthesis of 2	167
5.2.3	Li/Br exchange test	168
5.2.4	Synthesis of complex 6	169
5.2.5	Stability test of complex 6	170
5.2.6	Study of the reactivity of complex 5 with Py-F ₅	170
5.2.7	Reactivity of complex 5 with Py-F ₃	171
5.2.8	Synthesis of 1-cyclohexenylzirconocene fluoride (7)	172
5.2.9	Addition of HCl to 7	172
5.2.10	Synthesis of 1-iodocyclohexene	173
5.2.11	Solvent effect investigation in the reaction of complex 6 with Py-F ₅	173
5.2.12	Temperature effect investigation for the reaction of complex 6 and Py-F ₅	174
5.2.13	Concentration effect investigation for the reaction of complex 6 and Py-F ₅	174
5.2.14	Reagent ratio study for the reaction of complex 6 and Py-F ₅	175
5.2.15	Mechanistic investigation on the formation of 7	175

5.2.16	Synthesis of complex 11	176
5.2.17	Synthesis of 2,4-difluoro-6-(2-iodocyclohexen-1-yl)-pyridine	177
5.2.18	Investigation on the solvent effect in the synthesis of complex 11.....	178
5.2.19	Synthesis of complex 12	178
5.2.20	Synthesis of complex 10 and its iodinolysis	179
5.3	Chapter 3 – Stoichiometric reactivity between trialkylphosphines and Py-F ₅	180
5.3.1	Stoichiometric reactivity of PMe ₃ and Py-F ₅	180
5.3.2	Reagent ratio study for the reaction of PMe ₃ and Py-F ₅	181
5.3.3	Temperature study for the reaction of PMe ₃ and Py-F ₅	182
5.3.4	Solvent study for the reaction of PR ₃ and Py-F ₅	182
5.3.5	Phosphine effect investigation on the reaction of PR ₃ and Py-F ₅	183
5.3.5.1	Spectroscopic data for the synthesised difluorophosphoranes.....	183
5.3.6	Synthesis of ylide 16	187
5.4	Chapter 4 – P ⁿ Bu ₃ -catalysed hydro- and aminodefluorination of polyfluoroaromatics	188
5.4.1	Difluorination and reduction of difluorophosphoranes by PhSiH ₃	188
5.4.2	Procedure for the solvent optimisation in the catalytic HDF reaction	188
5.4.3	Procedure for catalyst optimisation in the catalytic HDF reaction	189
5.4.4	Procedure for silane optimisation in the catalytic hydrodefluorination reaction	189
5.4.5	Procedure for optimisation of the catalyst loading in the catalytic HDF reaction.....	189
5.4.6	Procedure for optimisation of the silane loading in the catalytic HDF reaction.....	190
5.4.7	General procedure for the catalytic HDF	190
5.4.7.1	Spectroscopic data for the hydrodefluorinated products:	191
5.4.8	Preparation of Ph ₂ Si(Cl)(NEt ₂)	193
5.4.9	Preparation of Ph ₂ Si(Cl)(pro)	194
5.4.10	Procedure for the catalytic aminodefluorination reaction	195
5.4.11	Reactivity test of 4-dimethylamino-tetrafluoropyridine and Ph ₂ Si(Cl)(NEt ₂)	197
5.4.12	Mechanistic studies for the catalytic HDF reaction	197
5.4.12.1	Reactivity test of PhSiH ₃ and pentafluoropyridine.....	197
5.4.12.2	Reactivity test of Ph ₂ SiH ₂ and P ⁿ Bu ₃	198
5.4.12.3	Reactivity test of Ph ₂ SiH ₂ and pentafluoropyridine	198
5.4.12.4	Reactivity test of Ph ₂ SiH ₂ and pentafluoropyridine in the presence of [Me ₄ N]F 198	
5.4.12.5	Characterisation of phosphonium salt [31][Ph ₂ Si(H) ₃ F]	199
5.4.12.6	Characterisation and reactivity of phosphonium salt [31]Br	200
5.4.12.7	Observation of the phosphonium salt [32][Ph ₂ Si(H) _{3-n} F _n]	201

5.4.12.8	Characterisation and reactivity of the phosphonium salt [28]Br	202
5.5	Crystallographic data collection and structure determination	203
5.5.1	Molecular structure of 16.....	203
5.5.2	Molecular structure of 11.....	204
5.6	DFT Calculations	205
5.7	Tabulated energies for mechanism presented in scheme 4	206
5.8	3-component alternative mechanism for Si-H activation (c.f. Piers' mechanism).....	208
	List of abbreviations	210
	References	212

List of Figures

Figure 1 Selected examples of fluorine-containing organic molecules employed in pharmaceutical and agrochemical industries.	28
Figure 2 Selected examples of mild nucleophilic, electrophilic and trifluoromethylating reagents. (DAST = diethylaminosulfur trifluoride; DFI = 2,2-difluoro-1,3-dimethylimidazolidine; NFSI = N-fluorobenzenesulfonimide)	29
Figure 3 Possible intermediates and transition states for the C–F activation of pentafluoropyridine at a late transition metal: three-centred transition state (A), ion-pair formation (B) and Meisenheimer intermediate (C).	45
Figure 4 Possible reactivity of arynes and cycloalkynes.....	55
Figure 5 ^1H NMR (600 MHz, C_6D_6) of complex 6 prepared according to Scheme 36, dried and dissolved in C_6D_6 (some residual THF is still present from the reaction mixture).	60
Figure 6 X-ray crystal structure of complex 6 reported by Buchwald and coworkers (figure reused with permission from Buchwald, S. L.; Dewan, J. C. <i>J. Am. Chem. Soc.</i> 1986 , 108, 23, 7441–7442. Copyright 1986 American Chemical Society).	61
Figure 7 ^1H NMR (400 MHz, C_6D_6) spectrum of complex 7 obtained by treating 6 (1 equiv.) with Py-F₅ (1 equiv.) in C_6D_6 at 20 °C for 4 hours. Magnifications of the signals of 7 are given.....	63
Figure 8 ^{19}F NMR (377 MHz, C_6D_6) of the reaction mixture obtained by treating the zirconocene- PMe_3 adduct 6 (1 equiv.) and pentafluoropyridine (1 equiv.) after 4 hours at 20 °C.	64
Figure 9 ^{19}F NMR (377 MHz, C_6D_6) spectra of the crude reaction mixture between PMe_3 and pentafluoropyridine (1:1, in C_6D_6) (a) and after 3 hours from the addition of complex 6 (b).	67
Figure 10 ^{19}F NMR (377 MHz, C_6D_6) spectrum of the reaction mixture of 6 (1 equiv.) and Py-F₄ (1 equiv.) in C_6D_6 after 48 hours at 50 °C. Magnifications of the signals of complex 10 are given.	69
Figure 11 ^{19}F NMR (377 MHz, C_6D_6) spectrum of the crude reaction mixture of the reaction between the zirconocene- PMe_3 adduct 6 (1 equiv.) with Py-F₃ (5 equiv.) in cyclohexane at 40 °C for 42 hours, dried and dissolved in C_6D_6 . Magnifications of the signals of complex 11 are given.....	70

Figure 12 ¹ H NMR (500 MHz, C ₆ D ₆) spectrum of the crude reaction mixture of the reaction between the zirconocene-PMe ₃ adduct 6 (1 equiv.) with Py-F₃ (5 equiv.) in cyclohexane at 40 °C for 42 hours, dried and dissolved in C ₆ D ₆ . Magnifications of the signals of complex 11 are given.....	71
Figure 13 ¹ H NOESY (500 MHz, C ₆ D ₆) spectrum of the crude reaction mixture of the reaction between the zirconocene-PMe ₃ adduct 6 (1 equiv.) with Py-F₃ (5 equiv.) in cyclohexane at 40 °C for 42 hours, dried and dissolved in C ₆ D ₆	72
Figure 14 GC(EI)-MS spectrum of 2,4-difluoro-6-(2-iodocyclohexen-1-yl)-pyridine obtained by reaction of 11 (1 equiv.) with I ₂ (1 equiv.) in C ₆ D ₆ at 20 °C for 15 minutes.....	73
Figure 15 Molecular structure of 11 in the solid. Ellipsoids drawn at the 25% probability level. Selected bond lengths (Å) and angles (°): Zr1-F1 2.008(1), Zr1-C1 2.321(2), Zr1-N1 2.479(2), N1-C7 1.372(3), C1-C6 1.354(3), C6-C7 1.456(3), F1-Zr1-C1 80.26(6), C1-Zr1-N1 68.35(6), F1-Zr1-N1 148.46(6), N1-C11-F3 114.7(2).	73
Figure 16 Fluorine substituent effects on the regioselectivity of S _N Ar reactions.	80
Figure 17 ³¹ P NMR (162 MHz, C ₆ D ₆ , spectrum on the top) and ¹⁹ F NMR (377 MHz, C ₆ D ₆ , spectrum on the bottom) of the reaction of Py-F₅ (3 equiv.) and PMe ₃ (1 equiv.) in C ₆ D ₆ after 20 minutes at 20 °C.....	101
Figure 18 ¹ H NMR (400 MHz, C ₆ D ₆) of the reaction of Py-F₅ (3 equiv.) and PMe ₃ (1 equiv.) in C ₆ D ₆ after 20 minutes at 20 °C.....	102
Figure 19 Molecular structure of 16 in the solid. Ellipsoids drawn at the 50% probability level. .	104
Figure 20 Set of tested phosphines.	105
Figure 21 Three types of catalytic cycles for the HDF reaction involving Si-based electrophiles. (LA = Lewis acid; LG = leaving group; Do = electron donating species).....	116
Figure 22 General preferential redox reactivity of compounds containing elements between group 13 and 17.	126
Figure 23 Qualitative frontier orbital diagram of a σ ³ -P compound in a C _{3v} , C _s and C _{2v} symmetry (top). Bending modes of an NPN compound (bottom).	127
Figure 24 Comparison of the key features between TM- and Pn-based redox cycles.....	128

Figure 25 $^{31}\text{P}\{^1\text{H}\}$ NMR spectrum (243 MHz, CD_3CN) of the reaction mixture of Py-F₅ (1 equiv.), Ph_2SiH_2 (1 equiv.) and P^nBu_3 (10 mol%) after 20 minutes at 20 °C.	133
Figure 26: ^{19}F NMR spectrum (565 MHz, CD_3CN) of the reaction mixture of Py-F₅ (1 equiv.), Ph_2SiH_2 (1 equiv.) and P^nBu_3 (10 mol%) after 20 minutes at 20 °C. Magnifications of the signals of Py-F₄ are shown.	134
Figure 27 Results of substrate scope studies for the HDF reaction catalysed by P^nBu_3 . ^a Isolated yield after flash column chromatography shown in parentheses.	135
Figure 28 Assigned coupling constants for compound 17	136
Figure 29 ^{19}F NMR spectrum (565 MHz, CD_3CN) of the reaction mixture of Py-F₄ (1 equiv.), Ph_2SiH_2 (1 equiv.) and P^nBu_3 (10 mol%) after 5 days at 70 °C. Magnifications of the signals of 17 are given.	136
Figure 30 ^{19}F NMR spectrum (565 MHz, CD_3CN) of the reaction mixture of 2,4,6-trifluoropyridine (1 equiv.), Ph_2SiH_2 (1 equiv.) and P^nBu_3 (10 mol%) after 6 days at 60 °C.	137
Figure 31 ^{19}F NMR spectrum (565 MHz, CD_3CN) of the reaction mixture of bromopentafluorobenzene (1 equiv.), Ph_2SiH_2 (1 equiv.) and P^nBu_3 (10 mol%) obtained after 20 minutes at 20 °C.	139
Figure 32 ^1H NMR spectrum (C_6D_6 , 600 MHz) of the isolated $\text{Ph}_2\text{Si}(\text{Cl})(\text{NEt}_2)$	141
Figure 33 ^{19}F NMR spectrum (565 MHz, CD_3CN) of the reaction mixture of Py-F₅ (1 equiv.), $\text{Ph}_2\text{Si}(\text{Cl})(\text{NEt}_2)$ (1.1 equiv.) and P^nBu_3 (10 mol%) obtained after 18 hours at 60 °C. Magnifications of the signals of 24 are given.	142
Figure 34 ^1H NMR spectrum (600 MHz, CD_3CN) of the reaction mixture of Py-F₅ (1 equiv.), $\text{Ph}_2\text{Si}(\text{Cl})(\text{NEt}_2)$ (1.1 equiv.) and P^nBu_3 (10 mol%) obtained after 18 hours at 60 °C.	143
Figure 35 $^{31}\text{P}\{^1\text{H}\}$ NMR spectrum (243 MHz, CD_3CN) of the reaction mixture of Py-F₅ (1 equiv.), $\text{Ph}_2\text{Si}(\text{Cl})(\text{NEt}_2)$ (1.1 equiv.) and P^nBu_3 (10 mol%) obtained after 18 hours at 60 °C. A magnification of the signal of 29 is given.	143
Figure 36 Possible structure of the unidentified species 29	144
Figure 37 Proton coupling constants of $\text{Ph}_2\text{Si}(\text{Cl})(\text{pro})$	145

Figure 38 ^1H NMR spectrum (600 MHz, C_6D_6) of the reaction mixture obtained from the final step of Scheme 120, after filtration of the precipitated $[\text{HNEt}_3]\text{Cl}$ salt and extraction with pentane of the products.	146
Figure 39 ^{19}F NMR spectrum (565 MHz, CD_3CN) of the reaction mixture of Py-F₅ (1 equiv.), $\text{Ph}_2\text{Si}(\text{Cl})(\text{pro})$ (1.1 equiv.) and P^nBu_3 (10 mol%) obtained after 18 hours at 60 °C. Magnifications of the signals of product 25 are given.	147
Figure 40 ^1H NMR spectrum (600 MHz, C_6D_6) of the reaction mixture of Py-F₅ (1 equiv.), $\text{Ph}_2\text{Si}(\text{Cl})(\text{pro})$ (1.1 equiv.) and P^nBu_3 (10 mol%) obtained after 18 hours at 60 °C. Magnifications of the signals of product 25 are given.	148
Figure 41 ^{19}F NMR spectrum (565 MHz, CD_3CN) of the mixture of HDF reaction of Py-F₅ (1 equiv.) with PhSiH_3 (1 equiv.) and P^nBu_3 (10 mol%) in CD_3CN at 20 °C after $t = 0$ (spectrum a)), 1 hour (spectrum b)) and 2 hours at 60 °C (spectrum c)).	151
Figure 42 $^{31}\text{P}\{^1\text{H}\}$ NMR spectrum (243 MHz, CD_3CN) of the mixture of HDF reaction of Py-F₅ (1 equiv.) with PhSiH_3 (1 equiv.) and P^nBu_3 (10 mol%) in CD_3CN at 20 °C after $t = 0$ (spectrum a)), 1 hour (spectrum b)) and 2 hours at 60 °C (spectrum c)).	151
Figure 43 ^{19}F NMR spectrum (565 MHz, CD_3CN) of the reaction mixture of Scheme 123 after 18 hours at 40 °C from the addition of Ph_2SiH_2 (spectrum a)) and after 10 minutes at 20 °C from the addition of $[\text{Me}_4\text{N}]\text{F}$ (spectrum b)).	153
Figure 44 Considered activation mode of the silane according to a FLP-type mechanism.	154
Figure 45 ^{19}F NMR (471 MHz, CD_3CN) spectra of the system described in Scheme 126 after 18 hours at 20 °C from the further addition of 0.9 equivalents of P^nBu_3 (spectrum a)) and after 10 minutes at 20 °C from the addition of $[\text{Me}_4\text{N}]\text{F}$ (spectrum b)).	156
Figure 46 $^{31}\text{P}\{^1\text{H}\}$ NMR (202 MHz, CD_3CN) spectra of the system described in Scheme 126 after 18 hours at 20 °C from the further addition of 0.9 equivalents of P^nBu_3 (spectrum a)) and after 10 minutes at 20 °C from the addition of $[\text{Me}_4\text{N}]\text{F}$ (spectrum b)).	157
Figure 47 Transition states for addition of PMe_3 to Py-F₅ (TS₁₂) and elimination of Py-F₄ from phosphorane M6 (TS₆₁). Hydrogen is shown in white, carbon in grey, phosphorus in orange, nitrogen in blue and fluorine in green. Selected distances (in Å) are shown.	160

List of Schemes

Scheme 1 Synthesis of fluticasone propionate via late-stage fluorination by Selectfluor.	30
Scheme 2 Examples of Zr-catalysed HDF of polyfluoropyridines reported by Rosenthal <i>et al.</i> (left) ³² and Ti-catalysed HDF of fluoroalkenes by Lentz and coworkers (right) and their proposed mechanisms. ²⁷	34
Scheme 3 Challenges in the metalation of fluoroarenes using organolithium reagents.....	36
Scheme 4 Monoalkylation and -arylation of perfluorinated arenes with Grignard reagents.	37
Scheme 5 <i>Ortho</i> -alkylation and arylation of 2-(2-fluorophenyl)pyridine and perfluoroaryl imine derivatives with Grignard reagents and proposed mechanism.	37
Scheme 6 Proposed mechanism for the alkylation and arylation of 2-(2,4-difluorophenyl)pyridine with a Mg(II) complex ($\text{Ar}^* = 2,6\text{-}^i\text{Pr}_2\text{-C}_6\text{H}_3$; $\text{R} = ^n\text{Bu, Ph}$).	38
Scheme 7 Selected example for the Sonogashira-type cross-coupling reactions promoted by strong bases.....	38
Scheme 8 Suzuki–Miyaura cross-coupling reaction of octafluorotoluene catalysed by $[\text{Ni}_2(^i\text{Pr}_2\text{Im})_4(\text{cod})]$ in the presence of boronic acid and NEt_3	39
Scheme 9 Selected example for the Suzuki–Miyaura cross-coupling reaction of polyfluorinated aromatics catalysed by $[\text{Ni}(^i\text{Pr}_2\text{Im})_2]_2(\text{cod})$ in the presence of aryl boronate.	40
Scheme 10 Ni-catalysed Hiyama cross-coupling reaction reported by Ogoshi and coworkers.....	40
Scheme 11 Ni-catalysed Negishi cross-coupling reaction in the presence of ZnR'_2	40
Scheme 12 Ni-mediated cross-coupling reactions of perfluorobenzene with aryl zinc or Grignard reagents; suggested transition state for the C–F bond cleavage step (bottom right).....	41
Scheme 13 Kumada–Tamao cross-coupling reaction of 1,4-difluorobenzene with aryl Grignard reagents and the diamidophosphine sulfide as ligand precursor; generation of the heterobimetallic complex (bottom right).	41
Scheme 14 Selected example of cross-coupling reaction of perfluoroaromatics with aryl zinc compounds and LiI as additive.	42

Scheme 15 Pd-catalysed Sonogashira-type cross coupling reaction of perfluoroarenes and terminal alkynes (dba = dibenzylideneacetone).	42
Scheme 16 Selected example of photocatalytic C–F bond alkylation of perfluoroarenes catalysed by <i>fac</i> -Ir(ppy) ₃	42
Scheme 17 Directing group-promoted C–F bond activation of polyfluorophenyl imines at [Pt(Me) ₂ (μ-SMe ₂) ₂].	43
Scheme 18 Catalytic methylation of polyfluoroaryl imines with a [Pt(Me) ₂ (μ-SMe ₂) ₂] as catalyst..	44
Scheme 19 <i>Ortho</i> -CF bond activation of Py-F₅ and Py-F₄ and subsequent functionalisation assisted by a Ni(cod) ₂ complex in the presence of PEt ₃ (top); proposed mechanism based on density functional theory (DFT) studies (bottom). ¹⁰⁰	46
Scheme 20 Catalytic conversion of fluorinated pyridines with [NiF(2-C ₅ NF ₄)(PEt ₃) ₂].	46
Scheme 21 C–F bond activation at Py-F₅ using either ^{<i>i</i>} Pr ₂ P(CH ₂ CH ₂ OMe) (top) or ^{<i>i</i>} Pr ₂ P(CH ₂ CH ₂ NMe ₂) (bottom) and [Ni(cod) ₂] (the ratio between the two products is reported).	47
Scheme 22 Suzuki-Miyaura-type cross-coupling of Py-F₅ and PhB(OH) ₂ catalysed by mixture A (top) and B (bottom).	47
Scheme 23 C–F bond activation of Py-F₅ assisted by Rh-silyl (top) and Rh-phosphine complexes (bottom).	48
Scheme 24 Suzuki-Miyaura- and Stille-type cross-coupling reactions catalysed by Pd complexes.	49
Scheme 25 C–F bond cleavage reactions by ETM complexes.	50
Scheme 26 Some examples of group 4 metallocene bis(trimethylsilyl)acetylene complexes.	51
Scheme 27 Reaction of [Cp ₂ Ti{η ² -C ₂ (SiMe ₃) ₂ }] with Py-F₄ and Py-F₅	51
Scheme 28 Reaction of ‘masked’ [Cp ₂ Zr] fragments with pentafluoropyridine and Py-F₄	52
Scheme 29 1,2-CF addition across a transient titanium alkylidyne (PNP)Ti≡C ^{<i>t</i>} Bu to afford (PNP)Ti=C[^{<i>t</i>} Bu(NC ₅ H ₃ F)](F).	53
Scheme 30 1,2-CF addition of pentafluoropyridine across a transient [<i>rac</i> -(<i>ebthi</i>)Zr(=NCMe ₃)]....	53
Scheme 31 C–F bond activation promoted by [Cp ₂ Zr(η ² - <i>c</i> -C ₃ H ₄)] and release of the ligand.	54

Scheme 32 Tentative catalytic C–C coupling reaction with dicyclopropylzirconocene as precatalyst and Al-(<i>c</i> -C ₃ H ₅) ₃ as transmetalating agent.....	54
Scheme 33 Resonance structures of complex [Cp ₂ Zr(η ² - <i>c</i> -C ₃ H ₄)].	54
Scheme 34 Cycloaddition reactions assisted by a zirconocene-η ² -cyclohexyne complex.....	56
Scheme 35 Synthetic strategy for the regioselective Zr-promoted C–F alkenylation of polyfluoropyridines.	56
Scheme 36 Synthetic protocol for the synthesis of the zirconocene-η ² -cyclohexyne (5) and its corresponding PMe ₃ adduct (6).	57
Scheme 37 Synthesis of 1-bromocyclohexene by reaction of cyclohexanone (1 equiv.), Br ₂ (1.5 equiv.), P(OPh) ₃ (1.1 equiv.), NEt ₃ (1.3 equiv.) in CH ₂ Cl ₂	58
Scheme 38 Proposed reaction mechanism for the synthesis of 1-bromocyclohexene.....	58
Scheme 39 Stability study of 3 in THF at –78 °C over time.	59
Scheme 40 Strategies (i), (ii) and (iii) for the synthesis of the methylzirconocene chloride.	59
Scheme 41 Extreme resonance structures of complex 6	61
Scheme 42 Attempts of C–F functionalisation of pentafluoropyridine with zirconocene-cyclohexyne complexes 5 and 6	62
Scheme 43 Synthesis of 1-cyclohexenylzirconocene fluoride complex 7 from reaction of the zirconocene-PMe ₃ adduct 6 (3 equiv.) with Py-F₅ (1 equiv.) and subsequent release of the organic ligand by addition of I ₂ (1 equiv.) in C ₆ D ₆	64
Scheme 44 Synthesis of 1-cyclohexenylzirconocene fluoride complex from reacting the zirconocene-PMe ₃ adduct 6 (3 equiv.) with Py-F₅ (1 equiv.) and release of the organic ligand by addition of HCl·Et ₂ O in C ₆ D ₆	65
Scheme 45 Reactivity test of Py-F₅ (1 equiv.) with PMe ₃ (1–3 equiv.) in C ₆ D ₆ or THF- <i>d</i> ₈ at 20 °C... ..	66
Scheme 46 Reaction of 6 (3 equiv.) with the compounds issued by the reaction of PMe ₃ (1 equiv.) and Py-F₅ (1 equiv.) in C ₆ D ₆ at 20 °C.	66

Scheme 47 Synthesis of the C–H activation product 10 by reaction of 6 (1 equiv.) and Py-F₄ (1 equiv.) in C ₆ D ₆ at 50 °C for 48 hours and its iodinolysis by addition of I ₂ (1 equiv.).....	68
Scheme 48 Synthesis of 11 and 12 by reaction of 6 (1 equiv.) with Py-F₃ or Py-F₂ (3–5 equiv.) in C ₆ D ₁₂ at 40 °C.....	70
Scheme 49 Iodinolysis of 11 (1 equiv.) by addition of I ₂ (1 equiv.) in C ₆ D ₆ after 15 min at 20 °C....	72
Scheme 50 Proposed synthetic strategy for the regio- and stereoselective preparation of a new fluorinated organic molecule.	77
Scheme 51 Banks and Tatlow’s methodology for the synthesis of perfluoro(hetero)aromatic compounds.	78
Scheme 52 Halex fluorination process for the synthesis of perfluoro(hetero)aromatic compounds.	79
Scheme 53 Stepwise (top) and concerted (bottom) S _N Ar mechanism.....	80
Scheme 54 Regioselectivity in the S _N Ar reaction of pentafluorobenzoate with NaOEt.	81
Scheme 55 Sequential functionalisation of pentafluoropyridine for the synthesis of pyridinylimidazole derivatives.....	81
Scheme 56 S _N Ar reaction of hexafluorobenzene with ⁿ BuLi.	81
Scheme 57 Polysubstitution of Py-F₅ with pyrazole anions.	82
Scheme 58 Polysubstitution of pentafluoropyridine and hexafluorobenzene with LDA.....	82
Scheme 59 Hydrodefluorination reaction of pentafluoropyridine with lithium aluminium hydride.	83
Scheme 60 Alkylation of polyfluoroarenes and perfluoroheteroarenes with phosphonium ylides.	83
Scheme 61 Proposed mechanism for the alkylation reaction of polyfluoroarenes and perfluoroheteroarenes with phosphonium ylides.	84
Scheme 62 S _N Ar reaction of pentafluoropyridine with NHC nucleophiles.....	84
Scheme 63 S _N Ar reaction of pentafluoropyridine with an NHC nucleophile and BF ₃ . ¹⁹⁰	85

Scheme 64 S_NAr reaction of perfluoro(hetero)aromatics with a CAAC nucleophile.	86
Scheme 65 Selected example of a negative Friedel-Crafts reaction.....	87
Scheme 66 Synthesis of polyfluoroaromatic containing polymers.....	87
Scheme 67 S_NAr reaction of perfluoro(hetero)aromatics with carbocations of methylphosphonate derivatives.	88
Scheme 68 Regioselective defluoroalkylation of polyfluoroarenes with nitroalkanes.....	88
Scheme 69 Synthesis of perfluoro(hetero)aryldimethylphosphines from Si or Sn-phosphide derivatives.	89
Scheme 70 Aromatic nucleophilic substitution reactions on pentafluoropyridine by silylphosphide derivatives.	90
Scheme 71 Fluoroalkanes C–F bond activation assisted by FLPs.....	90
Scheme 72 Synthesis of monofluoroalkenes <i>via</i> C–F bond activation of fluoroalkanes with FLPs.	91
Scheme 73 Nucleophilic substitution reactions of simple phosphines (PPh_3 and P^nBu_3) with perfluorinated alkenes.	91
Scheme 74 Synthesis of phosphonium betaines <i>via</i> PPh_3 -assisted C–F bond activation.	92
Scheme 75 Hydrodefluorination of polyfluoro(hetero)aromatics promoted by PEt_3	92
Scheme 76 Initial mechanistic proposal for the PEt_3 -assisted hydrodefluorination reaction.	93
Scheme 77 Proposed decomposition processes of the fluorophosphine.....	93
Scheme 78 Revised mechanism for the PEt_3 -assisted hydrodefluorination reaction.	94
Scheme 79 S_NAr reaction of perfluoro(hetero)aromatics by a σ^3 -phosphorus triamide compound and subsequent fluoride transfer.....	94
Scheme 80 S_NAr reaction of perfluoro(hetero)aromatics by a geometrically constrained P^{III} species.	95
Scheme 81 Unexpected synthesis of 15 and the difluorophosphorane.	95

Scheme 82 Proposed mechanism for the reductive coupling of perfluoroarenes promoted by P(NEt ₂) ₃ in Et ₂ O.	96
Scheme 83 General reaction for the metalation of perfluoroaromatics promoted by P(NEt ₂) ₃	96
Scheme 84 Synthesis of difluorophosphoranes <i>via</i> fluorination of phosphine oxides with (COCl) ₂ and KF.	97
Scheme 85 Synthesis of difluorophosphoranes <i>via</i> fluorination of phosphines with TCICA and KF.	97
Scheme 86 Electrochemical fluorination of PPh ₃ using KF.....	98
Scheme 87 Reaction of complex 6 with an equimolar amount of Py-F₅ in THF or C ₆ D ₆ at 20 °C.....	98
Scheme 88 Reaction between Py-F₅ (1 equiv.) and PMe ₃ (1 equiv.) in THF or C ₆ D ₆ after 20 minutes at 20 °C.....	99
Scheme 89 Reaction of Py-F₅ (1–3 equiv.) and PMe ₃ (1 equiv.) in C ₆ D ₆ after 20 minutes at 20 °C.	100
Scheme 90 Reaction mixture obtained after heating up to 20 °C for 4 hours a cold solution (0 °C) of PMe ₃ (1 equiv.) and Py-F₅ (3 equiv.) in toluene.	103
Scheme 91 Reaction of Py-F₅ (2.2 equiv.) and PMe ₃ (1 equiv.) in C ₆ D ₆ after 30 minutes at 20 °C.	105
Scheme 92 Reactivity tests on a set of PR ₃ (1 equiv.) with Py-F₅ (2.2 equiv.) in C ₆ D ₆ after 1 hour at 20 °C.....	106
Scheme 93 Reactivity of P(^t Bu) ₂ Cy and P ^t Bu ₃ with Py-F₅ in C ₆ D ₆ at 40°C for 4 hours and 7 days, respectively.....	106
Scheme 94 Reactivity of P ⁱ Pr ₃ , PMe ₂ Ph, PMe ₃ and PCy ₃ towards Py-F₅ in CD ₃ CN after 30 minutes at 20 °C.....	107
Scheme 95 Proposed reaction mechanism of Scheme 89.	108
Scheme 96 Proposed reaction mechanism for the formation of 16 ; an alternative mechanism for the synthesis of 9 is displayed (blue box).....	109
Scheme 97 Proposed mechanism for the formation of 15	110

Scheme 98 Proposed mechanism for the intermolecular acylfluorination of alkynes catalysed by PCy ₃ in toluene.	111
Scheme 99 Proposed deoxyfluorination reaction of alcohols with difluorophosphoranes.	113
Scheme 100 General reaction scheme for HDF.	114
Scheme 101 Selected example for the HDF of C(sp ³)-F catalysed by [Et ₃ Si][X].	117
Scheme 102 B(C ₆ F ₅) ₃ -catalysed hydrodefluorination of alkyl fluorides.	118
Scheme 103 HDF of fluoromethanes catalysed by silylium-like surface species. (ACF = aluminium chlorofluoride).....	119
Scheme 104 Catalytic HDF reaction using cooperative Si-H bond activation by a Ru-S bond.	119
Scheme 105 Stoichiometric HDF of glycosylfluoride promoted by AlH ₃	120
Scheme 106 Stoichiometric HDF of alkyl monofluorides promoted by B(C ₆ F ₅) ₃ and [tBu ₃ PH][HB(C ₆ F ₅) ₃].	120
Scheme 107 HDF of alkyl, benzyl and acyl fluorides catalysed by <i>in situ</i> generated [Ph ₃ Ge][B(C ₆ F ₅) ₄].	121
Scheme 108 Selected example of HDF of aryl fluorides catalysed by a pyrene-based photocatalyst and relative proposed mechanism.	122
Scheme 109 HDF of hexafluoropropene promoted by AlH ₃ ·NMe ₃	123
Scheme 110 HDF of polyfluoroaromatics catalysed by TBAT and proposed reaction mechanism.	123
Scheme 111 HDF of polyfluoroarenes catalysed by diazaphospholenes.....	124
Scheme 112 Stoichiometric HDF of polyfluoroaromatics promoted by PEt ₃	124
Scheme 113 HDF of polyfluoroarenes catalysed by Bi ^I complexes.....	128
Scheme 114 Stepwise OA, LM and RE at a P ^{III} centre.....	129
Scheme 115 HDF of polyfluoroaromatics catalysed by a geometrically constrained σ ³ -P compound.	129

Scheme 116 Synthesis of the difluorophosphoranes F_2PR_3 ($R = Me, 'Pr$) and 15 (first step) and reduction of F_2PR_3 with $PhSiH_3$ (second step).....	130
Scheme 117 Reaction of Ph_2SiCl_2 (1 equiv.) and dried Et_2NH (2 equiv.) in dried Et_2O under N_2 atmosphere resulted in the synthesis of $Ph_2Si(Cl)(NEt_2)$ and precipitation of $[Et_2NH_2]Cl$	140
Scheme 118 Reaction of aminodefluorination of Py-F₅ (1 equiv.) in the presence of $Ph_2Si(Cl)(NEt_2)$ (1.1 equiv.) and P^nBu_3 (10 mol%).....	141
Scheme 119 Reaction test between 4-dimethylamino-tetrafluoropyridine (1 equiv.), P^nBu_3 (1 equiv.) and $Ph_2Si(Cl)(NEt_2)$ (1 equiv.) carried out in CD_3CN for 18 hours at 60 °C.	144
Scheme 120 Synthesis of $Ph_2Si(Cl)(pro)$ <i>via</i> esterification of <i>L</i> -proline to form the <i>L</i> -proline methyl ester hydrochloride (30) and amidation of Ph_2SiCl_2	145
Scheme 121 Catalytic aminodefluorination of pentafluorobenzonitrile and perfluorotoluene using P^nBu_3 as catalyst.....	149
Scheme 122 HDF reaction of Py-F₅ (1 equiv.) with $PhSiH_3$ (1 equiv.) and P^nBu_3 (10 mol%) in CD_3CN at 20 °C.....	150
Scheme 123: Preparation of [31]Br and its reactivity towards silanes in the presence, and absence, of a fluoride source.....	152
Scheme 124 Reaction of Py-F₅ (1 equiv.) with Ph_2SiH_2 (1 equiv.) and $[Me_4N]F$ (10 mol%) in CD_3CN at 20 °C to test the catalytic ability of $[Ph_2Si(F)_nH_{3-n}]^-$ in absence of the phosphine.	154
Scheme 125 Reaction of perfluorotoluene (1 equiv.) with Ph_2SiH_2 (1 equiv.) and P^nBu_3 (10 mol%) in CD_3CN at 20 °C showed the formation of the intermediate phosphonium [32]⁺	155
Scheme 126 Mono- and dihydrodehalogenation of bromopentafluorobenzene (1 equiv.) with Ph_2SiH_2 (1 equiv.) and P^nBu_3 (1 equiv.) in CD_3CN at 20 °C <i>via</i> the phosphonium intermediate [28]⁺ formation.	155
Scheme 127 Proposed catalytic cycle and computed potential energy surface (PES) for $R = Me$. All energies at the PBE0/def2-TZVP//BP86/SV(P) level in CH_3CN . Relative Gibbs energies (in kJ/mol at 298 K) shown outside brackets and relative enthalpies (in kJ/mol at 298 K) shown in brackets. .	158
Scheme 128 Synthetic strategy for pyridine functionalisation <i>via</i> the formation of a phosphorane intermediate proposed by McNally <i>et al.</i> ³⁴⁵	159

Scheme 129 Representative scheme of our system for the catalytic reaction of HDF and hydroamination. 163

List of Tables

Table 1 Comparison of the Van der Waals radii between H and some elements from the <i>p</i> -block (top); bond dissociation energy (BDE) of relevant C–X bonds (bottom).....	27
Table 2 Different reaction types for intermolecular HDF reactions ([M] = transition-metal complex fragment, E = fluorophilic ligand).	35
Table 3 Product distribution from the reaction of Py-F₅ (1–3 equiv.) and PMe ₃ (1 equiv.) in C ₆ D ₆ after 20 minutes at 20 °C. ^a According to ¹⁹ F NMR analysis.	104
Table 4: Reaction optimisation for HDF of Py-F₅ . NMR yields determined by integration of ¹⁹ F NMR spectra using α,α,α -trifluorotoluene as internal standard.....	132
Table 5: Energies and corrections at the PBE0/def2-TZVPP//BP86/SV(P) level. As described above, vibrational frequencies and derived corrections were at the BP86/SV(P) level and electronic energies, both in the gas phase and COSMO solvation, in addition to DFT-D3 corrections were at the PBE0/def2-TZVPP level.....	206
Table 6 Relative energies of different states in the gas phase, with COSMO solvation in MeCN and with both COSMO solvation and DFT-D3 corrections.	207
Table 7 Energies and corrections at the PBE0/def2-TZVPP//BP86/SV(P) level. As described above, vibrational frequencies and derived corrections were at the BP86/SV(P) level and electronic energies, both in the gas phase and COSMO solvation, in addition to DFT-D3 corrections were at the PBE0/def2-TZVPP level.....	208
Table 8 Relative energies of different states in the gas phase, with COSMO solvation in MeCN and with both COSMO solvation and DFT-D3 corrections.	209

Acknowledgments

First of all, I would like to thank my supervisors, Dr. Christian Lorber, Prof. Jason Lynam, Dr. Antoine Simonneau and Dr. John Slattery for their huge support and guidance during these three years of PhD. With their enthusiasm, dedication to their work and huge chemistry knowledge, they have taught me how to conduct high-quality research. Beyond science, they have always encouraged me to persevere, push myself and embrace challenges. Honestly, I could not have hoped for better supervision.

I thank Dr. Emmanuel Gras, my 'parrain' at LCC, for his support and Prof. Anne-Duhme Klair for her interesting suggestions during the TAP meetings and for being there when I needed help.

I am also grateful to Prof. Robin Perutz for his interest in this research, our stimulating scientific discussions and for giving me valuable advice when I needed it.

I would like to thank Prof. Dr. Thomas Braun, Dr. Ruth Webster, Prof. Anne-Duhme Klair and Prof. Laurent Maron for accepting to be part of the jury members for my PhD defence.

I would like to thank all members of equipe N in Toulouse and the SLUG group, especially Quentin, Marie Christine, Aswin, Theo, Spencer and Jonny, for their presence and support during these three years. Thanks also to the CCIMC project, the European Union's Horizon 2020 research and innovation programme for the funding and the PMT who made this project possible. I am grateful to have known and been able to share this experience and many adventures with the other students in this project.

I would like to thank my friends in Italy (especially Marion and Elena) for their long-distance support, and Mylo and Ginevra, who made me feel like part of a family while abroad.

Finally, I deeply thank my parents Daniele and Maria Grazia and my siblings Marta and Andrea for their constant presence, encouragement and guidance in difficult times. Without your care and love I would not have been able to get here.

This PhD project has received funding from the *European Union's Horizon 2020 research and innovation programme* under the Marie Skłodowska-Curie grant agreement No. 860322.

Author's declaration

I declare that the research presented in this thesis, to the best of my knowledge, original and was carried out as part of the double doctoral degree programme under the MSCA-ITN CCIMC program under the supervision of Dr. Christian Lorber, Prof. Jason Lynam, Dr. Antoine Simonneau and Dr. John Slattery in LCC-CNRS, University of Toulouse III – Paul Sabatier and the Chemistry Department of the University of York between October 2020 and December 2023. Contributions from other authors and coworkers are listed below and referenced in the appropriate chapters throughout this thesis.

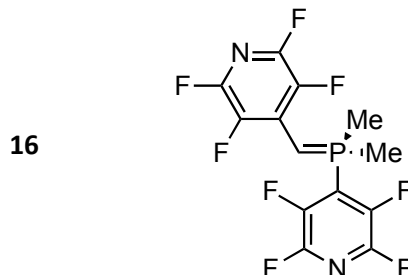
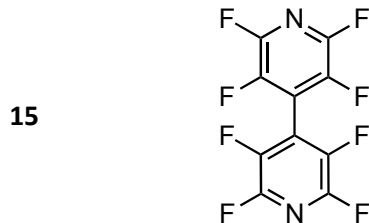
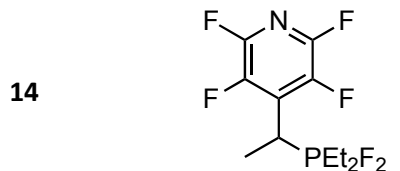
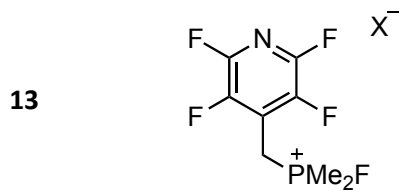
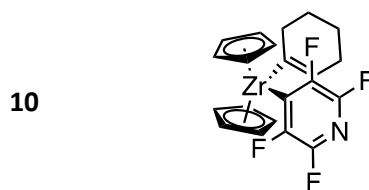
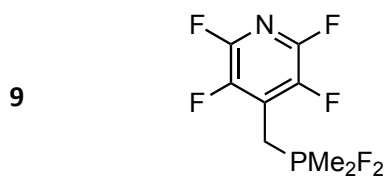
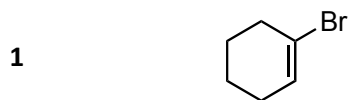
- Mass spectrometry experiments were performed by Karl Heaton (UoY).
- X-ray crystallography data were collected by Theo Tanner and Dr. Adrian Whitwood (UoY).
- Elemental analyses were performed by Isabelle Borget (CHN analysis service – LCC-CNRS).
- DFT calculations were performed by Prof. Jason Lynam and Dr. John Slattery.

The results presented in Chapter 4 were published in:

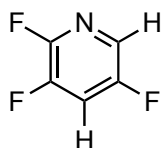
“Metallomimetic C–F Activation Catalysis by Simple Phosphines.”; Sara Bonfante,^{1,2} Christian Lorber,^{*1} Jason M. Lynam,^{*2} Antoine Simonneau,^{*1} John M. Slattery^{*2}

¹ Laboratoire de Chimie de Coordination, UPR CNRS 8241, 205 Route de Narbonne, 31077 Toulouse, France; ² Department of Chemistry, University of York, Heslington, York, YO10 5DD, North Yorkshire, United Kingdom. *J. Am. Chem. Soc.* **2024**, *146*, 2005–2014.

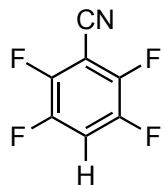
Summary of compounds



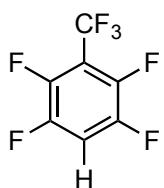
17



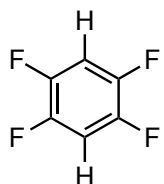
18



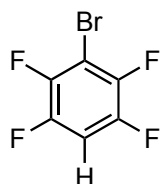
19



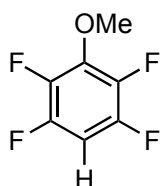
20



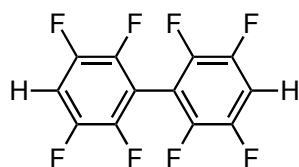
21



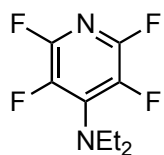
22



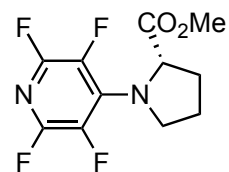
23



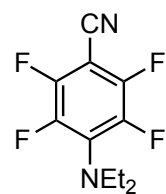
24



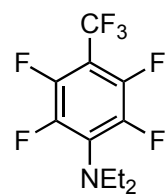
25



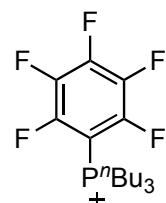
26



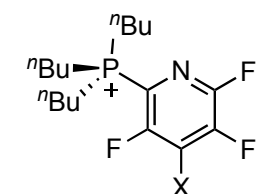
27



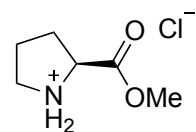
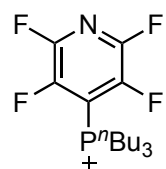
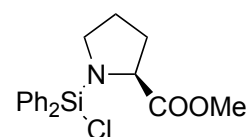
28



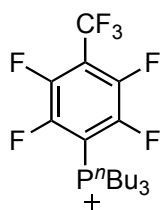
29



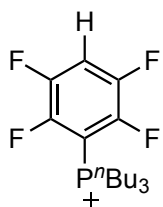
30

[31]⁺Ph₂Si(Cl)(pro)

[32]⁺



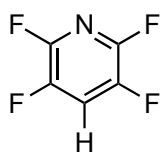
[33]⁺



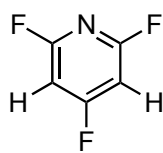
Py-F₅



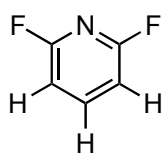
Py-F₄



Py-F₃



Py-F₂



Chapter 1 – Introduction

1.1 Properties of fluorine

Fluorine is the 9th element of the periodic table and it is the most electronegative, with a Pauling scale value (χ) of 4.0.¹ It also exhibits a high first ionisation energy ($IE_1 = 1679$ kJ/mol), making it challenging to abstract an electron from its 2p shell. Furthermore, fluorine exhibits a high electron affinity ($EA = -328$ kJ/mol), meaning that the addition of an electron to atomic fluorine releases energy.² Many of these effects are a consequence of fluorine having the smallest van der Waals atomic radius ($r_{vdw} = 1.47$ Å) among the period 2 elements (Table 1, top). The C–F bond is the strongest C–X bond (bond dissociation energy = 513 kJ/mol; Table 1, bottom),² deriving its strength mainly from the high ionic character (approximately 43%) resulting from the electronegativity difference between C and F ($\Delta\chi = 1.5$).³ Due to the high strength of this bond, the cleavage of C–F bonds is generally challenging.

Van der Waals radii (Å)	H	C	N	O	F	Si	P	S	Cl
	1.2	1.70	1.55	1.52	1.47	2.1	1.8	1.8	1.74

Bond	BDE (kJ/mol)
C–F	513
C–H	413
C–O	351
C–C	348
C–Cl	328
C–N	292

Table 1 Comparison of the Van der Waals radii between H and some elements from the *p*-block (top); bond dissociation energy (BDE) of relevant C–X bonds (bottom).

The high biological activity of fluorinated organic compounds stems from the fact that fluorine can be used as isostere for hydrogen in organic molecules, causing dramatic changes in the properties of the molecule comparing to the corresponding hydrocarbon but usually preserving its geometry and shape due to the small radius.⁴ The incorporation of fluorine often results in an increase in the

acidity of adjacent functional groups and organic acids, along with an enhancement in the lipophilicity of the molecule.⁵ Furthermore, the presence of fluorine in an organic molecule facilitates the formation of hydrogen bonding interactions. These phenomena strongly influence the biological activity of fluorinated organic compounds.⁴

1.2 Origin of fluorine and applications of fluorinated organic molecules

Fluorine is the 13th most abundant element in the Earth's crust, mainly occurring in the form of fluoride minerals such as fluorite (CaF₂).⁶ However, naturally occurring fluorinated organic compounds are limited and their biosynthesis remains unclear.⁷ The industrial synthesis of fluorine-containing organic molecules typically involves the use of elemental F₂ or HF. These compounds are obtained through the upgrading of CaF₂ to acid spar, which is a purer form of CaF₂ containing less than 1% of SiO₂, achieved through flotation.⁸

Fluorinated organic molecules can be found in a wide range of applications, including pharmaceuticals (where approximately 20% of commercial drugs contain at least one fluorine atom or a fluorinated functional group),⁹ agrochemicals, medical imaging (such as Positron Emission Tomography),¹⁰ materials (including fluoropolymers and liquid crystals), and more (Figure 1). Hence, there is a significant interest in developing efficient strategies for the synthesis of valuable fine chemicals that incorporate fluorine.

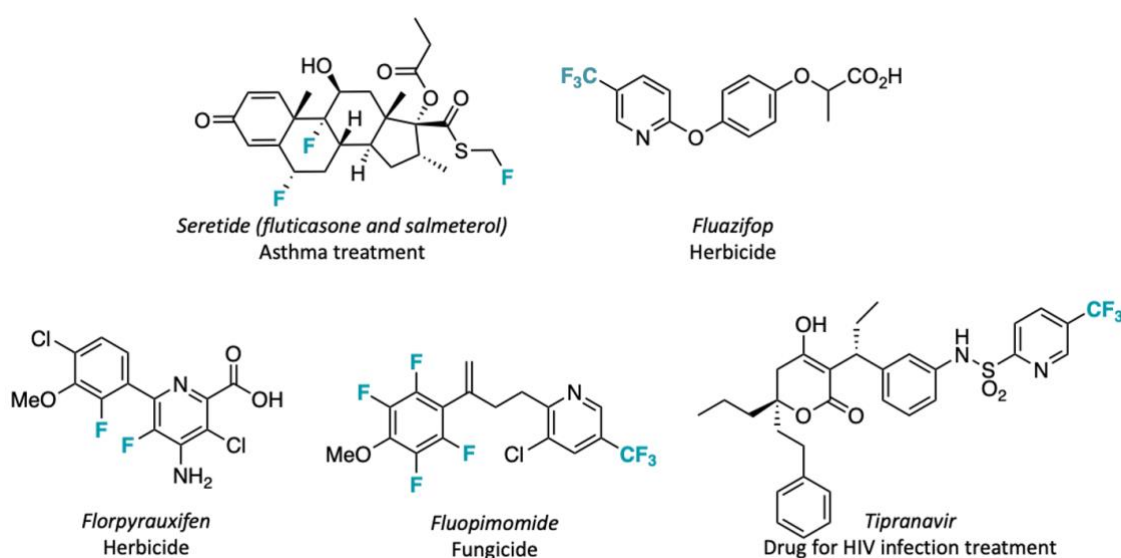


Figure 1 Selected examples of fluorine-containing organic molecules employed in pharmaceutical and agrochemical industries.

Moreover, due to their inert nature upon decomposition, fluorocarbons can be persistent in the environment. Hydrofluorocarbons (HFCs) and hydrofluoroolefins (HFOs) find applications in refrigeration, air-conditioning, foam-blowing, electronics and fire protection. Their high volatility leads to their release into the atmosphere as fluorinated gases, contributing to environmental pollution.^{11,12} Therefore, there is a need to explore alternative methods for the defluorination of fluorinated organic molecules.

1.3 Synthesis of fluorinated organic compounds

Two main pathways for the synthesis of partially fluorinated molecules have been developed:

- I. selective fluorination of non-fluorinated substrates;
- II. selective defluorination of perfluorinated and polyfluorinated molecules.

The first approach involves the use of fluorinating reagents, including nucleophilic, electrophilic and trifluoromethylating agents (Figure 2).

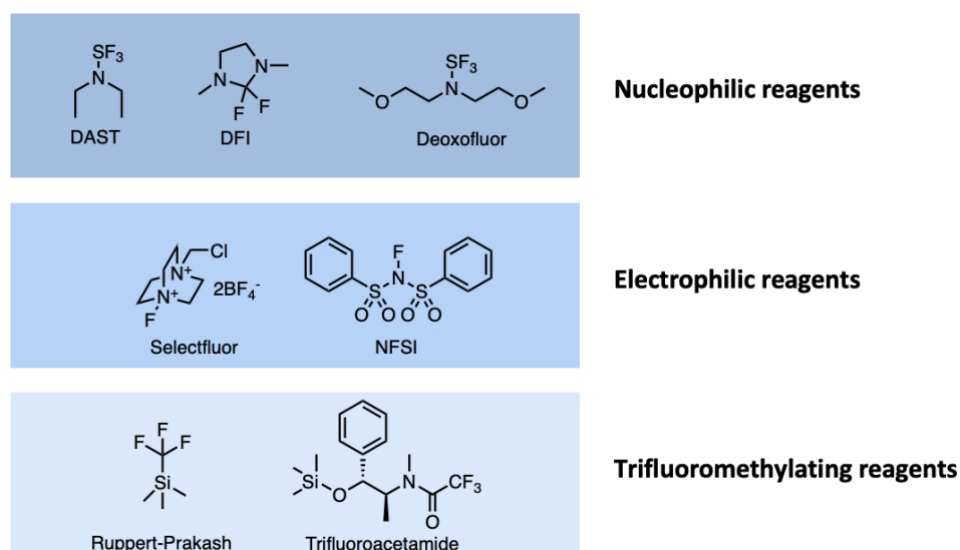


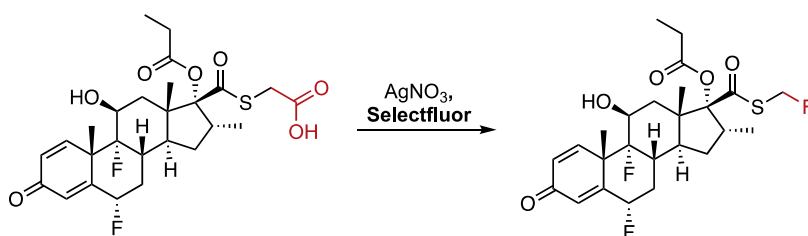
Figure 2 Selected examples of mild nucleophilic, electrophilic and trifluoromethylating reagents.

(DAST = diethylaminosulfur trifluoride; DFI = 2,2-difluoro-1,3-dimethylimidazolidine;
NFSI = N-fluorobenzenesulfonimide)

The main challenge in this method arises from controlling the reactivity of fluorine sources. With strong nucleophilic fluoride sources (e.g., HF, KF or Me₄NF), the fluoride anion exhibits weak nucleophilicity in the presence of hydrogen bond donors, leading to the formation of the stable

anion HF_2^- .⁵ When hydrogen bond donors are rigorously excluded, fluoride's strong basicity and nucleophilicity often result in undesired side reactions. Among the electrophilic fluorinating reagents, the simplest is fluorine gas, which is highly reactive, very difficult and hazardous to handle. It is often unselective and can react with many common functional groups. Consequently, due to the harsh conditions usually required in these systems, the substrate scope and selectivity of these reactions are restricted to simple substrates, which can be employed as building blocks for subsequent functionalisations.⁵

Researchers are overcoming this limitation by developing mild electrophilic fluorination reagents that enable the late-stage fluorination of complex organic molecules. These reagents allow milder reaction conditions to be used, they are easy to handle, less toxic and hazardous than traditional fluorinating reagents and exhibit enhanced selectivity. For instance, among the electrophilic fluorination reagents, the so-called "NF-reagents" stand out. These compounds feature a fluorine atom directly bonded to the electronegative nitrogen, which can be further activated by electron-withdrawing groups (e.g., carbonyl, sulfonyl) or a positive charge in the molecule. The advantage of all these reagents is that most are solid, non-volatile and non-explosive compounds, which may be handled with standard synthetic chemistry techniques.⁴ For example, Selectfluor, an NF-reagent developed thirty years ago, is industrially employed in the synthesis of fluticasone propionate (Scheme 1), an active ingredient in Seretide, a drug used for asthma treatment (Figure 1).¹³



Scheme 1 Synthesis of fluticasone propionate via late-stage fluorination by Selectfluor.

Nevertheless, often directing groups (such as pyridyl, amino, N-perfluorotolylamide groups) are necessary to ensure regioselectivity in these reactions.¹⁴ Alternatively, pre-activation of the substrate (β -ketocarbonyl compounds) can be necessary to promote the reaction.⁵

The second strategy for the synthesis of complex fluorinated organic compounds is the selective activation of C–F bonds in polyfluorinated and perfluorinated organic molecules. This approach is interesting as it allows the transformation of highly fluorinated molecules, readily available through bulk industrial fluorination processes (e.g., employing HF , KF , F_2), into more valuable fluorinated compounds. This is achieved through the selective activation of C–F bonds, converting them into C–H, C–C, C–O, C–S, C–N, C–P bonds. Transition metals (TMs) mainly promote these processes,

either catalytically or stoichiometrically, although examples involving main-group elements are also present in the literature.¹⁵ Considering the high strength of the C–F bond, as discussed in chapter 1.1, the thermodynamic requirement to make this process feasible is the formation of other strong E–F bonds, where E typically is H, Si, B, Al and TMs.¹⁶ This method is a viable alternative to the C–F formation strategy, as it can lead to the synthesis of new compounds, new selectivity and synthetic routes that might not be accessible with the first approach.¹⁷ The challenges associated with this method involve achieving precise control over the regio- and stereoselectivity and improving the functional group tolerance of the transformation.¹⁵

Chapters 2, 3 and 4 begin with introductions that provide comprehensive overviews of the literature related to their respective topics. The introduction in chapter 2 deals with the hydrodefluorination reactions catalysed by transition metals and *f*-block metals. Following this, a literature review is presented on defluorinative C–C coupling of polyfluorinated aromatics, involving *s*-block, *f*-block and transition metals. The focus then shifts to zirconium complexes incorporating highly strained cycloalkyne ligands and their potential applications in C(*sp*²)–C coupling reactions *via* C–F bond activation. The introduction of chapter 3 focuses on the selective derivatisation of readily available polyfluoro(hetero)aromatics, achieved through the cleavage of one or more C–F bonds, yielding valuable building blocks that can be further functionalised. This introduction section provides a description of the substitution reactions involving nucleophilic reagents, with particular emphasis placed on the reactivity of polyfluoro(hetero)aromatics towards phosphorus-containing compounds. In chapter 4, the introduction deals with hydrodefluorination reactions assisted by main-group elements.

1.4 Aims and objectives

The aim of this Ph.D. project was to explore novel strategies for the regioselective activation and functionalisation of C–F bonds in readily available polyfluoroaromatic compounds promoted by early-transition metals and by *p*-block elements.

This project is structured into three sections. The aim of the first section (chapter 2) was to establish a novel synthetic protocol for the controlled and regioselective functionalisation of fluorinated pyridines using a strained zirconocene-cycloalkyne complex. The objective was to obtain a fluorinated pyridine alkenylated in *ortho*-position, which could subsequently be further functionalised to yield a more complex, stereo-defined fluorinated organic compound. This investigation demonstrated that the zirconocene-cycloalkyne complex followed three different

reactivity pathways, depending on the fluorination pattern of the polyfluoropyridine.

In the second section (chapter 3), the investigation of a side reaction observed in chapter 2 is described. This reaction involved the C–F bond activation in *para*-position of pentafluoropyridine promoted by simple trialkylphosphines. The outcome of this activation reaction depends on the reaction conditions, leading to either the hydrodefluorinated product or the reductive C–C homocoupling product. Additionally, the generation of differently substituted difluorophosphoranes was observed. This research highlighted the potential of metal-free systems, employing only simple phosphines to selectively and efficiently functionalise electron-poor perfluoroheteroaromatics.

The final objective was to demonstrate that simple trialkylphosphines are able to catalyse hydrodefluorination and aminodefluorination reactions in the presence of silanes and silyl amides, without the need for complex constrained structures or the use of metals, as reported in the existing literature (chapter 4). The research showed that $P^n\text{Bu}_3$ could exhibit reactivity akin to transition metals during the catalytic cycle, characterised by reversible two-electron redox processes like oxidative addition and reductive elimination.

Chapter 2 – C–F bond functionalisation promoted by a zirconium-cyclohexyne complex

2.1 Introduction

As discussed in Chapter 1.3, taming the reactivity of fluoride ions in solution has prompted the development of mild fluorination agents^{5,18,19} to introduce fluorine atoms into non-fluorinated molecules (i) and methods to selectively activate the strong C–F bonds of polyfluorinated compounds (ii).¹⁷ This thesis deals with the second strategy, more precisely focusing on the selective activation and functionalisation of C–F bonds in polyfluorinated (hetero)aromatics.

This introduction section provides a brief overview of hydrodefluorination reactions promoted by transition metals and *f*-block metals. A literature review on defluorinative C–C coupling reactions of polyfluorinated aromatics promoted by *s*-block, *f*-block and transition metals is then presented. The focus then shifts to zirconium complexes incorporating highly strained cycloalkyne ligands and their potential applications in C(*sp*²)-C coupling reactions *via* C–F bond activation. The scope of this introduction is limited to hydrodefluorination and C–C coupling reactions because these areas are strongly overlapping with the new research reported in chapter 2.3. This section does not cover C–F bond functionalisations involving alkyl, benzylic or allylic fluorides as substrates.

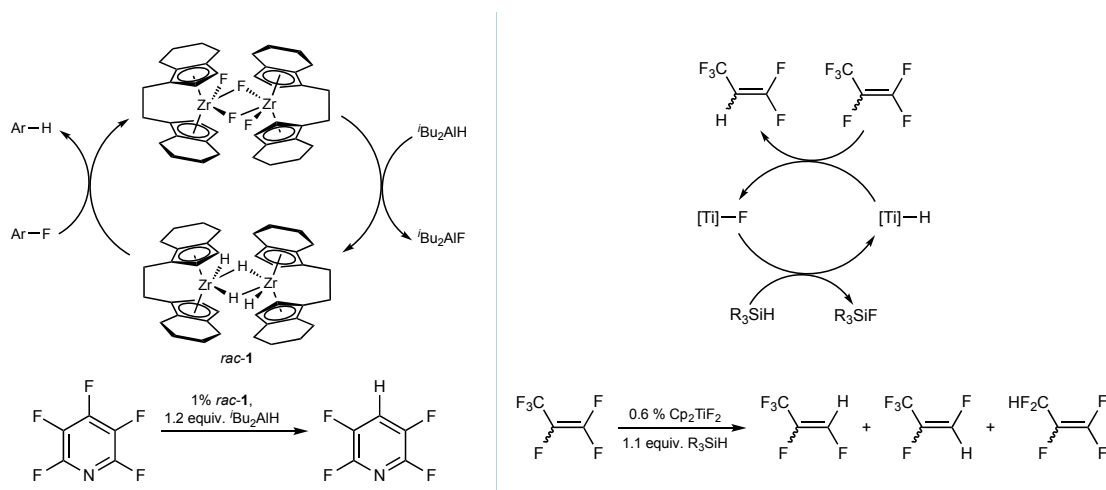
The main objective of this chapter was to develop a novel protocol for the regioselective alkenylation of polyfluorinated pyridines assisted by a zirconium complex bearing a highly strained unsaturated ligand. This complex exhibited distinct C–F bond activation pathways depending on the fluorinated compounds employed, enabling the regioselective synthesis of new organic fluorinated compounds.

2.1.1 Hydrodefluorination reaction

The C–F bond activation approach often relies on transition-metal- or main-group element-mediated (or catalysed) hydrodefluorination (HDF) reactions of readily available polyfluoroaromatic compounds.²⁰ This transformation involves the cleavage of a C–F bond and the subsequent formation of a new C–H bond. Extensive studies have been conducted in this area,

leading to the development of many approaches, including transition-metal^{20,21} and main-group element-mediated,²² heterogeneous,²³ gas-phase²⁴ and microbial HDF reactions.²⁵ The first strategy involves both early transition metals (ETMs) and late transition metals (LTMs).

Among the ETMs, group 4 metals have been mainly investigated and their reaction mechanisms usually result in the formation of a fluoro complex, due to the high affinity of these metals for fluoride ligands (Table 2, first row).²⁶ Ti,²⁷ Zr^{28–30} and Hf³¹ complexes promote, and in some cases catalyse, the HDF of polyfluorinated aromatics and olefins. Rosenthal *et al.*³² reported the Zr-catalysed HDF of pentafluoropyridine (**Py-F₅**) in the presence of aluminium hydrides as catalyst regenerators while Lentz and coworkers²⁷ demonstrated the Ti-catalysed HDF of fluoroalkenes with silanes as the hydride source (Scheme 2).



Scheme 2 Examples of Zr-catalysed HDF of polyfluoropyridines reported by Rosenthal *et al.* (left)³² and Ti-catalysed HDF of fluoroalkenes by Lentz and coworkers (right) and their proposed mechanisms.²⁷

Another example involves the HDF of benzylic CF₃ groups catalysed by Ti complexes in the presence of B(C₆F₅)₃ and Et₃SiH.³³ Aside from group 4 metals, group 5 metals such as Nb³⁴ and Ta³⁵ have also demonstrated the ability to promote the HDF of perfluoroaromatics in the presence of Grignard reagents and Et₃SiH, respectively. Additionally, there are a few examples of HDF reactions involving reduction^{36,37} and oxidative-addition mechanisms³⁸ with Zr complexes (Table 2, third and fourth row). Furthermore, *f*-block complexes such as Sm^{II}[N(SiMe₃)₂] have been employed as reducing agents for the HDF of alkyl fluorides.³⁹ In contrast, mechanisms involving metal-carbon bond formation, oxidative addition, reductive HDF and intramolecular HDF are typical of LTMs.²⁰ Rh, Ni, Pd, Cu, and Ir complexes are commonly employed in these reactions.

Profile	General equation
Fluorido complex	$[M]-H \xrightarrow{R-F} [M]-F + R-H$
Metal-carbon bond formation	$[M]-E \xrightarrow{R-F} [M]-R + E-F$
Oxidative addition	$[M] \xrightarrow{R-F} R-[M]-F$
Reductive hydrodefluorination	$2/n [M]^N \xrightarrow{R-F} 2/n [M]^{N+n} + R^- + F^-$

Table 2 Different reaction types for intermolecular HDF reactions ([M] = transition-metal complex fragment, E = fluorophilic ligand).

Furthermore, a promising field of research lies in main-group element-mediated C–F bond activation, which has demonstrated great efficiency in HDF, but also cross-coupling and other functionalisation reactions.^{21,40–42} These research areas will be discussed in more detail in chapters 3 and 4. Further detail on transition-metal-mediated HDF reactions is provided in the review article by Braun *et al.*²⁰

2.1.2 C–F bond functionalisation of perfluoro(hetero)arenes

Reactions resulting in the net, selective functionalisation of aromatic C(sp²)–F bonds^{15,17,43–45} have also been developed and they represent an attractive way to access fluoro(hetero)arene scaffolds that are frequently introduced in fluorinated pharmaceuticals, agrochemicals and dyes. Focusing on the functionalisation of polyfluoropyridines and polyfluoroarenes, an important body of work exists based on the use of LTMs in stoichiometric or catalytic amounts.¹⁷ These approaches generally rely on oxidative addition (OA) of the C–F bond and introduction of aryl,^{46,47} vinyl,⁴⁸ alkyl,⁴⁹ acyl⁴⁹ as well as silyl^{48,50} or boryl^{51,52} groups. Furthermore, examples of C(sp²)–F functionalisation promoted by main-group elements appear to be promising. These processes rely mainly on nucleophilic aromatic substitution-type mechanisms and enable the formation of new C–C cross-coupling products,^{53,54} but also C–N,⁵⁵ C–P⁵⁶ and C–O bonds.⁵⁷ On the other hand, examples with early transition metals are limited.²⁶

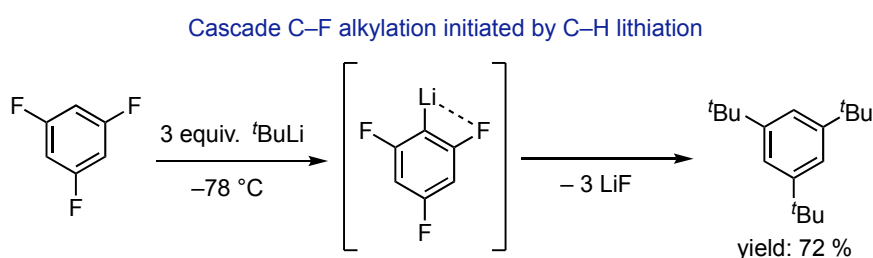
In this chapter, main-group metal- and transition-metal-assisted C–F bond activation of perfluorinated (hetero)aromatics that lead to the formation of new C–C bonds are discussed. Only homogeneous systems are considered, with a specific focus on group 1 and 2 for the main-group elements and on group 4 and 10 for the transition metals. The discussion will subsequently centre

on zirconium complexes incorporating highly ring-strained ligands and their potential applications in these $C(sp^2)$ -C coupling reactions, to set the scene for the new research described in chapter 2.3, where a zirconocene-cyclohexyne complex was employed for the C-F bond functionalisation of polyfluorinated pyridines.

2.1.3 Main-group metal-mediated $C(sp^2)$ -C coupling reactions *via* C-F activation

The study of cross-coupling reactions involving C-F bond activation of polyfluoro(hetero)aromatic compounds has gained increasing interest over the past few decades, leading to numerous examples reported in the literature.^{16,17,58-60}

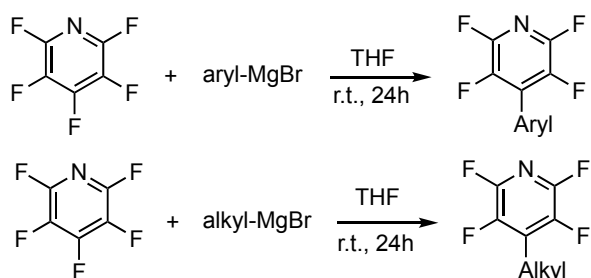
Within the main-group metals, the *s*-block metals are the only elements which have been reported to promote this kind of transformation. Grignard reagents⁶¹⁻⁶⁵ and organolithium compounds⁶⁶ have been employed and these reactions typically follow a nucleophilic aromatic substitution-type mechanism. Organolithium compounds are very reactive towards fluoroarenes and have been used for alkylation and alkenylation reactions of many per-⁶⁶⁻⁶⁸ and polyfluoro(hetero)aromatics.⁶⁹⁻⁷¹ However, the high instability of the metalated fluoroaromatics requires the use of very strict reaction conditions and the reactivity of the system can be quite complex and uncontrolled. Schlosser *et al.* demonstrated that the treatment of *t*BuLi with 1,3,5-trifluorobenzene at $-78\text{ }^\circ\text{C}$ led to an initial deprotonative metalation, which then underwent several H/Li interconversions and benzyne formation to yield the polyalkylated product (Scheme 3).⁷²



Scheme 3 Challenges in the metalation of fluoroarenes using organolithium reagents.

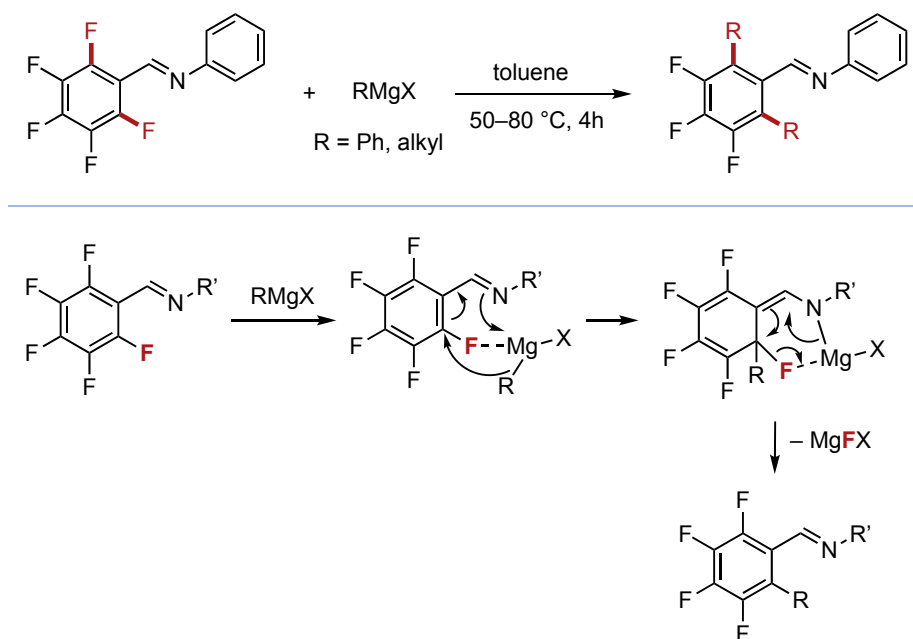
Alternatively, Grignard reagents can be employed in cross-coupling reactions involving the C-F bond activation of polyfluoroaromatic compounds, with or without directing groups. Early examples of these reactions demonstrated that Grignard reagents with benzyl and alkyl R groups could promote C-C coupling reactions with hexafluorobenzene, but the yields were relatively low due to the poor selectivity of these reactions.⁷³⁻⁷⁵ More recently, Li and coworkers⁵³ proposed an improved protocol for the alkylation and arylation of perfluorinated (hetero)arenes, assisted by

alkyl and aryl-based Grignard reagents (Scheme 4). This new procedure achieved high reaction selectivity by relying on lower temperatures than those employed in the early examples, resulting in the formation of the desired products in good yields.



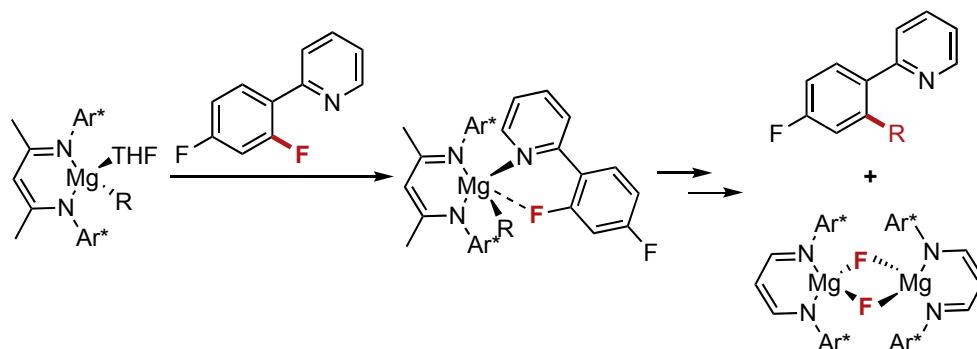
Scheme 4 Monoalkylation and -arylation of perfluorinated arenes with Grignard reagents.

Li and coworkers⁷⁶ reported a similar reaction with polyfluoroarenes bearing an imino directing group. The pre-coordination of the N of the directing group to the Mg allows the interaction between Mg and the *ortho*-F, leading to a partial weakening of the C–F bond (Scheme 5). This sets the stage for the nucleophilic attack of the R-group of the Grignard reagent on the *ortho*-carbon atom. The formation of the new C–C bond occurs through the generation of the six-membered chelate ring intermediate and the final cleavage of the C–F bond of the Meisenheimer complex analogue results in the monoalkylated or -arylated compound. A second cycle completes the process, liberating the targeted double cross-coupling product in excellent yields.



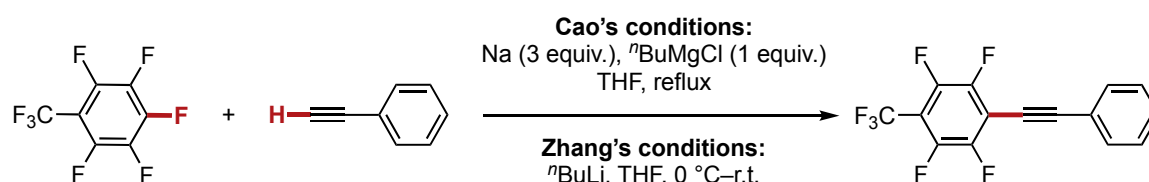
Scheme 5 *Ortho*-alkylation and arylation of 2-(2-fluorophenyl)pyridine and perfluoroaryl imine derivatives with Grignard reagents and proposed mechanism.

Similarly, Hevia *et al.* reported the alkylation and arylation of 2-(2,4-difluorophenyl)pyridine assisted by a Mg complex with a sterically demanding β -diketiminato ligand (Scheme 6).^{77,78} The proposed mechanism proceeds *via* a six-membered ring intermediate, in a similar way as in Scheme 5.



Scheme 6 Proposed mechanism for the alkylation and arylation of 2-(2,4-difluorophenyl)pyridine with a Mg(II) complex ($\text{Ar}^* = 2,6\text{-}i\text{Pr}_2\text{-C}_6\text{H}_3$; $\text{R} = n\text{Bu, Ph}$).

Base-promoted Sonogashira-type cross-coupling reactions of terminal alkynes with perfluoroarenes have been reported by Cao^{79,80} and Zhang and coworkers.⁸¹ In both cases, the presence of a strong base was crucial for the formation of the acetylene anion, which, *via* a nucleophilic aromatic substitution ($\text{S}_{\text{N}}\text{Ar}$) (or a radical-nucleophilic aromatic substitution in the first case), led to the formation of the cross-coupling product (Scheme 7).



Scheme 7 Selected example for the Sonogashira-type cross-coupling reactions promoted by strong bases.

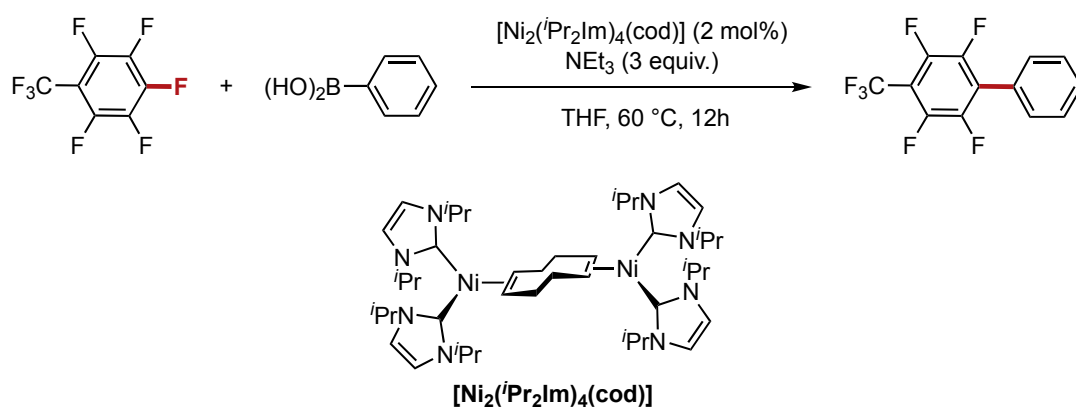
As an alternative to organometallic nucleophiles, examples of C–F functionalisation with other types of common nucleophiles (e.g., C-, O-, N-, P-based) have been reported. These examples will be discussed in detail in chapter 3.1.

2.1.4 LTM-mediated C(sp²)-C coupling reactions *via* C-F activation

Generally, Ni, Pd and Pt are the most commonly employed metals in this field.^{4,39} A shared mechanistic step is the oxidative addition of the fluorinated aromatic to the metal whereby, in general, the reaction is more favoured with more electron-deficient substrates. This section focuses on stoichiometric and catalytic C(sp²)-C coupling reactions and is categorised into three groups: C(sp²)-F bond activation of (1) fluorinated benzene derivatives, (2) polyfluorinated aromatics supported by a remote group and (3) polyfluorinated pyridines. The most emblematic examples of each category and their reaction mechanisms are discussed.

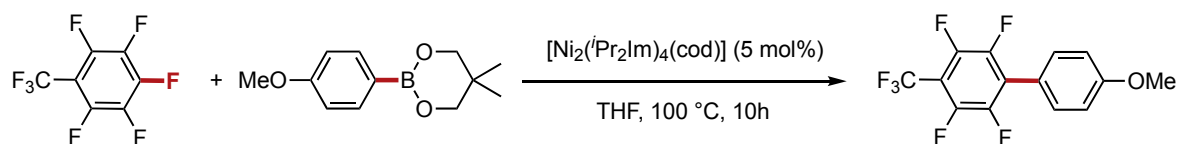
2.1.4.1 C(sp²)-C bond formation at polyfluorinated benzene derivatives

In 2006, Radius *et al.* made a significant advancement in this field by reporting a Ni-catalysed Suzuki-Miyaura-type cross-coupling reactions of polyfluoroarenes.⁸² The N-heterocyclic carbene (NHC)-stabilised nickel complex $[\text{Ni}_2(\text{}^i\text{Pr}_2\text{Im})_4(\text{cod})]$ ($\text{}^i\text{Pr}_2\text{Im}$ = 1,3-di(isopropyl)imidazole-2-ylidene, cod = 1,5-cyclooctadiene, Scheme 8) was a source of $[\text{Ni}(\text{}^i\text{Pr}_2\text{Im})_2]$ fragments, which readily underwent OA with perfluorinated aromatic compounds. The system was made catalytic for Suzuki-type cross-coupling reactions by employing aryl boronic acids as coupling partners in addition to a base (Scheme 8). The proposed reaction mechanism involved the initial η^2 -coordination of the substrate to a $[\text{Ni}(\text{}^i\text{Pr}_2\text{Im})_2]$ fragment, followed by a concerted oxidative addition.⁸³ It then proceeded according to the typical Suzuki-Miyaura coupling reaction mechanism.



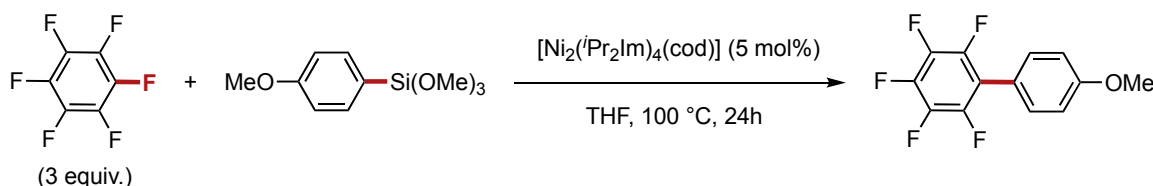
Scheme 8 Suzuki-Miyaura cross-coupling reaction of octafluorotoluene catalysed by $[\text{Ni}_2(\text{}^i\text{Pr}_2\text{Im})_4(\text{cod})]$ in the presence of boronic acid and NEt_3 .

Following this discovery, various Ni-based catalytic systems have been developed. For instance, Ogoshi *et al.* demonstrated the possibility of performing the Suzuki-Miyaura-type cross-coupling reaction using the Ni catalyst $[\text{Ni}_2(\text{iPr}_2\text{Im})_4(\text{cod})]$ without the need for a base, employing 4-anisylboronate instead of aryl boronic acids (Scheme 9).⁸⁴



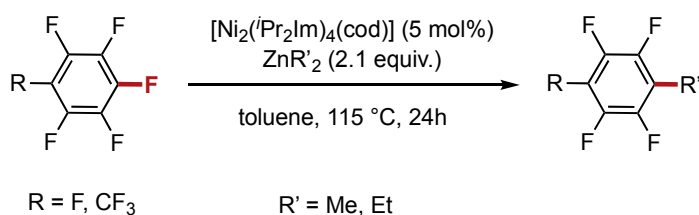
Scheme 9 Selected example for the Suzuki–Miyaura cross-coupling reaction of polyfluorinated aromatics catalysed by $[\text{Ni}(\text{iPr}_2\text{Im})_2]_2(\text{cod})$ in the presence of aryl boronate.

Ogoshi *et al.* also reported the base-free Hiyama cross-coupling reaction of perfluoroarenes catalysed by $[\text{Ni}_2(\text{iPr}_2\text{Im})_4(\text{cod})]$ in the presence of aryl trimethoxysilanes (Scheme 10).⁸⁵



Scheme 10 Ni-catalysed Hiyama cross-coupling reaction reported by Ogoshi and coworkers.

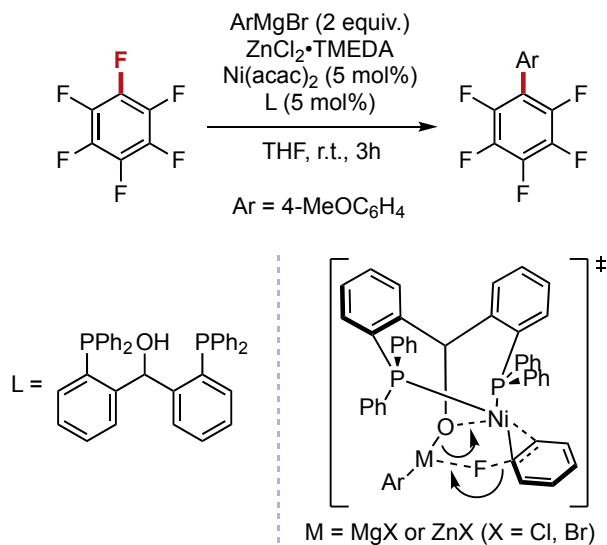
The same Ni complex was recently employed by Radius *et al.* to perform the catalytic Negishi-type cross-coupling reaction of perfluoroaromatics in the presence of ZnR'_2 ($\text{R}' = \text{Me}, \text{Et}$).⁸⁶



Scheme 11 Ni-catalysed Negishi cross-coupling reaction in the presence of ZnR'_2 .

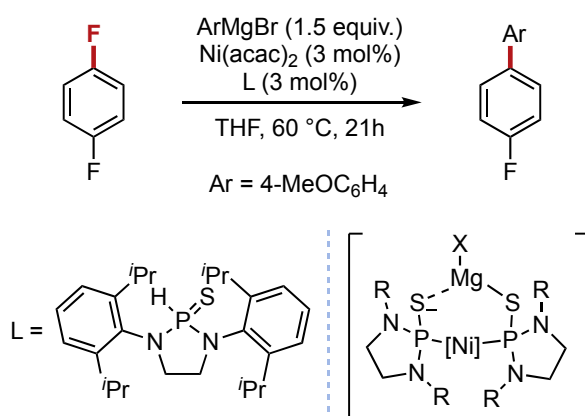
Nakamura and coworkers demonstrated that nickel complexes were able to catalyse the cross-coupling between polyfluoroarenes and organozinc or Grignard reagents in the presence of a tridentate diphosphine ligand bearing an alkoxide group (Scheme 12).⁸⁷ In this example, the ligand cooperated in the C–F bond activation step and the presence of the phosphine significantly enhanced the efficiency of this system. The two phosphine groups stabilised the Ni(0) centre, while the alkoxide unit coordinated with both the Zn (or Mg) and Ni(II) intermediates in the OA step,

accelerating the C–F bond activation process through a push-pull mechanism (Scheme 12). This was followed by transmetalation and reductive elimination.



Scheme 12 Ni-mediated cross-coupling reactions of perfluorobenzene with aryl zinc or Grignard reagents; suggested transition state for the C–F bond cleavage step (bottom right).

In a similar trend, Ackermann *et al.* proposed a Ni-catalysed Kumada-Tamao-type cross-coupling of fluoroarenes using aryl Grignard reagents.⁸⁸ The employed ligand, a diamidophosphine sulfide, enabled the formation of a heterobimetallic complex, considered the active catalyst in the reaction (Scheme 13, bottom right).

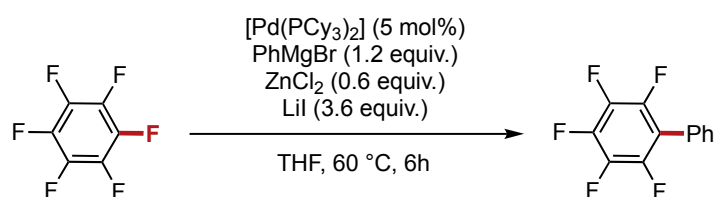


Scheme 13 Kumada–Tamao cross-coupling reaction of 1,4-difluorobenzene with aryl Grignard reagents and the diamidophosphine sulfide as ligand precursor; generation of the heterobimetallic complex (bottom right).

In a similar context, Jin *et al.* described the Kumada-Tamao cross-coupling reaction of fluoroarenes with PhMgBr, employing a diamidophosphine oxide as a ligand precursor.⁸⁹ More examples of Ni-

catalysed cross-coupling reactions with aryl Grignard reagents were proposed by Tamao⁹⁰ and Herrmann and coworkers.⁹¹

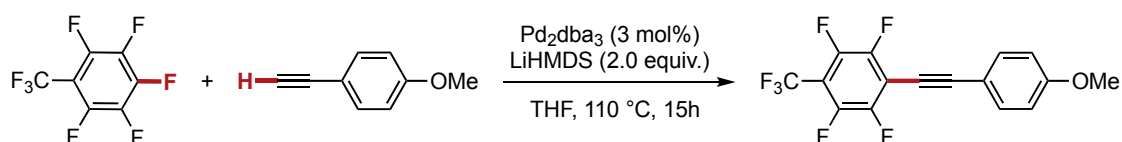
Shifting focus to other metals of group 10, Ogoshi *et al.* reported a cross-coupling reaction of perfluoroarenes catalysed by $[\text{Pd}(\text{PCy}_3)_2]$ (Cy = cyclohexyl) with aryl zinc compounds in the presence of LiI as an additive (Scheme 14).⁹² The oxidative addition of the fluorinated arene to Pd was followed by a halogen exchange reaction between the fluoride and LiI and this final step enabled the formation of the cross-coupling product.



Scheme 14 Selected example of cross-coupling reaction of perfluoroaromatics with aryl zinc compounds and LiI as additive.

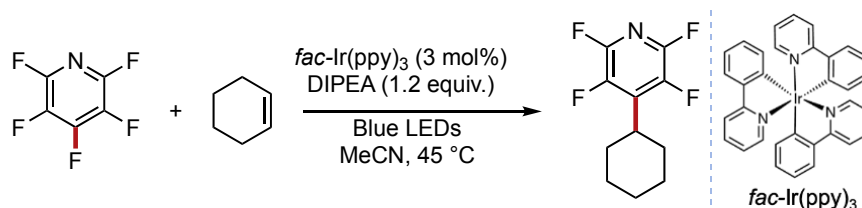
Tamao *et al.* also reported another example of a Pd-catalysed Kumada-Tamao cross-coupling reaction involving polyfluorinated benzenes in the presence of aryl Grignard reagents.⁹⁰

Base-promoted palladium-catalysed Sonogashira cross-coupling reaction of polyfluorinated aromatics with terminal alkynes was also proposed by Cao and coworkers (Scheme 15).⁹³



Scheme 15 Pd-catalysed Sonogashira-type cross-coupling reaction of perfluoroarenes and terminal alkynes (dba = dibenzylideneacetone).

Finally, photocatalytic defluoroalkylation of perfluoroarenes was also reported. One example was proposed by Weaver *et al.* in the presence of *fac*-Ir(ppy)₃ (ppy = 2-phenylpyridine) as catalyst and N(Et)₂Pr as base and sacrificial electron donor (Scheme 16).⁹⁴

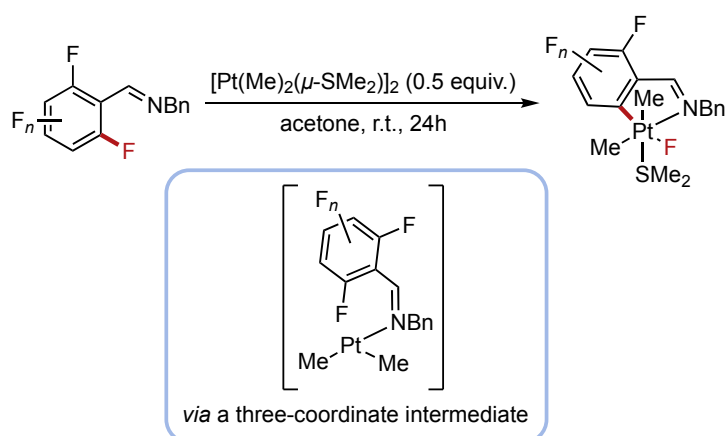


Scheme 16 Selected example of photocatalytic C–F bond alkylation of perfluoroarenes catalysed by *fac*-Ir(ppy)₃.

2.1.4.2 C(sp²)-C bond formation at polyfluorinated aromatics supported by a remote group

The incorporation of directing groups such as imines, oxazolines, pyridines, nitro, keto and hydroxo groups into a fluoroaromatic can promote the C-F bond activation process and direct the C-C coupling to the *ortho*-position relative to them.

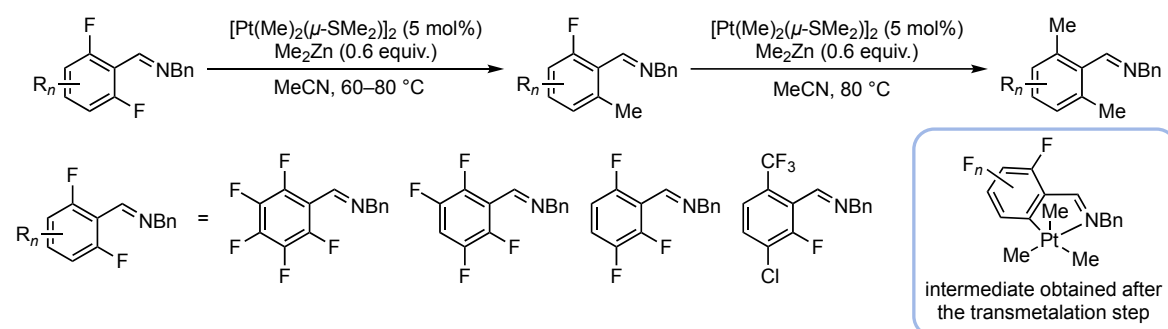
The first example of directed C-F bond activation dates back to the 1990s, pioneered by Crespo *et al.*, who demonstrated the regioselective C-F cleavage in polyfluoroaryl imines using the binuclear complex [Pt(Me)₂(μ-SMe₂)]₂ (Scheme 17).^{95,96} Mechanistic studies demonstrated that the coordination of the imine nitrogen to the Pt centre led to the dissociation of SMe₂ and the formation of a three-coordinate Pd complex intermediate. Intramolecular concerted oxidative addition led to the cleavage of the C-F bond and re-coordination of SMe₂, which eventually resulted in the formation of the unstable Pt^{IV} complex (product of Scheme 17).



Scheme 17 Directing group-promoted C-F bond activation of polyfluorophenyl imines at [Pt(Me)₂(μ-SMe₂)]₂.

Based on the results of Crespo and coworkers, Love *et al.* developed a catalytic cross-coupling system catalysed by the same Pt complex and employing an organozinc compound for the catalyst regeneration (Scheme 18).⁹⁷ The regioselective methylation of the arene in the *ortho*-position occurred through the coordination of the aryl imine to Pt^{II}, leading to the release of a SMe₂ ligand (similar to the mechanism proposed by Crespo in Scheme 17) and the formation of the active catalyst. The transmetalation with Me₂Zn formed MeZnF and the methylated complex (reported in Scheme 18) which subsequently liberated the cross-coupling product *via* reductive elimination took place. Interestingly, the rate-determining step in this reaction can be either the oxidative addition or the reductive elimination, depending on the substrate used. If the aryl imine is sufficiently electron-deficient, the oxidative addition product will be stabilised, making the elimination of the

product the rate-determining step. Conversely, if the substrate is electron-rich, oxidative addition will limit the rate of the process.



Scheme 18 Catalytic methylation of polyfluoroaryl imines with a $[\text{Pt}(\text{Me})_2(\mu\text{-SMe}_2)]_2$ as catalyst.

Further examples of Pt-, Ni-, and Pd-catalysed aromatic C–F functionalisation in the presence of directing groups are discussed in the reviews by Braun *et al.*¹⁷ and Weaver *et al.*⁹⁸

2.1.4.3 $\text{C}(sp^2)$ –C bond formation at polyfluorinated pyridines

Fluorinated pyridine compounds are essential building blocks in the pharmaceutical, agrochemical and dye industries. The last few decades have witnessed extensive research into novel methods enabling the regioselective functionalisation of these compounds. Furthermore, polyfluorinated heteroaromatics, such as pentafluoropyridine, exhibit enhanced electrophilicity compared to their non-heteroaromatic counterparts like hexafluorobenzene. Consequently, reactions involving oxidative addition by metals or nucleophilic attack are generally more favoured with polyfluorinated heteroaromatics.

The regioselectivity of C–F bond activation of polyfluorinated pyridines by group 10 metals is generally determined by the mechanism of the oxidative addition step. Several potential routes for oxidative addition to metal centres exist, including three-coordinate transition states that might involve ligand cooperation (**A**), tight ion-pairs formed through electron transfer from electron-rich metal complexes (**B**) and Meisenheimer intermediates *via* $\text{S}_{\text{N}}\text{Ar}$ reactions (**C**), as illustrated in Figure 3.

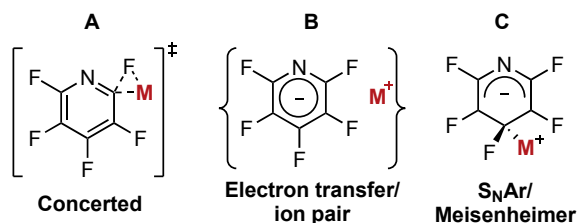
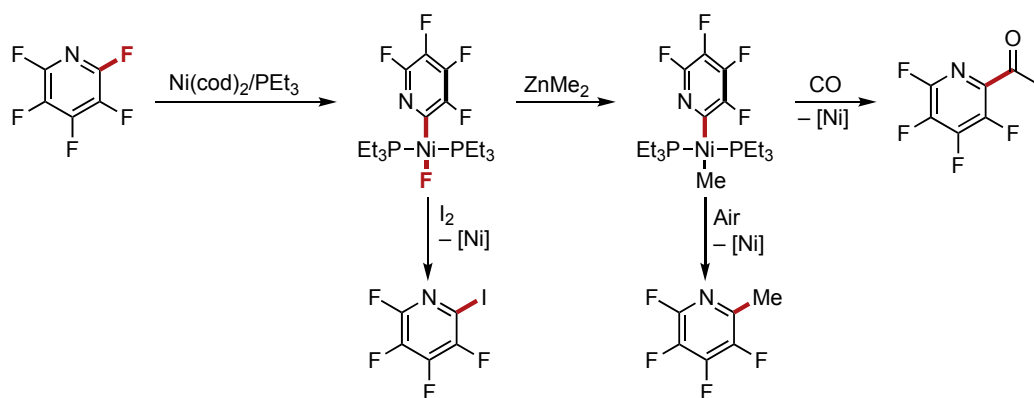
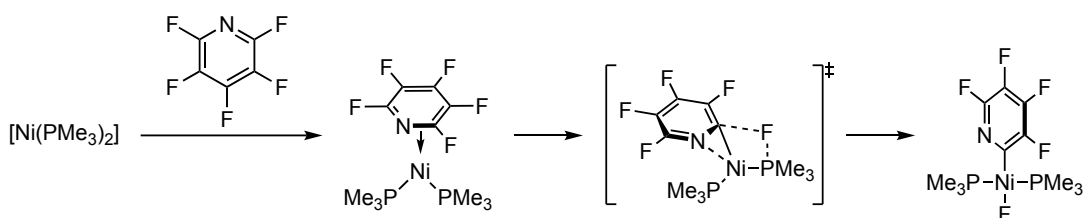


Figure 3 Possible intermediates and transition states for the C–F activation of pentafluoropyridine at a late transition metal: three-centred transition state (**A**), ion-pair formation (**B**) and Meisenheimer intermediate (**C**).

The activation at the 4-position of **Py-F₅** is the most common and thermodynamically favoured, whereas activation at the 2-position is less frequent. The regioselectivity of the transformation is influenced by the metal and pyridine substituents. For instance, Perutz and coworkers⁹⁹ reported the oxidative addition **Py-F₅** and 2,3,5,6-tetrafluoropyridine (**Py-F₄**) to the Ni(cod)₂ complex in the presence of PEt₃ (Scheme 19). The C–F activation occurred at the *ortho*-position, providing indirect evidence for concerted mechanism (**A**) and resulting in the formation of a square planar nickel(II) fluoride complex. Computational investigations into this reaction mechanism revealed that the activation at the *ortho*-position of the pyridine was kinetically favoured.¹⁰⁰ This preference was ascribed to the neighbouring group effect: the pyridine nitrogen pre-coordinates to the nickel centre *via* its lone pair, while simultaneously a fluoride transfers to one of the phosphine ligands, forming a transient metallophosphorane intermediate. Eventually, the fluoride migrated to the metal centre, yielding the OA product (Scheme 19, reaction at the top, first step). This complex enabled further stoichiometric functionalisation of the pyridine, such as methylation, carbonylation, iodination and protonation in the pyridine *ortho*-position.^{101,102}

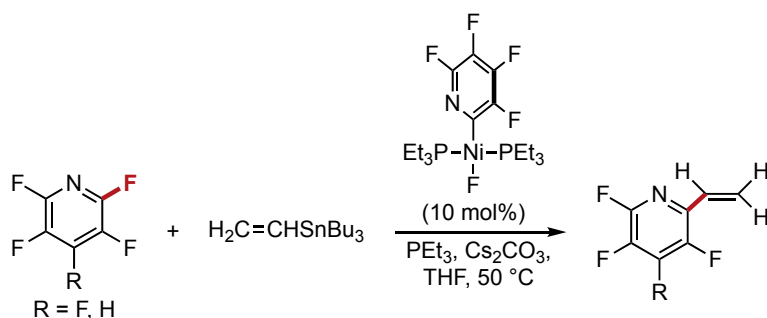


Proposed mechanism:



Scheme 19 *Ortho*-CF bond activation of **Py-F₅** and **Py-F₄** and subsequent functionalisation assisted by a Ni(cod)₂ complex in the presence of PEt₃ (top); proposed mechanism based on density functional theory (DFT) studies (bottom).¹⁰⁰

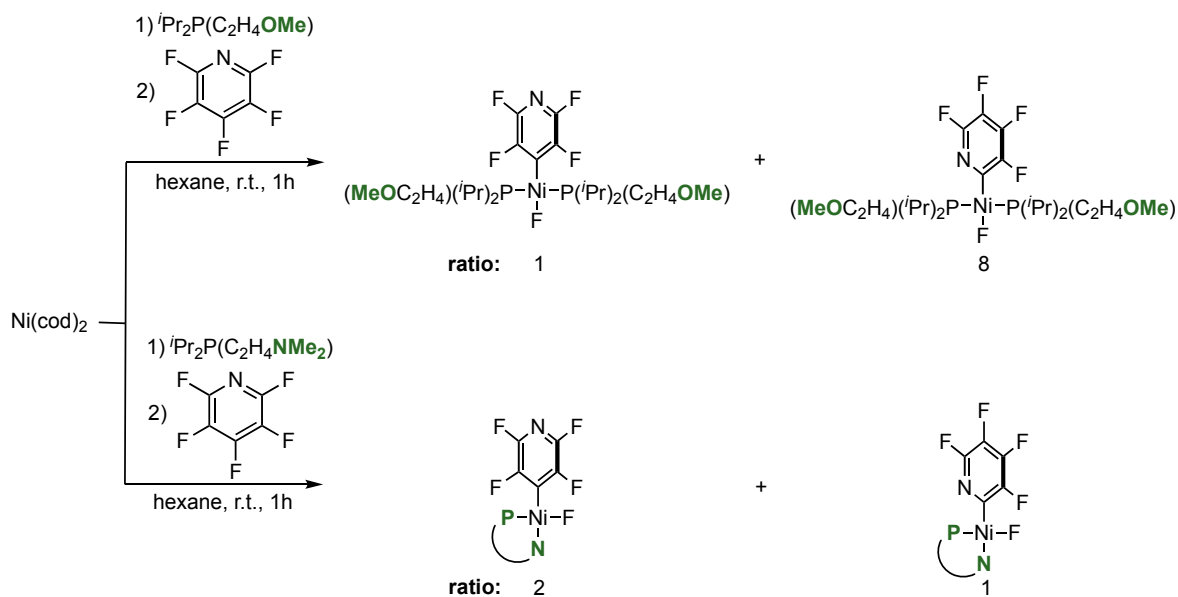
Furthermore, Stille coupling reactions of **Py-F₅** (or **Py-F₄**) with tributyl(vinyl)tin to afford the cross-coupling product 2-vinyltetrafluoropyridine (or 2-vinyl-3,5,6-trifluoropyridine) were possible using [NiF(2-C₅NF₄)(PEt₃)₂] as a catalyst (Scheme 20).¹⁰³



Scheme 20 Catalytic conversion of fluorinated pyridines with [NiF(2-C₅NF₄)(PEt₃)₂].

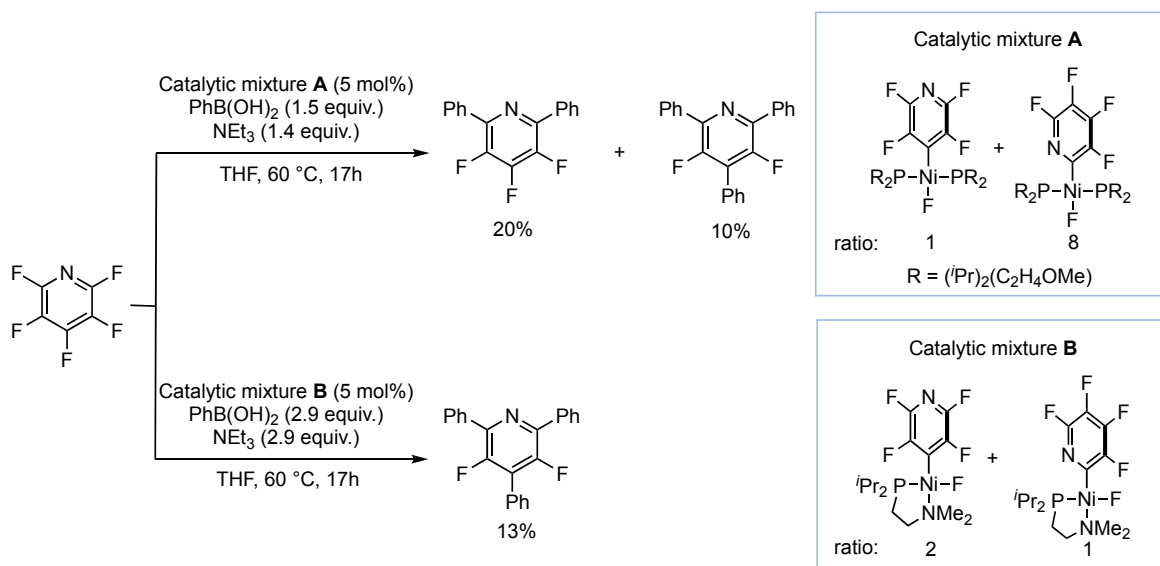
In a similar fashion, Braun *et al.* demonstrated that [Ni(P(^{*i*}Pr)₂){(CH₂CH₂OMe)}₂] underwent OA of **Py-F₅** mainly at 2-position (Scheme 21, top).¹⁰⁴ The authors proposed a similar phosphine-assisted mechanism to that of Perutz (Scheme 19). However, when ^{*i*}Pr₂P(CH₂CH₂NMe₂) was employed as a chelating ligand instead of ^{*i*}Pr₂P(CH₂CH₂OMe), C–F bond activation preferentially occurred at the 4-position (Scheme 21, bottom). In this case, the phosphine coordinated with both donor atoms (P,

N) at the nickel centre and was less prone to cooperate during the OA step. Consequently, the formation of the thermodynamic product was preferred (Scheme 21).



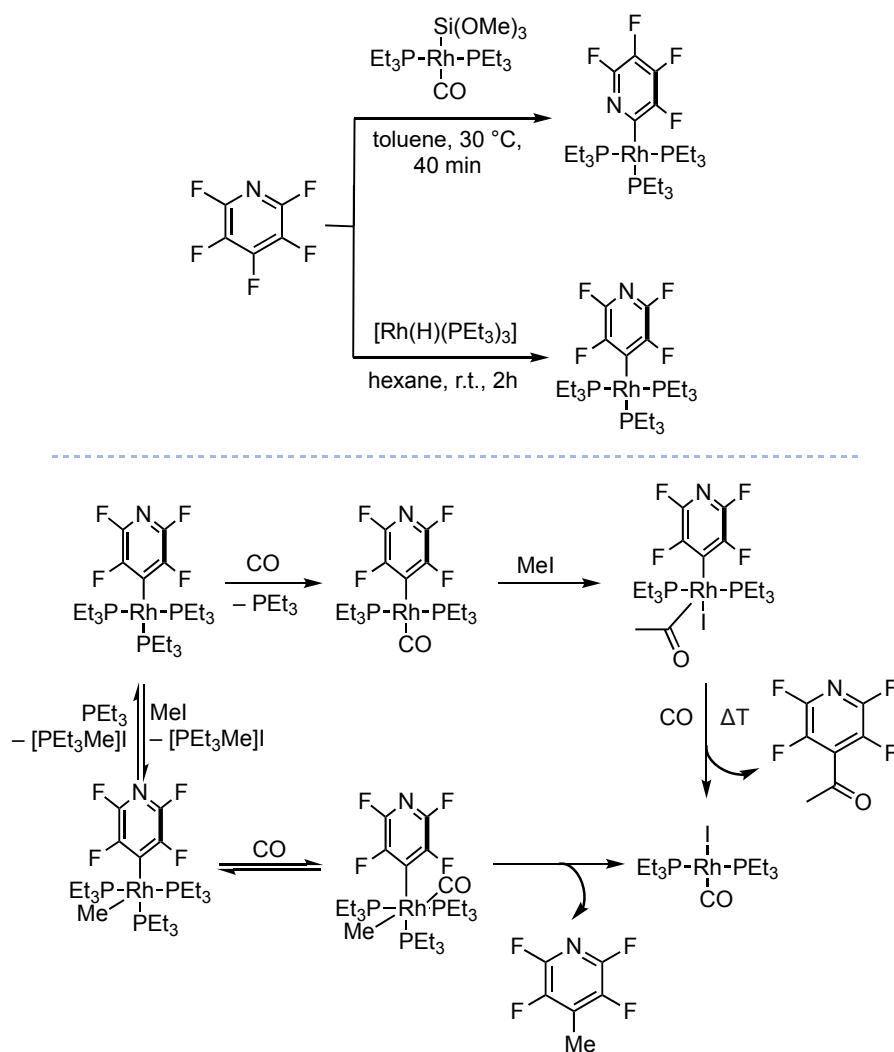
Scheme 21 C-F bond activation at **Py-F₅** using either $i\text{Pr}_2\text{P}(\text{CH}_2\text{CH}_2\text{OMe})$ (top) or $i\text{Pr}_2\text{P}(\text{CH}_2\text{CH}_2\text{NMe}_2)$ (bottom) and $[\text{Ni}(\text{cod})_2]$ (the ratio between the two products is reported).

Furthermore, the two mixtures obtained were able to catalyse Suzuki-Miyaura-type cross-coupling reactions in the presence of $\text{ArB}(\text{OH})_2$ as nucleophile (Scheme 22).



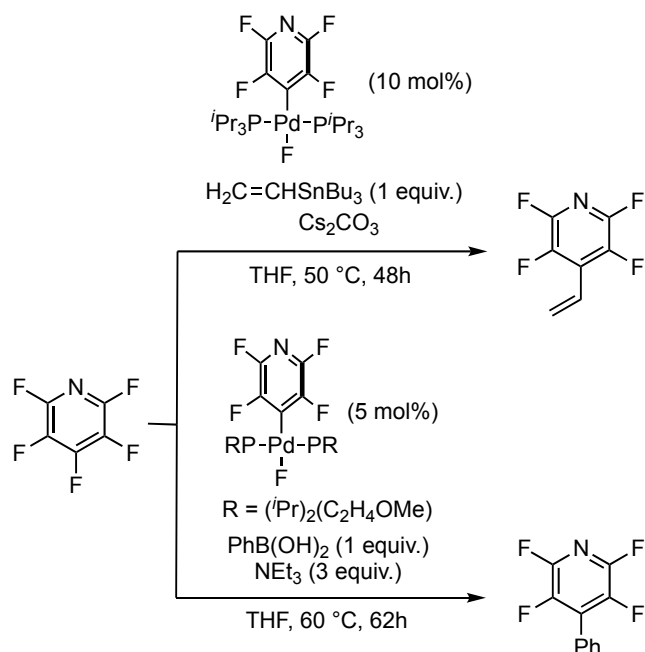
Scheme 22 Suzuki-Miyaura-type cross-coupling of **Py-F₅** and $\text{PhB}(\text{OH})_2$ catalysed by mixture **A** (top) and **B** (bottom).

The dependence of the reaction's regioselectivity on the metal ligand was also reported by Braun and coworkers in the case of rhodium complexes. Silyl ligands assisted the OA process leading to C–F bond activation of **Py-F₅** in *ortho*-position (Scheme 23, left).¹⁰⁵ Conversely, when phosphine ligands were used, the activation occurred predominantly at the *para*-position (Scheme 23, top).¹⁰⁶ Stoichiometric methylation and acylation were also possible in this system (Scheme 23, bottom).



Scheme 23 C–F bond activation of **Py-F₅** assisted by Rh-silyl (top) and Rh-phosphine complexes (bottom).

Finally, some examples of Suzuki-Miyaura¹⁰⁷ and Stille-type cross-coupling reactions¹⁰⁸ catalysed by Pd complexes were reported by Braun and coworkers (Scheme 24).¹⁰⁹ In all these studies, the C–F bond was activated at the 4-position of the fluorinated pyridine, which is typical of $\text{S}_{\text{N}}\text{Ar}$ reactions (Figure 3).



Scheme 24 Suzuki-Miyaura- and Stille-type cross-coupling reactions catalysed by Pd complexes.

2.1.5 ETM-mediated C–F activation

A limited number of ETM and *f*-block metal complexes have been employed in the C–F bond activation of polyfluorinated organic compounds.

The cleavage of C–F bonds assisted by lanthanides and actinides typically involves a homolytic mechanism and it is favoured by the high fluoride-ion affinity of these species. For instance, U^{III} complexes exhibit the ability to activate C–F bonds in hexafluorobenzene, resulting in the formation of the corresponding fluoride complex and a range of organic compounds, including the product of HDF and alkylation.¹¹⁰ Another approach for C–F functionalisation involves the use of nucleophiles that attack the activated fluorinated compound. LnI₃ and La[N(SiMe₃)₂]₃ were employed in the iodo-¹¹¹ and aminodefluorination of alkyl fluorides.¹¹² Deacon and coworkers documented the thermal decomposition of La(CF₃Form)₃ (CF₃Form = N,N'-bis(2-trifluoromethylphenyl)formamidine) to LaF₃, yielding polyamidines through the activation of all fluorine atoms of the CF₃ substituent.¹¹³ Bart *et al.* proposed the alkylation of perfluoroaromatics promoted by Tp*₂U(CH₂C₆H₅) (Tp* = hydrotris(3,5-dimethylpyrazolyl)borate), which led to the formation of Tp*₂U–F and the alkylated product.¹¹⁴

From group 5, TaCl₅ and imido-coordinated Nb complexes were found to be active towards C–F functionalisation of polyfluoroarenes and CF₃ groups. TaCl₅ performed single and double defluorinative alkylation of hexafluorobenzene in the presence of Grignard reagents.¹¹⁵ Nb^{III}

complexes bearing an imido group can activate all the F atoms of a benzylic CF₃ group leading to the formation of a new C–N bond between the aryl fragment and the *tert*-butylimido ligand.¹¹⁶ Furthermore, Arnold *et al.* reported the cleavage of the C–F bond of fluoroarenes promoted by the same Nb^{III} complex leading to the formally oxidised Nb^V aryl fluoride complex.³⁴ Akiyama *et al.* demonstrated that NbCl₅ can activate the F atoms of benzylic CF₃ groups and, in the presence of LiAlH₄, form new C–H and intramolecular C–C bonds resulting in the generation of polycyclic compounds such as fluorene,¹¹⁷ indoles¹¹⁸ and indenenes.¹¹⁹ Alternatively, NbCl₅ can catalyse defluorinative triallylation of benzylic CF₃ in the presence of allyltrimethylsilane.¹²⁰

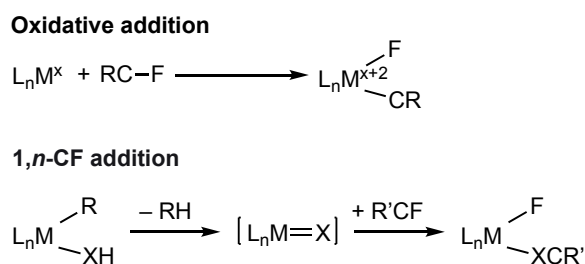
Shifting to group 4 metals, Ti complexes can cleave the C–F bond of acyl and benzylic CF₃ groups by forming strong Ti–F and either coordinating¹²¹ or liberating the defluorinated organic fragment.¹²² Cp₂ZrCl₂ can catalytically activate one F from a vinylic CF₃ substituent in the presence of trialkylaluminum to form new C–C bonds.¹²³

Since the main body of work on ETM-assisted C(sp²)–F bond activation reactions involves group 4 metals and polyfluoropyridines as substrates, section 2.1.5.1 focuses specifically on these systems, emphasising their reaction mechanisms. More comprehensive insights into the reactivity of ETMs with fluoroalkenes and fluoroarenes are discussed in the reviews by Braun *et al.*¹⁷ and Rosenthal *et al.*²⁶

2.1.5.1 C(sp²)–F activation at polyfluorinated pyridines assisted by group 4 metals

While numerous strategies have been developed for the functionalisation of C(sp²)–F bonds promoted or catalysed by LTMs, the interest in investigating these transformations assisted by ETMs stems from the complementary reaction mechanisms they offer in comparison to LTMs, leading to different reaction selectivity. Furthermore, most of ETMs are more abundant than LTMs (e.g., Ti 5650 ppm and Zr 165 ppm abundance vs. Pd 0.015 ppm and Pt 0.005 ppm abundance), they are cheaper and generally exhibit a lower toxicity.¹²⁴

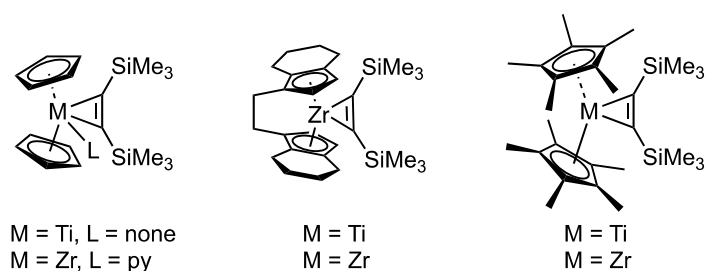
C–F bond cleavage by ETMs can be classified into two main reaction types, as depicted in Scheme 25.



Scheme 25 C–F bond cleavage reactions by ETM complexes.

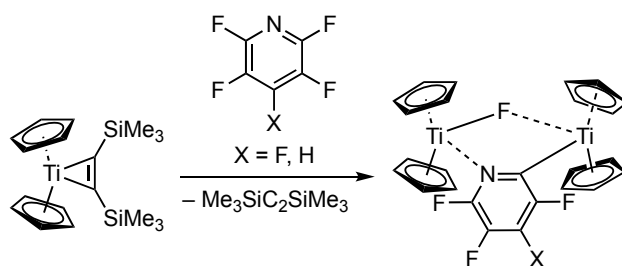
2.1.5.1.1 C–F bond cleavage via oxidative addition mechanism

The OA of fluorinated pyridines to low-valent metals (Scheme 25, top), which is the most common pathway for LTMs, has been reported for $[\text{Cp}'_2\text{M}^{\text{II}}]$ metallocenes ($\text{M} = \text{Ti}$, $\text{Cp}' = \text{Cp}$, Cp^* ; $\text{M} = \text{Zr}$, $\text{Cp}' = \text{Cp}$, *rac*-ethylene-1,2-bis(η -5-4,5,6,7-tetrahydro-1-indenyl)). These complexes are generally stabilised by an η^2 -coordinated bis(trimethylsilyl)acetylene (btmsa) ligand and act as 'masked' M^{II} fragments (Scheme 26). The dissociation of btmsa releases highly reactive low-valent titanium or zirconium complexes of the type $[\text{Cp}'_2\text{M}^{\text{II}}]$, as they are coordinatively and electronically unsaturated (14-electron complexes with metals in d^2 configuration).^{125,126}



Scheme 26 Some examples of group 4 metallocene bis(trimethylsilyl)acetylene complexes.

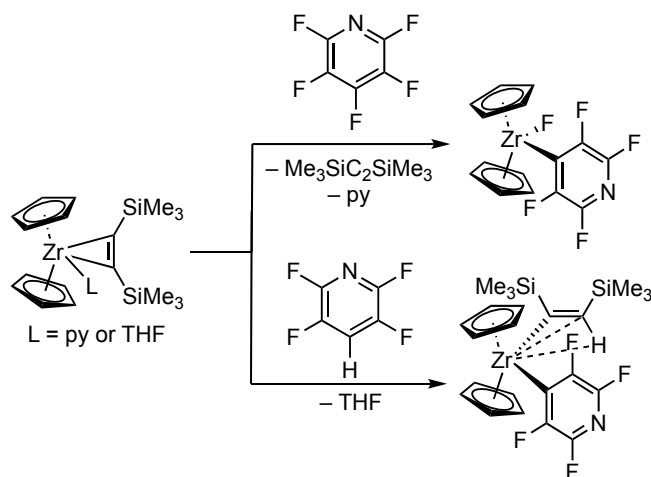
Beckhaus and coworkers reported the activation in the *ortho*-position of 2-fluoropyridine, **Py-F₄** and **Py-F₅** using titanocene fragments $[\text{Cp}_2\text{Ti}^{\text{II}}]$, generated *in situ* from the corresponding btmsa complexes.¹²⁷ This process resulted in the formation of a dimeric fluoride-bridged titanocene at room temperature (Scheme 27). The authors proposed that a concerted oxidative addition step *via* a three-centred transition state (Figure 3) occurred and led to the formation of a mononuclear Ti^{IV} intermediate. This then underwent a comproportionation reaction with another *in situ* generated $[\text{Cp}_2\text{Ti}^{\text{II}}]$ fragment to yield the observed bimetallic Ti^{III} complex. It is worth mentioning that this Ti complex exhibited a preference for C–F activation over C–H activation in fluorinated pyridines.



Scheme 27 Reaction of $[\text{Cp}_2\text{Ti}\{\eta^2\text{-C}_2(\text{SiMe}_3)_2\}]$ with **Py-F₄** and **Py-F₅**.

Interestingly, the reactivity and regioselectivity patterns differ in the case of the zirconocene complex $\text{Cp}_2\text{Zr}(\text{py})(\text{btmsa})$.¹²⁸ For instance, the reaction with **Py-F₅** resulted in C–F bond activation at the 4-position, contrary to the expected attack at the 2-position (Scheme 28). The regioselectivity

can be best explained by the formation of a Meisenheimer intermediate in an S_NAr reaction (see Figure 3). Additionally, when the zirconocene complexes $Cp_2Zr(L)(btmsa)$ ($L=THF, pyridine$) was reacted with **Py-F₄**, C–H activation occurred instead of C–F activation, leading to the formation of 4-substituted pyridyl complexes with agostic alkenyl groups (Scheme 28).

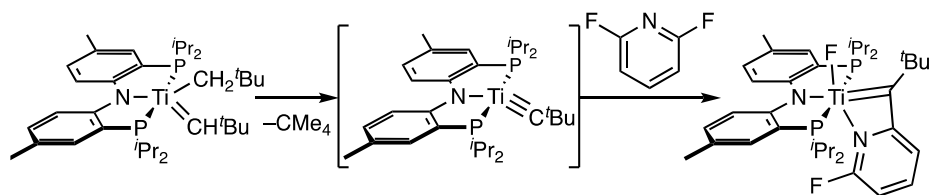


Scheme 28 Reaction of ‘masked’ $[Cp_2Zr]$ fragments with pentafluoropyridine and **Py-F₄**.

2.1.5.1.2 C–F bond cleavage via 1,*n*-C–F addition reaction

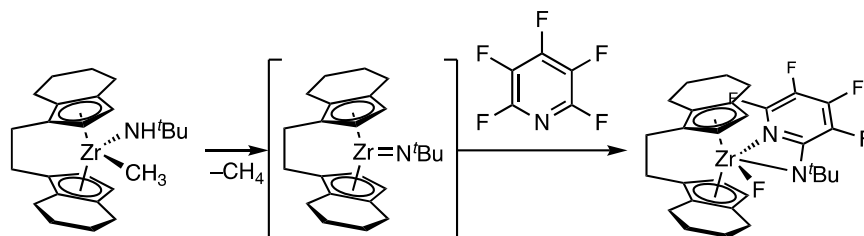
Examples of 1,*n*-C–F addition reactions in the literature are limited (Scheme 25, bottom). Unlike the late transition metal systems, which are based on OA, these transformations share as a common mechanistic feature the formal 1,*n*- ($n = 2$ or 3) addition of the C–F bond over a reactive metal–ligand bond and the formation of a new C–E bond (where E is usually C or N). The undeniable advantage of these reaction systems is their perfect regioselectivity, likely dictated by interaction of the substrate with the metal centre prior to the C–F bond activation event, leading to functionalisation of the challenging 2-position of fluorinated pyridines.

An example of this reactivity was reported by Mindiola and coworkers.¹²⁹ Complex $(PNP)Ti(CH^tBu)(CH_2^tBu)$ ($PNP = \text{bis}(2\text{-(diisopropylphosphino)-4-methylphenyl)amide}$) was activated by elimination of neopentane, generating the intermediate $(PNP)Ti\equiv C^tBu$ (Scheme 29). This transient species efficiently cleaved the *ortho*-C–F bond of 2,6-difluoropyridine (**Py-F₂**) and 2-fluoropyridine at room temperature, leading to the formation of new C–C and Ti–F bonds in the resulting alkylidene–fluoride complexes. In this and subsequent examples within this chapter, no other products besides the addition product were observed. DFT calculations provide evidence for pre-coordination of the pyridine through the N atom, followed by a [2+2] cycloaddition and β -F elimination, resulting in the formation of the formal 1,2-C–F bond addition product.



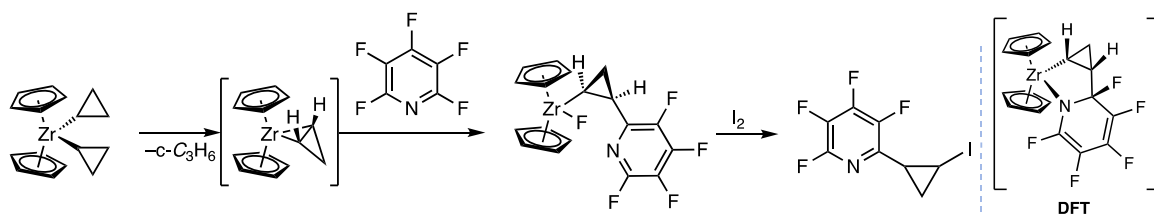
Scheme 29 1,2-CF addition across a transient titanium alkylidyne (PNP)Ti \equiv C^tBu to afford (PNP)Ti=C[^tBu(NC₅H₃F)](F).

A similar example was reported by Bergman *et al.* for an amidozirconocene complex of the type *rac*-(ebthi)Zr-(NHCM₃)Me (Scheme 30).¹³⁰ Intramolecular α -H abstraction and methane release generated the proposed imidozirconocene transient intermediate [*rac*-(ebthi)Zr(=N^tBu)]. This species regioselectively coupled **Py-F₅** at 2-position resulting in the formation of new C–N and Zr–F bonds.



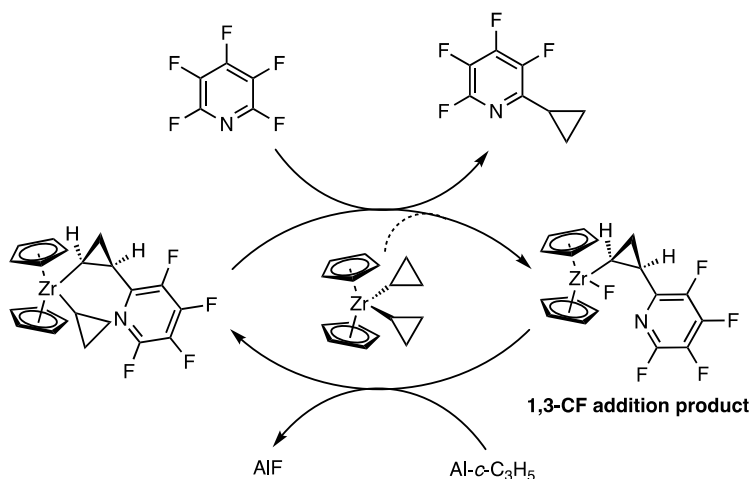
Scheme 30 1,2-CF addition of pentafluoropyridine across a transient [*rac*-(ebthi)Zr(=N^tBu)].

A more recent example was reported by Etienne *et al.*,¹³¹ where a zirconabicyclobutane [Cp₂Zr(η^2 -c-C₃H₄)], generated *in situ* by thermal activation of dicyclopropylzirconocene, [Cp₂Zr(c-C₃H₅)₂], enabled the regio- and stereoselective 1,3-C–F bond addition of 2,4,6-trifluoropyridine (**Py-F₃**) and **Py-F₅** forming new Zr–F and C–C bonds (Scheme 31). The driving forces for this reaction are the ring strain release of the cyclopropenyl ligand and the formation of a strong Zr–F bond (BDE = 623 \pm 63 kJ/mol).¹³² The recovery of the coupling product was also possible by iodolysis of the Zr–C bond, which released *cis*-1-iodo-2-(tetrafluoropyridyl)cyclopropane. DFT calculations showed that the regioselectivity in *ortho*-position of the polyfluorinated pyridine arose from the initial formation of an azazirconacycle intermediate (Scheme 31), which then underwent ring opening and C–F bond cleavage.



Scheme 31 C–F bond activation promoted by $[\text{Cp}_2\text{Zr}(\eta^2\text{-}c\text{-C}_3\text{H}_4)]$ and release of the ligand.

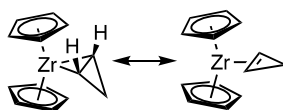
A stoichiometric synthetic cycle was developed by formation of the 1,3-addition product, transmetalation of the cyclopropyl fragment by using $\text{Al}(\text{-}c\text{-C}_3\text{H}_5)_3$, formation of $[\text{Cp}_2\text{Zr}(c\text{-C}_3\text{H}_5)\{\text{-}c\text{-cis-CHCH}_2\text{CH}(2\text{-NC}_5\text{F}_4)\}]$ and release of the 2-($c\text{-C}_3\text{H}_5$) NC_5F_4 product by reaction with another molecule of **Py-F₅** (Scheme 32). Nevertheless, one-pot catalytic reactions failed, due to the decomposition of the active species in the system and multiple C–F bond activations by $\text{Al}(\text{-}c\text{-C}_3\text{H}_5)_3$.



Scheme 32 Tentative catalytic C–C coupling reaction with dicyclopropylzirconocene as precatalyst and $\text{Al}(\text{-}c\text{-C}_3\text{H}_5)_3$ as transmetalating agent.

2.1.6 Zirconocene complexes of unsaturated organic molecules

The exceptional reactivity of the transient zirconabicyclobutane intermediate shown in Scheme 31, which could be represented by two extreme resonance structures (Scheme 33), can be attributed to the high ring strain of the ligand.



Scheme 33 Resonance structures of complex $[\text{Cp}_2\text{Zr}(\eta^2\text{-}c\text{-C}_3\text{H}_4)]$.

Metal complexes incorporating strained unsaturated organic ligands have been investigated and, among these species, the reactivity of metal-benzyne or -cycloalkyne complexes has gained significant interest.^{133,134} The distinctive feature of strained cycloalkynes lies in the bent nature of the C≡C bonds. Unlike stable linear alkynes, whose structure is dictated by *sp*-hybridization, strain in the triple bond reduces the overlap of the in-plane *p*-orbitals, significantly weakening the C–C bond.¹³⁵ Moreover, moving from linear to bent alkynes results in a lower energy of the LUMO, while the HOMO energy remains relatively unchanged.¹³⁶ Consequently, cycloalkynes and arynes typically exhibit more electrophilic reactivity.

Metal-free cycloalkyne and benzyne systems undergo a wide range of reactions such as cycloadditions, Diels Alder, ring insertions and multicomponent reaction (involving a nucleophilic attack to the strained alkyne followed by an electrophilic attack).¹³⁷ Transition metals like Pd and Ni can coordinate and stabilise these highly reactive cycloalkynes (Figure 4). They can also promote or catalyse the aforementioned reactions with more challenging substrates and in an asymmetric fashion.^{133,134, 138}

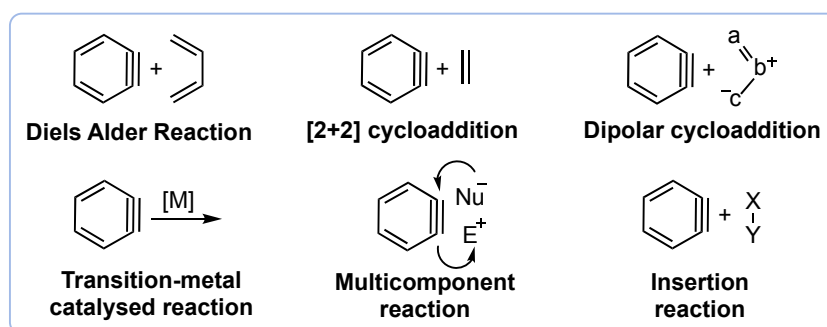
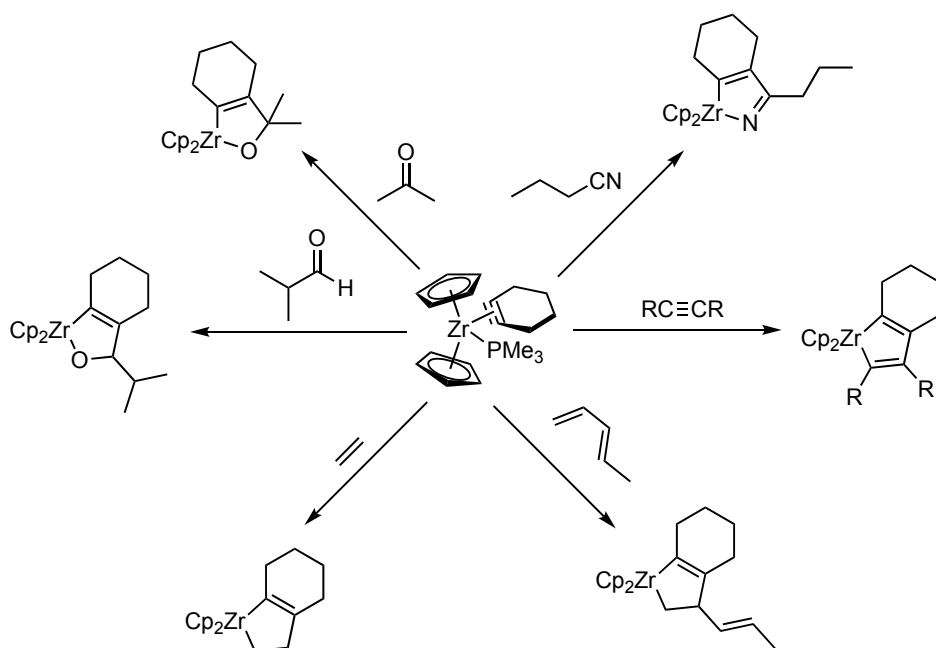


Figure 4 Possible reactivity of arynes and cycloalkynes.

Erker¹³⁹ and Buchwald *et al.*^{140,141} thoroughly investigated group 4 metal-based organometallic compounds bearing cycloalkynes or benzyne ligands. More specifically, they focused on the C–C bond formation assisted by zirconocene complexes of strained alkynes. These complexes have been employed for insertion reactions of unsaturated molecules such as ketones, aldehydes, imines, nitriles, olefins and alkynes. Some reactivity examples of a zirconocene- η^2 -cyclohexyne complex are presented in Scheme 34.

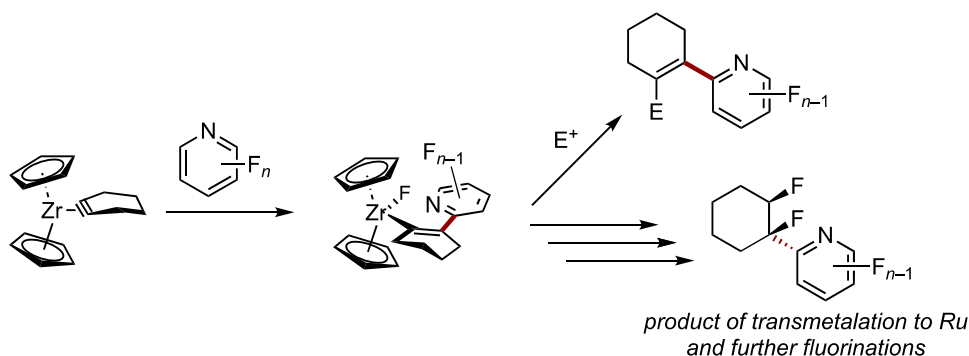


Scheme 34 Cycloaddition reactions assisted by a zirconocene- η^2 -cyclohexyne complex.

Yet, the use of metal-benzynes and -cycloalkyne complexes for the activation of strong σ -bonds has remained elusive. Only one example of intramolecular C–H bond activation assisted by a Zr-(η^2 -benzyne) intermediate has been reported in the literature.^{142,143}

2.2 Aims and objectives

The aim of this chapter was to establish a novel synthetic protocol for a controlled and regioselective functionalisation of fluorinated pyridines using a strained cycloalkynyl-zirconocene complex. Based on the results obtained by Etienne and coworkers¹³¹ who employed a zirconocene-cyclopropene complex for the 1,2-CF activation of polyfluoropyridines (Scheme 31), it was envisioned that the ring strain of the cyclohexynyl ligand might drive, in cooperation with the Zr centre, the 1,3-addition of the polyfluoropyridine's C–F bond (Scheme 35).

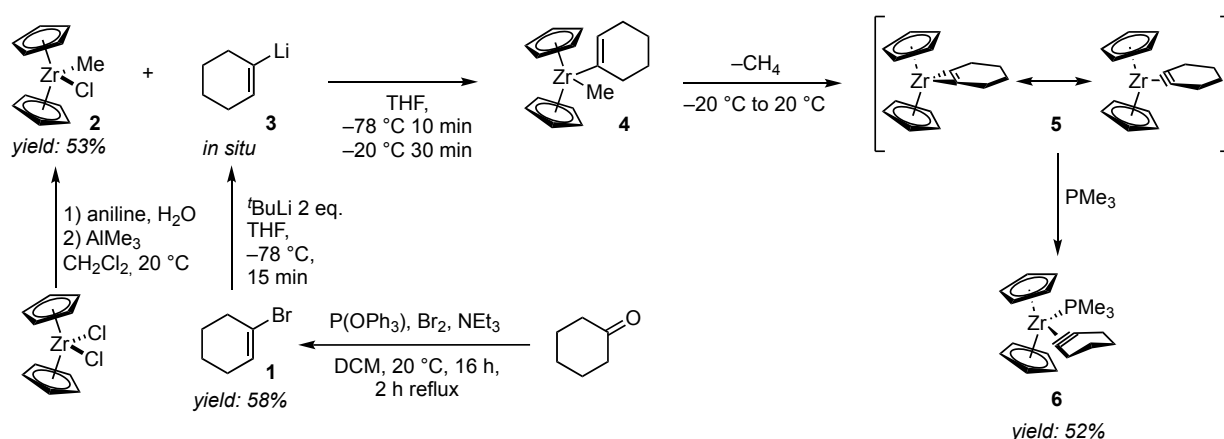


Scheme 35 Synthetic strategy for the regioselective Zr-promoted C–F alkenylation of polyfluoropyridines.

Our specific interest in this type of transformation stemmed from two main reasons. Firstly, the alkenylation of perfluorinated pyridines typically occurs at the 4-position, following an S_NAr -type mechanism. Hence, our strategy aimed to offer an alternative regioselectivity for this type of compound by leveraging a chemistry akin to that elucidated by Etienne and coworkers (Scheme 31), which involves an initial pre-coordination of the fluorinated aromatic heteroatom with the metal. Secondly, we envisaged the possibility of further functionalising the fluorinated ligand, either through insertion reactions within the Zr–C bond and subsequent liberation of the product by the addition of electrophiles (e.g., H^+ , I_2) or by transmetalation to another metal, as many ligand redistribution reactions between Zr and *p*-block elements, as well as LTMs,¹⁴⁴ are documented in the literature.

2.3 Results and discussion

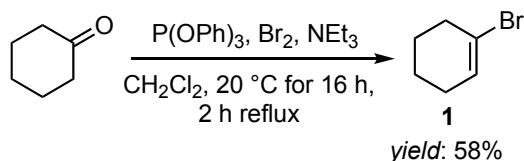
2.3.1 Synthesis of the zirconocene-cyclohexyne complex



Scheme 36 Synthetic protocol for the synthesis of the zirconocene- η^2 -cyclohexyne (5) and its corresponding PMe₃ adduct (6).

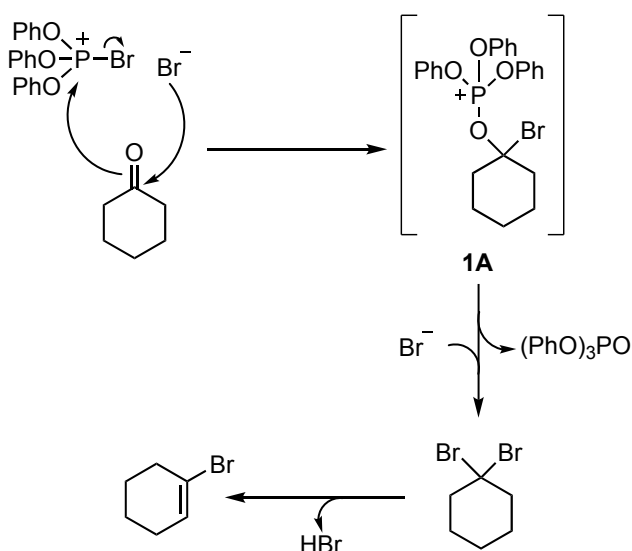
The investigation started with the study of the synthesis of the zirconocene- η^2 -cyclohexyne complex (5) reported by Buchwald (Scheme 36).¹⁴⁵ The targeted Zr complex was prepared by degradation of an *in situ* generated 1-cyclohexenyl-methyl-zirconocene complex (4) *via* β -H abstraction, leading to methane evolution and the zirconocene-cyclohexyne complex 5. To facilitate its isolation, Buchwald *et al.* stabilised 5 with PMe₃, resulting in the phosphine adduct 6. Complex 6, or *in situ* prepared 5, were shown to react with various unsaturated organic molecules by insertion in the Zr–C bond.¹⁴⁰

To begin, 1-bromocyclohexene (**1**) was synthesised by reacting cyclohexanone with a slight excess of bromine, triphenylphosphite and NEt_3 (Scheme 37).¹⁴⁶



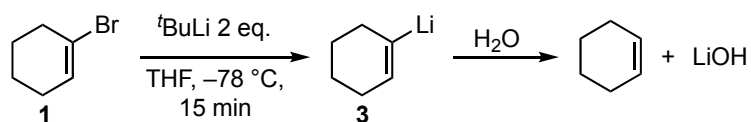
Scheme 37 Synthesis of 1-bromocyclohexene by reaction of cyclohexanone (1 equiv.), Br_2 (1.5 equiv.), P(OPh)_3 (1.1 equiv.), NEt_3 (1.3 equiv.) in CH_2Cl_2 .

In this reaction, the strong oxophilicity of triphenylphosphite is believed to trigger the formation of an oxyphosphonium halide intermediate **1A**, which then transforms into a *gem*-dihalide through elimination of triphenyl phosphate. Subsequently, this species undergoes base-promoted dehydrohalogenation, forming the desired product (Scheme 38).



Scheme 38 Proposed reaction mechanism for the synthesis of 1-bromocyclohexene.

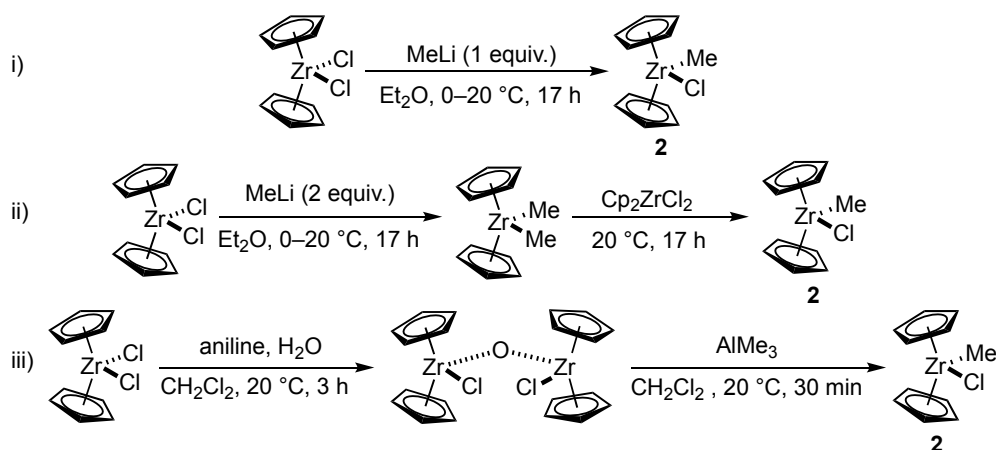
Anticipating the high reactivity of 1-lithiocyclohexene **3**, a stability study on this compound was carried out. The formation of **3** occurs through a metal-halogen exchange between **1** (1 equivalent) and $^t\text{BuLi}$ (2 equivalents) in THF at $-78\text{ }^\circ\text{C}$ (Scheme 36). It is worth noting that $^t\text{BuLi}$ is highly reactive towards THF, with a half-life of 40 minutes at $-20\text{ }^\circ\text{C}$.¹⁴⁷ Therefore, the solvent must be carefully cooled to $-78\text{ }^\circ\text{C}$ before starting the reaction. Furthermore, to assess the formation of **3** in solution, aliquots of the reaction mixture were quenched with water over time. This process resulted in the production of lithium hydroxide and cyclohexene from **3**, as illustrated in Scheme 39.



Scheme 39 Stability study of **3** in THF at $-78\text{ }^\circ\text{C}$ over time.

Compound **1** was quantitatively converted into **3**, as evidenced by ^1H NMR spectroscopy showing the formation of the free cyclohexene and the absence of **1** within only 15 minutes at $-78\text{ }^\circ\text{C}$. However, traces of unidentified secondary species were already observed during this period and their concentration increased over time. Therefore, it was crucial to carefully conduct the metal-halogen exchange step at $-78\text{ }^\circ\text{C}$ and within a 15-minute timeframe to avoid the reaction of $^t\text{BuLi}$ with THF and the decomposition of **3**.

Subsequently, three strategies were tested for the synthesis of $\text{Cp}_2\text{Zr}(\text{Me})\text{Cl}$ (**2**): (i) the transmetalation reaction between Cp_2ZrCl_2 and one equivalent of MeLi ,¹⁴⁸ (ii) the dimethylation of Cp_2ZrCl_2 with 2 equivalents of MeLi , followed by a ligand redistribution step by adding one equivalent of Cp_2ZrCl_2 ¹⁴⁹ and (iii) the formation of **2** via $[(\text{Cp}_2\text{ZrCl})_2(\mu\text{-O})]$ (Scheme 40).¹⁵⁰ Among these approaches, the last one, depicted at the bottom of Scheme 40, was selected as it showed the highest selectivity towards **2** while maintaining a moderate and reproducible overall yield (ca. 50%).



Scheme 40 Strategies (i), (ii) and (iii) for the synthesis of the methylzirconocene chloride.

The formation of the desired oxo-bridged complex $[(\text{Cp}_2\text{ZrCl})_2(\mu\text{-O})]$ was achieved in high isolated yields (78%) by reacting equimolar amounts of zirconocene dichloride, aniline and a slight excess of water (Scheme 40, reaction iii). The subsequent methylation with two equivalents of trimethylaluminium allowed the formation of **2** in moderate yields of 62% (relative to the oxo-bridged complex) and the reaction could be conducted on a relatively large scale (8 g). However,

due to the presence of a 3% of Cp_2ZrCl_2 (detected by ^1H NMR analysis) in the obtained solid, purification was attempted. Both sublimation (90 °C, 0.05 mbar) and crystallisation attempts (by slowly cooling concentrated solutions in hexane, toluene, dichloromethane) failed due to the partial decomposition of **2** into different zirconocene side products, as observed by ^1H NMR spectroscopy (one of these species being the starting oxo-bridged complex). Given that the quantity of unreacted Cp_2ZrCl_2 detected from the synthesis of the methylzirconocene chloride complex was only limited (3%) and considering the high instability and moisture-sensitivity of **2**, the synthesis of **6** using the unpurified complex **2** was tested.

The zirconocene- PMe_3 adduct **6** was successfully synthesised according to reaction Scheme 36 in 52% isolated yield. The formation of this complex was evidenced by the appearance of a singlet at $\delta = -2.3$ ppm in the $^{31}\text{P}\{^1\text{H}\}$ NMR spectrum, corresponding to the phosphorus nucleus of the coordinated phosphine, and the disappearance of the signal for free PMe_3 ($\delta(^{31}\text{P}) = -62.0$ ppm). The targeted complex also displayed a broad triplet at $\delta = 2.93$ ppm ($^3J_{\text{HH}} = 5.4$ Hz) and a triplet of multiplets at $\delta = 2.35$ ppm ($^3J_{\text{HH}} = 5.7$ Hz) corresponding to the $-\text{CH}_2$ protons adjacent to the triple bond in the η^2 -cyclohexyne ligand in the ^1H NMR spectrum (labelled in yellow in Figure 5). The two multiplets centred at $\delta = 1.81$ and 1.77 ppm correspond to the two remaining methylene groups (highlighted in green in Figure 5) and the two doublets at $\delta = 5.33$ ($J_{\text{HP}} = 1.69$ Hz) and 0.95 ppm ($^2J_{\text{HP}} = 5.83$ Hz) represent the Cp and the methyl signals coupling with the P nucleus, respectively. 2D-NMR analyses further proved the identity of the product.

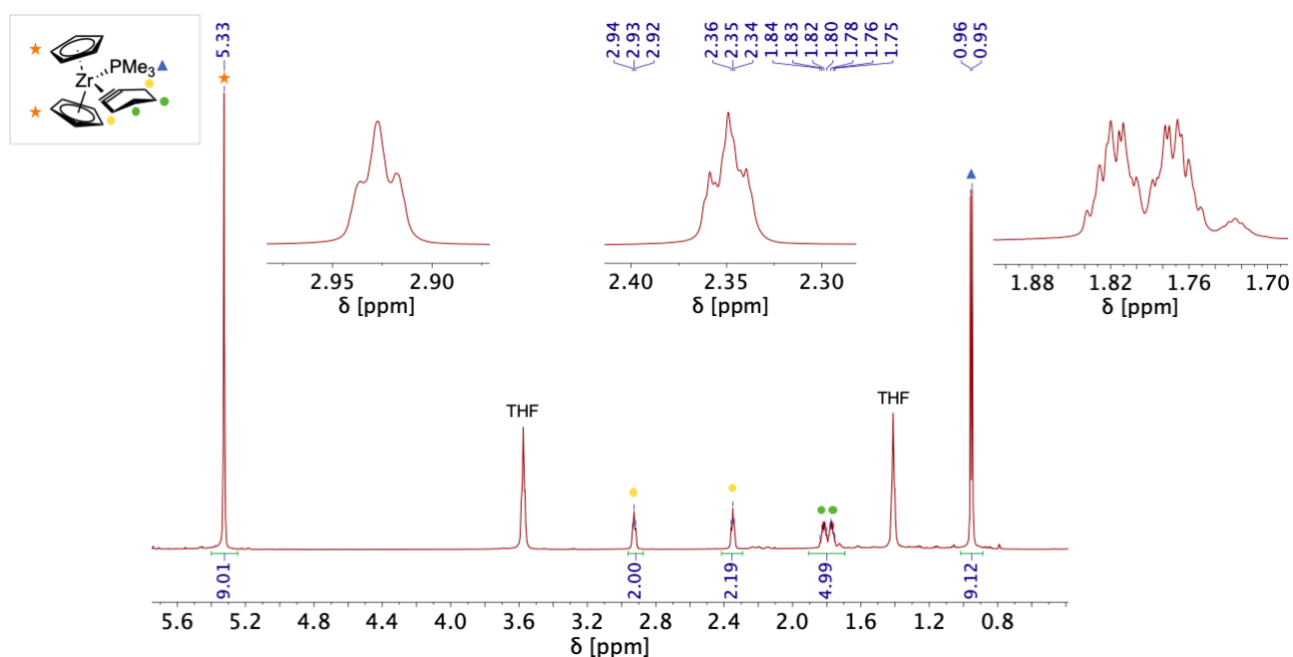
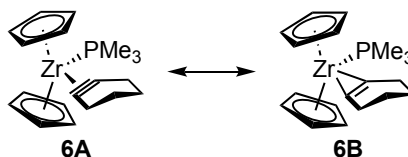


Figure 5 ^1H NMR (600 MHz, C_6D_6) of complex **6** prepared according to Scheme 36, dried and dissolved in C_6D_6 (some residual THF is still present from the reaction mixture).

The PMe_3 adduct **6** is an 18-electron complex and can be represented in the form of two extreme resonance structures (**6A** and **6B**, Scheme 41).



Scheme 41 Extreme resonance structures of complex **6**.

The Zr centre of structure **6A** is in the +2 oxidation state and the π bond of the cycloalkyne acts as a σ -donor ligand (2-electron donor). In structure **6B**, instead, the Zr is in a +4 oxidation state and the π backdonation from the metal to the π^* antibonding orbital of the triple bond is so high that it reduces the bond order of one unit, resulting in the formation of a metallacycle. In this case the ligand is no longer formally a 2-electron donor ligand, but a 4-electron one.

Crystallisation attempts of complex **6** (by slowly cooling down concentrated solutions in diethyl ether, toluene, pentane and by layering of pentane as antisolvent on a concentrated solution in toluene) failed. However, from the crystal structure reported in the literature it is possible to obtain structural information about this strained complex in solid state (Figure 6).¹⁴⁵

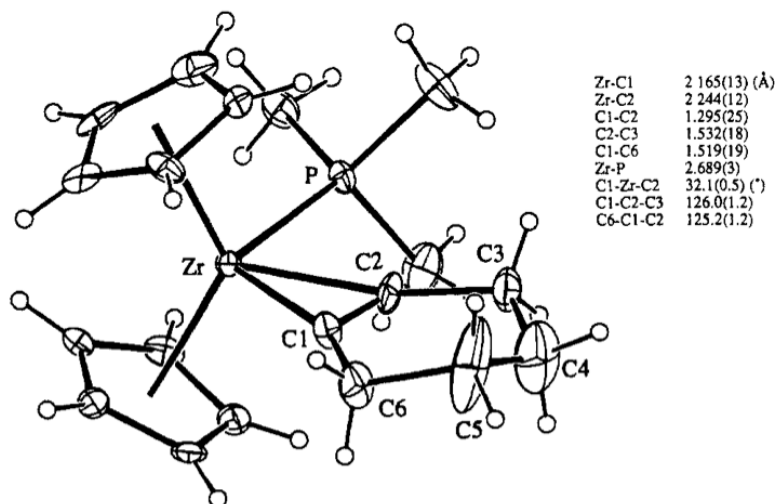


Figure 6 X-ray crystal structure of complex **6** reported by Buchwald and coworkers (figure reused with permission from Buchwald, S. L.; Dewan, J. C. *J. Am. Chem. Soc.* **1986**, 108, 23, 7441–7442.

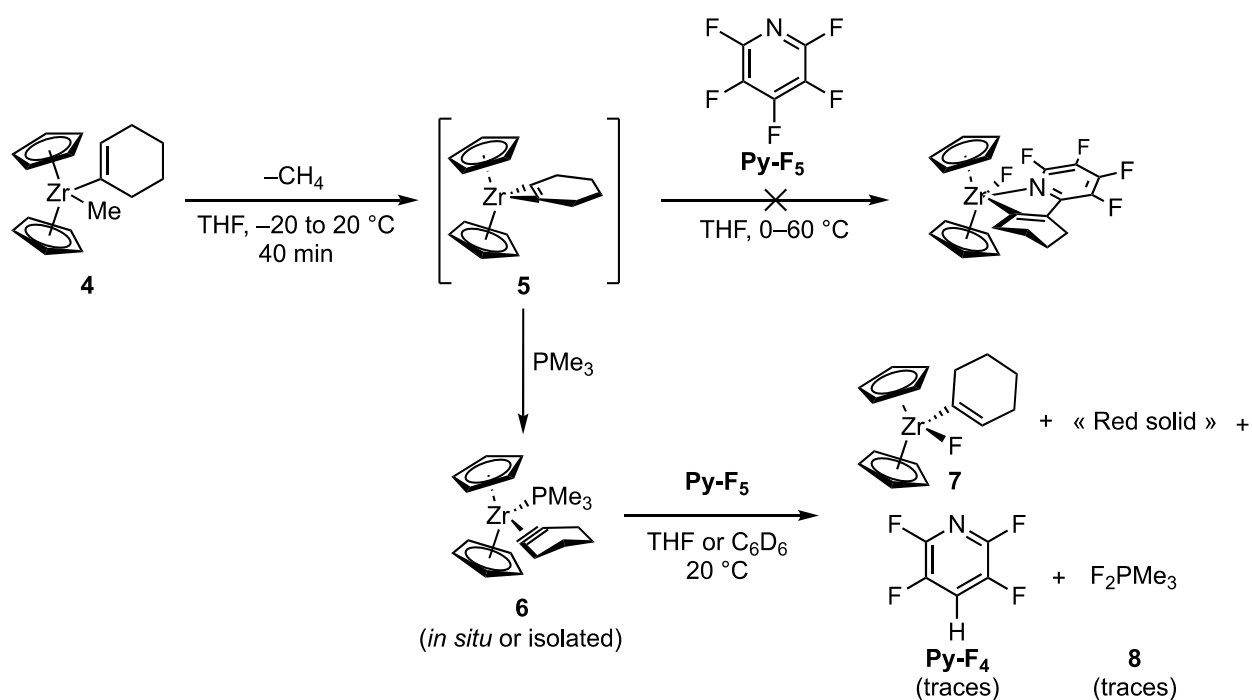
Copyright 1986 American Chemical Society).

The C–C multiple bond length (1.295(25) Å) and the C6–C1–C2 and C1–C2–C3 angles (126.0(1.2)° and 125.2(1.2)°) are more similar to those of sp^2 -hybridised (1.339 Å, 120°)¹⁵¹ carbons rather than sp -hybridised ones (1.203 Å, 180°).¹⁵¹ This means that the complex in solid state structurally resembles more a metallacycle, corresponding to resonance structure **6B**.

2.3.2 Reactivity of the Zr-cyclohexyne complex with pentafluoropyridine

The reactivity of complex **6** and the *in situ* generated **5** with differently fluorinated pyridines was investigated. **Py-F₅** was chosen as the initial polyfluorinated pyridine for this study due to its reported high reactivity in the C–F bond addition reaction, as indicated in the study conducted by Etienne and coworkers.¹³¹

As the 16-electron complex **5** is expected to be the active species for the C–F activation process, a solution of the *in situ* generated complex was treated with an excess of **Py-F₅** but no reaction was observed according to ¹H and ¹⁹F NMR spectroscopy, even upon heating up to 60 °C for several hours (Scheme 42, top reaction). Surprisingly, when PMe₃ was added to the reaction mixture, the complete consumption of the heteroaromatic compound occurred after 16 hours at 20 °C (Scheme 42, bottom reaction). Analysis of the mixture by ¹⁹F NMR revealed a singlet at $\delta = 51.0$ ppm in the spectrum, matching well with a Zr-bound fluoride, along with numerous signals in the region of the aromatic *ortho*, *meta* and *para* fluorine. From this observation, it was assumed that the presence of trimethylphosphine was crucial for the C–F bond activation and may act as an assisting ligand. As discussed in the introduction chapter 2.1.4.3, phosphine assistance in metal-mediated C–F bond activation is a known phenomenon.^{100,102,152,153} Typically, these examples involve the formation of a metallofluorophosphorane intermediate, which then undergoes either an alkyl or a fluoride transfer from the P^V centre to the metal, leading to an alkylated or fluorinated metal complex, respectively.¹⁰⁹



Scheme 42 Attempts of C–F functionalisation of pentafluoropyridine with zirconocene-cyclohexyne complexes **5** and **6**.

The reactivity of the isolated PMe_3 adduct **6** with an equimolar amount of Py-F_5 (Scheme 42, bottom reaction) was therefore investigated. After four hours at 20 °C in C_6D_6 , the starting complex, **6**, was fully converted into 1-cyclohexenylzirconocene fluoride (**7**), accompanied by the formation of an unidentified dark red solid (17 mg out of 43 mg of starting complex **6** used) and unreacted Py-F_5 . Two more equivalents of **6** were needed to consume all the Py-F_5 . Complex **7** was characterised by a singlet resonance in the ^{19}F NMR spectrum (Figure 8) at $\delta = 51.0$ ppm corresponding to the Zr–F bond (the same chemical shift observed in the previous experiment). In the ^1H NMR spectrum (Figure 7), **7** featured a singlet at $\delta = 5.86$ ppm associated with the Cp protons, two multiplets at $\delta = 2.10$ and 1.67 ppm related to the eight $-\text{CH}_2$ protons of the cyclohexenyl ring and the distinctive multiplet at $\delta = 6.03$ ppm consistent with the vinylic proton.

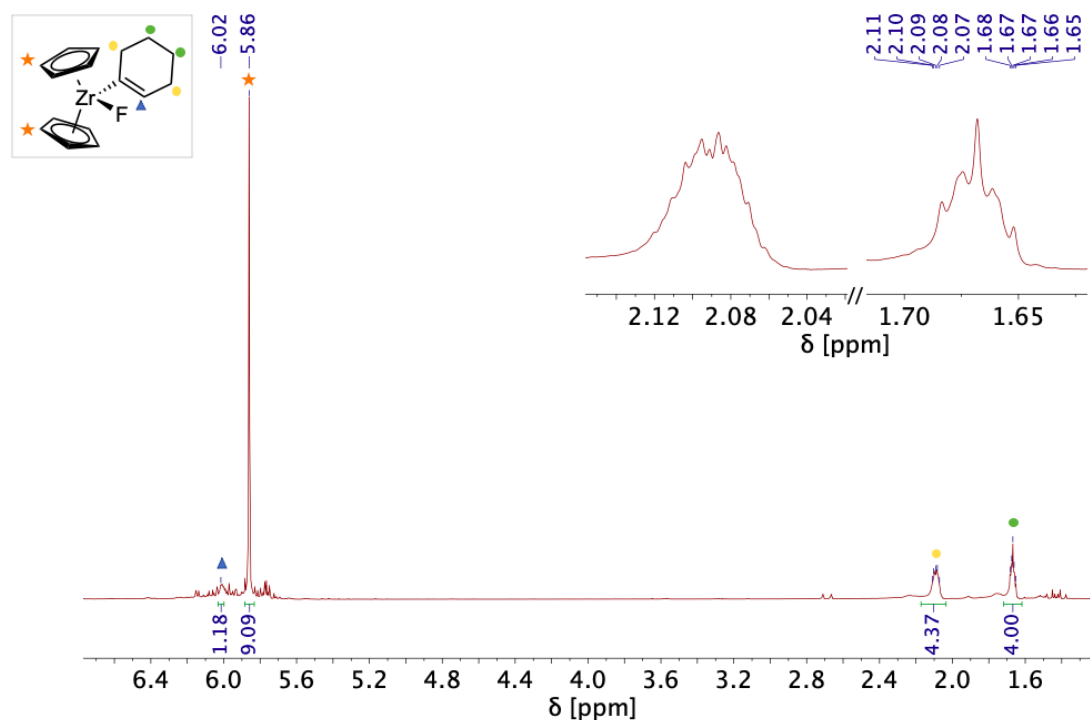


Figure 7 ^1H NMR (400 MHz, C_6D_6) spectrum of complex **7** obtained by treating **6** (1 equiv.) with Py-F_5 (1 equiv.) in C_6D_6 at 20 °C for 4 hours. Magnifications of the signals of **7** are given.

Traces of the hydrodefluorination product Py-F_4 were identified by two multiplets at $\delta(^{19}\text{F}) = -91.6$ (*ortho-F*) and -140.2 ppm (*meta-F*) along with trimethyldifluorophosphorane (F_2PMe_3 , **8**, $\delta(^{19}\text{F}) = -5.7$ ppm (*pseudo* dsext, $^1J_{\text{FP}} = 544$ Hz, $^3J_{\text{FH}} = 12.2$ Hz)). Additionally, a product presumably resulting from the reaction of pentafluoropyridine with a phosphorus species, featuring two multiplets at $\delta(^{19}\text{F}) = -91.6$ and -140.2 ppm, the precise identification of which remained challenging, was also observed in the ^{19}F NMR spectrum (Figure 8). The formation of **7**, Py-F_4 and **8** was ascertained by multinuclear (^1H , ^{31}P , ^{19}F , ^{13}C) and 2D-NMR spectroscopy.

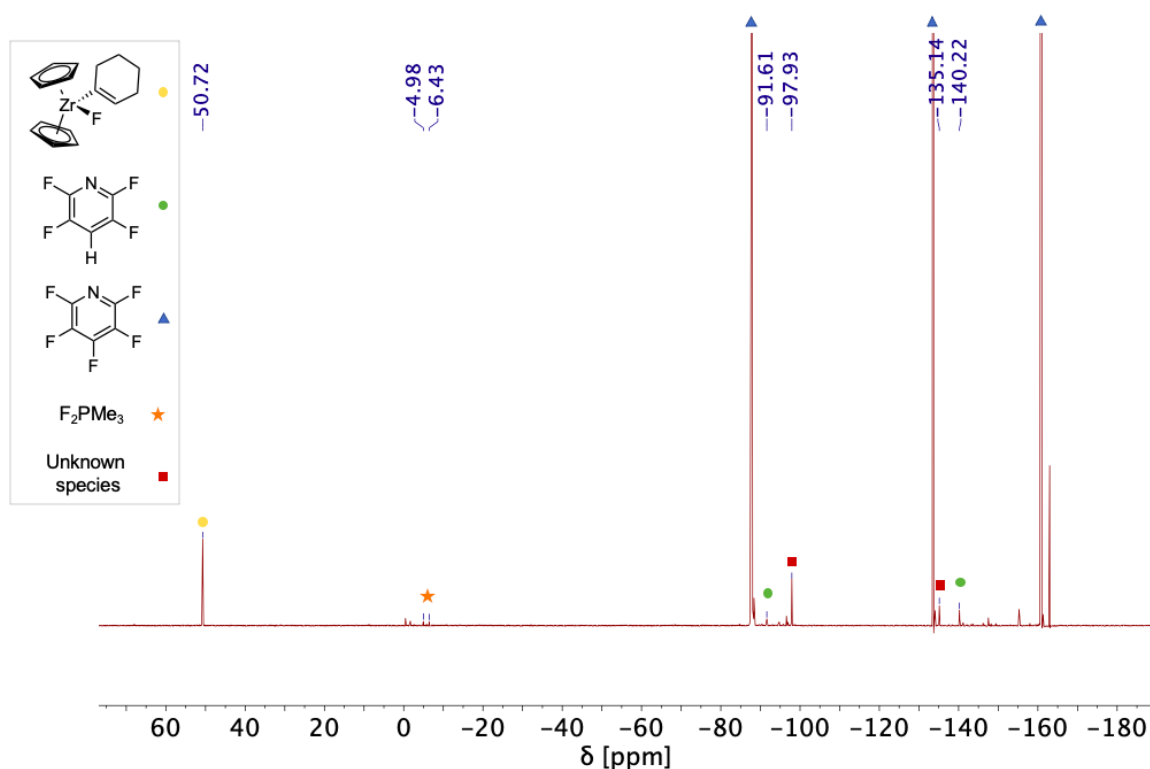
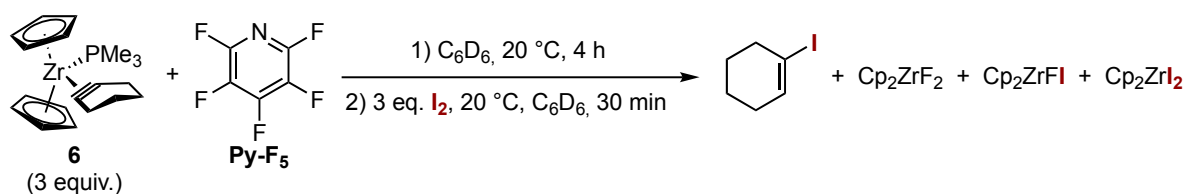


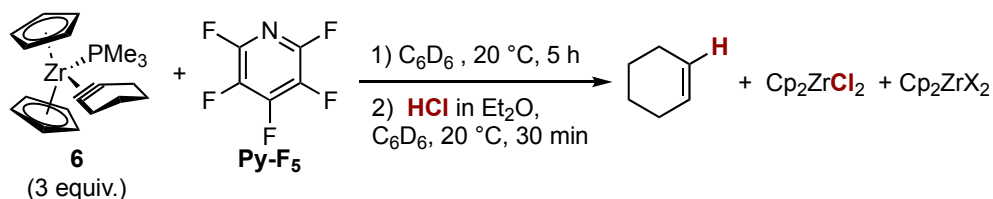
Figure 8 ^{19}F NMR (377 MHz, C_6D_6) of the reaction mixture obtained by treating the zirconocene- PMe_3 adduct **6** (1 equiv.) and pentafluoropyridine (1 equiv.) after 4 hours at 20 °C.

To further confirm the formation of **7**, one equivalent of I_2 was added into the mixture obtained from the first reaction step of Scheme 43. The formation of 1-iodocyclohexene was identified through ^1H NMR signals at $\delta = 6.15$ ppm (tt, $^3J_{\text{HH}} = 4.0$ Hz, $^4J_{\text{HH}} = 1.8$ Hz) matching with the $-\text{C}(\text{sp}^2)\text{H}$, along with three multiplets at $\delta = 2.28$, 1.63 and 1.22 ppm corresponding to the other eight protons of the ring. Cp_2ZrFI , Cp_2ZrF_2 and Cp_2ZrI_2 were also produced.



Scheme 43 Synthesis of 1-cyclohexenylzirconocene fluoride complex **7** from reaction of the zirconocene- PMe_3 adduct **6** (3 equiv.) with Py-F_5 (1 equiv.) and subsequent release of the organic ligand by addition of I_2 (1 equiv.) in C_6D_6 .

In parallel, the addition of hydrochloric acid to the same crude mixture led to the liberation of cyclohexene, Cp_2ZrCl_2 and other zirconocene halides (identified by ^1H NMR analysis) (Scheme 44).

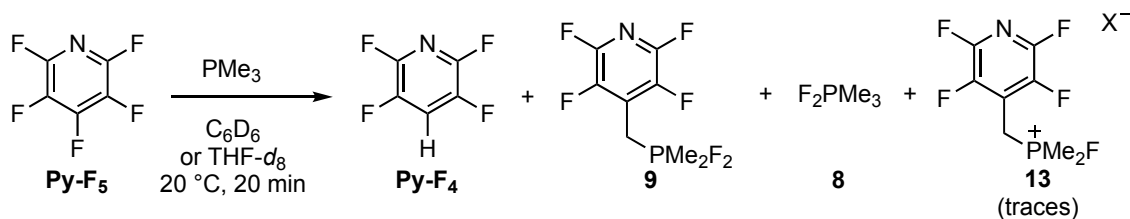


Scheme 44 Synthesis of 1-cyclohexenylzirconocene fluoride complex from reacting the zirconocene- PMe_3 adduct **6** (3 equiv.) with **Py-F₅** (1 equiv.) and release of the organic ligand by addition of $\text{HCl}\cdot\text{Et}_2\text{O}$ in C_6D_6 .

Different conditions for the C–F bond activation reaction of **6** with **Py-F₅** were investigated (Scheme 42, bottom reaction), but changing the solvent (benzene, toluene and cyclohexane), concentration of the zirconocene- PMe_3 adduct (0.1 M, 0.3 M), reagent ratio (complex **6** : **Py-F₅** = 1:1, 3:1, 5:1), lowering the temperature to 0 °C, and using pre-cooled solvent and reagents (–40 °C) had only little influence on the reaction outcome. At –40 °C the system was unreactive.

The elemental analysis of the red solid showed the presence of carbon (35.46%), hydrogen (2.74%) and nitrogen (3.64%). This suggests it may incorporate a pyridinic moiety, probably together with zirconocene-derived motifs, but its insolubility in all the tested solvents prevented further analysis. Furthermore, considering that Zr complexes are known to undergo reactions *via* radical mechanisms, as seen in the oligomerisation of hexafluorobenzene,¹⁵⁴ and given that three equivalents of **6** were needed in our system to consume one equivalent of **Py-F₅**, it may be possible that a radical process leading to the polymerisation of Zr complexes occurs in this context.

Even though the mechanism leading to **7** is still unclear, its vinylic proton seems to come from the phosphine ligand of complex **6**, as the solvents used for the reaction were deuterated and both the solvents and the fluorinated pyridine had been carefully dried and stored in the glovebox. To shed more light on the mechanism of this reaction, a control experiment on the reactivity of trimethylphosphine towards pentafluoropyridine was carried out. Addition of an equimolar amount of PMe_3 to a solution of **Py-F₅** in C_6D_6 or $\text{THF-}d_8$ at 20 °C triggered an immediate reaction noticeable by colour change from colourless to yellow. The main products, according to mass and NMR analyses, were **Py-F₄**, F_2PMe_3 , the 4-methylenetetrafluoropyridine-substituted difluorophosphorane **9** and a phosphonium salt **13**, along with unreacted PMe_3 (Scheme 45). The red solid was not observed.

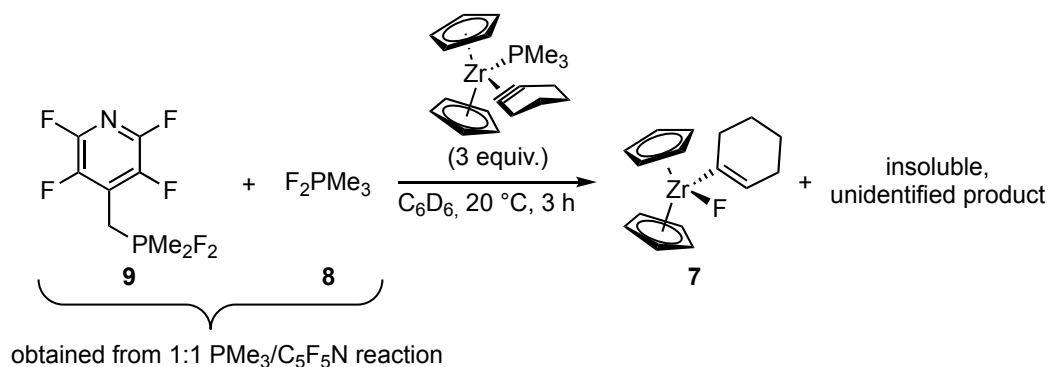


Scheme 45 Reactivity test of **Py-F₅** (1 equiv.) with **PMe₃** (1–3 equiv.) in C_6D_6 or $\text{THF-}d_8$ at 20°C .

Compound **9** exhibited similar coupling constant $^1J_{\text{PF}}$ to **8**, displaying a doublet of multiplets at $\delta(^{19}\text{F}) = -10.4$ ppm ($^1J_{\text{PF}} = 595$ Hz) and two multiplets at $\delta(^{19}\text{F}) = -93.1$ ppm and -144.9 ppm corresponding to the tetrafluoropyridyl fragment (Figure 9, a).

The presence of the formal HDF product **Py-F₄** is reminiscent of the recent work from the group of García on the PEt_3 -promoted HDF of fluoroaromatics,^{155,156} although in that case traces of water were critical to observe the desired outcome as H_2O is proposed to be the hydrogen source (this work is discussed in more detail in chapter 3.1.3.1, Scheme 75). Strict exclusion of moisture in our case rules out the involvement of García's mechanism to explain the formation of **Py-F₄**, although nucleophilic attack of the phosphine onto the 4-position of **Py-F₅** must be a common initial elementary step in both reactions. This intriguing stoichiometric reactivity between trialkylphosphines and pentafluoropyridine was further studied and more details of this investigation are discussed in chapter 3.3.

The spontaneous reaction of **PMe₃** with **Py-F₅** casts doubt on a Zr-mediated C–F bond activation for this substrate. The treatment of the mixture produced by the 1:1 **PMe₃/Py-F₅** reaction in C_6D_6 with the cyclohexyne complex **6**, according to Scheme 46, resulted in the consumption of **8** and **9** and the appearance of the zirconocene-fluoride **7** after 3 hours at 20°C , as evidenced by the ^{19}F NMR spectrum (Figure 9, b). Three equivalents of **6** (vs. **Py-F₅**) were needed to consume all **8** and **9** to afford **7** rather selectively.



Scheme 46 Reaction of **6** (3 equiv.) with the compounds issued by the reaction of **PMe₃** (1 equiv.) and **Py-F₅** (1 equiv.) in C_6D_6 at 20°C .

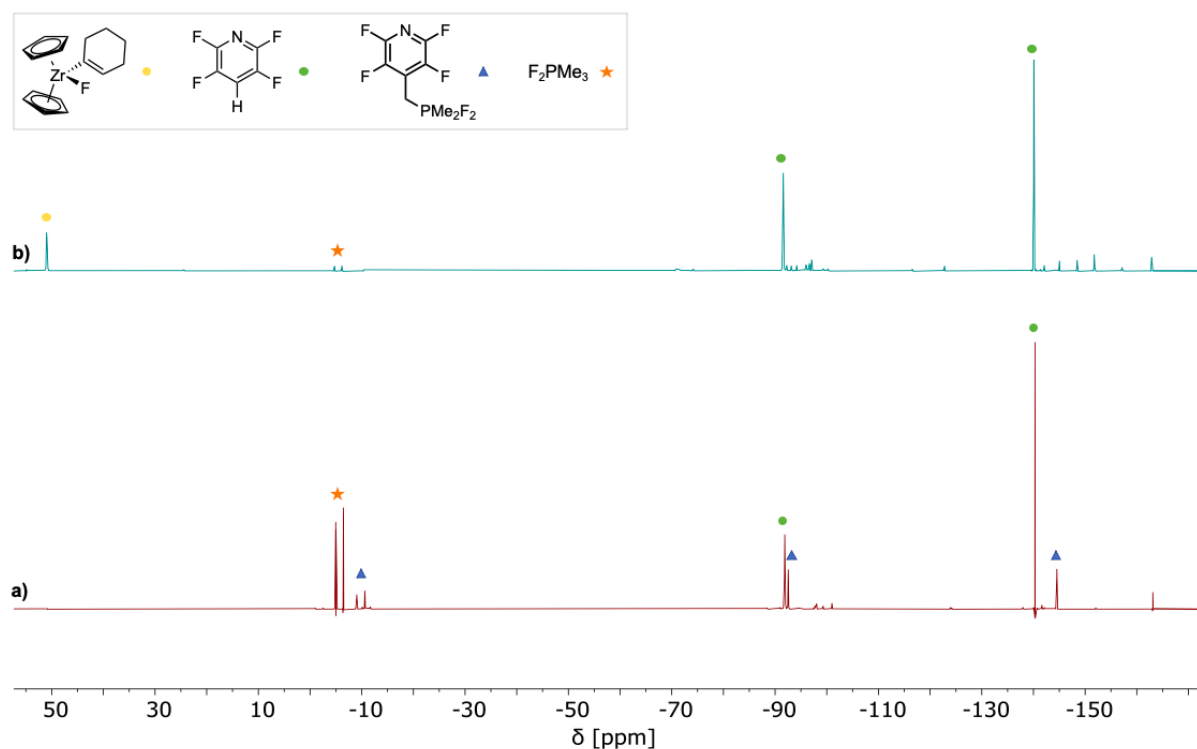


Figure 9 ^{19}F NMR (377 MHz, C_6D_6) spectra of the crude reaction mixture between PMe_3 and pentafluoropyridine (1:1, in C_6D_6) (a) and after 3 hours from the addition of complex **6** (b).

This outcome strongly suggests that the C–F bond activation event observed in the reaction of **6** with **Py-F₅** was initiated by dissociated PMe_3 reacting with the heteroaromatic to give **8** and **9**, which subsequently reacted with **6** to provide **7**. This is consistent with the dissociation energy values of the bonds involved: the Zr–F bond (BDE = 623 ± 63 kJ/mol) is indeed stronger than the P–F (BDE ≤ 405 kJ/mol) and C–F bonds (BDE = 513 kJ/mol).¹³²

In order to avoid the reaction between the phosphine and the fluorinated heteroaromatic, three alternative solutions were examined:

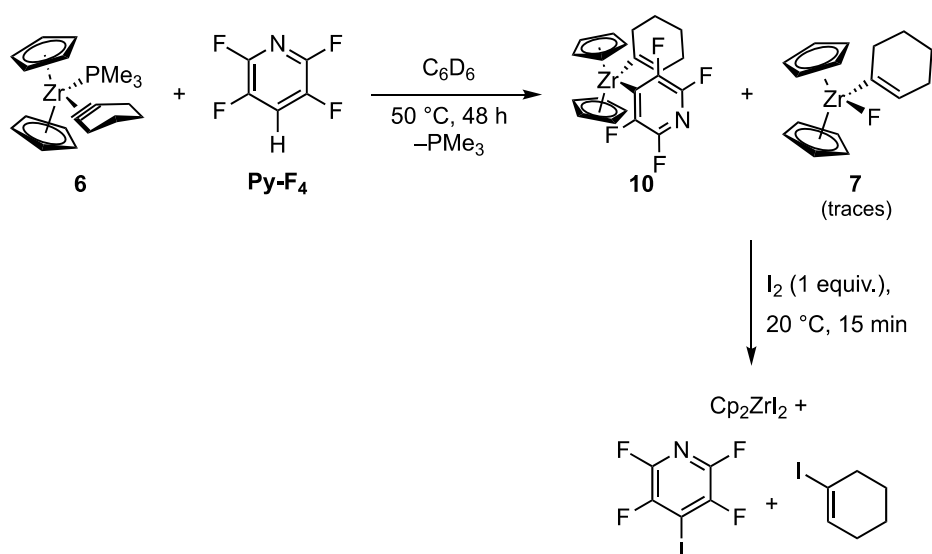
- addition of a Lewis acid in the reaction mixture to neutralise PMe_3 by forming an acid-base adduct;
- changing the stabilising ligand of complex **6**, by using a more sterically hindered trialkylphosphine;
- screening less electrophilic fluoropyridines, e.g. tetra-, tri- and difluoropyridines.

Preliminary tests on the first strategy by using tris(pentafluorophenyl)borane (BAR^{F_3}) were unsuccessful. In addition to the synthesis of the $\text{Me}_3\text{P}\cdot\text{BAR}^{\text{F}_3}$ adduct, PMe_3 underwent secondary reactions, leading to a complex reaction mixture. The second approach will be extensively discussed in chapter 3, while the third method is described in the following section.

2.3.3 Reactivity of the zirconocene-cyclohexyne complex with Py-F₄, Py-F₃ and Py-F₂

Considering the nucleophilic attack of the phosphine on the fluoroheteroaromatic as a crucial mechanistic step in the reaction outlined in Scheme 45, it was expected that the use of a less electron-poor pyridine (e.g., with a reduced degree of fluorination) could circumvent the undesired reactivity of PMe₃ with the fluoroheteroarene (for a more detailed mechanistic explanation, see chapter 3.3.3). Therefore, **Py-F₄**, **Py-F₃** and **Py-F₂** were identified as suitable candidates for this investigation.

When **6** was reacted with an equimolar amount of **Py-F₄**, complete consumption of the reagents was observed after 48 hours at 50 °C in C₆D₆. The main product was identified as the C–H activation product **10**, characterised by two multiplets in the ¹⁹F NMR at $\delta = -97.7$ and -114.8 ppm, along with small amounts of **7** (Scheme 47 and Figure 10). Multinuclear and 2D-NMR analyses further proved the formation of **10**. Additionally, a tiny quantity of a dark red solid was also observed.



Scheme 47 Synthesis of the C–H activation product **10** by reaction of **6** (1 equiv.) and **Py-F₄** (1 equiv.) in C₆D₆ at 50 °C for 48 hours and its iodolysis by addition of I₂ (1 equiv.).

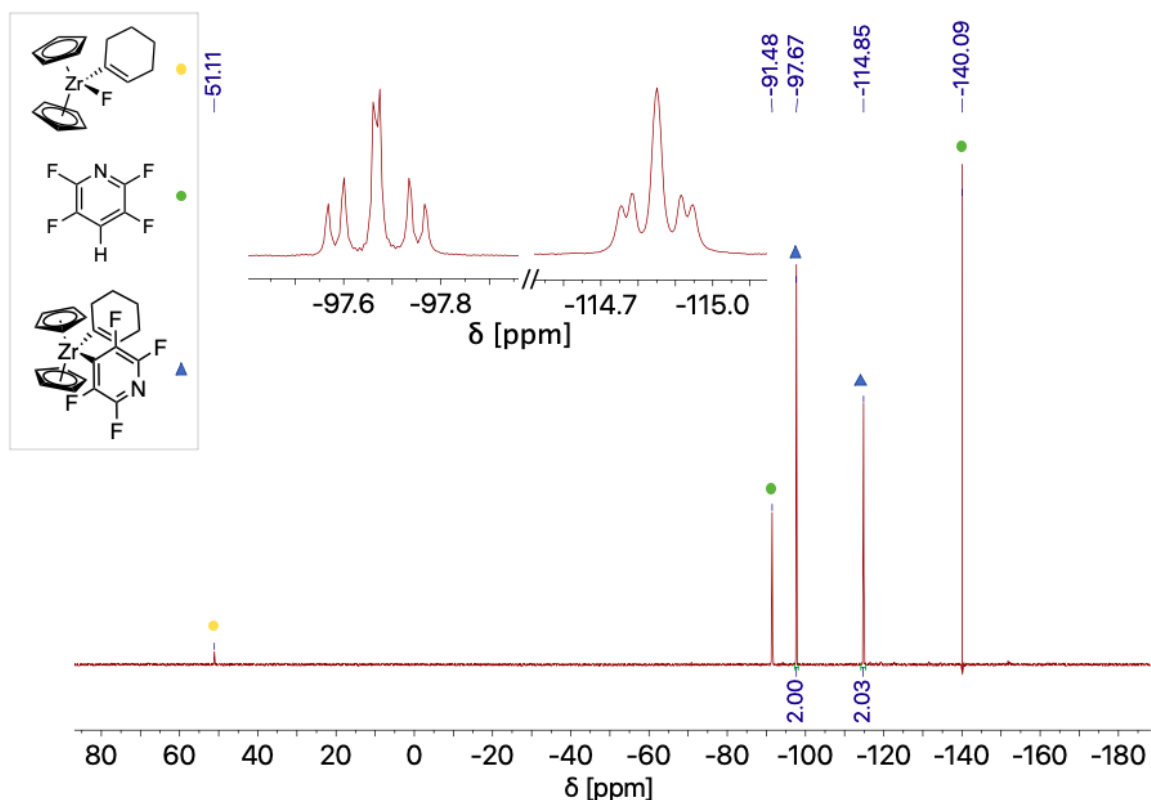
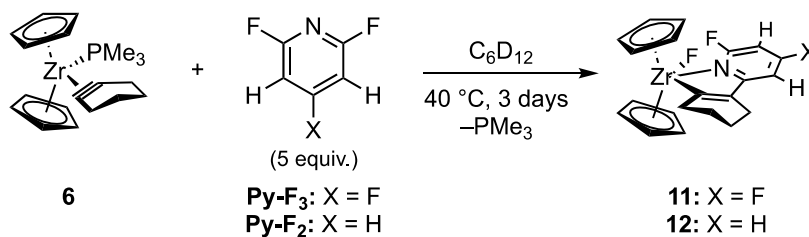


Figure 10 ^{19}F NMR (377 MHz, C_6D_6) spectrum of the reaction mixture of **6** (1 equiv.) and **Py-F₄** (1 equiv.) in C_6D_6 after 48 hours at 50 °C. Magnifications of the signals of complex **10** are given.

Complex **10** is believed to result from 1,2-C–H addition over the Zr–($\eta^2\text{-C}\equiv\text{C}$) bond in **6**, a hypothesis further supported by the absence of deuterium incorporation when the reaction was conducted in deuterated benzene. As mentioned in chapter 2.1.5.1.1, similar reactivity was also observed for bis(trimethylsilyl) acetylene complexes of zirconocene derivatives.¹²⁸ Compound **7** possibly arises from a side reaction involving, as mentioned earlier, fluorophosphines or -phosphoranes and the Zr centre. Further evidence for C–H activation was collected through NMR analyses of the reaction mixture after treatment with I_2 (Scheme 47), with the detection of 1-iodocyclohexene in the ^1H NMR spectrum and 4-iodo-2,3,5,6-tetrafluoropyridine, characterised by two multiplets at $\delta = -90.2$ and -123.5 ppm in the ^{19}F NMR spectrum.

Remarkably, in the case of **Py-F₃** and **Py-F₂** the targeted 1,3-C–F bond addition over the Zr– η^2 -cycloalkyne motif took place, affording **11** and **12**, respectively (Scheme 48). Various solvents (THF, chlorobenzene, toluene, benzene, diethyl ether, cyclohexane) and temperatures were tested to find the optimal conditions for these reactions. The system exhibited the highest yield (71% isolated yield of **11**) and selectivity when cyclohexane was used as solvent at 40 °C.



Scheme 48 Synthesis of **11** and **12** by reaction of **6** (1 equiv.) with **Py-F₃** or **Py-F₂** (3–5 equiv.) in C₆D₁₂ at 40 °C.

The addition product **11** is characterised by a singlet at $\delta(^{19}\text{F}) = -35.4$ ppm, corresponding to the Zr–F bond, a doublet at $\delta(^{19}\text{F}) = -60.7$ ppm ($^4J_{\text{FF}} = 24.0$ Hz) and a doublet of doublets of doublets at $\delta(^{19}\text{F}) = -94.8$ ppm ($^4J_{\text{FF}} = 24.0$, $^3J_{\text{FH}} = 9.5$ Hz, $^3J_{\text{FH}} = 7.5$ Hz), associated with the *ortho*- and *para*-fluorine of the pyridine, respectively (Figure 11). The *ortho*-fluorine shows only the coupling with the fluorine in *para*-position because the $^3J_{\text{FH}}$ with the nearby proton is relatively small (*ca.* 2 Hz).

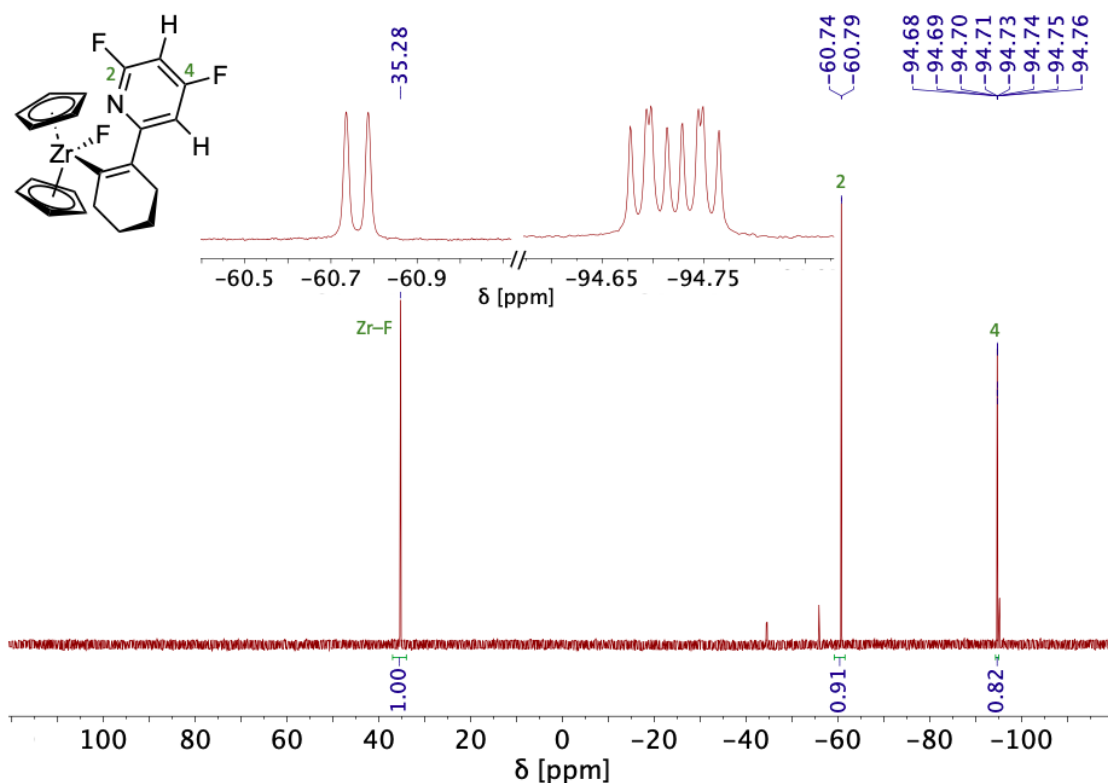


Figure 11 ^{19}F NMR (377 MHz, C₆D₆) spectrum of the crude reaction mixture of the reaction between the zirconocene-PMe₃ adduct **6** (1 equiv.) with **Py-F₃** (5 equiv.) in cyclohexane at 40 °C for 42 hours, dried and dissolved in C₆D₆. Magnifications of the signals of complex **11** are given.

In the ^1H NMR spectrum (Figure 12), the diagnostic peaks for complex **11** were observed as a doublet of doublets at $\delta = 6.35$ ppm ($^3J_{\text{HF}} = 9.7$ Hz, $^4J_{\text{HH}} = 2.3$ Hz), a *pseudo* doublet of triplets at $\delta = 5.58$ ppm ($^3J_{\text{HF}} = 7.3$, $^4J_{\text{HH}} \approx ^3J_{\text{HF}} \approx 2$ Hz), corresponding to the pyridine protons in position 5 and 3, respectively, and a singlet at $\delta = 5.96$ ppm, gathering the cyclopentadienyl protons. Additionally, three multiplets at 2.97, 1.93 and 1.68 ppm are related to protons of the cyclohexenyl fragment. The ^1H NOESY NMR spectrum (Figure 13) displayed a spatial correlation between the signal at $\delta = 6.35$ ppm and $\delta = 1.93$ ppm, which was therefore associated with protons in position 8.

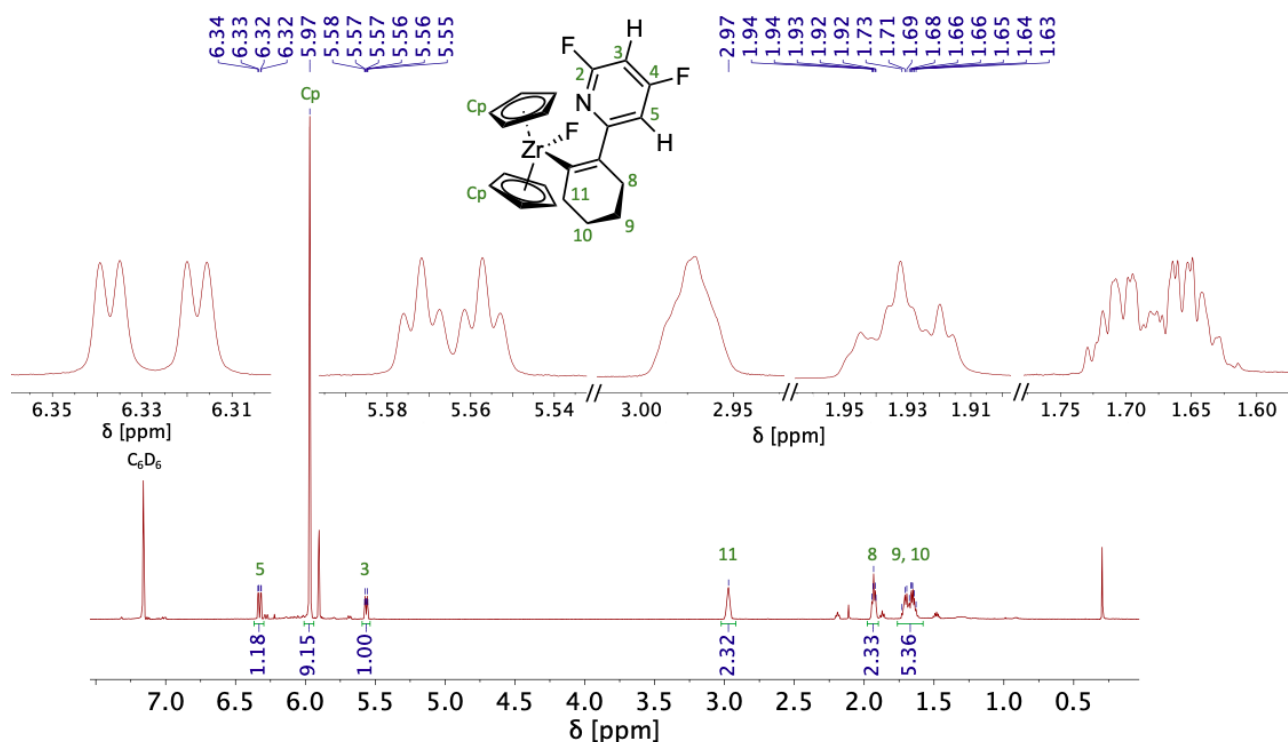


Figure 12 ^1H NMR (500 MHz, C_6D_6) spectrum of the crude reaction mixture of the reaction between the zirconocene- PMe_3 adduct **6** (1 equiv.) with **Py-F₃** (5 equiv.) in cyclohexane at 40 °C for 42 hours, dried and dissolved in C_6D_6 . Magnifications of the signals of complex **11** are given.

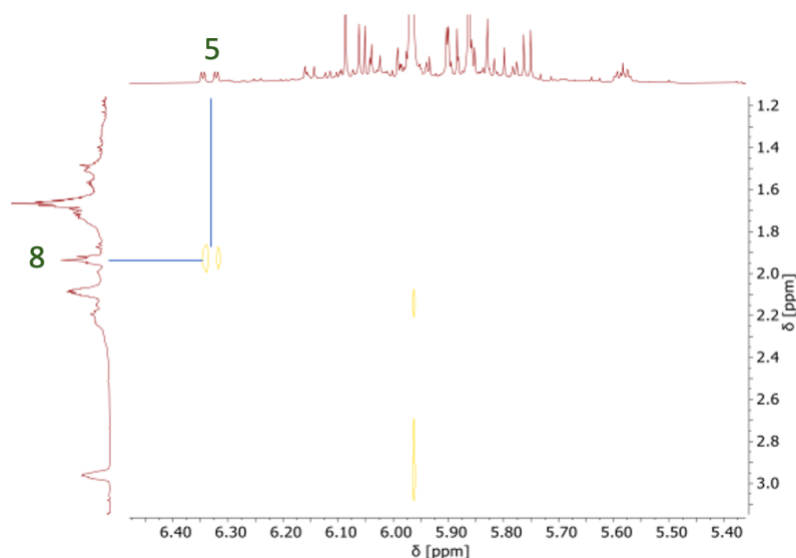
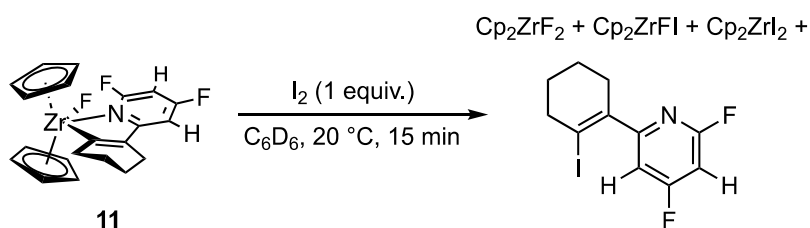


Figure 13 ^1H NOESY (500 MHz, C_6D_6) spectrum of the crude reaction mixture of the reaction between the zirconocene- PMe_3 adduct **6** (1 equiv.) with **Py-F₃** (5 equiv.) in cyclohexane at 40 °C for 42 hours, dried and dissolved in C_6D_6 .

Further confirmation of the identity of the product was provided by the ^1H - ^{19}F HMBC spectrum, displaying a correlation between the Zr-F signal at $\delta(^{19}\text{F}) = -35.4$ ppm and the cyclopentadienyl protons at $\delta(^1\text{H}) = 5.96$ ppm. $^{13}\text{C}\{^1\text{H}\}$ and $^{13}\text{C}\{^1\text{H}\}$ - ^1H 2D NMR spectra further verified the nature of complex **11**.

Additionally, the formation of **11** was evidenced by the generation of 2-(2-iodocyclohexen-1-yl)-4,6-difluoropyridine, characterised by GC(EI)-MS and NMR analyses, after iodinolysis of the complex (Scheme 49).



Scheme 49 Iodinolysis of **11** (1 equiv.) by addition of I_2 (1 equiv.) in C_6D_6 after 15 min at 20 °C.

The iodinolysed organic product is characterised by a doublet at $\delta = -63.3$ ppm ($J = 22.6$ Hz) and a multiplet at $\delta = -97.9$ ppm in the ^{19}F NMR spectrum. Multinuclear (^1H , ^{19}F , ^{13}C) and 2D-NMR spectra are consistent with the formation of 2,4-difluoro-6-(2-iodocyclohexen-1-yl)-pyridine. In addition, GC(EI)-MS analysis exhibited its characteristic fragmentation pattern (Figure 14).

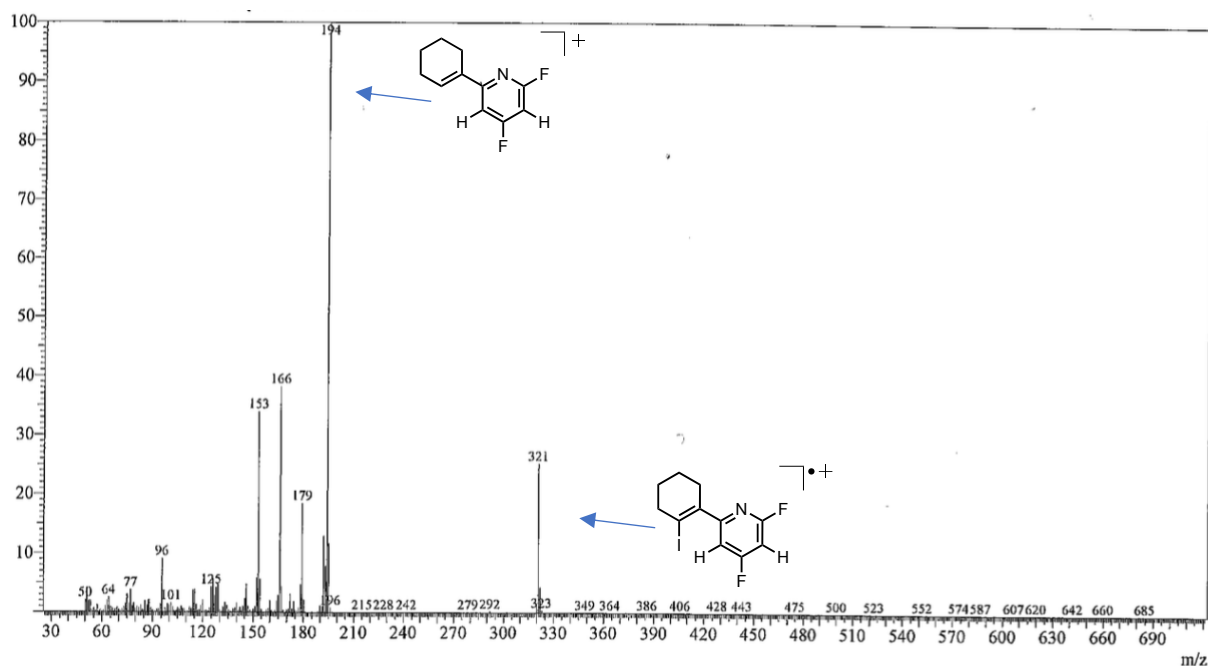


Figure 14 GC(EI)-MS spectrum of 2,4-difluoro-6-(2-iodocyclohexen-1-yl)-pyridine obtained by reaction of **11** (1 equiv.) with I₂ (1 equiv.) in C₆D₆ at 20 °C for 15 minutes.

Crystals suitable for a single crystal X-ray diffraction (sc-XRD) analysis were grown after vapour diffusion of tetramethylsilane, as an antisolvent, into a concentrated toluene solution of **11**. Its molecular structure is shown in Figure 15.

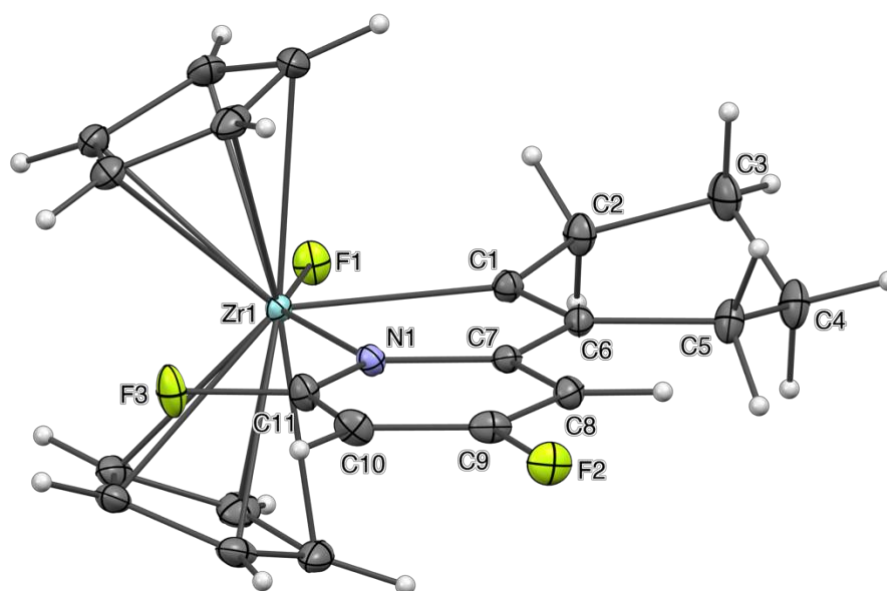


Figure 15 Molecular structure of **11** in the solid. Ellipsoids drawn at the 25% probability level. Selected bond lengths (Å) and angles (°): Zr1-F1 2.008(1), Zr1-C1 2.321(2), Zr1-N1 2.479(2), N1-C7 1.372(3), C1-C6 1.354(3), C6-C7 1.456(3), F1-Zr1-C1 80.26(6), C1-Zr1-N1 68.35(6), F1-Zr1-N1 148.46(6), N1-C11-F3 114.7(2).

The Zr atom lies in a distorted trigonal bipyramidal environment, with apical sites occupied by the nitrogen of the pyridine ligand and the fluoride. The former belongs to a 1-zircona-2-aza-cyclopentadiene motif that connects it to the alkenyl carbon found in the equatorial plane, forcing the F-Zr-N array to deviate significantly from linearity [F1-Zr1-N1 148.46(6)°] and imposing a tilt angle for the Cp-Zr-Cp moiety of 135.8°. Similar deviations from the ideal trigonal bipyramidal geometry are found in other crystallographically characterised five-coordinated, Cp-supported 1-zircona-2-aza-cyclopentadienes.^{157–162} Compared to structurally related species,^{157–163} the angles measured within the five-membered ring as well as the bond lengths of the conjugated part show no significant irregularity. However, the Zr–C bond is rather short and the Zr–N, rather long. In the considered family of compounds selected for comparison, the former varies slightly in length, while the Zr–N distance fluctuates depending on the L or X character of the nitrogen ligand and the N-substituent. In the present case, we explain the long Zr–N bond by the presence of the fluoride in *trans* relationship, coupled with the electron-poor properties of the difluoropyridine ring. The elongation of the Zr–N bond mechanically impacts the length of the Zr–C bond due to the rigidity of the 1-zircona-2-aza-cyclopentadiene core. An additional observation is that the N1-C11-F3 angle is quite acute [114.7(2)°], presumably as a result of a long-range interaction of the fluorine atom with the electropositive Zr atom.

Interestingly, the addition of an excess of **Py-F₃** to the *in situ* generated **5** did not trigger any C–F activation process, leaving the system almost unchanged, as it was observed with **Py-F₅** (Scheme 42, top). The reaction of **6** with **Py-F₃** in THF resulted in a complex mixture where **7** was identified as the main product and no **11** was detected, suggesting that the PMe₃-assisted C–F activation process is prevalent in this system. These observations may provide an explanation for the lack of 1,3-CF addition product when **5** and **Py-F₅** or **Py-F₃** are treated in tetrahydrofuran. Probably, the solvent coordinates to the Zr centre to stabilise the coordinatively and electronically unsaturated complex **5** and other less energy-demanding reactions than the C–F bond activation step are occurring.

Complex **12**, obtained from treating the zirconocene-PMe₃ adduct **6** with **Py-F₂** (5 equivalents) in cyclohexane at 40 °C for 3 days (Scheme 48), exhibits similar NMR features to **11**. The ¹⁹F NMR spectrum displays a singlet at δ = 34.7 ppm, corresponding to the Zr–F bond, and a doublet at δ = –64.3 ppm (d, *J* = 7.6 Hz). In the ¹H NMR spectrum, three signals at δ = 8.33 (*pseudo q*, 1H, *J* = 7.9 Hz, *para-H*), 7.61 (*pseudo dt*, ³*J*_{HH} = 8.0 Hz, *J* = 1.2 Hz, *meta-H*) and 7.16 ppm (*pseudo dt*, ³*J*_{HH} = 8.0 Hz, *J* = 1.2 Hz, *meta-H*) are associated with the pyridine protons. A triplet of triplet at δ = 2.86 ppm (³*J*_{HH} = 6.4 Hz, ⁴*J*_{HH} = 2.2 Hz) and two multiplets at 2.32 and 2.11 ppm correspond to the cyclohexenyl ring protons. It is remarkable to note that the system was highly selective and, despite

the presence of a proton in the *para*-position, the C–H bond activation product was not detected.

Several hypotheses may be given to explain the differences in reactivity of the four polyfluoropyridines towards **6**. The absence of a 1,3-C–F addition product after treatment with **Py-F₅** can reasonably be attributed to the fast reaction of the latter with dissociated PMe_3 . The low Lewis basicity of **Py-F₅** may also lead to a loosely bound adduct with the transient phosphine-free cyclohexyne complex **5**, hampering a C–F bond activation step to occur before the substrate reacts with the phosphine. Additionally, the structure of **11** (Figure 15) reveals a 1,3-allylic (^{1,3}A) strain between the cycles' backbones (carbons C5 to C8), along the ring junction. This destabilising interaction would be exacerbated if the heteroaromatic ring was fully fluorinated and may exist before the C–C bond formation event, imparting a kinetic penalty for a C–F bond activation pathway.

The observation of the C–H activation product in the reaction with **Py-F₄** may be the result of two factors: on the one hand, the high level of fluorination of the heterocycle makes it, akin to **Py-F₅**, a poor Lewis base that is not likely to strongly bind the Zr centre. Besides, a potential C–F/CH₂ repulsion, resulting in the above-spotted ^{1,3}A strain in the cyclometalated product (Figure 15), is likely to arise from **Py-F₄** coordination. Moreover, Perutz and coworkers conducted an extensive study on the competition between metal-assisted C–H and C–F bond activation processes and identified several factors, such as the nature of the metal and its ligands, as well as the fluorinated compound and its fluorine substitution pattern, both playing crucial roles in the selectivity of the system.^{153,164,165} An important parameter is the presence of *ortho*-fluorine substituents in the generated metal-fluororaryl complex, which makes C–H bond activation more energetically favourable. The presence of fluorine atoms in *ortho* to the M–C bond increases the ionic character of this bond, resulting in a negative charge at the *ipso*-carbon of the M-aryl bond. This charge is stabilised by *ortho*-fluorine substituents through hyperconjugation to the C–F antibonding σ^* orbitals and due to the electron-withdrawing character of fluorine.¹⁶⁴ In our system, the metalation of the acidic C–H provides a metal-4-pyridyl compound with highly stabilising two-fold *ortho*-fluorine substitution.

In the case of **Py-F₃** and **Py-F₂**, higher Lewis basicity may allow the heteroarene to better interact with the Zr atom after PMe_3 dissociation and thus bringing its *ortho* C–F bonds closer to the reactive cyclohexyne ligand. This sets the stage for a regioselective C–F bond activation to take place.¹³¹ The formation of complex **7** was not observed in these systems as the fluorinated pyridines were not sufficiently electrophilic to react with the dissociated PMe_3 . Remarkably, in the case of **Py-F₂** the 4-position is not fluorinated, yet complete chemoselectivity for C–F over C–H activation was

observed. This is likely the result of a stronger Zr...N interaction favouring C–F activation as well as the absence of fluorine in the 3- and 5-positions that would stabilise the C–H activation product.

2.4 Summary, conclusions and perspectives

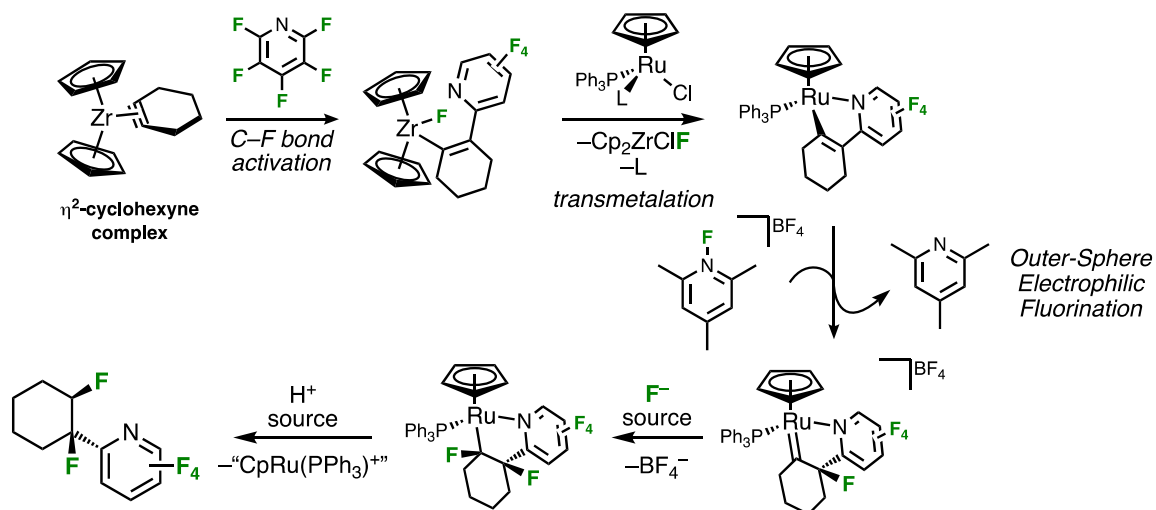
The PMe_3 adduct of the zirconocene η^2 -cyclohexyne complex (**6**) was successfully synthesised (52% isolated yield) and its reactivity towards differently fluorinated pyridines was investigated. Interestingly, depending on the fluorination pattern of the heteroaromatic, three distinctive reaction pathways were observed.

Complex **6** reacted at room temperature with **Py-F₅** to form 1-cyclohexenylzirconocene chloride (**7**) along with some unidentified solid and other fluorine- and phosphorus-containing minor products. Control experiments pointed out that an initial dissociation of PMe_3 , followed by its reaction with the heteroaromatic to yield F_2PMe_3 and **9**, subsequently triggered the formation of **7** through the reaction of F_2PMe_3 and **9** with **6**. The high reactivity of this system is ascribed to the electrophilicity of **Py-F₅**, making it an excellent candidate for undergoing $\text{S}_{\text{N}}\text{Ar}$ by nucleophiles such as PMe_3 . When complex **6** was treated with an equimolar amount of **Py-F₄**, the major product detected was the 1,2-C–H addition product **10**, accompanied by some traces of **7**. Remarkably, the targeted 1,3-C–F bond addition reaction occurred with **Py-F₃** and **Py-F₂**, the former affording crystals suitable for XRD analysis that display coordination of the N of the fluorinated pyridine to the Zr centre. The products obtained from the reactions with the various fluorinated pyridines were treated with electrophiles, allowing the release of the fluorinated ligands for further characterisation.

We envision that further functionalisation of the fluorinated ligand in complexes **11** and **12**, such as through insertion (e.g. of CO or carbonyl), will be feasible. Additionally, inspired by the work of Zeng and coworkers,¹⁶⁶ it would be interesting to explore the ability of Zr complexes **11** and **12** in the synthesis of fluorinated indolizines. Zeng *et al.* demonstrated that a Co complex containing 2-alkenylpyridine as a ligand underwent an insertion reaction of an α -keto aldehyde. Subsequent protonation and Co-promoted nucleophilic substitution involving the nitrogen led to the release of indolizines.

Furthermore, we envisioned the possibility of transmetalating the fluorinated ligand to other metals, considering the many ligand redistribution reactions involving zirconium and *p*-block elements, group 7, 9, 10, 11 and 12 metals reported in the literature.^{144,167,168} Our specific interest was focused on the formation of a pyridine ligand with a vinyl group in 2-position because it was envisaged the possibility to transfer it to a ruthenium complex of the type

$[\text{Ru}(\eta^5\text{-C}_5\text{H}_5)(\text{PPh}_3)(\text{py})_2]\text{PF}_6$. Subsequent outer-sphere electrophilic fluorination, nucleophilic fluorination and product release reactions would allow the synthesis of a new fluorinated organic compound in a regio- and stereoselective manner.^{14,169}



Scheme 50 Proposed synthetic strategy for the regio- and stereoselective preparation of a new fluorinated organic molecule.

Finally, we envisage the possibility of broadening the scope of fluorinated substrates beyond pyridines and investigating the reactivity of **6** towards other perfluoroaromatic compounds. Additionally, the synthesis of other Zr complexes bearing ring-strained ligands (e.g., Zr-benzynes complex) could be carried out to explore their potential for activating the C-F bonds of polyfluoropyridines and -aromatics.

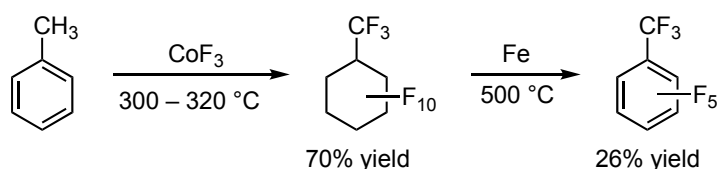
Chapter 3 –Stoichiometric reactivity between trialkylphosphines and Py-F₅

3.1 Introduction

3.1.1 Synthesis of perfluoroaromatic compounds

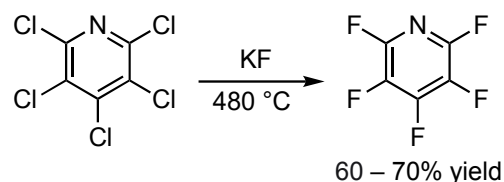
Fluoro(hetero)aromatic compounds find many applications as intermediates in the production of agrochemicals, pharmaceuticals, reactive dyes and liquid crystals.^{170,171}

The investigation of their reactivity has significantly broadened since the discovery of efficient protocols for their synthesis in the late 1950s. Banks and Tatlow reported the synthesis of perfluorinated (hetero)aryl compounds through fluorination and saturation of the aromatics using CoF₃ and subsequent rearomatisation (*via* defluorination or hydrodefluorination) with metals (such as iron or nickel) at high temperatures or electrochemically (Scheme 51). This process has also been developed industrially.¹⁷²



Scheme 51 Banks and Tatlow's methodology for the synthesis of perfluoro(hetero)aromatic compounds.

In 1963 the synthesis of perfluoro(hetero)aromatics using the corresponding perchlorinated (hetero)aromatic and anhydrous KF as a source of fluoride anion was developed (Scheme 52).¹⁷³ This method, currently employed in industry, relies on halogen exchange (referred to as Halex fluorination) and occurs *via* an S_NAr mechanism.



Scheme 52 Halex fluorination process for the synthesis of perfluoro(hetero)aromatic compounds.

As an alternative strategy, a second industrial approach for a more selective fluorination of aromatic compounds is the diazotisation approach (Balz-Schiemann reaction) and its extensions.^{171,174}

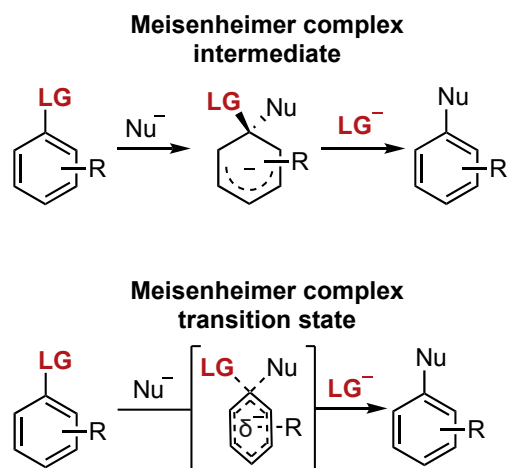
The straightforward synthesis of these compounds makes them cheap and readily available substrates. Their selective derivatisation can be achieved by cleaving one or more C–F bonds, yielding valuable building blocks that can be further functionalised. Since the chemistry of polyfluoro(hetero)aromatic compounds is mainly characterised by substitution reactions with nucleophilic reagents, the following sections provide a description of this reactivity. In this introduction section, a particular focus on the reactivity of polyfluoro(hetero)aromatics with phosphorus-containing compounds is given, as the new research described in chapter 3.3 deals with the functionalisation of pentafluoropyridine using simple phosphines.

3.1.2 S_NAr reactions with polyfluoro(hetero)aromatic compounds

3.1.2.1 Mechanism and regioselectivity

Polyfluorinated (hetero)arenes can undergo nucleophilic aromatic substitution reactions under relatively mild conditions. A huge number of nucleophiles, including those based on C, O, N and S, readily react with polyfluoro(hetero)aromatic compounds *via* S_NAr reactions.^{175,176}

The ease of these transformations stems from the presence of many highly electronegative fluorine substituents on the ring, which makes the aromatic compound more electrophilic. This lowers the energy of the π^* antibonding orbital compared to that of a simple aromatic hydrocarbon, making it more susceptible to nucleophilic attack. Recent studies on S_NAr reactions highlight their high dependency on both the substrate and nucleophile. These transformations can proceed through a stepwise mechanism, involving the formation of a charged Meisenheimer complex intermediate, or a concerted mechanism, characterised by the formation of a Meisenheimer complex transition state (Scheme 53).^{177–179}



Scheme 53 Stepwise (top) and concerted (bottom) S_NAr mechanism.

When fluoride is the leaving group (LG), the stepwise mechanism mainly occurs. Furthermore, the anionic Meisenheimer complex is stabilised by the presence of electron-withdrawing substituents on the ring, such as fluorine, and the rearomatisation thereof promotes fluoride elimination.¹⁸⁰

Extensive studies have investigated the regioselectivity of S_NAr reactions with polyfluorinated aromatic and heteroaromatic compounds.^{181–183} In both cases, this is mainly dictated by maximising the number of F substituents in *ortho*- and in *meta*-position to the site of the nucleophilic attack, attributed to the ion-dipole and inductive effects. Furthermore, F atoms in the *para*-position are deactivating, due to electronic repulsion in the Meisenheimer complex intermediate (Figure 16).¹⁷⁵

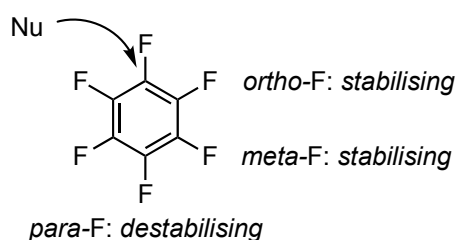
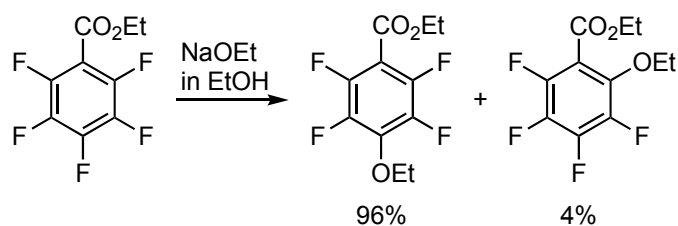


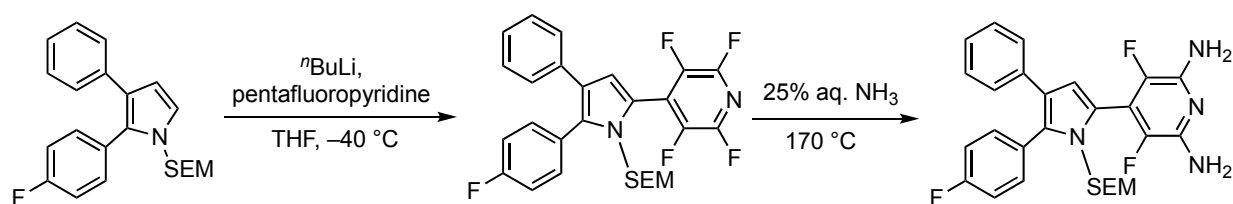
Figure 16 Fluorine substituent effects on the regioselectivity of S_NAr reactions.

Therefore, for compounds with substituents other than F (e.g., C_6F_5X , where X is any substituent, electron-withdrawing or donating) or perfluoroheteroaromatic compounds, the activation of the C–F bond primarily occurs in *para*-position relative to the substituent or the heteroatom and, secondarily, in *ortho*-position. This can be observed in the reaction of ethyl pentafluorobenzoate with NaOEt, wherein the *para*-substituted derivative was the major product, although the *ortho*-functionalised one was also observed (Scheme 54).¹⁸⁴



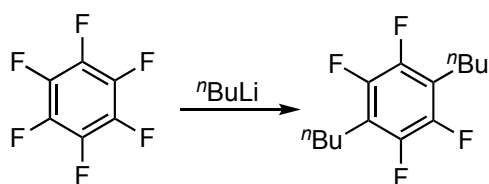
Scheme 54 Regioselectivity in the S_NAr reaction of pentafluorobenzoate with NaOEt.

The greater activation of the *para*- than the *ortho*-position to the heteroatom in perfluoroheteroaromatic compounds can be exploited to synthesise targeted polysubstituted species. For instance, the synthesis of biologically active 2,6-diamino-3,5-difluoropyridinyl-substituted pyridinylimidazoles, able to treat chronic inflammatory diseases, can be achieved through sequential S_NAr reactions.¹⁸⁵ Deprotonation of the trimethylsilylethoxymethyl (SEM)-protected imidazole generated a carbanion that nucleophilically attacked **Py-F₅** in 4-position. Subsequently, diamination in 2- and 6-positions occurred *via* reaction with NH_3 in aqueous solution at high temperatures (Scheme 55).



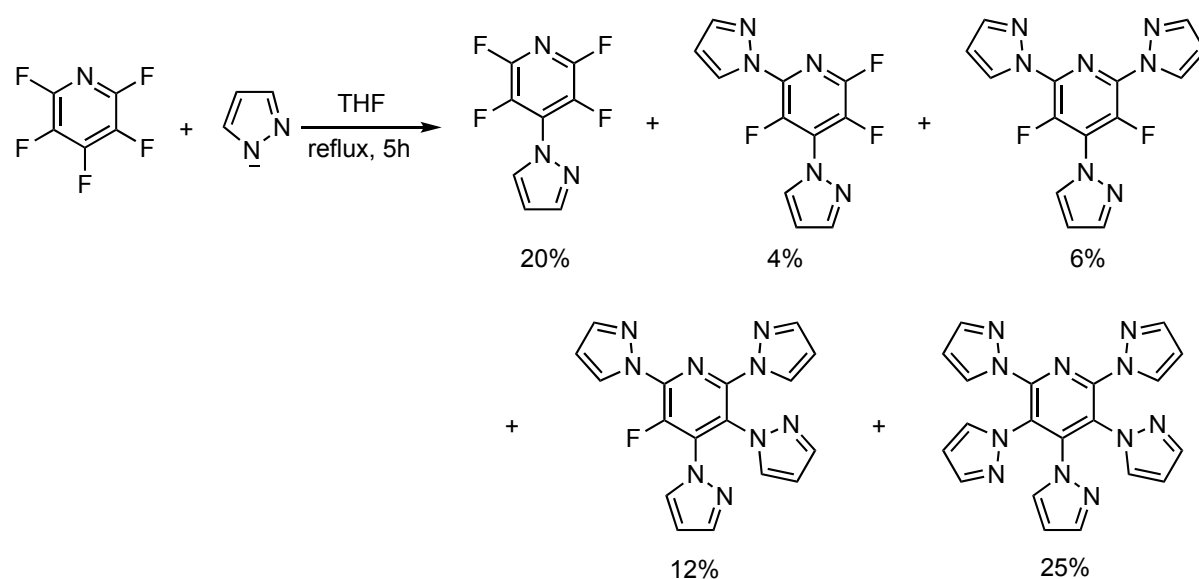
Scheme 55 Sequential functionalisation of pentafluoropyridine for the synthesis of pyridinylimidazole derivatives.

However, the use of highly reactive nucleophiles, strong bases or harsh reaction conditions is sometimes necessary for nucleophilic substitution to take place. In such cases, the reactions may lead to multiple substitutions, making the control of the selectivity challenging. For instance, as discussed in chapter 2.1.3, the use of organolithium compounds like $nBuLi$ led to the polysubstitution of hexafluorobenzene (Scheme 56).¹⁸¹



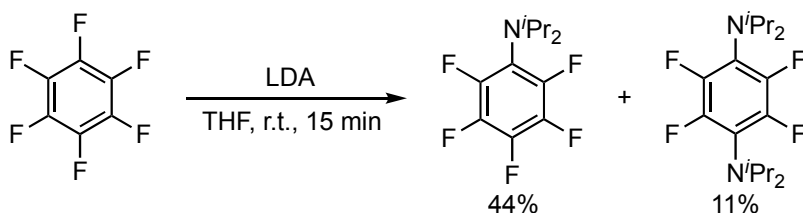
Scheme 56 S_NAr reaction of hexafluorobenzene with $nBuLi$.

Furthermore, simple amines (such as ammonia, primary and sometimes secondary amines) can be employed for the synthesis of polyfluoroaromatic amines only if they are sufficiently nucleophilic. Alternatively, less basic amines (or less electrophilic polyfluoroaromatics) can be used in the additional presence of strong bases (such as LiHMDS, BuLi, LiH, ^tBuOK) that deprotonate them. However, these systems often require harsh reaction conditions (high temperatures and extended reaction times). The use of very strong bases and vigorous conditions can lead to poor reaction selectivity and side reactions may occur. For example, the reaction of equimolar amounts of **Py-F₅** with pyrazolide anions, generated by deprotonation with NaH, produced a mixture of substituted mono-, bis-, tris-, tetrakis- and pentakis-pyrazole pyridines (Scheme 57).⁵⁵



Scheme 57 Polysubstitution of **Py-F₅** with pyrazole anions.

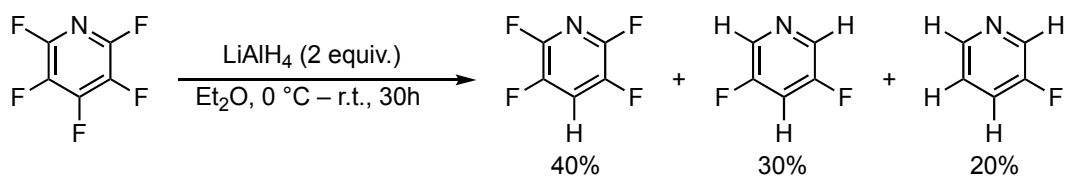
Moreover, the reactions of lithium diisopropylamide (LDA) with hexafluorobenzene or **Py-F₅** resulted in a mixture of monosubstitution and 1,4-disubstitution products in the first case, and 2,4-disubstitution along with 2- and 4-monosubstitution in the second case (Scheme 58).¹⁸⁶



Scheme 58 Polysubstitution of pentafluoropyridine and hexafluorobenzene with LDA.

On the other hand, hydride ions can be used as nucleophiles for the HDF reaction of **Py-F₅**. Diisobutylaluminium hydride (DIBAL) have been employed, but harsh reaction conditions

(100 °C, sealed tube, 24 hours) were necessary to obtain the monosubstitution product **Py-F₄**. However, when a more reactive hydride source, such as lithium aluminium hydride, was used at low temperatures (between 0 °C and room temperature for 32 hours), a mixture of polysubstitution products was formed (Scheme 59).¹⁸⁷



Scheme 59 Hydrodefluorination reaction of pentafluoropyridine with lithium aluminium hydride.

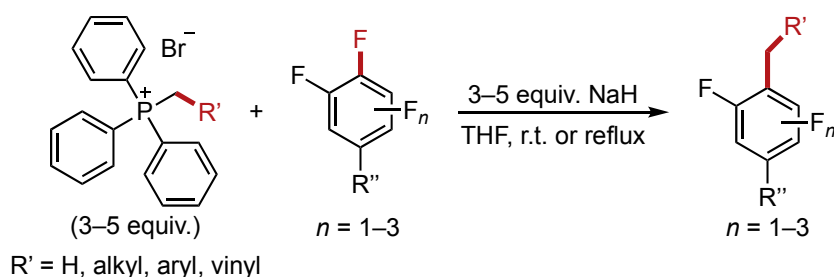
Therefore, the challenge in this type of functionalisation reactions is to control the regioselectivity (and stereoselectivity where applicable) while maintaining high efficiency of the system.

3.1.2.2 Metal-free C(sp²)-C bond forming reactions in polyfluoroaromatics

As shown in chapter 2.1, organometallic compounds are mainly used to promote C-C bond coupling reactions *via* the cleavage of C-F bonds. However, metal-free alternative routes that involve the use of neutral and anionic carbon-based nucleophiles have been developed.

3.1.2.2.1 Neutral nucleophiles

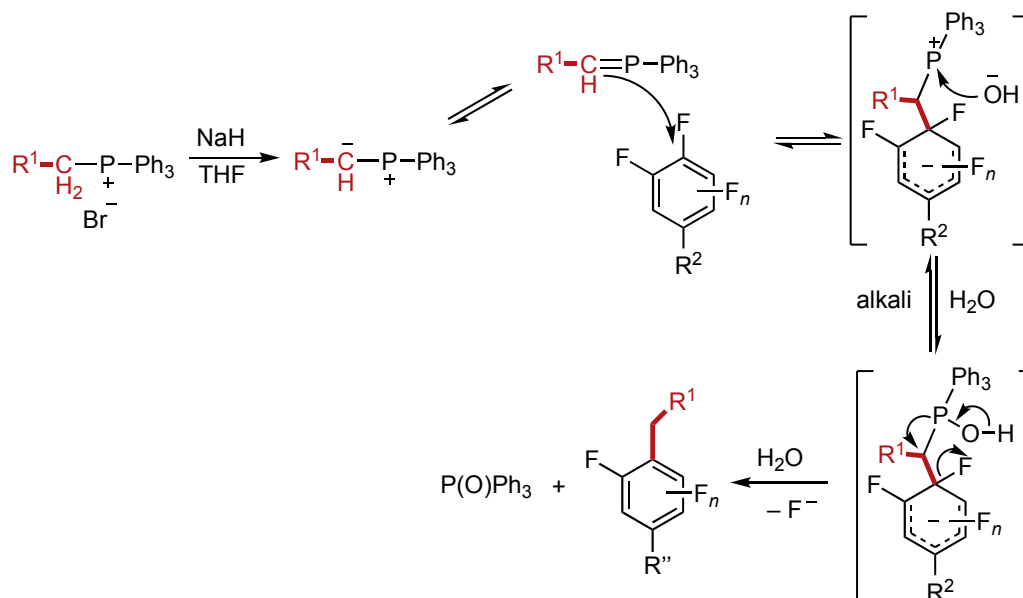
Phosponium ylides are able to replace fluorides with alkyl groups in a regioselective manner in polyfluoroarenes and perfluoroheteroarenes (Scheme 60).⁵⁴ The alkyl group is introduced in the *para*-position to the arene substituent or the heteroatom.



Scheme 60 Alkylation of polyfluoroarenes and perfluoroheteroarenes with phosphonium ylides.

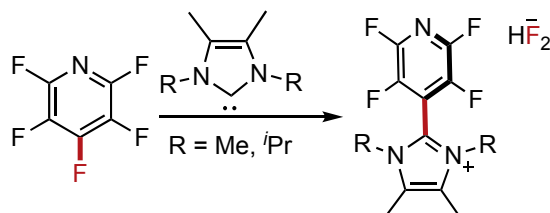
A mechanism for this reaction was proposed (Scheme 61). The *in situ* generated ylide, obtained by deprotonation of the phosphonium salt with a strong base (NaH), attacks the polyfluoro(hetero)aromatic compound in *para*-position to the substituent (or heteroatom) following an S_NAr mechanism. This results in the formation of a Meisenheimer intermediate with a

phosphonium-containing substituent. Subsequently, a hydroxide attacks the phosphorus-centre, which is then hydrolysed in the presence of H₂O and alkali, resulting in the expected product of C–C coupling and phosphine oxide. The high steric hindrance of the ylide appears to be an important factor for the high regioselectivity of the system.



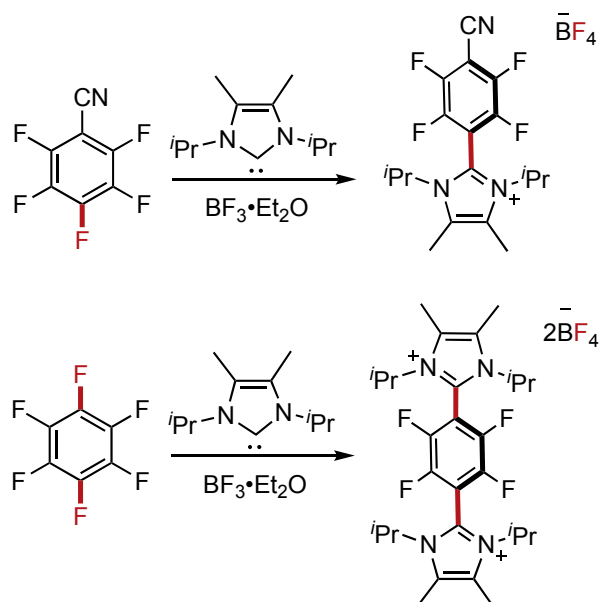
Scheme 61 Proposed mechanism for the alkylation reaction of polyfluoroarenes and perfluoroheteroarenes with phosphonium ylides.

An alternative pathway for C–C bond coupling reactions relies on the use of NHCs as nucleophiles. These are electron-rich species and they are usually employed as spectator ligands in organometallic chemistry and catalysis. The chemistry of carbenes with perfluoroaromatics has been developed in the past 20 years. Kuhn and coworkers in 1998 were the first to show that the carbon-centre in tetraalkylimidazol-2-ylidenes was sufficiently nucleophilic to directly attack **Py-F₅** at low temperature.¹⁸⁸ The product obtained was the 2-tetrafluoropyridylimidazolium salt shown in Scheme 62.



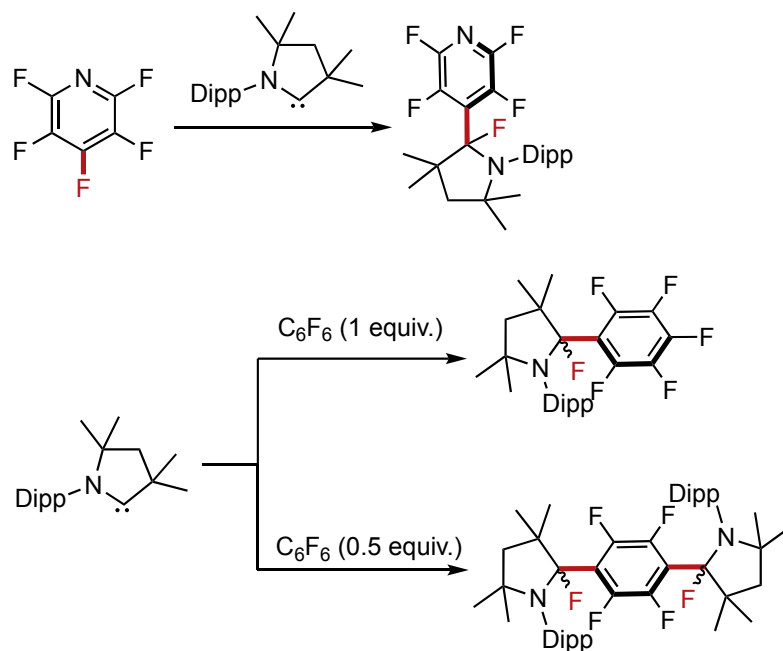
Scheme 62 S_NAr reaction of pentafluoropyridine with NHC nucleophiles.

Furthermore, the same type of NHC reacted with differently substituted polyfluoroarenes in the presence of boron trifluoride to synthesise perfluoroaryl-substituted imidazolium tetrafluoroborate salts (Scheme 63). The addition of BF_3 was necessary to form stable salts. In the case of hexafluorobenzene, double substitution occurred, resulting in the formation of a dicationic salt.¹⁸⁹



Scheme 63 $\text{S}_{\text{N}}\text{Ar}$ reaction of pentafluoropyridine with an NHC nucleophile and BF_3 .¹⁹⁰

Finally, another class of carbenes, such as cyclic alkyl amino carbenes (CAACs), proved to undergo $\text{S}_{\text{N}}\text{Ar}$ reactions with Py-F_5 and perfluorotoluene (Scheme 64).¹⁹¹ In these cases, an oxidative addition process occurred, as the carbon oxidation state changed from +2 to +4 and the fluorinated pyridine was added to the carbon-centre. When Me^2CAAC was treated with hexafluorobenzene, double substitution of the arene took place instead.

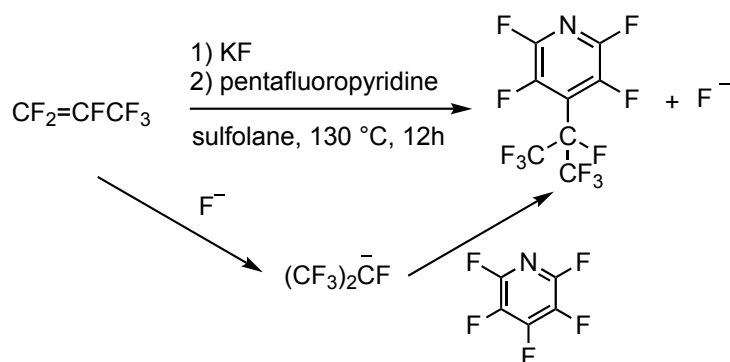


Scheme 64 S_NAr reaction of perfluoro(hetero)aromatics with a CAAC nucleophile.

The ease with which the newly formed C–F bond in these products could be broken by the subsequent addition of a Lewis acid (e.g., BF_3) leading to the formation of perfluoroaryl-substituted 1-pyrrolinium salts, demonstrated the possibility of using these compounds as fluoride transfer or mild fluorinating agents.

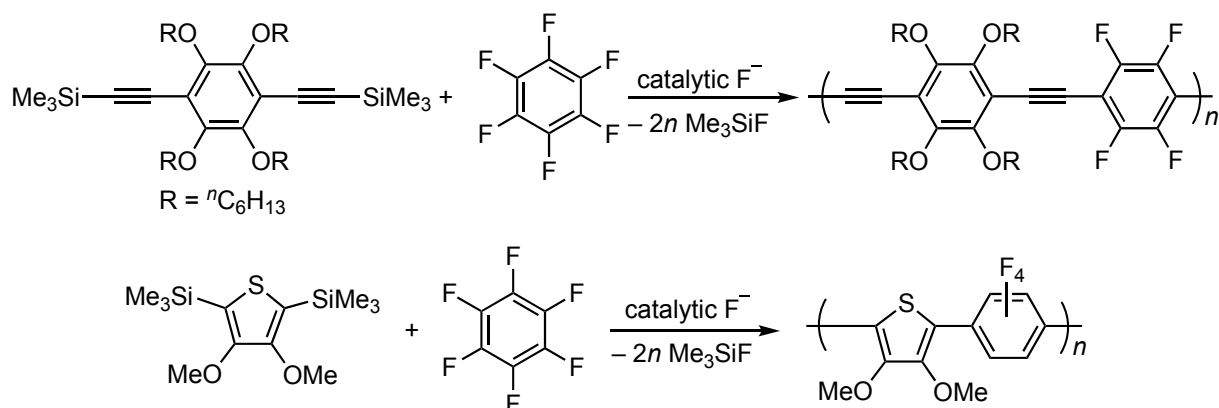
3.1.2.2.2 Charged nucleophiles

Other S_NAr reactions involve the use of anionic carbon-based nucleophiles generated *in situ*. For example, the so-called negative Friedel-Crafts reaction consists of the polyfluoroalkylation of polyfluorinated (hetero)aromatic compounds (Scheme 65). In this transformation, the polyfluorinated carbanions, generated by the reaction between fluoroalkenes and fluoride ions, are trapped by the fluoroaromatic. **Py-F₅** reacts with the widest variety of polyfluoroalkyl groups, resulting in mono- and di-substitutions at 4- and 2-positions.¹⁸²



Scheme 65 Selected example of a negative Friedel-Crafts reaction.

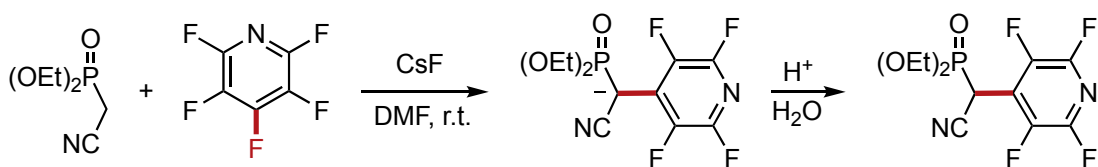
Another approach to generate carbon-centred nucleophiles is through the use of tetraorganosilanes (such as Me_3SiR), considered synthetic equivalents of carbanions R^- . In particular, trimethylsilylethynyl¹⁹² or trimethylsilylthiopene derivatives¹⁹³ underwent polymerisation reactions when treated with electron-poor perfluoroarenes in the presence of a catalytic amount of fluoride anion (Scheme 66).



Scheme 66 Synthesis of polyfluoroaromatic containing polymers.

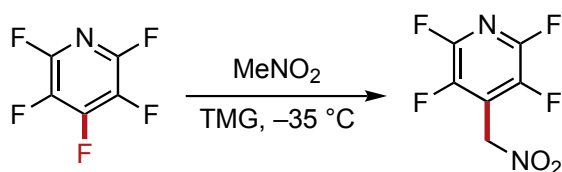
The fluoride ion attacks the Si centre, forming a fluorosilicate ion, enabling the transfer of the R fragment to an electrophile such as a perfluoroarene. This process liberates the C–C coupling product, Me_3SiF and a fluoride ion, restarting the catalytic cycle.

Alternatively, other types of carbanions have been employed for the formation of new C–C bonds in perfluoroarenes. For example, carbanions derived from diethyl methylphosphonates of the type $(\text{EtO})_2\text{P}(\text{O})(\text{CH}_2\text{X})$ (where X is an electron-withdrawing substituent in β -position to the phosphorus) generated by reaction with a base (e.g., CsF or NaH), reacted with perfluorinated aromatics and heteroaromatics yielding the C–C coupling product (Scheme 67).¹⁹⁴ Similarly to the reaction involving ylides in Scheme 60, the negative charge of the carbanion was located in α -position to the phosphorus and a new C–C bond was formed at that position.



Scheme 67 S_NAr reaction of perfluoro(hetero)aromatics with carbocations of methylphosphonate derivatives.

Similarly, the formation of a carbanion derived from the deprotonation of nitroalkanes using strong bases, such as 1,8-diazabicyclo(5.4.0)undec-7-ene (DBU) or 1,1,3,3-tetramethylguanidine (TMG), at low temperatures led to the perfluoro(hetero)arylation of the compound (Scheme 68).¹⁹⁵



Scheme 68 Regioselective defluoroalkylation of polyfluoroarenes with nitroalkanes.

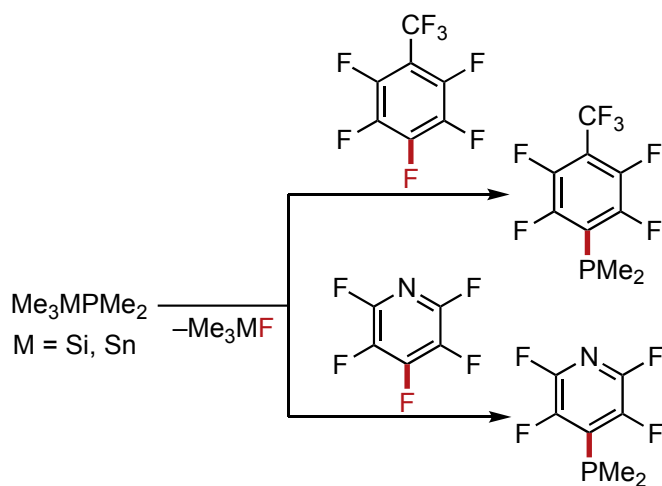
3.1.3 C–F bond activation promoted by phosphorus-containing species

Although phosphorus-containing compounds are generally considered as spectator ligands in complexes with transition metals and are often inert in strong σ -bond activation reactions, there are several reported examples where the phosphine ligand actively participates in the transformation.^{100,152,196} Recent studies demonstrated that phosphorus-containing compounds exhibit the ability to activate C–F bonds even in the absence of metals.¹⁵⁶ The ambiphilic nature of phosphorus, along with its high fluoride affinity, allows for different types of reactivity, acting as both Lewis acid or Lewis base depending on its oxidation state (P^V or P^{III}) and whether they are cationic or neutral species.

Stephan and his group conducted extensive investigations into C–F bond activation and functionalisation reactions promoted by highly Lewis acidic phosphonium^{197–200} and phosphonium cations.^{201,202} However, since this chapter focuses on transformations involving nucleophilic substitutions, C–F bond activation processes assisted by Lewis acids are not addressed here. Nevertheless, representative examples from this research are discussed in chapter 4.1 and more details can be found in the review by Stephan *et al.*²⁰³

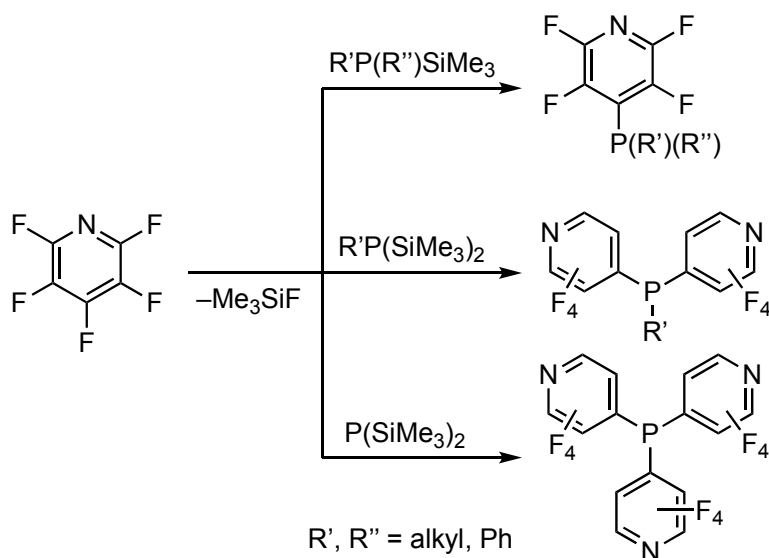
3.1.3.1 Phosphorus-containing Lewis bases

P^{III} Lewis bases can promote the C–F bond activation of electron-poor polyfluoroarenes through S_NAr mechanisms. Many examples in the literature exploit the enhanced basicity of P^{III}-containing species achieved through the use of alkali or *p*-block metal and metalloid phosphides to perform the C–F bond functionalisation of perfluoro(hetero)aromatics. These compounds are formed by treating secondary phosphines with phenyllithium,²⁰⁴ potassium *tert*-butoxide or hydroxide, as well as by reacting triphenylphosphine with lithium,²⁰⁵ sodium or potassium.²⁰⁶ An alternative approach is the formation of compounds with *p*-block metals or metalloids (such as Sn or Si). For example, Mück-Lichtenfeld and coworkers reported the synthesis of a variety of perfluoro(hetero)aryldimethylphosphines through the reaction of Si or Sn-phosphide derivatives and perfluoroarenes (Scheme 69).²⁰⁷



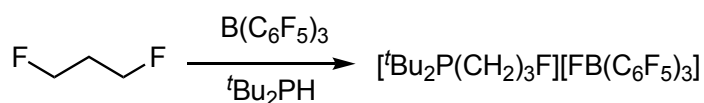
Scheme 69 Synthesis of perfluoro(hetero)aryldimethylphosphines from Si or Sn-phosphide derivatives.

Furthermore, Beletskaya *et al.* demonstrated that mono-, di- or trisilylphosphides performed mono-, double and triple aromatic nucleophilic substitution reactions on **Py-F₅** (Scheme 70).²⁰⁸



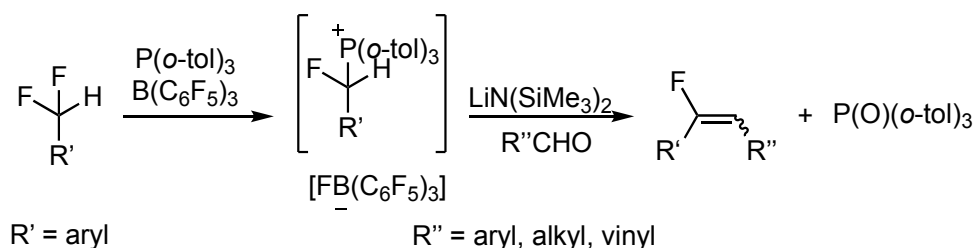
Scheme 70 Aromatic nucleophilic substitution reactions on pentafluoropyridine by silylphosphide derivatives.

An alternative approach involves the use of P^{III} Lewis bases incorporated into Frustrated Lewis Pairs (FLPs) for the functionalisation of fluoroalkanes. Stephan *et al.* demonstrated that it is possible to stoichiometrically activate fluoroalkanes using the B(C₆F₅)₃/^tBu₃P FLP, leading to the formation of the corresponding fluoroborate salt and the alkylated phosphonium (Scheme 71).²⁰⁹ The generation of the alkylation product resulted from the weakening of the C–F bond through the interaction of the fluoride with the Lewis acid, thus making the carbon more electrophilic.



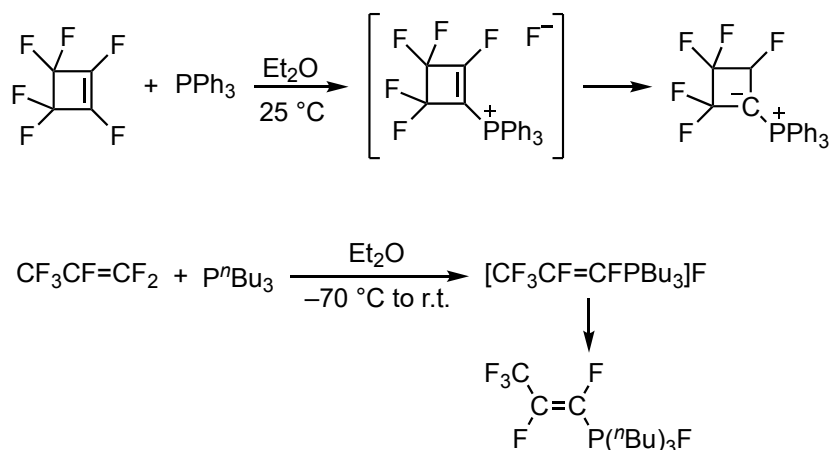
Scheme 71 Fluoroalkanes C–F bond activation assisted by FLPs.

^{209,209}Young and coworkers employed an FLP formed by P(*o*-tol)₃ and B(C₆F₅)₃ to activate the C–F bond in *gem*-difluoroalkanes. This activation led to the formation of an α-fluoroalkylphosphonium product, which subsequently underwent a Wittig reaction to produce monofluoroalkenes (Scheme 72).²¹⁰



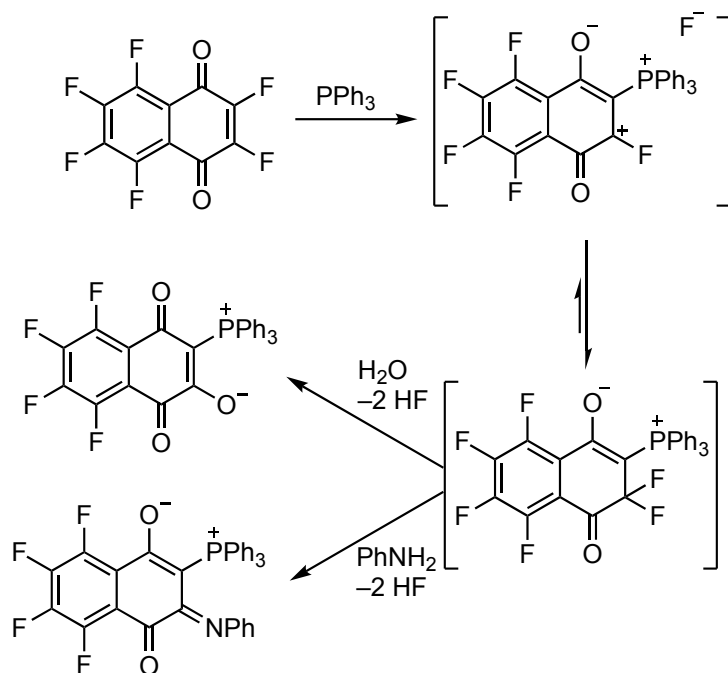
Scheme 72 Synthesis of monofluoroalkenes *via* C–F bond activation of fluoroalkanes with FLPs.

Nevertheless, examples where simple tertiary phosphines are used in C–F bond functionalisation reactions, without requiring activation by metals or metalloids and without the assistance of a Lewis acid, are scarce. In the 1970s Burton and coworkers were the first to demonstrate that simple phosphines such as PPh₃ and PⁿBu₃ were sufficiently nucleophilic to attack perfluorinated cyclic alkenes, leading to the formation of stable phosphonium ylides, as well as perfluorinated linear terminal alkenes, resulting in the production of a fluorophosphorane, at room temperature (Scheme 73).²¹¹



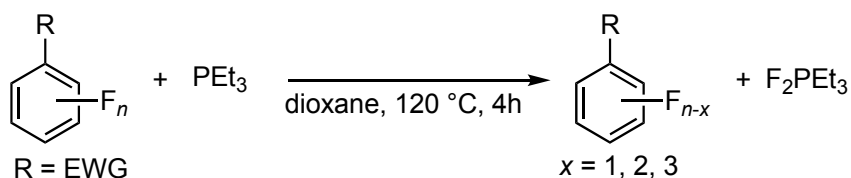
Scheme 73 Nucleophilic substitution reactions of simple phosphines (PPh₃ and PⁿBu₃) with perfluorinated alkenes.

A few other examples involve S_NAr reactions of poly- and perfluoroaromatic compounds by tertiary phosphines. For instance, the nucleophilic attack of PPh₃ on fluorinated quinones (in Scheme 74 hexafluoro-1,4-naphthoquinone is shown) resulted in the formation of a phosphonium salt.^{56,212} This would subsequently hydrolyse in contact with water or react with aniline to form the zwitterionic compounds reported in Scheme 74.



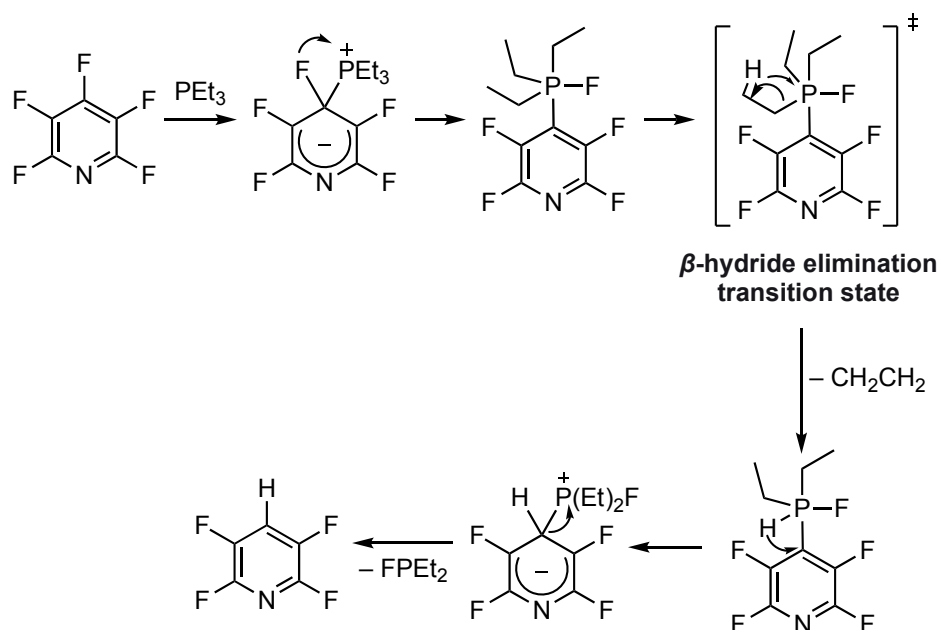
Scheme 74 Synthesis of phosphonium betaines *via* PPh₃-assisted C–F bond activation.

Furthermore, García and coworkers reported the hydrodefluorination reaction of a series of polyfluoro(hetero)aromatics promoted by PEt₃ as the sole defluorinating agent at high temperatures (Scheme 75).^{155,156}



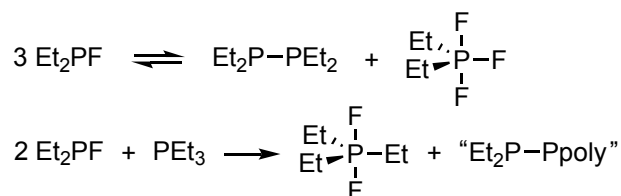
Scheme 75 Hydrodefluorination of polyfluoro(hetero)aromatics promoted by PEt₃.

The initially proposed mechanism envisioned the phosphine itself as the proton source for the hydrodefluorination product (Scheme 76). The process started with the nucleophilic attack of the phosphine on the aromatic ring, followed by fluoride transfer to generate a fluorophosphorane. Subsequently, β -hydride elimination occurred, releasing ethylene and a fluorohydridophosphorane. Hydride transfer to the aromatic ring resulted in the formation of the hydrodefluorination product and the liberation of a fluorophosphine.¹⁵⁶



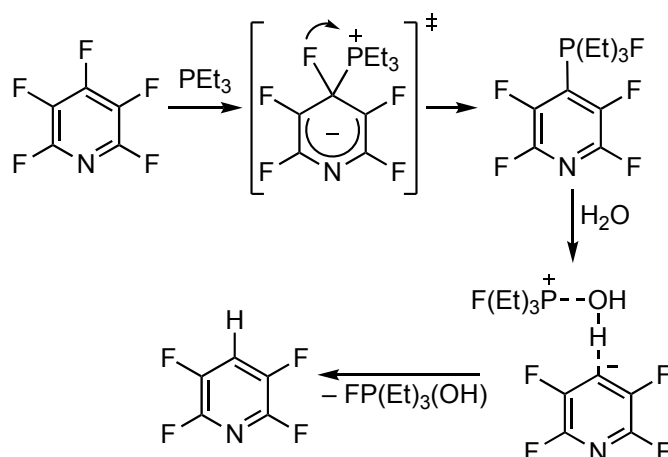
Scheme 76 Initial mechanistic proposal for the PEt_3 -assisted hydrodefluorination reaction.

The fluorophosphine generated would undergo further decomposition reactions, ultimately resulting in the formation of a difluorophosphorane, along with dimerisation or polymerisation (Scheme 77).



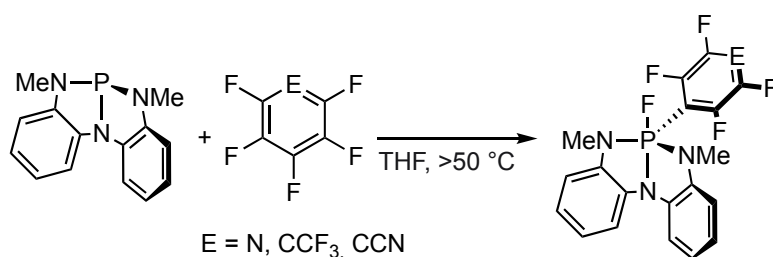
Scheme 77 Proposed decomposition processes of the fluorophosphine.

In a subsequent study supported by computational calculations, the same authors proposed a more energetically feasible mechanism in which the proton source was trace water in the system.¹⁵⁵ This revised mechanism retained the nucleophilic attack and the formation of a fluorophosphorane (Scheme 78), similar to the initial proposal. Then, the introduction of a water molecule in the reaction resulted in the formation of an ion pair, where the $\text{P}-\text{C}(sp^2)$ bond had broken and the water molecule was positioned between the aromatic compound and the phosphine. Ultimately, the formation of the new $\text{C}(sp^2)\text{-H}$ bond led to the release of the hydrodefluorination product and $\text{PEt}_3(\text{F})(\text{OH})$.



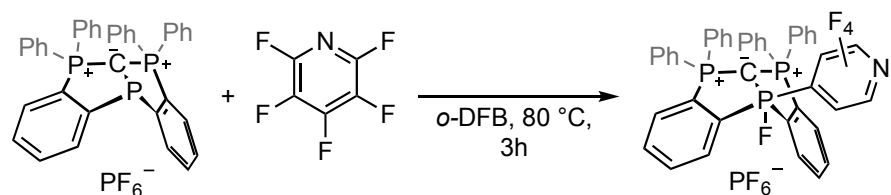
Scheme 78 Revised mechanism for the PEt_3 -assisted hydrodefluorination reaction.

A sophisticated investigation by Radosevich *et al.* demonstrated the ability of a C_3 -symmetric phosphorus triamide compound to conduct regioselective $\text{S}_{\text{N}}\text{Ar}$ reactions on perfluorotoluene, **Py-F₅** and pentafluorobenzonitrile, followed by fluoride transfer to the phosphorus-centre, resulting in a stable perfluoroaryl-substituted fluorophosphorane (Scheme 79).²¹³ As the so-formed species is reminiscent to the OA product in transition-metal-based catalytic cycles, the authors conducted preliminary stoichiometric studies to develop a metallomimetic hydrodefluorination catalytic system. Further details on this work are discussed in chapter 4.1.4.



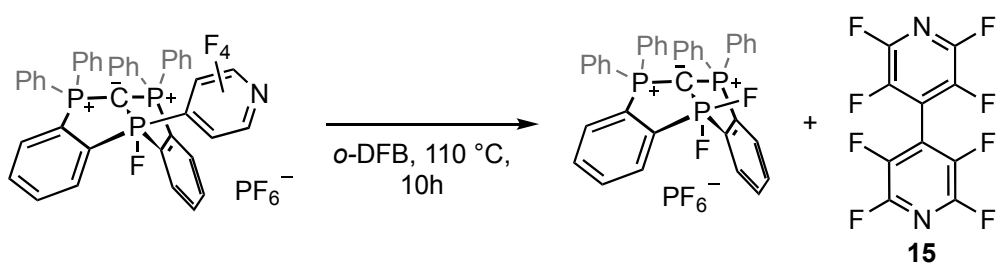
Scheme 79 $\text{S}_{\text{N}}\text{Ar}$ reaction of perfluoro(hetero)aromatics by a σ^3 -phosphorus triamide compound and subsequent fluoride transfer.

More recently, Dobrovetsky and coworkers reported the use of a geometrically constrained P^{III} species featuring an hexaphenylcarbodiphosphoranyl-based CCC pincer-type ligand as a catalyst in the hydrodefluorination and C–N coupling reactions of electron-poor perfluoro(hetero)arenes in the presence of silanes and silylamides in *ortho*-difluorobenzene (*o*-DFB) (Scheme 80).²¹⁴ Once again, the initial step of the catalytic cycle (supported by both experimental and computational evidence) involved the nucleophilic attack of the P nucleophile on the fluorinated aromatic substrate and the fluoride transfer (akin to Radosevich's example reported in Scheme 79).



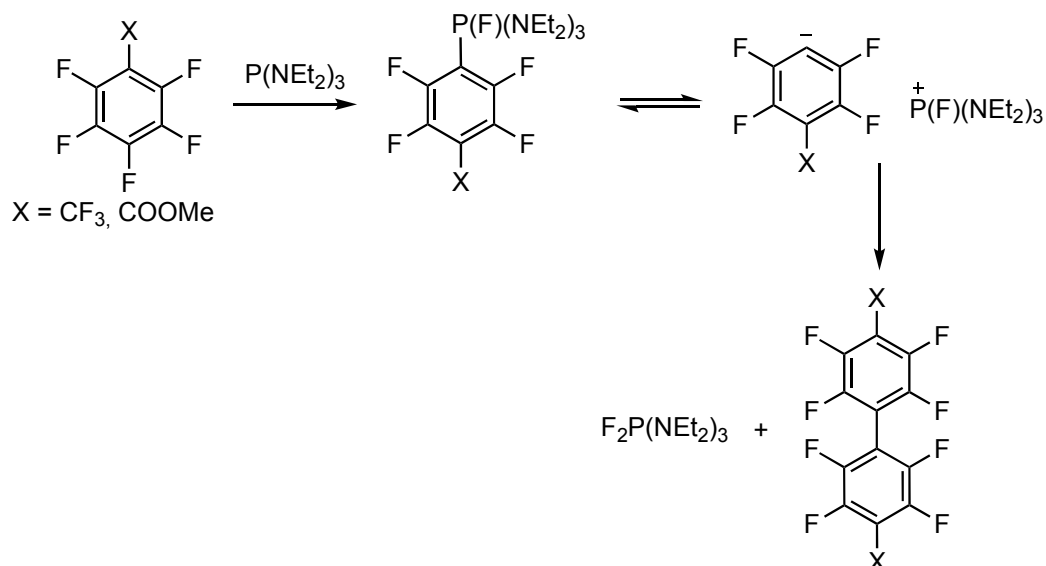
Scheme 80 S_NAr reaction of perfluoro(hetero)aromatics by a geometrically constrained P^{III} species.

In the same study, Dobrovetsky and his group reported an alternative reactivity within this system. Heating the fluorophosphorane, obtained through S_NAr reaction and fluoride transfer, resulted in the formation of the homocoupling product 4,4'-perfluorobipyridine (**15**) and the difluorophosphorane (Scheme 81). The proposed mechanism involves a series of ligand exchanges followed by elimination of the final product.



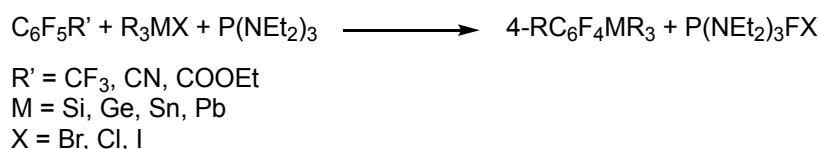
Scheme 81 Unexpected synthesis of **15** and the difluorophosphorane.

A similar reactivity involving $P(NEt_2)_3$ has already been reported. Yakobson²¹⁵ and, later, Chernega and coworkers²¹⁶ reported the reductive coupling of perfluorinated arenes and phosphine fluorination. Their research showed that treatment of triamidophosphines with octafluorotoluene, methyl pentafluorobenzoate or **Py-F₅** led to the formation of the reductive homocoupling product and the corresponding difluorophosphorane. The proposed mechanism consists of the nucleophilic attack of the phosphine to the aromatic ring in *para*-position, fluoride transfer and subsequent dissociation of the polyfluoroaromatic anion forming an ion pair with fluorophosphonium (Scheme 82). The (hetero)aryl anion then undergoes another S_NAr reaction resulting in the homocoupling product.



Scheme 82 Proposed mechanism for the reductive coupling of perfluoroarenes promoted by P(NEt₂)₃ in Et₂O.

Interestingly, Furin exploited this reactivity by defining a protocol for the synthesis of polyfluoroaryl-containing silanes, germanes, stannanes and plumbanes using P(NEt₂)₃ (Scheme 83).²¹⁷ Apparently, the generated perfluoroaryl anion preferentially attacked metals and metalloids bearing more mobile halogen atoms (like Br, Cl and I) than F.



Scheme 83 General reaction for the metalation of perfluoroaromatics promoted by P(NEt₂)₃.

3.1.4 Synthesis of fluorophosphoranes

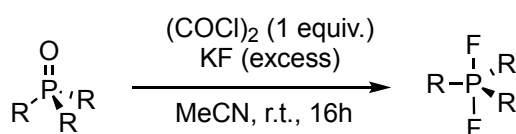
As demonstrated in the previous section, the interaction of phosphines with polyfluoroaromatic compounds often results in the production of mono- and difluorophosphoranes. Fluorophosphoranes are fluorinated neutral P^V compounds of the formula R_nPF_{5-n}, where R can be an aliphatic or aromatic group.

Whether in their neutral or charged states (either cationic or anionic), fluorinated P^V-containing species exhibit versatile applications in organocatalysis. These species are involved in C–F bond functionalisation,²⁰⁰ carbonyl activation,^{199,218} olefin hydrogenation,²¹⁹ CO₂ capture²²⁰ and

hydroxylation processes.^{197,199} Moreover, they are used as electrolytes,²²¹ ionic liquids,²²² deoxyfluorinating agents^{223,224} and for ¹⁸F-radiolabeling.²²⁵

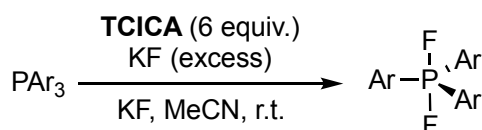
Several methods have been developed for the synthesis of fluorophosphoranes, with the most common approaches involving the fluorination of substituted phosphines using fluorinating agents such as XeF₂,²²⁶ F₂,²²⁷ HF,²²⁸ COF₂,²²⁹ N₂F₄,²³⁰ NF₃,²³¹ N₂F₂,²³¹ N₃CF₂R²³² and IF₅.²³³ Alternative methods include the use of alkyl- or arylchlorophosphines (or phosphoranes) in combination with metalloid fluorides like SbF₅, AsF₃ and SbF₃ as fluorinating agents.²³⁴ Triorganophosphine sulfides and tetraalkyldiphosphine disulfides can undergo conversion into difluoro- and trifluorophosphoranes, respectively, through fluorination with AsF₃ and SbF₃. Additionally, phosphine oxides, phosphonic acids and phosphinic acids can be transformed into difluoro-, trifluoro- and tetrafluorophosphoranes *via* reaction with SF₄.^{235,236}

Remarkably, Togni *et al.* developed a deoxygenative fluorination method that involved the use of mild fluorinating reagents with phosphine oxides, resulting in the production of di-, tri- and tetrafluorophosphoranes.²³⁹ This process employed a combination of oxalyl chloride and potassium fluoride as fluorinating reagents and exhibited versatility across a broad range of phosphine oxides (Scheme 84). Furthermore, this approach also enabled the formation of hexafluorophosphate salts and fluorinated antimony and arsenic compounds.



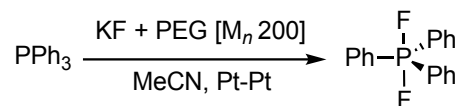
Scheme 84 Synthesis of difluorophosphoranes *via* fluorination of phosphine oxides with (COCl)₂ and KF.

A recently developed approach involved the use of mild oxidative fluorinating agents, such as trichloroisocyanuric acid (TCICA) and KF to synthesise a wide variety of fluorinated phosphoranes, including difluorophosphoranes derived from tertiary phosphines (Scheme 85).²⁴⁰ Also in this case, the system was extended to the synthesis of hexafluorophosphate salts and fluorinated arsenic compounds.



Scheme 85 Synthesis of difluorophosphoranes *via* fluorination of phosphines with TCICA and KF.

Moreover, an electrochemical approach has been developed involving the anodic fluorination of triphenylphosphine in the presence of poly(ethylene glycol) as an additive and KF, acting as both the fluorine source and supporting electrolyte (Scheme 86).^{241,242}

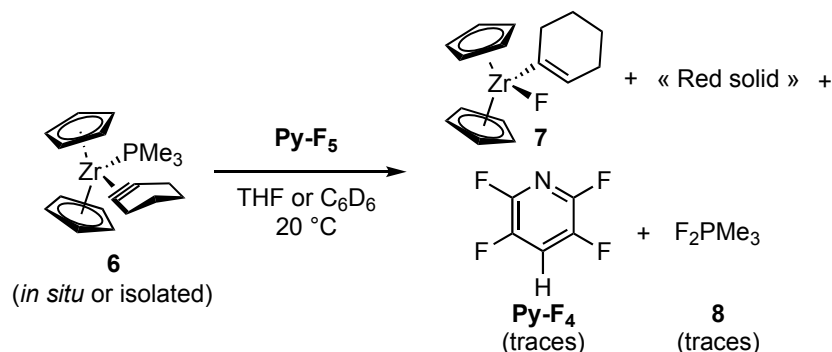


Scheme 86 Electrochemical fluorination of PPh₃ using KF.

Additionally, methods for the photochemical oxidative fluorination of tertiary phosphines have been developed. For instance, triarylphosphines and phosphites can be transformed into their corresponding difluorophosphoranes using TiO₂ as a photocatalyst and AgF as a fluoride source.²⁴³

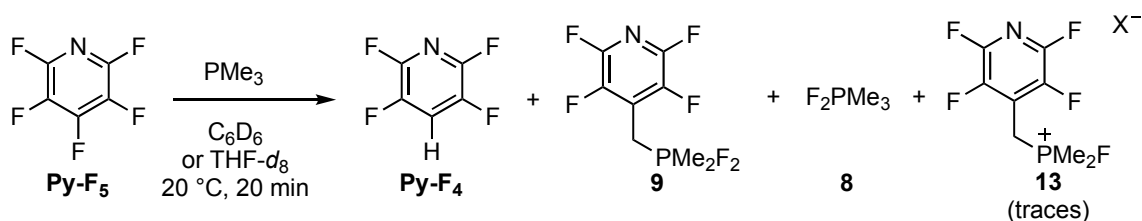
3.2 Aims and objectives

In chapter 2.3.2 it was demonstrated that the zirconocene-PMe₃ adduct **6** reacted at room temperature with **Py-F₅** to form 1-cyclohexenylzirconocene fluoride (**7**), an unidentified solid and traces of other fluorine- and phosphorus-containing products (Scheme 87).



Scheme 87 Reaction of complex **6** with an equimolar amount of **Py-F₅** in THF or C₆D₆ at 20 °C.

Control experiments pointed out that the dissociation of the PMe₃ ligand and subsequent reaction with the fluorinated heteroaromatic led to the generation of F₂PMe₃ and the 4-methylenetetrafluoropyridine-substituted difluorophosphorane (**9**), which would then trigger the formation of **7**. A reactivity test between equimolar amounts of PMe₃ and **Py-F₅** showed the immediate formation of **Py-F₄**, **9**, F₂PMe₃, traces of a fluorophosphonium salt (**13**) along with unreacted PMe₃ (Scheme 88).



Scheme 88 Reaction between **Py-F₅** (1 equiv.) and **PMe₃** (1 equiv.) in THF or C_6D_6 after 20 minutes at 20 °C.

Considering the unexpected reactivity between **PMe₃** and **Py-F₅**, this chapter further explores this chemistry. The primary objectives include:

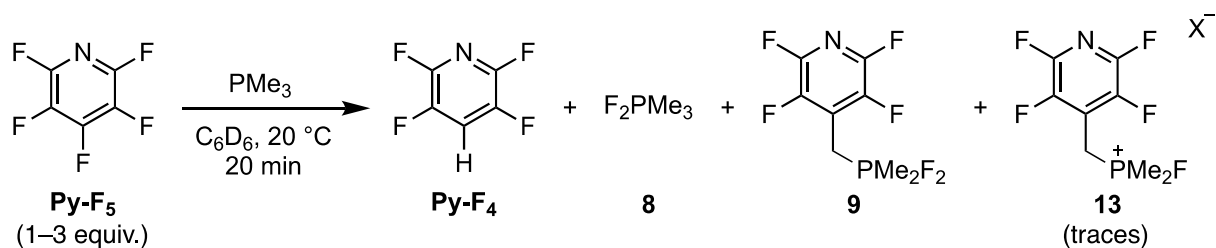
- Investigating the reactivity of **Py-F₅** with different sterically hindered phosphines to assess the possibility to circumvent this undesired reactivity; the final aim would be to synthesise a new phosphine-zirconocene adduct that enables the 1,3-CF addition reaction of **Py-F₅**.
- Modifying several parameters of the system (such as solvent, temperature and reagent ratios) to gain a better insight into the reaction mechanism.

3.3 Results and discussion

3.3.1 Spectroscopic characterisation of the products

The stoichiometric reactivity between **PMe₃** and **Py-F₅**, as discussed in section 2.3.2, was further investigated to gain a better understanding of the system. The objective was to assess whether changing the system conditions, including the phosphine, solvent, temperature and reagent ratio, could limit or suppress this reactivity.

The preparation of an equimolar solution of **PMe₃** and **Py-F₅** in C_6D_6 triggered the formation of **Py-F₄**, **8** and **9**, along with a fourth minor species **13** not unambiguously identified and unreacted **PMe₃**, according to NMR analysis (Scheme 89).



Scheme 89 Reaction of **Py-F₅** (1–3 equiv.) and **PMe₃** (1 equiv.) in **C₆D₆** after 20 minutes at 20 °C.

Compound **8** is characterised by a doublet of multiplets at $\delta = -5.5$ ppm in the ^{19}F NMR spectrum and a triplet of multiplets at $\delta = -16.2$ ppm in the ^{31}P NMR spectrum, both sharing the same coupling constant ($^1J_{\text{PF}}$) of 544 Hz (Figure 17). As previously discussed in chapter 2.3.2, **9** displays similar spectroscopic features to **8**, exhibiting a doublet of multiplets at $\delta(^{19}\text{F}) = -9.7$ ppm ($^1J_{\text{PF}} = 595$ Hz) and a triplet of multiplets at $\delta(^{31}\text{P}) = -20.5$ ppm ($^1J_{\text{PF}} = 595$ Hz). The chemical shift, multiplicity and large coupling constants of these signals strongly suggest the presence of the $-\text{PF}_2$ fragment characteristic of difluorophosphoranes. Additionally, **8** features a doublet of triplets resonance at $\delta(^1\text{H}) = 1.42$ ppm ($^2J_{\text{HP}} = 17.3$ Hz, $^3J_{\text{HF}} = 12.3$ Hz; C_6D_6), originating from the coupling of the methyl protons with P and F nuclei (Figure 18). Similarly, a signal at $\delta(^1\text{H}) = 1.34$ ppm (dt, $^2J_{\text{HP}} = 17.3$ Hz, $^3J_{\text{HF}} = 12.5$ Hz; C_6D_6) belongs to species **9** and represents the two methyl groups. This compound is also associated with an additional, more downfield, doublet of triplets of triplets corresponding to the protons of the methylene bridge at $\delta(^1\text{H}) = 3.09$ ppm ($^2J_{\text{HP}} = 23.5$ Hz, $^3J_{\text{HF}} = 5.0$ Hz, $^4J_{\text{HF}} = 1.8$ Hz). **Py-F₄** is characterised by two multiplets at $\delta(^{19}\text{F}) = -141.2$ ppm and -92.4 ppm, corresponding to the four *ortho*- and *meta*-fluorine substituents, respectively. Analogously, **9** displays two multiplets at $\delta(^{19}\text{F}) = -144.9$ and -93.1 ppm representing the four fluorine atoms of the pyridine ring. The identity of **9** was further validated through ^{13}C and 2D NMR experiments.

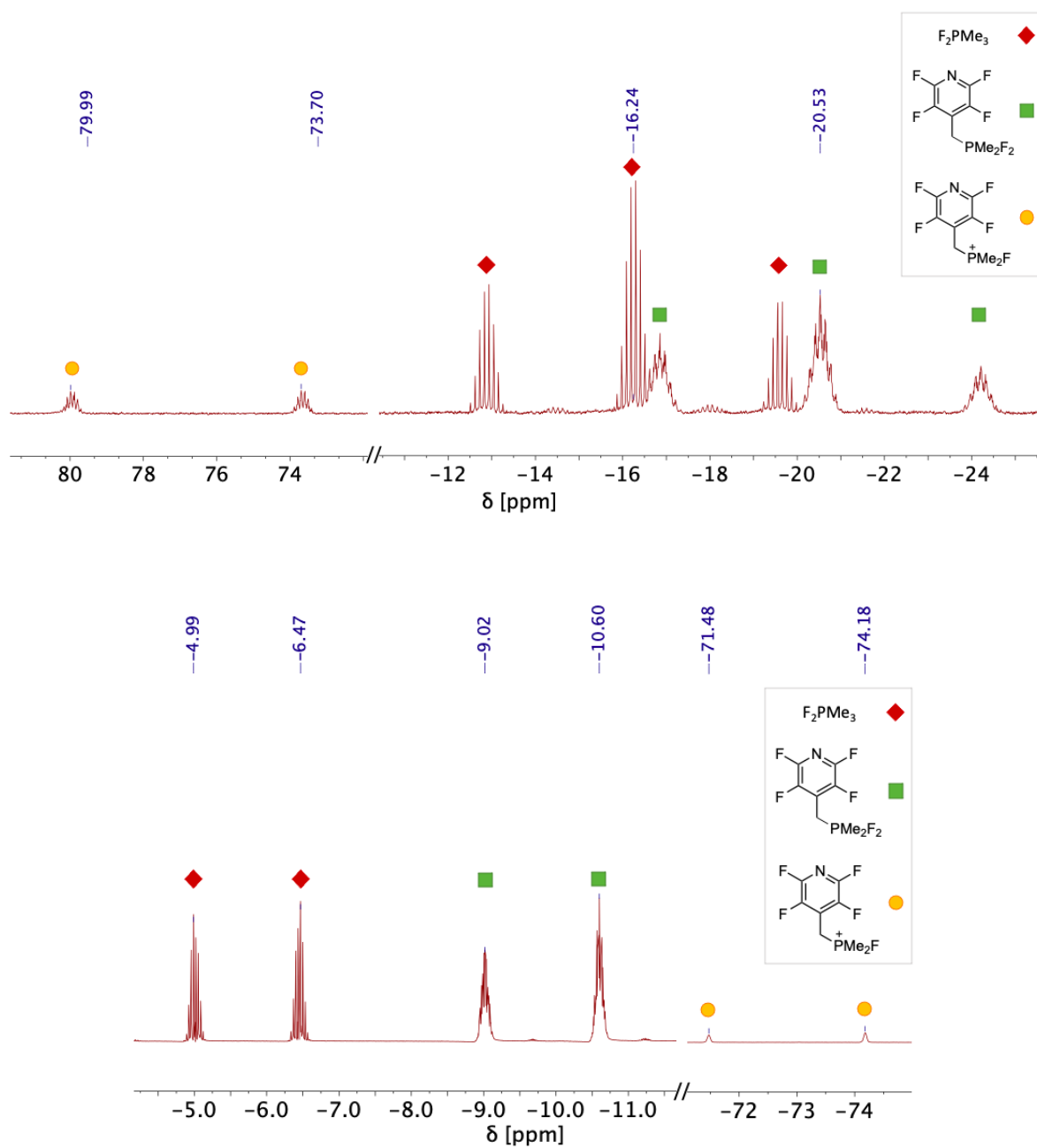


Figure 17 ^{31}P NMR (162 MHz, C_6D_6 , spectrum on the top) and ^{19}F NMR (377 MHz, C_6D_6 , spectrum on the bottom) of the reaction of **Py-F₅** (3 equiv.) and **PMe₃** (1 equiv.) in C_6D_6 after 20 minutes at 20 °C.

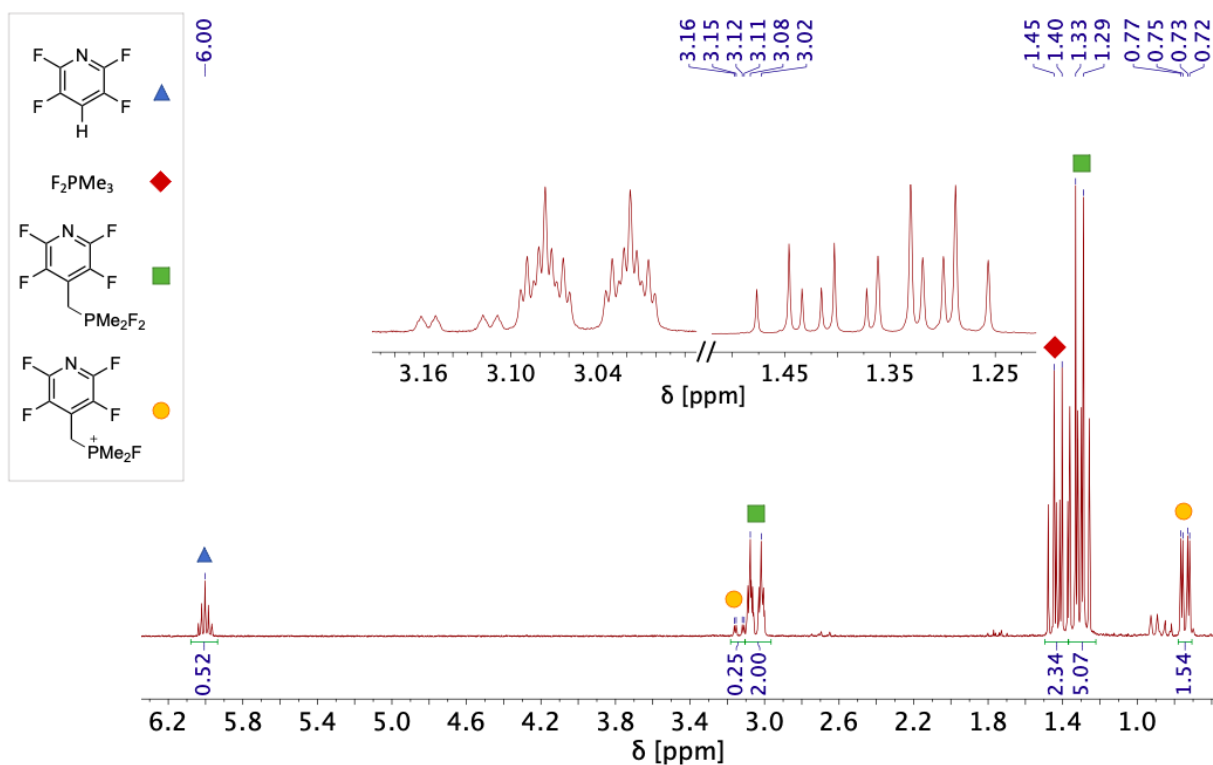
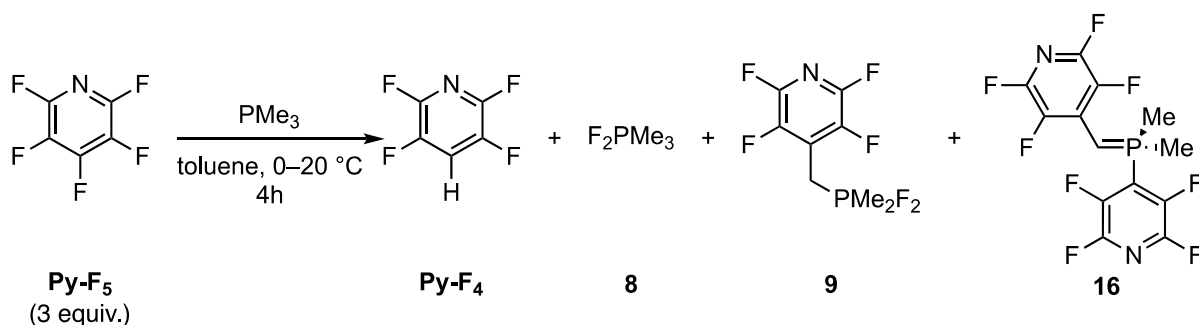


Figure 18 ^1H NMR (400 MHz, C_6D_6) of the reaction of **Py-F₅** (3 equiv.) and PMe_3 (1 equiv.) in C_6D_6 after 20 minutes at 20 °C.

Further evidence of the identity of species **9** was provided by GC(EI)-MS analysis of the crude reaction mixture showing the presence of the molecular radical cation $[\text{H}_8\text{C}_8\text{F}_6\text{NP}]^+$ of 263.02931 m/z (3.10 ppm deviation from theoretical) and the characteristic fragmentation pattern of the compound.

A fourth minor species **13** was present in the crude reaction mixture but could not be unambiguously identified, although it shares similar spectroscopic features with **9**. It is characterised by two doublets of doublets of triplets at $\delta = 0.74$ ($^2J_{\text{PH}} = 14.6$ Hz, $^3J_{\text{FH}} = 4.6$ Hz, $^4J_{\text{FH}} = 1.0$ Hz) and 3.14 ppm ($^2J_{\text{PH}} = 16.7$ Hz, $^3J_{\text{FH}} = 3.8$ Hz, $^4J_{\text{FH}} = 1.0$ Hz) in C_6D_6 in the ^1H NMR spectrum, suggesting the presence of a $\text{Me}_2(\text{F})\text{P}-$ fragment linked to the pyridinic ring through a methylene bridge at the 4-position. Additionally, the doublet of multiplets detected in both the ^{31}P and ^{19}F NMR spectra exhibits a $^1J_{\text{PF}}$ of 1021 Hz, which is significantly larger than those encountered so far. Furthermore, the signal in the ^{31}P NMR spectrum is located at $\delta = 76.2$ ppm, a considerably more downfield chemical shift than the signals belonging to compounds **8** and **9**. These two last features align with what is reported in the literature for fluorophosphonium salts,²⁴⁵ even though no trace of the negatively charged counterpart could be detected. Ions such as PF_6^- or, assuming some reactivity due to etching of the reaction flask glass by released HF, BF_4^- or SiF_5^- were not evident in the ^{19}F NMR spectra.

The reaction in Scheme 89 was scaled up to obtain a sufficient quantity of product for the isolation and crystallisation of difluorophosphorane **9**. Due to the high reactivity of the system, the following reaction protocol was adapted: PMe_3 was added dropwise to a cold solution ($0\text{ }^\circ\text{C}$) of **Py-F₅** in toluene. After 4 hours at $20\text{ }^\circ\text{C}$, the NMR analysis showed the formation of **Py-F₄**, F_2PMe_3 , **9** and an additional product **16** (in a 4:1 **9**:**16** ratio) (Scheme 90). Compound **16** corresponds to an ylide bearing two tetrafluoropyridyl groups, one directly bonded to the P centre and the other to the P=C carbon.



Scheme 90 Reaction mixture obtained after heating up to $20\text{ }^\circ\text{C}$ for 4 hours a cold solution ($0\text{ }^\circ\text{C}$) of PMe_3 (1 equiv.) and **Py-F₅** (3 equiv.) in toluene.

In its ^1H NMR spectrum in C_6D_6 , a doublet was observed at $\delta = 2.71\text{ ppm}$ (d, $^2J_{\text{HP}} = 18.4\text{ Hz}$) corresponds to the P=C–H proton, with both the chemical shift and the $^2J_{\text{HP}}$ consistent with similar ylides reported in the literature.^{246,247} Another doublet at $\delta = 0.92\text{ ppm}$ (d, $^2J_{\text{HP}} = 13.8\text{ Hz}$) represents the two methyl groups. The correlation of these peaks in the ^1H - ^{31}P HMBC spectrum to a multiplet at $\delta(^{31}\text{P}) = -1.7\text{ ppm}$ confirms the absence of a P–F fragment in this species. ^1H - ^{19}F HMBC and ^{19}F COSY showed that four multiplets centred at $\delta = -88.3, -97.7, -135.0, -155.1\text{ ppm}$, corresponding to the *ortho*- and *para*-F of the two pyridines, belong to **16**.

Crystals suitable for a sc-XRD analysis were grown through vapour diffusion of pentane, as an antisolvent, into a concentrated toluene solution containing compounds **9** and **16**. However, only crystals of compound **16** were obtained and its molecular structure is depicted in Figure 19.

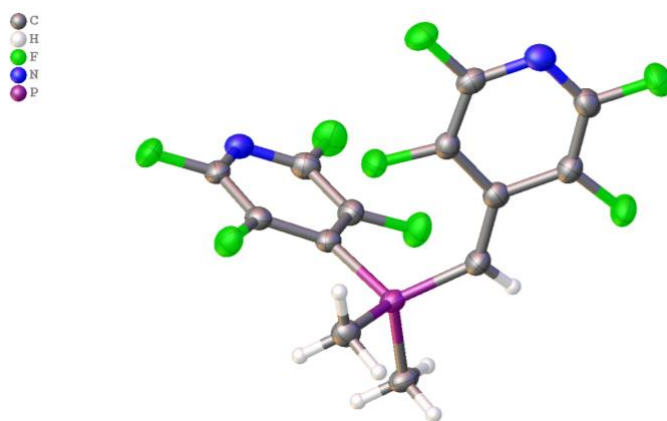
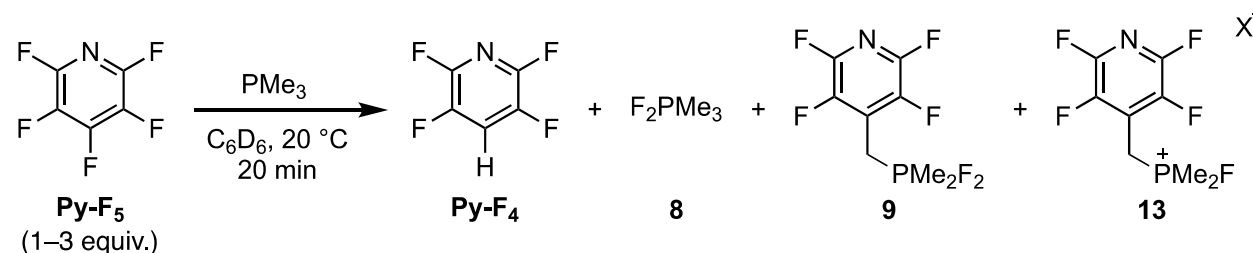


Figure 19 Molecular structure of **16** in the solid. Ellipsoids drawn at the 50% probability level.

The P=C bond length of compound **16** is 1.707(17) Å, which is comparable to the distance of the same bond in simple ylides such as Me₃P=CH₂ (1.678(2) Å)²⁴⁸ and ⁱPr₃P=CMe₂ (1.731(3) Å).²⁴⁹ This bond length is not significantly influenced when comparing ylides with a simple²⁴⁷ and fluorinated aryl²⁵⁰ on the carbon of the P=C bond, remaining between 1.693(2) and 1.757(4) Å, respectively. In compound **16**, the P–C^{pyr} length is longer (1.842(17) Å), along with the P–CH₃ bond distance (1.794(18), 1.797(18) Å), consistent with the lengths reported in the literature.^{247–250}

3.3.2 Analysis of experimental conditions

Different parameters, including temperature, reagent ratio, phosphine and solvent were screened at an NMR scale. Lowering the system temperature to –40 °C resulted in the same products as obtained in Scheme 89 with a comparable distribution. Using a 3:1 **Py-F**₅/PMe₃ ratio, the phosphine was completely consumed, but some **Py-F**₅ remained (Table 3).

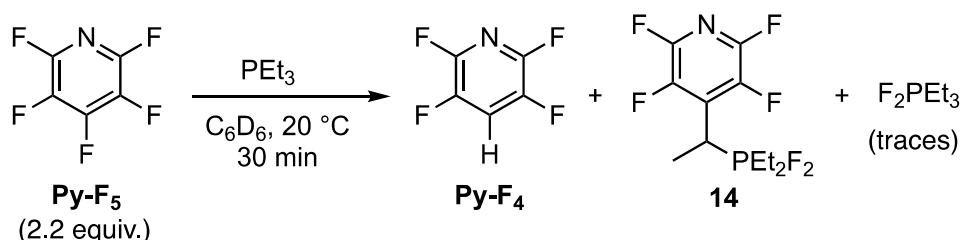


Product distribution ^a	PMe ₃	Py-F ₄	8	9	13
1 equiv. Py-F₅	21%	25%	20%	28%	6%
3 equiv. Py-F₅	0%	28%	30%	36%	6%

Table 3 Product distribution from the reaction of **Py-F**₅ (1–3 equiv.) and PMe₃ (1 equiv.) in C₆D₆ after 20 minutes at 20 °C. ^a According to ¹⁹F NMR analysis.

Note that no traces of ylide **16** or similar ylides were detected by NMR analysis in these tests and in the following experiments.

Subsequently, the possibility of using PEt_3 instead of PMe_3 as nucleophile was considered. The slightly higher steric hindrance of the ethyl group compared to the methyl group and the harsh reaction conditions (140 °C, 3 days) used by García *et al.*¹⁵⁶ for the reaction of PEt_3 with various fluorinated compounds, including pentafluoropyridine, pointed to a reduced reactivity compared to PMe_3 . Nevertheless, a control experiment on the reactivity of triethylphosphine towards **Py-F₅** revealed that the former exhibited comparable reactivity to its methyl analogue. The 4-methanetriyltetrafluoropyridine-substituted difluorophosphorane **14**, **Py-F₄** and traces of F_2PET_3 were selectively produced (Scheme 91).



Scheme 91 Reaction of **Py-F₅** (2.2 equiv.) and PMe_3 (1 equiv.) in C_6D_6 after 30 minutes at 20 °C.

The formation of difluorophosphoranes was observed also by Perutz and coworkers when they treated $\text{Ni}(\text{COD})_2$ and an excess of PEt_3 with different perfluoro(hetero)aromatics.^{251,252} Although the authors could not precisely identify the difluorophosphoranes, the NMR peaks reported when using **Py-F₅** are consistent with those identified as species **14** and F_2PET_3 in our system. Initially, it was proposed that the formation of these P^{V} species was promoted by nickel complexes. However, subsequent reactivity tests revealed that the formation of difluorophosphoranes and **Py-F₄** occurred even in the absence of the metal complex.

Next, a set of phosphines with varying steric hindrance was selected to investigate the scope and limits of this reactivity (Figure 20). These reactions were monitored by multinuclear NMR, GC(EI)-MS or ESI-MS.

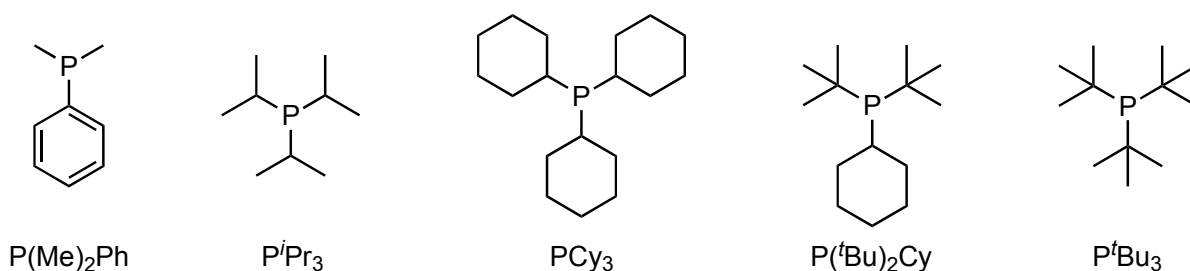
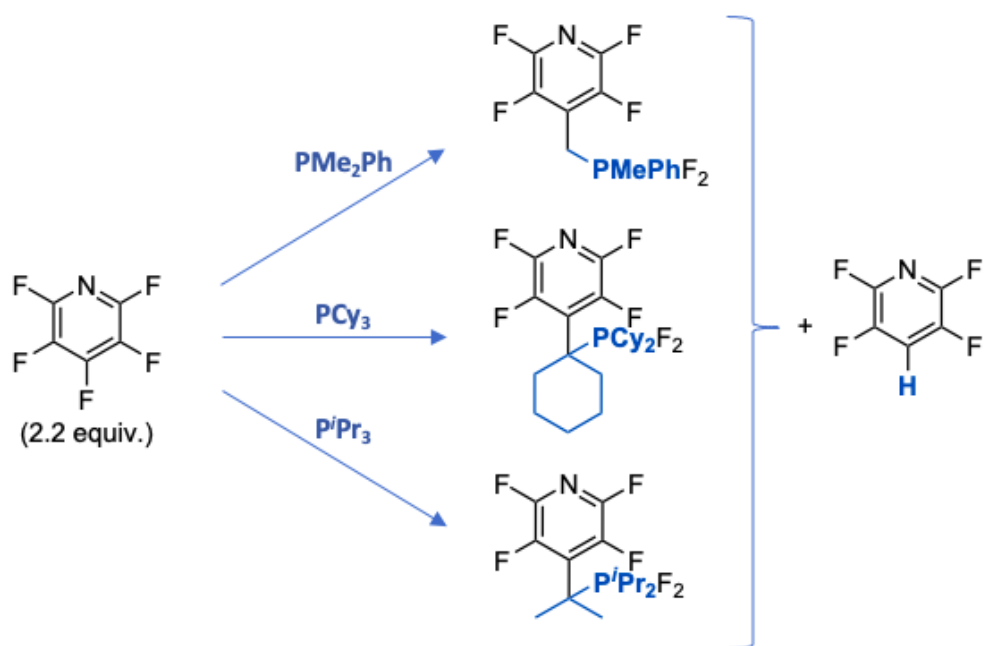


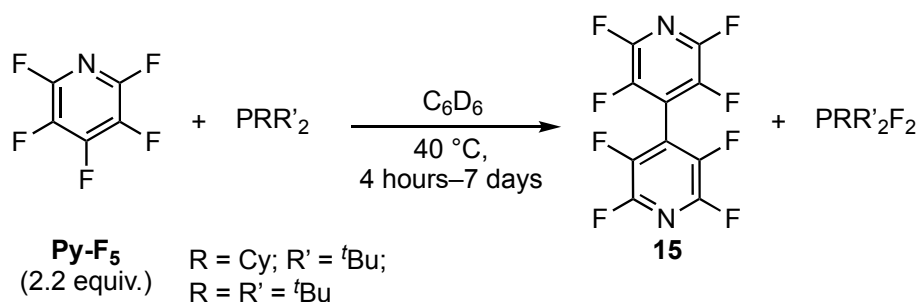
Figure 20 Set of tested phosphines.

Dimethylphenylphosphine (PMe_2Ph), triisopropylphosphine (P^iPr_3) and tricyclohexylphosphine (PCy_3) reacted with 2.2 equivalents of **Py-F₅** (vs. PR_3) in C_6D_6 within 30 minutes at 20 °C. The reactions selectively yielded the expected **Py-F₄**, the tetrafluoropyridyl-substituted phosphorane (in a 1:1 ratio) and, in some cases, traces of simple difluorotriorganophosphorane (Scheme 92). The phosphine was quantitatively consumed and only traces of unreacted **Py-F₅** remained in the system.



Scheme 92 Reactivity tests on a set of PR_3 (1 equiv.) with **Py-F₅** (2.2 equiv.) in C_6D_6 after 1 hour at 20 °C.

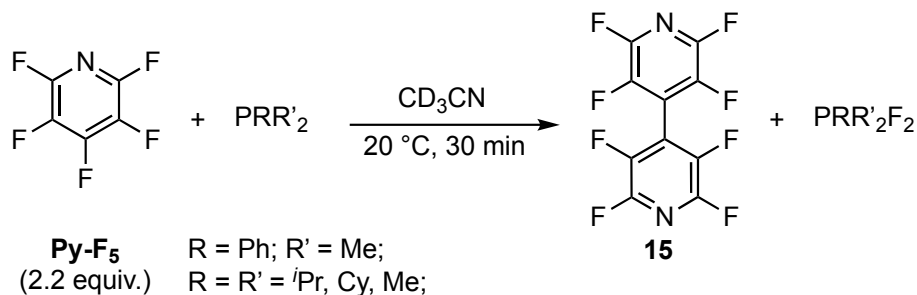
In contrast, di-*tert*-butyl-cyclohexylphosphine ($\text{P}^t\text{Bu}_2\text{Cy}$) and tri-*tert*-butylphosphine (P^tBu_3) exhibited a slow reaction with **Py-F₅** (taking 4 hours and 7 days at 40 °C, respectively, to achieve complete consumption of the phosphine). These reactions resulted in the formation of **15** and the corresponding simple difluorophosphoranes in a 1:1 ratio (vs. **15**) (Scheme 93).



Scheme 93 Reactivity of $\text{P}^t\text{Bu}_2\text{Cy}$ and P^tBu_3 with **Py-F₅** in C_6D_6 at 40 °C for 4 hours and 7 days, respectively.

Product **15** exhibited two multiplets at $\delta(^{19}\text{F}) = -88.2$ and -138.7 ppm and GC(EI)-MS analysis further confirmed its identity by showing the presence of its molecular radical cation.

The investigation of the solvent effect revealed that changing the solvent to toluene- d_8 , THF- d_8 and CD_2Cl_2 resulted in the formation of the same products observed in Scheme 92 with a comparable distribution. Nevertheless, CD_3CN led to the exclusive formation of the simple difluorophosphoranes and the reductive coupling product **15** within 30 minutes at 20 °C for each tested phosphine (Scheme 94).



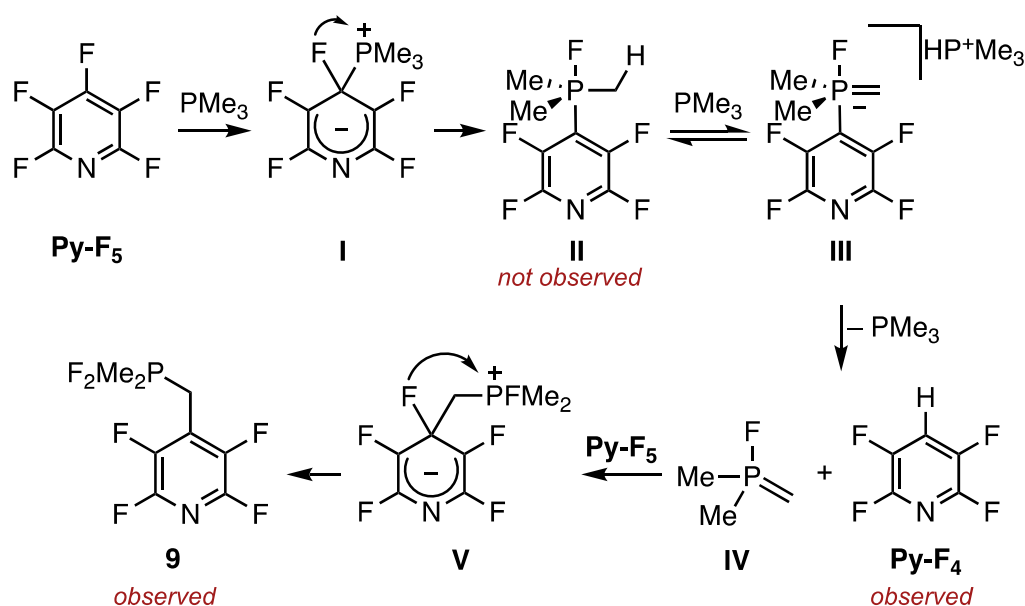
Scheme 94 Reactivity of P^iPr_3 , PMe_2Ph , PMe_3 and PCy_3 towards **Py-F₅** in CD_3CN after 30 minutes at 20 °C.

Based on these results, it can be concluded that the reactivity observed between PMe_3 and **Py-F₅** extends to other more sterically hindered phosphines while still maintaining high reactivity and that for most solvents (excluding CD_3CN) there is no solvent effect on the reaction outcome. The conditions for the reaction of Scheme 92 require the phosphine to have a proton in the α -carbon to the phosphorus and not excessively bulky R groups. The kinetic limit of the system was reached when $\text{P}^t\text{Bu}_2\text{Cy}$ was employed. In this case an alternative reactivity pathway was favoured, resulting in the formation of the simple difluorophosphorane and **15**. The same outcome was observed in the absence of a proton in the α -carbon in the phosphine, such as with P^tBu_3 . Furthermore, the investigation of the solvent effect suggested that this second reaction pathway was promoted, even with less sterically hindered phosphines, by the use of a more polar solvents such as acetonitrile.

Difluorophosphoranes can be used in many valuable transformations and applications such as CO_2 capture,²²⁰ deoxofluorination²⁵³ and for ^{18}F -radiolabeling.²²⁵ Therefore, in parallel to other strategies reported in the literature for the synthesis of these species (see chapter 3.1.4), this approach offers a useful and versatile route for preparing F_2PR_3 compounds under simple and mild reaction conditions. The potential advantage of this method lies in the generally low cost of phosphines and **Py-F₅**. Moreover, it could also be used as a pathway for the synthesis of compound 4,4'-perfluorobipyridine (**15**).

3.3.3 Mechanistic proposal

The presence of the formal HDF product **Py-F₄** in the reaction of Scheme 89 and Scheme 92 is reminiscent of the recent work from the group of García on the PEt₃-promoted HDF of fluoroaromatics (see chapter 3.1.3.1).^{155,156} The methodology they reported differs from the above-mentioned experiments by the reaction conditions, in their case traces of water were critical to observe the desired outcome. Strict exclusion of moisture in our case rules out the involvement of García's mechanism to explain the formation of **Py-F₄**, although the nucleophilic attack of the phosphine onto the 4-position of **Py-F₅** must be a common initial elementary step in both reactions. Considering the reaction between PMe₃ and **Py-F₅** and given that the formation of **9** cannot be explained by other means than the occurrence of a PMe₃-derived ylide, it is proposed that the observed outcome of the reaction of **Py-F₅** and PMe₃ stems from the mechanism depicted in Scheme 95.

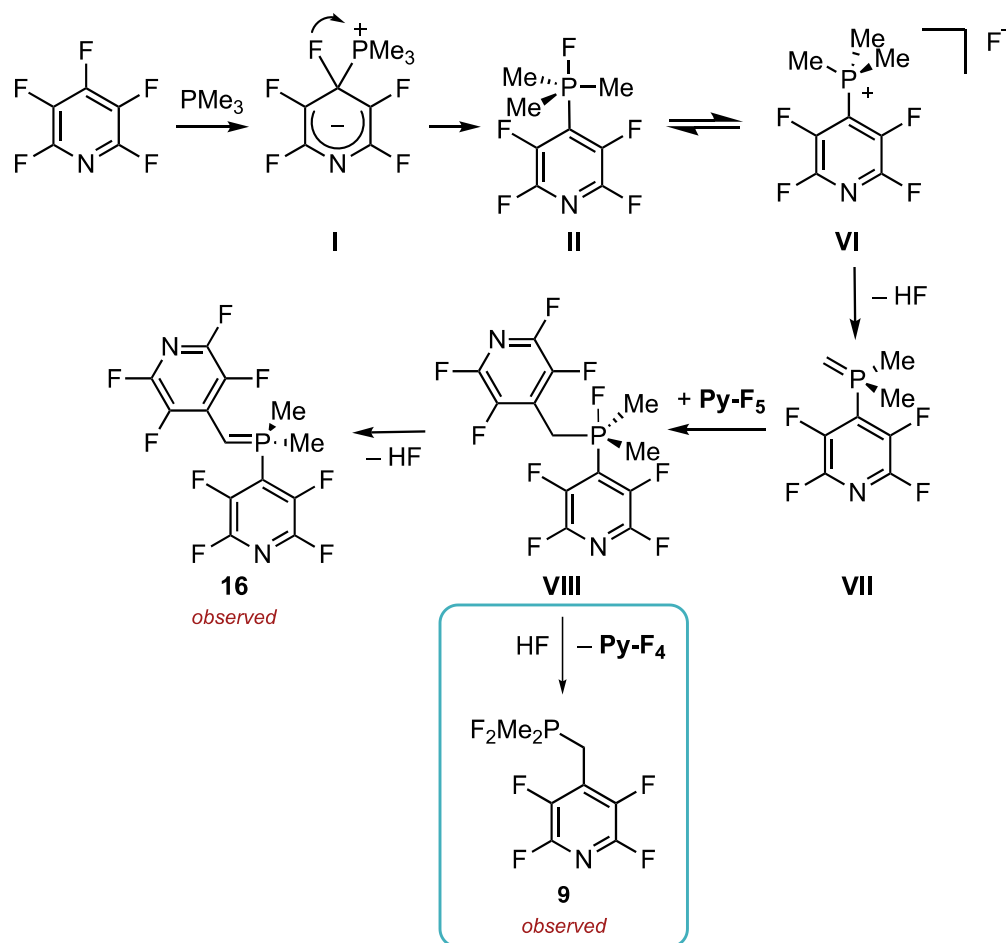


Scheme 95 Proposed reaction mechanism of Scheme 89.

After the nucleophilic attack of PMe₃ onto **Py-F₅**, the zwitterionic Meisenheimer complex **I** would evolve into the fluorophosphorane **II**. In the latter, the acidity of the Me groups may be high enough to be deprotonated by PMe₃ (pK_a varying from ~9 in THF up to 15.5 in CH₃CN), followed by proton transfer from [HPR₃]⁺ to the tetrafluoropyridyl carbon and formation of **Py-F₄**.^{254–257} Alternatively, a tetrafluoropyridyl anion, obtained by dissociation from fluorophosphorane **II**, may act as the base, deprotonating another molecule of intermediate **II**. This would result in ion pair **III**, with a hydro- or fluorophosphonium as counterion, that would undergo P-bond protolysis to release PMe₃, **Py-F₄** and the P-fluorinated ylide **IV**.²⁵⁸ The latter could then attack another equivalent of **Py-F₅** to

lead to complex **9** via another Meisenheimer complex **V**, followed by C-to-P fluoride transfer sequence. Overall, this rationale explains well the observed ~1:1 **Py-F₄**:**9** ratio. A light-activated mechanism was excluded, as a test experiment conducted in the absence of light yielded the same outcome.

The formation of ylide **16**, obtained from the large-scale reaction of Scheme 89, is proposed to occur following the mechanism in Scheme 96.



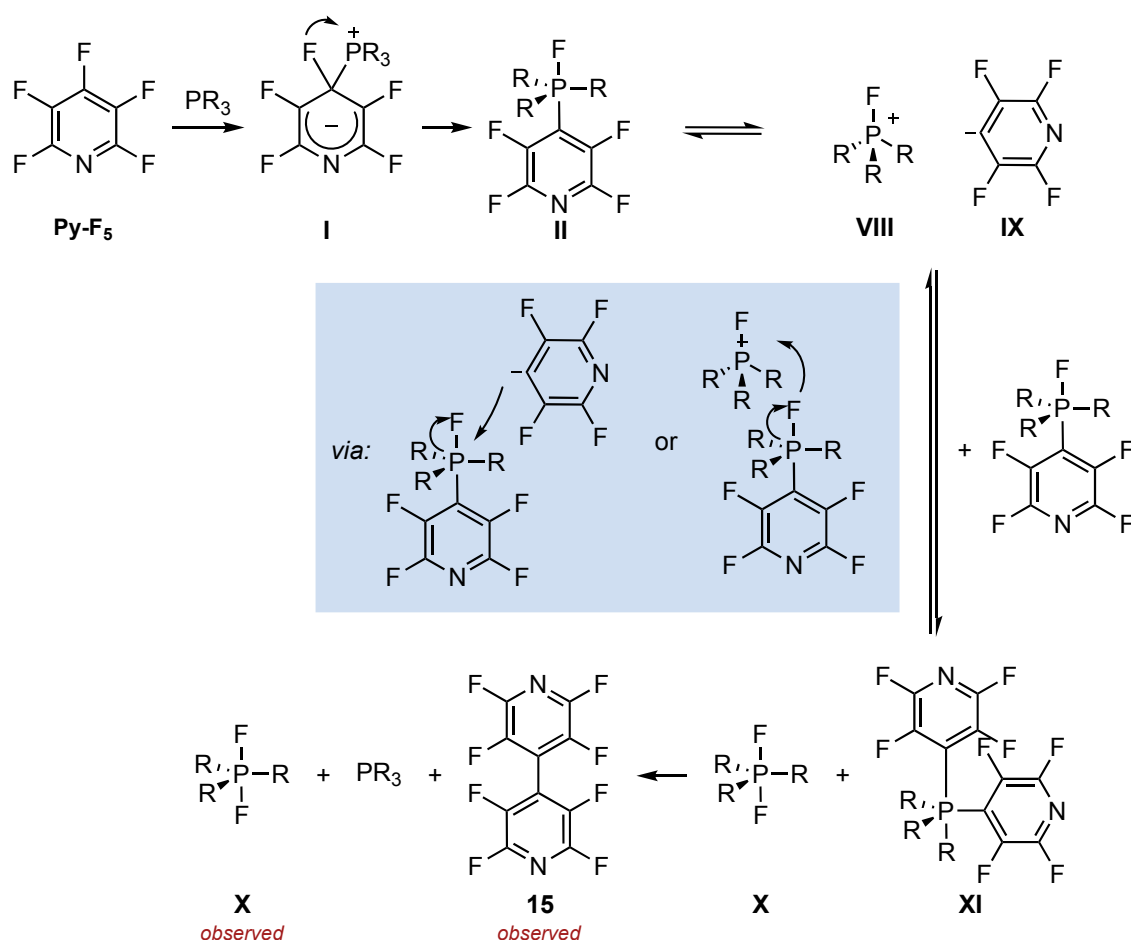
Scheme 96 Proposed reaction mechanism for the formation of **16**; an alternative mechanism for the synthesis of **9** is displayed (blue box).

Similar to Scheme 95, following the nucleophilic attack of PMe_3 on **Py-F₅**, the zwitterionic Meisenheimer complex **I** is proposed to evolve into fluorophosphorane **II**. This species would exist in equilibrium with the respective phosphonium **VI** with a dissociated fluoride, although presumably this equilibrium would lie strongly towards the fluorophosphorane.^{259–262} This fluoride would then deprotonate a methyl group, resulting in the formation of ylide **VII**.^{263,264} This step could be promoted by the release of HF and the formation of its strong bond. Subsequently, **VII** would nucleophilically attack another molecule of **Py-F₅** generating fluorophosphorane **VIII** which, after

HF loss, would form **16**. While the formation of this compound does not directly confirm any intermediate of the mechanism proposed in Scheme 95, it does provide evidence of the possibility of ylide formation in our system. Moreover, an alternative mechanism for the synthesis of compound **9** could involve the P–C^{pyr} bond cleavage *via* protonolysis with HF (blue box, Scheme 96).

The occurrence of compound **16** exclusively in the large-scale reaction and not in the NMR-scale experiments, suggests that reducing the reagent concentrations by half ([PMe₃] decreased from a 0.33 M solution to 0.17 M) and/or conducting the reaction at a lower temperature (0 °C) favours this reactivity pathway more than when the same reaction is performed at 20 °C on NMR scales.

When the reaction between trialkylphosphines and **Py-F₅** was conducted in CD₃CN, or when bulky phosphines (such as P(^tBu)₂Cy) or phosphines lacking a proton in the C_α were employed (e.g., P^tBu₃), the formation of the simple difluorophosphorane and the reductive coupling product **15** took place instead. The proposed mechanism for this reaction is reported in Scheme 97.



Scheme 97 Proposed mechanism for the formation of **15**.

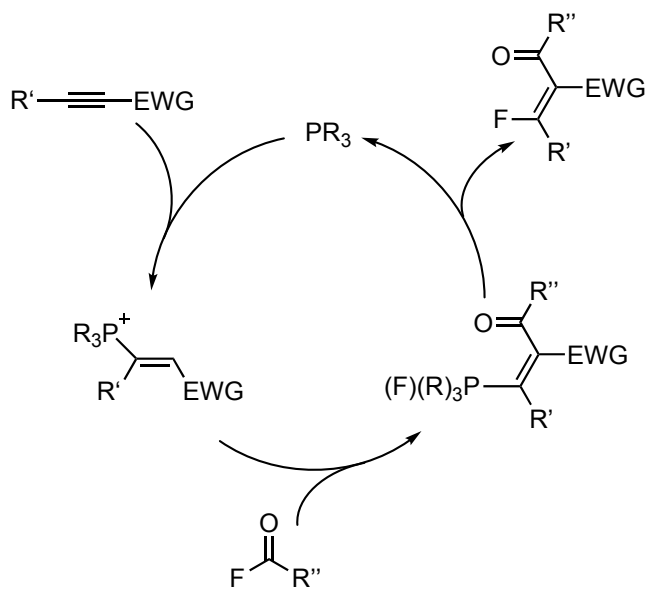
Similar to the previous mechanisms, the Meisenheimer complex **I** formation and its conversion into fluorophosphorane **II** take place. The 2,3,5,6-tetrafluoropyridyl group could be expected to be a

better leaving group than other Ar- fragments owing to the delocalisation of the negative charge due to the high degree of fluorination of $[\text{Py-F}_4]^-$, the presence of polar solvents and the steric repulsion arising from bulky R groups on the phosphine. Furthermore, the absence of any evidence of compound **II** in both our systems and the existing literature^{155,156} suggests that **II** is highly reactive. The generation of difluorophosphorane **X** and phosphorane **XI** could occur through two distinct pathways:

- *via* pyridyl attack on the phosphorus centre, leading to the release of fluoride, which then migrates to the P^+ of **VIII** (Scheme 97, blue box on the left);
- through the attack of **VIII** which acts as a Lewis acid by abstracting a fluoride from **II**, followed by the interaction of the resulting P^+ with the 2,3,5,6-tetrafluoropyridyl anion **IX** (Scheme 97, blue box on the right).

Finally, the ligand-ligand coupling in species **XI** would form **15**, as previously reported in similar systems,^{265–267} along with the liberation of free PR_3 .

A comparable solvent effect was observed in the context of the PCy_3 -catalysed intermolecular acylfluorination of alkynes in toluene.²⁶² Tobisu *et al.* proposed the participation of a fluorophosphorane intermediate in the catalytic cycle which, after ligand coupling and release of the acylfluorination product, regenerates the P^{III} catalyst (Scheme 98).



Scheme 98 Proposed mechanism for the intermolecular acylfluorination of alkynes catalysed by PCy_3 in toluene.

In polar solvents such as acetonitrile, the reaction yields the simple difluorophosphorane F_2PCy_3 and the hydroacylated product, with the acylfluorination product detected only in minimal amounts. The authors proposed that the fluorophosphorane is in equilibrium with the

corresponding phosphonium salt, which is more stable in acetonitrile. The phosphonium species is expected to decompose more readily than the fluorophosphorane and the protonation of the system would lead to the formation of F_2PCy_3 and the hydroacylated product. Traces of water (*via* nucleophilic attack onto phosphonium ion) or cyclohexyl groups (through β -hydrogen elimination) could act as proton sources in this system.

In conclusion, this study demonstrates that simple trialkyl phosphines readily undergo nucleophilic attack on **Py-F₅**. Subsequently, depending on the reaction conditions, two distinct reaction mechanisms may occur (Scheme 95 and Scheme 97). These results suggest that in transformations involving metal-catalysed C–F bond activation of pentafluoropyridine, trialkyl phosphines present as ligands in the metal complex could potentially play an active role in the system.

3.4 Summary, conclusions and perspectives

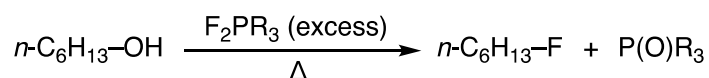
Complex **6** reacted at room temperature with **Py-F₅** to form 1-cyclohexenylzirconocene fluoride (**7**), an unidentified solid and traces of other fluorine- and phosphorus-containing products. Control experiments pointed out that the dissociation of the PMe_3 ligand and subsequent reaction with the fluorinated heteroaromatic led to the generation of F_2PMe_3 and the methylenetetrafluoropyridine-substituted difluorophosphorane (**9**), which would then trigger the formation of **7**. To circumvent the undesired reaction between PMe_3 and **Py-F₅**, a reactivity study between different trialkylphosphines and **Py-F₅** was conducted.

Upon preparation of an equimolar solution of PMe_3 and **Py-F₅**, the immediate quantitative consumption of the heteroaromatic and the generation of F_2PMe_3 , **9** and the HDF product **Py-F₄** took place. The phosphine scope study revealed that a similar reaction with a range of more sterically hindered phosphines occurred, provided they featured a proton in the carbon adjacent to the phosphorus. The kinetic limit was observed with P^tBu_2Cy , where an alternative reactivity pathway was favoured, resulting in the formation of the simple difluorophosphorane $F_2P^tBu_2Cy$ and 4,4'-octafluorobipyridine (**15**). A similar transformation occurred when the same range of phosphines was employed in the presence of a more polar solvent, such as acetonitrile. Furthermore, when a bulky phosphine lacking a proton in the α -carbon (e.g., P^tBu_3) was employed, the generation of the simple difluorophosphorane $F_2P^tBu_3$ and **15** was observed.

In summary, this investigation provided more insights into the unexpected reactivity of trialkylphosphines towards **Py-F₅** and the potential reaction mechanisms at play. It was concluded that, even by replacing PMe_3 with another phosphine, avoiding the undesired side reactivity with

Py-F₅ is challenging. Changing the ligand of the Zr-cyclohexyne complex to a labile pyridine or an NHC with bulky substituents (to avoid the side reactivity described in chapter 3.1.2.2) may enable the targeted 1,3-CF addition of **Py-F₅**. Nevertheless, the reactivity outlined in Scheme 94 offers a convenient and versatile route for preparing F₂PR₃ compounds under simple and mild reaction conditions, in addition to the other strategies already discussed in chapter 3.1.4. Moreover, it could also be used as a pathway for the synthesis of compound 4,4'-octafluorobipyridine.

An interesting application of the difluorophosphoranes obtained from Scheme 92 and Scheme 94 could be related to the deoxyfluorination reaction of alcohols.^{223,224} In this field, mild deoxyfluorinating agents include sulfur-based (such as DAST²⁶⁸ or, more recently, PyFluor)²⁶⁹ and carbon-based compounds (PhenoFluor,²⁷⁰ CpFluor)²⁷¹ have been reported. Inspired by Akashi and coworkers' strategy²²³ involving the deoxyfluorination of 1-octanol assisted by difluorotriphenylphosphine, the use of other difluorophosphoranes as potential deoxyfluorinating agents is envisioned (Scheme 94). Preliminary tests with compounds F₂P^{*i*}Pr₃, F₂PMe₃ and **9** showed the formation of a small amount of 1-fluorohexane when reacted with 1-hexanol, but further optimisation of the reaction conditions is required.



Scheme 99 Proposed deoxyfluorination reaction of alcohols with difluorophosphoranes.

Chapter 4 – PⁿBu₃-catalysed hydro- and aminodefluorination of polyfluoroaromatics

4.1 Introduction

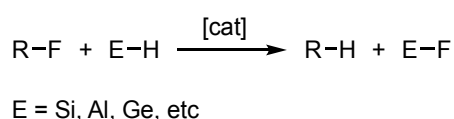
As expressed in chapter 2.1, among the various methods known for promoting C–F bond activation, significant progress has been made employing TMs, with these strategies usually proceeding *via* OA-type mechanisms.^{16,272} This approach proved to be efficient for chemoselective and catalytic transformations, however, the substrate scope was generally limited to C(sp²)–F bond of aromatic and vinylic fluorocarbons.²⁷³

In recent years, there has been a significant interest in the activation and functionalisation of small molecules and strong bonds using compounds that contain main-group elements and acting in similar ways to transition metals.^{41,78,274–276}

In the field of C–F bond activation, the simplest transformation is the hydrodefluorination reaction. Catalytic HDFs allow the conversion of readily available and inexpensive perfluorinated or polyfluorinated organic compounds into more valuable partially fluorinated species. This reaction has three main requirements:

- the parallel formation of a thermodynamically favoured E–H bond (Scheme 100), as the BDE of the C–F bond is generally higher than that of the C–H bond (500 ± 50 vs. 400 ± 50 kJ/mol);²⁷⁷
- the presence of a hydrogen source;
- a catalyst that promotes this transformation.

Typically, the first two requirements are addressed by employing a single species (which can be based on Si, Al, Ge, etc.) that features a high fluoride ion affinity (FIA) and acts as both hydrogen source and fluoride acceptor (Scheme 100).²⁰



Scheme 100 General reaction scheme for HDF.

As this chapter deals with the investigation of a metal-free system for HDF reactions catalysed by simple phosphines, this introduction section delves into HDF reactions assisted by main-group elements. Other types of transition-metal-free C–F bond functionalisations are discussed in the reviews by Braun *et al.*,²¹ Oestreich *et al.*²⁷⁸ and Wu *et al.*²⁷³

4.1.1 Main-group-mediated HDF reactions

Four main activation approaches have been developed for the HDF reaction assisted by main-group elements.²⁷³

- 1) abstraction of the fluoride anion by Lewis acids (LAs);
- 2) C–F bond homolysis through a radical pathway (light-activated or with radical initiators);
- 3) nucleophilic substitution of fluoride employing strong bases and/or strong nucleophilic reagents;
- 4) reversible two-electron redox catalysis.

In the following section, emblematic examples of transition-metal-free HDF reactions are presented and they are categorised based on the four activation methods listed above.

4.1.1.1 Fluoride abstraction by Lewis acids

Among the four C–F activation strategies, the one that has been mostly investigated involves the use of a strong Lewis acid with high FIA to abstract the fluoride (generally from an C(*sp*³)-F bond) of a fluorinated organic molecule. The main electrophilic reagents used in the literature are Si-, Al-, Ge- and B-based.

4.1.1.1.1 Si-based electrophiles

Depending on the activation mode by the Si-based electrophile, three different catalytic cycles can be identified (Figure 21).²⁷⁸

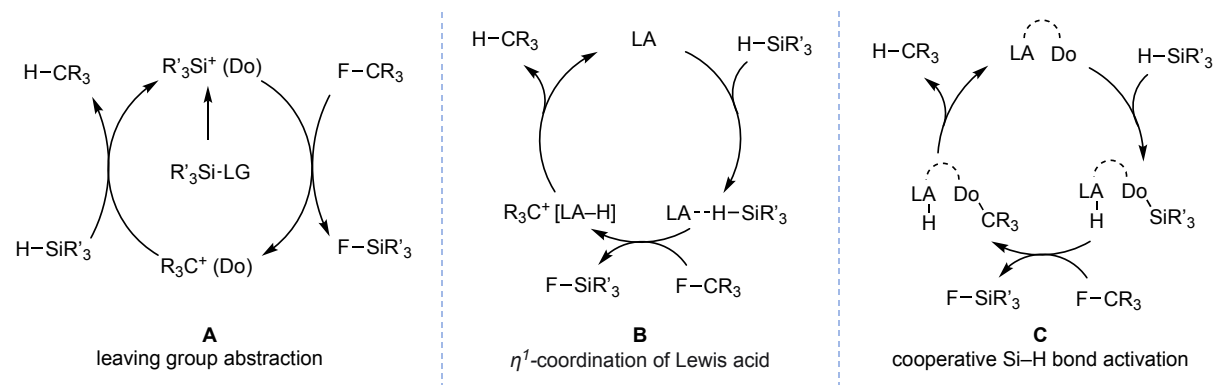


Figure 21 Three types of catalytic cycles for the HDF reaction involving Si-based electrophiles.

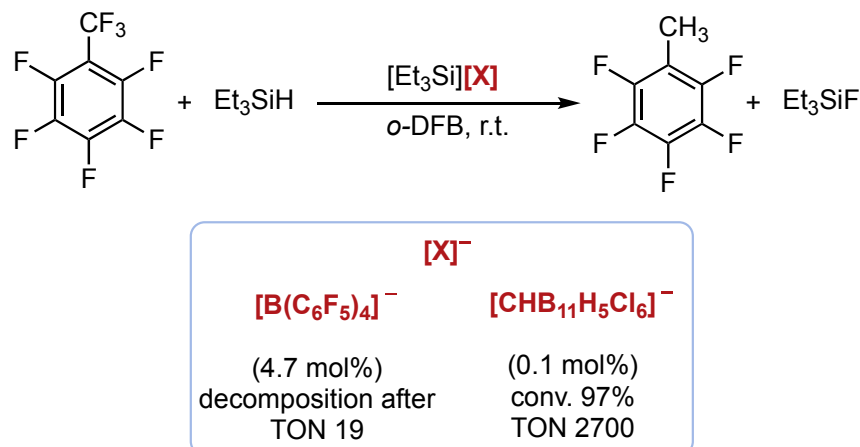
(LA = Lewis acid; LG = leaving group; Do = electron donating species)

All three approaches use a catalytically active silicon-based LA capable of fluoride abstraction, which is regenerated through hydride transfer to an intermediate carbenium ion ($[R_3C]^+$). A hydrosilane usually acts as both the catalyst and the hydride source.

Mechanism **A** involves the generation of a silylium cation ($[R_3Si]^+$) by abstraction of the LG. The extremely high Lewis acidity and FIA²⁷⁹ of $[R_3Si]^+$ enables the cleavage of the $C(sp^3)-F$ bond and the release of a $[R_3C]^+$ and a fluorosilane (R_3SiF). Finally, a hydride transfer from the stoichiometric hydrosilane to $[R_3C]^+$ yields the target HDF product and regenerates the silylium ion catalyst. The overall process can be viewed as a Si-H/C-F metathesis (with conversion to Si-F/C-H) and it is thermodynamically driven ($Si-H/C-F \rightarrow Si-F/C-H$), as C-H bonds (*ca.* 400 kJ/mol) are stronger than Si-H bonds (*ca.* 300 kJ/mol) and Si-F bonds (*ca.* 600 kJ/mol) are stronger than C-F bonds (*ca.* 500 kJ/mol).^{42,277}

The first work on the use of a LA to abstract the fluoride from fluoroalkanes was reported by Krause and Lampe in 1977.²⁸⁰ They studied the ion-molecule reactions characteristic of SiH_4-CF_4 mixtures and examined the ionic pathways of their exchange by tandem mass spectrometry.²⁸¹ From this investigation they observed Si-H/C-F redistribution favouring F on Si and H on C in the gas phase upon collision of $[SiH_3]^+$ with CF_4 . This was the first proof of the ability of silicon cations to abstract a fluoride from a C-F bond.

Subsequently, Ozerov *et al.* pioneered silylium ion-mediated HDF reactions.²⁸² In 2005 they demonstrated that the strong Lewis acidity, the high fluoride affinity and electrophilicity of $[\text{Et}_3\text{Si}]^+$ enable the heterolytic cleavage of $\text{C}(sp^3)\text{-F}$ bonds (Scheme 101).



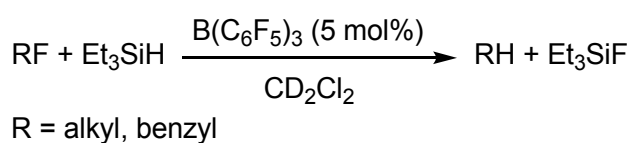
Scheme 101 Selected example for the HDF of $\text{C}(sp^3)\text{-F}$ catalysed by $[\text{Et}_3\text{Si}][\text{X}]$.

$[\text{Et}_3\text{Si}][\text{B}(\text{C}_6\text{F}_5)_4]$ was initially employed as catalyst and Et_3SiH as the hydride source. $[\text{Et}_3\text{Si}][\text{B}(\text{C}_6\text{F}_5)_4]$ is a synthetic equivalent of $[\text{Et}_3\text{Si}]^+$ and it is prepared *in situ* by treatment of Et_3SiH with a catalytic amount of $[\text{Ph}_3\text{C}][\text{B}(\text{C}_6\text{F}_5)_4]$. In this catalytic system, silylium ions readily reacted at room temperature with various fluoroorganic compounds, including α,α,α -trifluorotoluene derivatives and 1-fluoropentane, yielding the target HDF product (with aromatic C-F bonds remaining untouched). This study was noticeable as it was the first room temperature, transition-metal-free catalysis enabling non-activated $\text{C}(sp^3)\text{-F}$ bond cleavage.

Subsequently, the authors discovered that the catalytic efficiency of the system was significantly influenced by the nature of the solvent and the counteranion. The latter had not only to be weakly coordinating, but also resistant to high Lewis and Brønsted acidity.²² The decomposition of $[\text{B}(\text{C}_6\text{F}_5)_4]^-$ in the presence of carbocations and strong Brønsted acids generated over the reaction limited the turnover number (TON) of the catalytic system (up to 19 with perfluorotoluene). Changing the counteranion to halogenated monocarboranes,²² dramatically improved the TON (2700 with perfluorotoluene) (Scheme 101). Again, all HDF reactions exhibited complete chemoselectivity for aliphatic $\text{C}(sp^3)\text{-F}$ bonds. The proposed mechanism for this system follows the scenario **A** of Figure 21.

Mechanism **B** in Figure 21 involves the activation of the electrophile, a neutral tetracoordinate organosilicon compound, by another strong LA, which could be a main-group LA or a cationic transition metal complex. The coordination mode is usually η^1 -coordination and it generates a potent source of electrophilic silicon.²⁷⁸ The electrophilicity of the coordinated silane is high enough to abstract a fluoride from a C–F bond, resulting in the liberation of $[R_3C]^+$ and a stabilised $[LA-H]^-$. The hydride transfers to $[R_3C]^+$ leads to the formation of the HDF product.

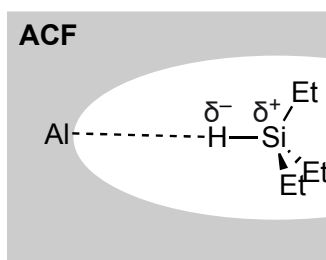
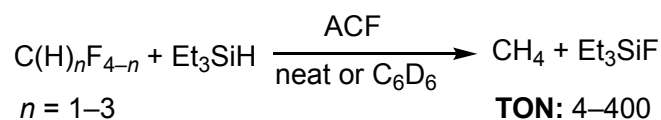
An example of HDF reaction following this mechanism was reported by Stephan and coworkers.²⁸⁴ Commercially available $B(C_6F_5)_3$ was used as catalyst for the hydrodefluorination of alkyl C–F bonds in the presence of Et_3SiH (Scheme 102).



Scheme 102 $B(C_6F_5)_3$ -catalysed hydrodefluorination of alkyl fluorides.

The electron-deficient borane was shown to activate the silane through η^1 -coordination (according to scenario **B**, Figure 21). The formation of the η^1 -H(Si) silane coordination increased the polarisation of the Si–H bond, with an accompanying increase in charge on silicon in comparison to the free silane and a decrease in the charge on hydrogen. Therefore, the η^1 -H(Si) coordinated silane is expected to be a more potent source of electrophilic silicon than the free one. Consequently, primary, secondary and tertiary alkyl fluorides were successfully converted into the corresponding alkanes.

Following a similar activation mode for silanes, Kemnitz and Braun's group performed a heterogeneous catalytic HDF reaction with nanoscopic amorphous aluminium chlorofluoride (ACF) as the catalyst (Scheme 103).²⁸⁶



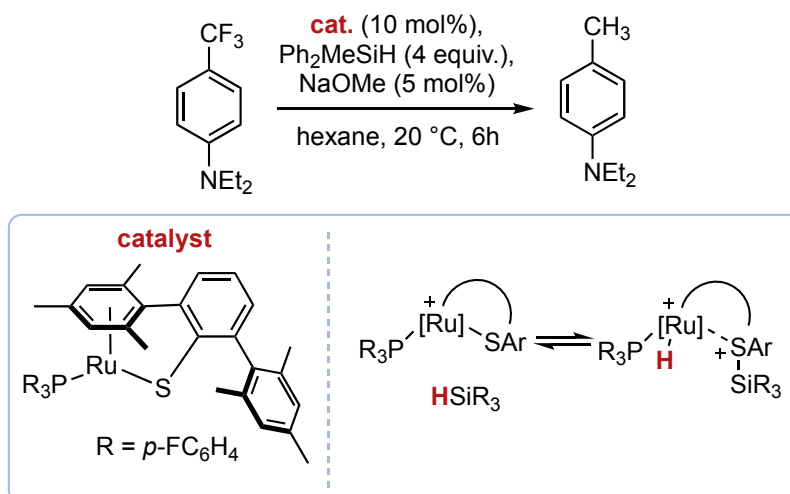
Scheme 103 HDF of fluoromethanes catalysed by silylium-like surface species.

(ACF = aluminium chlorofluoride)

ACF is an extremely strong Lewis acid of the formula $\text{AlCl}_x\text{F}_{3-x}$ ($x \approx 0.05-0.3$) and it was able to perform HDF of CH_3F and of CH_2F_2 (with TONs of 400 and 112, respectively). CHF_3 was also active in this system, however harsher conditions were required. The activated silane represented in Scheme 103 appeared to be the key intermediate of the catalytic mechanism.²⁸⁶

Finally, the third scenario (Figure 21, mechanism **C**) results from a combination of the first two approaches. The R_3SiH is simultaneously activated by a LA, which abstracts the hydride, and a Lewis base (Do), that stabilises the generated $[\text{R}_3\text{Si}]^+$. Fluoride abstraction from the fluoroalkane to the Si occurs, resulting in the release of the fluorosilane, formation of a stabilised $[\text{R}_3\text{C}]^+$ and final liberation of the HDF product.

Oestreich *et al.* introduced the concept of cooperative activation of the $\text{R}_3\text{Si-H}$ bond in the HDF of $\text{C}(sp^3)\text{-F}$ bonds (Scheme 104).²⁸⁷ In Figure 21, Mechanism **C**, LA would be Ru^{II} and Do ArS^- .

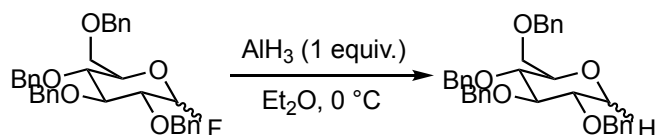


Scheme 104 Catalytic HDF reaction using cooperative Si-H bond activation by a Ru-S bond.

The polar Ru–S bond enabled the reversible splitting of the Si–H bond by a σ -bond metathesis. The activated Si was then able to abstract a fluoride from the $C(sp^3)$ –F bond initiating the catalytic cycle. Catalytic HDF of CF_3 -substituted anilines under mild reaction conditions was realised with this system.

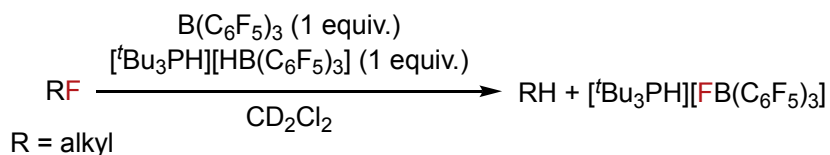
4.1.1.1.2 Other electrophiles

In addition to silicon, elements of group 13 are known for their electrophilicity. In 1984, Nicolaou *et al.* used an equimolar amount of AlH_3 to convert glycosylfluoride into the defluorinated tetrahydropyran under mild reaction conditions (Scheme 105).²⁸⁸ It is remarkable that the alane acted as both the hydride source and Lewis acid without the demand for further activation.



Scheme 105 Stoichiometric HDF of glycosylfluoride promoted by AlH_3 .

Another important class of main-group Lewis acids is represented by boron-based electrophiles. In particular, Stephan and coworkers reported that $B(C_6F_5)_3$ is capable of activating $C(sp^3)$ –F bonds in alkyl monofluorides when acting as the Lewis acidic component in FLPs (Scheme 106).²⁸⁴

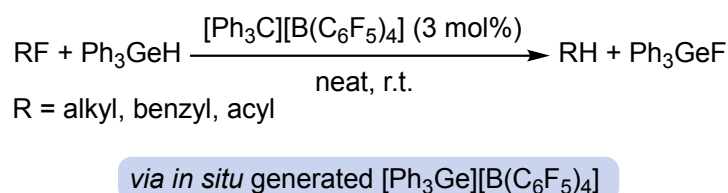


Scheme 106 Stoichiometric HDF of alkyl monofluorides promoted by $B(C_6F_5)_3$ and $[tBu_3PH][HB(C_6F_5)_3]$.

For example, treatment of fluoropentane with equimolar amounts of $B(C_6F_5)_3$ and $[tBu_3PH][HB(C_6F_5)_3]$ as the hydride source yielded the alkane and the salt $[tBu_3PH][FB(C_6F_5)_3]$. In the absence of $B(C_6F_5)_3$, no reaction was observed, indicating that LA activation of the C–F bond by the electron-deficient borane was critical to promote the nucleophilic attack of the hydridoborate. A more detailed discussion on FLP-mediated C–F bond activation can be found in the reviews by Stephan *et al.*^{203,284,291}

It has been demonstrated that germanium can act similarly to Si and Al electrophiles in HDF reactions.²⁹² Weinert's group reported a room temperature HDF of acid fluorides and alkyl

fluorides, involving an *in situ* generated germylium cation $[\text{Ph}_3\text{Ge}]^+$ (Scheme 107).²⁹³ Interestingly, no decarbonylation or reduction of the acid fluorides was observed.



Scheme 107 HDF of alkyl, benzyl and acyl fluorides catalysed by *in situ* generated $[\text{Ph}_3\text{Ge}][\text{B}(\text{C}_6\text{F}_5)_4]$.

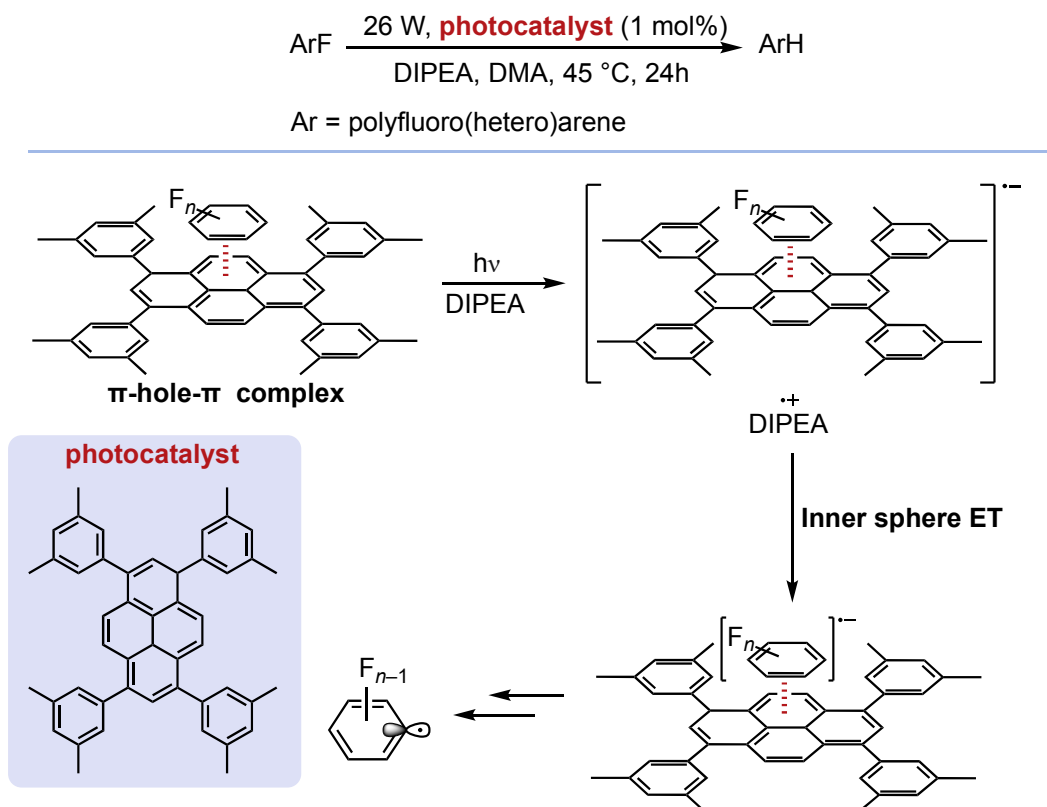
4.1.2 Photoinduced HDF

Photocatalytic hydrodefluorination reactions involve single electron transfer (SET) mechanisms promoted by photocatalysts through irradiation of visible light, enabling the cleavage of a C–F bond and the subsequent formation of a new C–H bond. The reaction mechanism usually includes the liberation of a fluoride from a radical anion, the reduction of the latter forming a neutral radical and the protonation of the product.²⁹⁴

This approach is new and promising because it does not need any stoichiometric amounts of reductants for the reaction to occur and it broadens the substrate scope in terms of the type of bond activated (for example, aryl C–F bonds can be cleaved) and functional group toleration.

In this section, only a selection of relevant examples is covered. For a more detailed discussion on photochemical strategies for HDF of fluorinated organic compounds see review by Yan.²⁹⁴

Zhang and coworkers developed a metal-free method for the HDF of polyfluoroarenes using a pyrene-based photocatalyst and N,N-diisopropylethylenamine (DIPEA) as the base/sacrificial electron donor (Scheme 108).²⁹⁵ Polyfluoroarenes underwent monoHDF in good yields and with excellent selectivity. A series of functional groups were tolerated, such as aryl groups, esters, ethers and CF_3 groups.



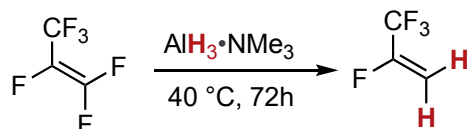
Scheme 108 Selected example of HDF of aryl fluorides catalysed by a pyrene-based photocatalyst and relative proposed mechanism.

The authors proposed the formation of a weak “ π -hole- π ” interaction between the photocatalyst and the aromatic substrate. When this complex was irradiated in the presence of DIPEA, it was reduced into a radical anion. An inner sphere ET to the fluoroarenes and the dissociation of the complex took place leading to the release of the photocatalyst and the intramolecular dissociative electron transfer in the fluoroarenes. The formation of the radical and liberation of a fluoride then occurred. Finally, the aryl radical abstracts a proton from DIPEA radical cation generating the desired product.²⁹⁶

4.1.3 HDF via nucleophilic substitution

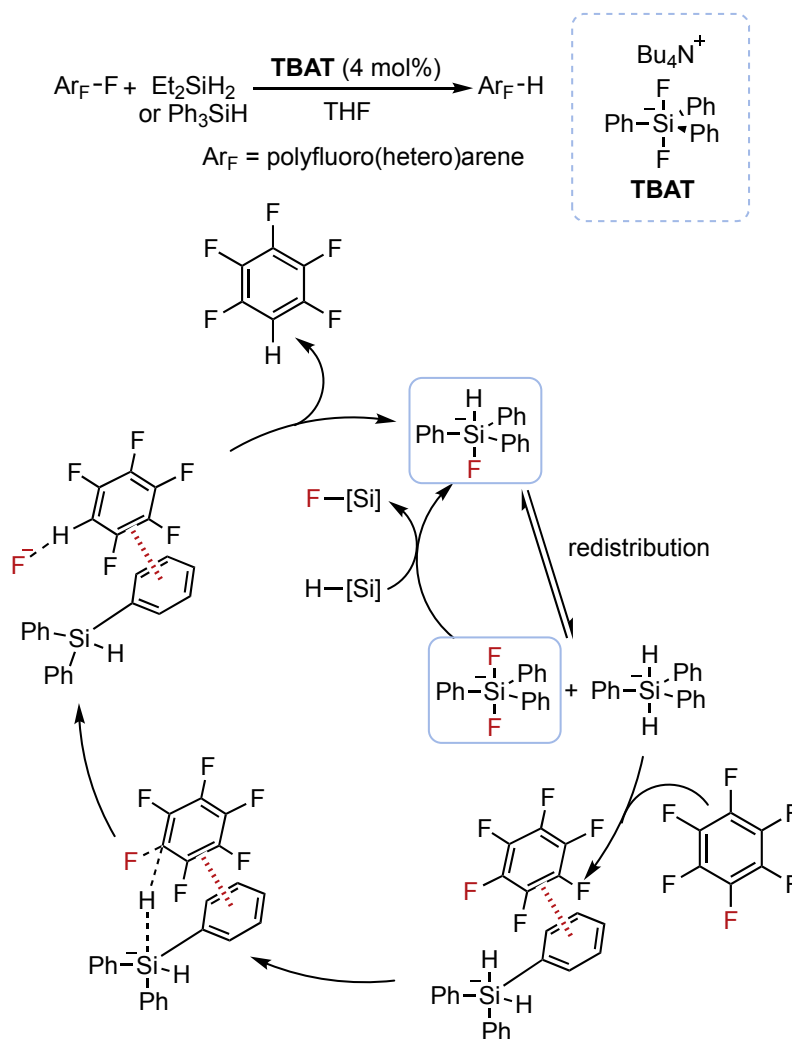
The third method for transition-metal-free C–F bond activation relies on S_NAr or nucleophilic vinylic substitution mechanisms with bases and/or nucleophilic reagents. This approach specifically targets aromatic or vinylic $C(sp^2)$ –F bonds and the system’s reactivity tends to decrease with higher electron density in the substrates. Consequently, substrates bearing electron withdrawing groups favour the nucleophilic attack, ultimately promoting the HDF process.

Crimmin *et al.* proposed the synthesis of commercially valuable hydrofluoroolefins *via* selective hydrodefluorination of hexafluoropropene (Scheme 109).²⁹⁷ The reaction occurred under mild conditions in the presence of $\text{AlH}_3 \cdot \text{NMe}_3$ as both the Lewis base and hydrogen source. The proposed mechanism proceeds *via* concerted nucleophilic vinylic substitution pathway, where the hydride is the nucleophile.²⁹⁸



Scheme 109 HDF of hexafluoropropene promoted by $\text{AlH}_3 \cdot \text{NMe}_3$.

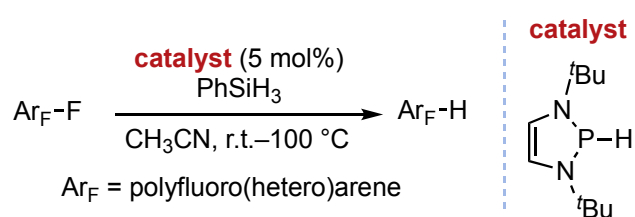
Another example was recently reported by Ogoshi *et al.*²⁹⁹ Tetrabutylammonium difluorotriphenylsilicate (TBAT) was used as the catalyst for the HDF of polyfluoroarenes in the presence of a stoichiometric amount of hydrosilane as the hydride source (Scheme 110).



Scheme 110 HDF of polyfluoroaromatics catalysed by TBAT and proposed reaction mechanism.

This catalytic system led to the generation of mono- and, in some cases, dihydrodefluorination products, while tolerating FGs that would instead react in the presence of a strong LA such as silylium cations (e.g., cyano, pyridine, ester, amides, nitro, chloride). The proposed mechanism involves the formation of a catalytic amount of dihydrosilicate through reaction with the stoichiometric hydrosilane and redistribution. Subsequently, π - π stacking of the fluoroarenes with the Ph of the catalyst favours the concerted S_NAr , resulting in the liberation of the HDF product.

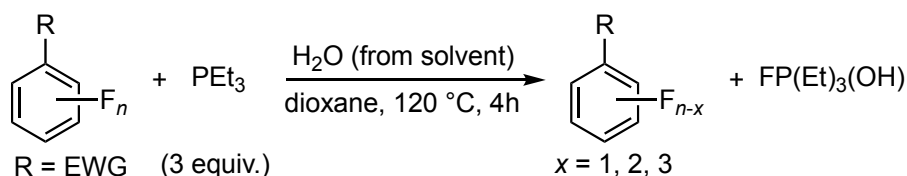
Following a strategy akin to Ogoshi's, where the enhanced hydricity of the Si-H bond triggered the S_NAr of fluorinated arenes, Cheng and coworkers introduced a metal-free catalytic HDF system assisted by diazaphospholenes in the presence of PhSiH₃ as the hydride source (Scheme 111).³⁰⁰



Scheme 111 HDF of polyfluoroarenes catalysed by diazaphospholenes.

The proposed mechanism involves the formation of a complex between the catalyst and the aromatic substrate *via* π - π stacking interactions. Subsequently, the activated P-H hydride attacks the fluoroaromatic through concerted S_NAr , resulting in the formation of the HDF product and fluorodiazaphospholene. The catalyst is then regenerated through σ -bond metathesis with PhSiH₃.

As already described in chapter 3.1.3.1, García and coworkers proposed the stoichiometric HDF of polyfluoroaromatics promoted by PEt₃, where the hydrogen source was proposed to be traces of water in the system (Scheme 112).¹⁵⁵ The proposed mechanism for this transformation is reported in Scheme 78.



Scheme 112 Stoichiometric HDF of polyfluoroaromatics promoted by PEt₃.

4.1.4 Reversible two-electron redox catalytic HDF

The activation and functionalisation of small molecules and strong bonds by main-group-element compounds acting in similar ways to transition metals has attracted significant interest in recent years.²⁷⁴ A fundamental concept underlying this research is the metallomimetic behaviour, where main-group-element species can exhibit reactivity analogous to TMs.³⁰¹ Reversible 2-e⁻ redox processes, such as OA and RE steps, characterise the most common TM-based catalytic cycles. Similar redox cycling in main-group elements is comparably less common, despite the increased interest in this field.²⁷⁵ A significant challenge emerges with main-group species due to their significant stability differences between various oxidation states, unlike TMs. This usually allows either the OA or RE steps to be performed, but the reverse process is much more difficult and poses challenges for catalysis.

For instance, considering the *p*-block elements, compounds containing low-valent elements from group 13 and 14 can usually undergo OA with substrates bearing C–X or E–H (E = H, C, N, O; X = F, Cl, Br, I) bonds.^{302–305} Nevertheless, RE processes involving the corresponding high-valent species are rarer. On the other hand, high-valent compounds containing group 16 and 17 elements are able to undergo RE, resulting in the formation of C–C, C–H and C–X (X = F, Cl) bonds.^{306,307} OA of the respective low-valent species is more difficult (Figure 22). Due to the preferential reactivity of low- and high-valent species, achieving reversible 2-e⁻ redox processes with *p*-block element-containing compounds proves challenging.³⁰⁸

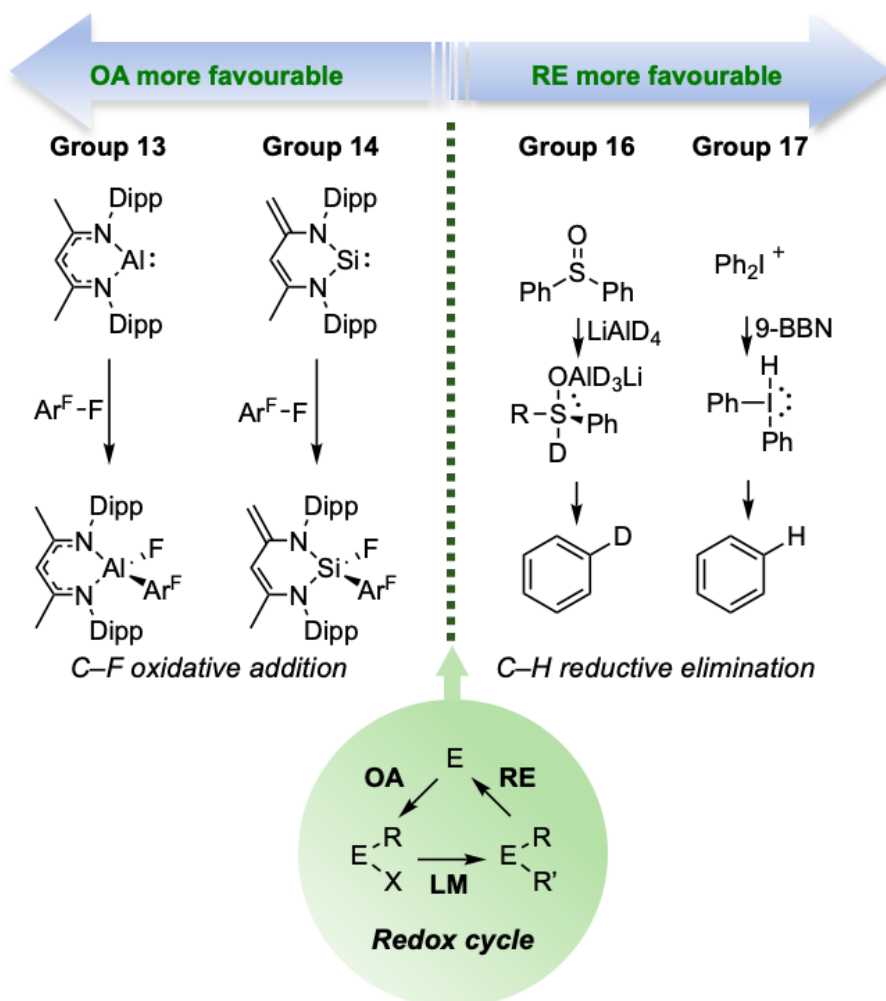


Figure 22 General preferential redox reactivity of compounds containing elements between group 13 and 17.

Elements from group 15, known as pnictogens (Pn), showed a distinctive reactivity compared to the other *p*-block elements. Their ability to stabilise various oxidation states could enable a bidirectional $\text{Pn}^n/\text{Pn}^{n+2}$ redox process, making them good candidates for the development of metallomimetic reactivity and catalysis.²⁷⁶ Despite these premises, catalytic processes employing redox catalysts based on group 15 elements remain rare.²⁷⁵ A key design concept that led to observations of redox-cycling in the few examples reported in the literature is the introduction of appropriate geometrical constraints around the Pn atoms. Constraining the molecular shape of these compounds allows their electronic structure to be tailored, thus significantly impacting their reactivity.³⁰⁹ Therefore, understanding the correlation between the geometry and the electronic structure of non-trigonal compounds is crucial. The frontier correlation diagram reported in Figure 23 provides insights into this intercorrelation.²⁷⁶ For example, Goicoechea and coworkers stated that the use of tridentate, meridionally coordinating ligands enables the tuning of the binding angles with the Pn and the overall molecular geometry, ultimately ensuring the biphilic reactivity

of the compound.³⁰⁹ Generally, PnL_3 species (where L is a monodentate ligand), exhibit C_{3v} symmetry (pyramidal geometry) and the Pn's lone pair is represented by the orbital of symmetry $2a_1$ (Figure 23). The antibonding orbitals of the Pn–L bonds correspond to the degenerate set of orbitals $2e$. Using polydentate ligands would move these species to a more planar configuration, for example, by changing their symmetry to C_s or C_{2v} (T-shaped geometry). In both cases the $2e$ orbitals are no longer degenerate. This splitting results in the reduction of the HOMO/LUMO gap, reminiscent of TMs, and it seems to be a crucial factor for the biphilic reactivity of these compounds.^{309,310}

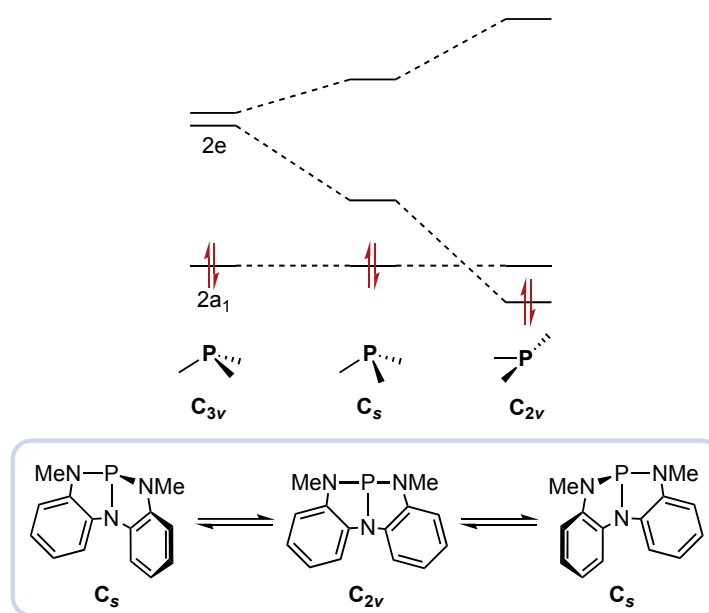


Figure 23 Qualitative frontier orbital diagram of a σ^3 -P compound in a C_{3v} , C_s and C_{2v} symmetry (top). Bending modes of an NPN compound (bottom).

Pincer ligands are often used as constraining ligands in these systems, although metal-ligand cooperativity is also frequently observed.³¹¹

Recent studies have demonstrated that geometrically constrained pnictogen systems can promote HDF, either through a series of stoichiometric steps, or catalytically, *via* $\text{P}^{\text{III}}/\text{P}^{\text{V}}$ or $\text{Bi}^{\text{I}}/\text{Bi}^{\text{III}}$ redox cycling.^{213,214,312} Crucially, the three key processes of OA, ligand metathesis (LM)/transmetallation, and RE that underpin many transition-metal catalytic mechanisms were seen in these systems (Figure 24).

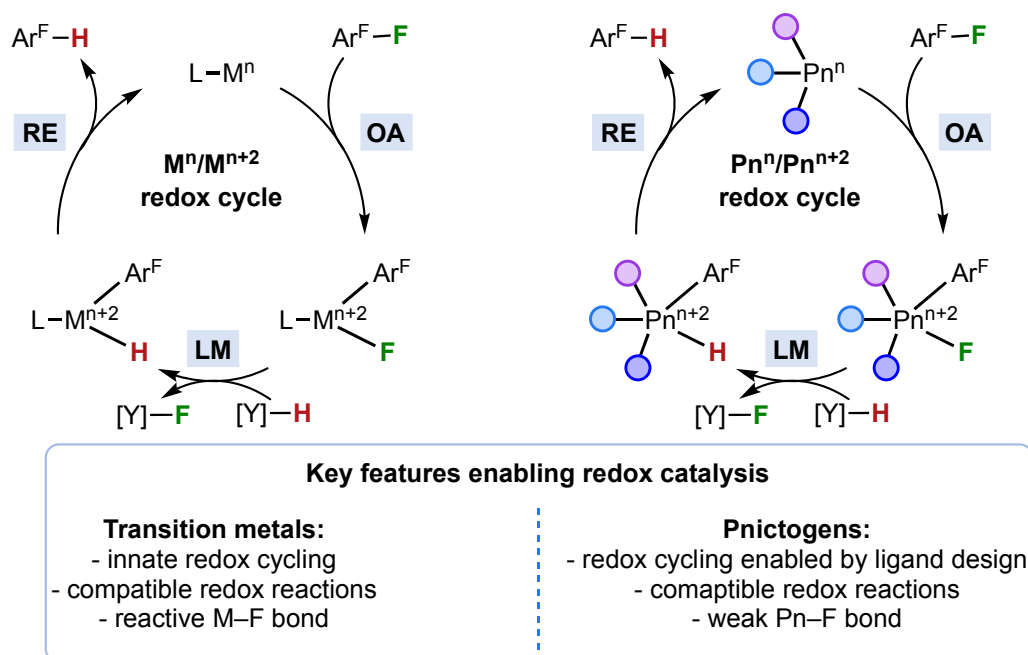
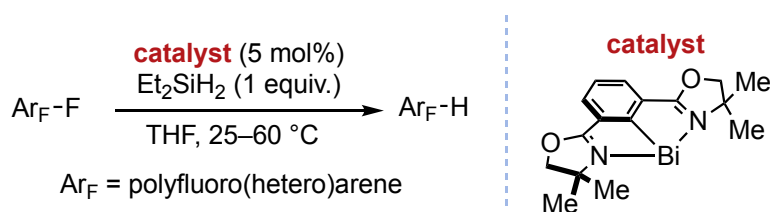


Figure 24 Comparison of the key features between TM- and Pn-based redox cycles.

Cornella and coworkers reported the hydrodefluorination reaction of a variety of polyfluoroarenes catalysed by bismuthinidenes, Phebox-Bi^I and OMe-Phebox-Bi^I under mild conditions (Scheme 113).³¹² Et₂SiH₂ was used as hydride source, yielding diethylfluorosilane upon completion of the reactions. Mechanistic studies supported the Bi^I/Bi^{III} redox cycle depicted in Figure 24.

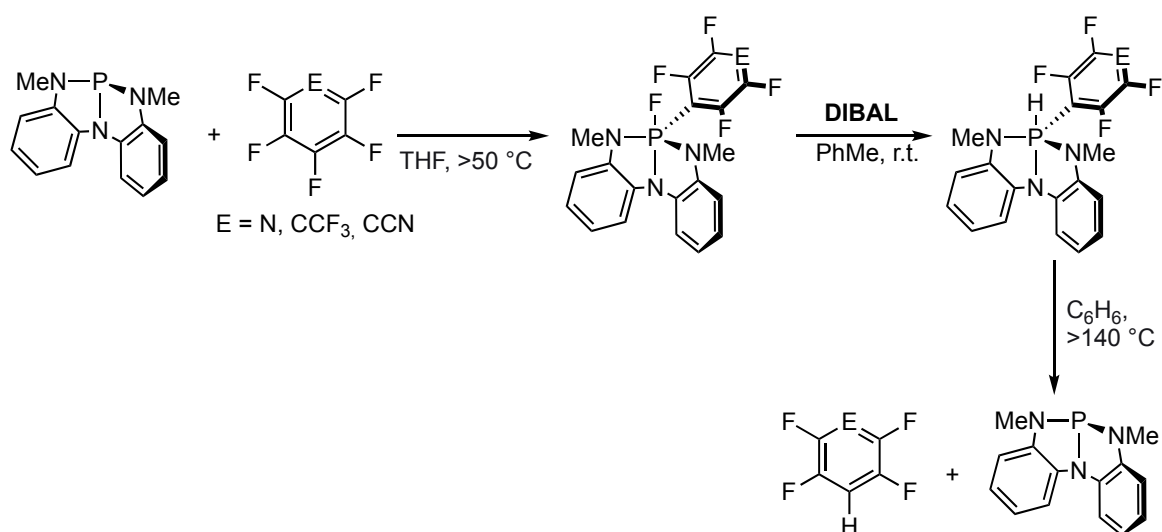


Scheme 113 HDF of polyfluoroarenes catalysed by Bi^I complexes.

Mild conditions were applied for electron-poor polyfluorinated arenes. The presence of an EDG made the reaction more challenging, requiring more forcing reaction conditions. This reactivity trend was observed also in the following examples reported by Radosevich²¹³ and Dobrovetsky.²¹⁴

Shifting focus to phosphorus, Radosevich and coworkers pioneered P^{III}/P^V redox cycling.²¹³ Applying the same structure-electronic relation concept as explained earlier, strained tridentate and bidentate ligands were employed to reduce the HOMO/LUMO gap, thus favouring the redox cycling. Firstly, they demonstrated that σ^3 -P triamide (Scheme 114) of molecular symmetry C_s underwent reversible OA and RE with amines.³¹³ Then, the same P-containing compound was employed to develop a stepwise process for the HDF of polyfluorinated arenes: OA, the

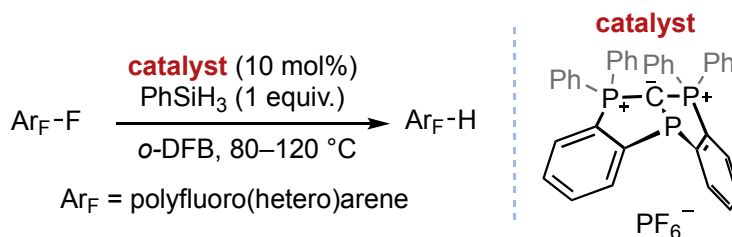
replacement of the fluoride with a hydride using DIBAL and the subsequent RE process resulted in the release of the hydrodefluorinated aromatic along with the regenerated phosphine.²¹³



Scheme 114 Stepwise OA, LM and RE at a P^{III} centre.

The paper provides a fully characterised examples of the three elementary steps at the bases of a typical TM-based catalytic cycle. However, the decomposition of DIBAL at high temperatures, which are required for the C–H RE, prevented the development of a catalytic cycle.

Following these results, Dobrovetsky and coworkers reported a catalytic HDF and aminodefluorination reaction assisted by a cationic, geometrically constrained, P^{III} species in a hexaphenyl-carbodiphosphoranyl-based CCC pincer-type ligand (Scheme 115).²¹⁴ Similarly to the previously mentioned bismuth example, the mechanism of this catalytic process proceeded *via* oxidative addition, ligand metathesis and reductive elimination.



Scheme 115 HDF of polyfluoroaromatics catalysed by a geometrically constrained σ^3 -P compound.

4.2 Aims and objectives

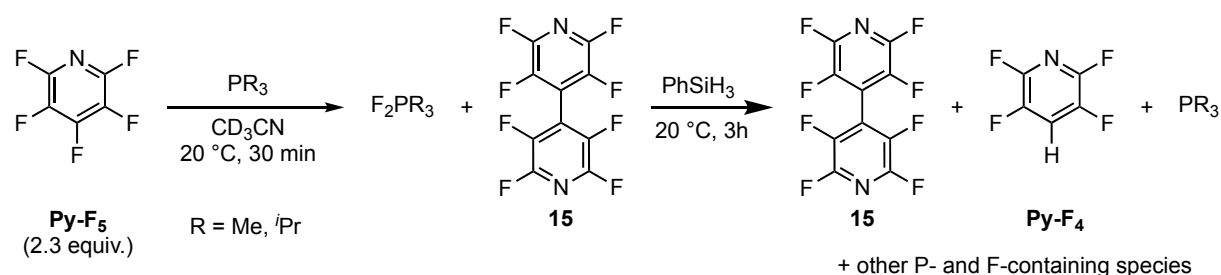
The works of Cornella,³¹² Radosevich²¹³ and Dobrovetsky²¹⁴ are remarkable demonstrations that main-group systems can mechanistically mimic the key steps in transition-metal catalysis. However, complex ligand architectures were employed and these were proposed to play an important role in the observed reactivity, due to their geometrical constraints on the pnictogen.

Inspired by the study of García *et al.*^{155,156} and considering the results obtained from the stoichiometric reaction of simple trialkylphosphines with pentafluoropyridine reported in chapter 3.3 (where it was shown that stoichiometric HDF was possible), it was decided to explore whether geometric constraints were a necessary prerequisite for redox cycling in HDF using pnictogen catalysts.

The aim of this chapter was to investigate whether a simple catalytic system, comprising commercially available alkylphosphines and silanes, can effectively perform the HDF reaction on a range of aromatic substrates. Some of the work described in this chapter has been published.³¹⁴

4.3 Results and discussion

The possibility of reducing simple difluorophosphoranes, such as F_2PMe_3 and $F_2P^iPr_3$, with silanes (Scheme 116) was investigated. These P^V compounds, along with compound **15**, were formed from the stoichiometric reaction between PR_3 and 2.3 equivalents of **Py-F₅** in CD_3CN (see chapter 3.3 for further details about this reaction). The introduction of $PhSiH_3$ to the mixture enabled the regeneration of the initial phosphine, which was evident in the ^{31}P NMR spectrum. Remarkably, compound **15** remained unaffected, whereas the slight excess of unreacted **Py-F₅** (approximately 0.3 equivalents remained in solution after the first reaction step in Scheme 116) converted into **Py-F₄** according to ^{19}F NMR analysis.



Scheme 116 Synthesis of the difluorophosphoranes F_2PR_3 (R = Me, *i*Pr) and **15** (first step) and reduction of F_2PR_3 with $PhSiH_3$ (second step).

This initial experiment demonstrated the ability of PhSiH₃ to reduce difluorotrialkylphosphoranes to simple trialkylphosphines. In addition, it suggested the system's potential to promote HDF, as evidenced by the formation of **Py-F₄**.

Subsequent investigations probed whether **Py-F₅** and PhSiH₃ could form **Py-F₄** in the presence of a catalytic amount of PⁱPr₃ (10 mol%) under similar reaction conditions to those used by Dobrovetsky and coworkers (*o*-DFB at 60 °C, Table 4, entry 1) with a geometrically constrained phosphine catalyst (see introduction chapter 4.1.4 for more details).²¹⁴ After 18 hours, the formation of **Py-F₄** was observed, albeit in a modest yield of 26%. Unreacted **Py-F₅** (65%) and 9% of **15** were also identified by ¹⁹F NMR spectroscopy. These results demonstrated for the first time that a catalytic HDF was achieved employing only a simple trialkylphosphine as the catalyst.

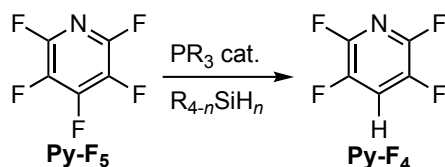
A control experiment under the same conditions showed that, in the absence of the phosphine, **Py-F₅** and PhSiH₃ or Ph₂SiH₂ did not react to form **Py-F₄**, even upon heating up to 60 °C for 18 hours. Additionally, the phosphines included in this study (PⁱPr₃ and PⁿBu₃) did not react with either silane in the absence of **Py-F₅**.

The HDF reaction with this catalytic system proceeded significantly more slowly than the one reported by Dobrovetsky and coworkers, who obtained a 95% yield of **Py-F₄** in only 3 hours at 80 °C using a geometrically constrained P^{III} catalyst.²¹⁴ Nevertheless, our protocol, which involves simple phosphines and silanes, allowed for straightforward reaction optimisation with various potential catalysts and hydride sources. The focus of this investigation was not only on improving the rate and selectivity of the system, but also on employing the simplest, most widely available and cost-effective catalysts and reagents to ensure the broad applicability of these reactions.

4.3.1 Reaction optimisation

A variety of conditions was explored to understand the effects of different phosphines, silanes and solvents on the HDF of **Py-F₅** (Table 4). As α,α,α -trifluorotoluene proved to be unreactive in the presence of phosphines and silanes in CD₃CN at high temperature (60 °C, 18 hours), it was selected as suitable internal standard in the following tests. The reaction mixtures were analysed by quantitative ¹⁹F NMR spectroscopy. The product conversion was calculated from the ratio of the integrals of the ¹⁹F NMR signals of the internal standard and **Py-F₅** before the reaction (blank sample) and the ratio of the integrals of α,α,α -trifluorotoluene and **Py-F₄** signals throughout the reaction. Due to an observed discrepancy between the signal integrals of the *meta*-F versus the *ortho*- and *para*-F of **Py-F₅** in ¹⁹F NMR spectra, inversion recovery experiments were performed on **Py-F₅** to

determine the appropriate recycle delay (D1). The *meta*-F signal at -162.7 ppm was on resonance throughout the experiment. The D1 was set at 10 seconds and a total of seven values ranging from 1 millisecond to 30 seconds were used for the inversion recovery delay (T1). It was observed that the *meta*-F exhibited the longest T1 value, measuring 7.8 seconds. Thus, the D1 parameter was set to 39 seconds ($5 \times T1$) for all the ^{19}F NMR experiments.



Entry	PR ₃	PR ₃ (mol%)	Silane	Silane (equiv.)	Solvent	Temp. / °C	Time / h	Yield of Py-F ₄ / %
1	P ⁱ Pr ₃	10	PhSiH ₃	1	<i>o</i> -DFB	60	18	26
2	P ⁱ Pr ₃	10	PhSiH ₃	1	CD ₃ CN	60	44	76
3	P ⁱ Pr ₃	10	Ph ₂ SiH ₂	1	CD ₃ CN	20	18	84
4	P ⁱ Pr ₃	10	Ph ₃ SiH	2	CD ₃ CN	20	18	2
5	P ⁿ Bu ₃	10	PhSiH ₃	1	CD ₃ CN	60	2	100
6	P ⁿ Bu ₃	10	Ph ₂ SiH ₂	1	CD ₃ CN	20	0.33	93
7	P ⁿ Bu ₃	10	Ph ₃ SiH	2	CD ₃ CN	20	18	6
8	P ⁿ Bu ₃	10	Ph ₂ SiH ₂	0.55	CD ₃ CN	20	3	87
9	P ⁿ Bu ₃	5	Ph ₂ SiH ₂	1	CD ₃ CN	20	1	93
10	P ⁿ Bu ₃	1	Ph ₂ SiH ₂	1	CD ₃ CN	20	18	83

Table 4: Reaction optimisation for HDF of **Py-F₅**. NMR yields determined by integration of ^{19}F NMR spectra using α,α,α -trifluorotoluene as internal standard.

Changing the solvent from *o*-DFB to CD₃CN significantly improved the reaction, yielding 67% of **Py-F₄** after 18 hours at 60 °C and 76% after 44 hours (Table 4, entry 2), along with a small amount of the perfluorinated bipyridine **15** (4%), traces of unreacted **Py-F₅** and minor quantities of unidentified fluorinated products. Substituting PhSiH₃ with Ph₂SiH₂ remarkably increased the reaction rate (Table 4, entry 3), enabling a lower temperature (20 °C) and resulting in 84% of **Py-F₄** after only 18 hours, along with 7% of **15**. However, further substitution of the hydride with phenyl

groups on the silicon led to limited formation of **Py-F₄**: when Ph₃SiH was employed (Table 4, entry 4), most of the starting material **Py-F₅** was left unreacted, along with 8% of **15**.

Higher yields and reaction rates were observed when PⁿBu₃ was used instead of PⁱPr₃, showing a similar relative reactivity trend with the silanes as with PⁱPr₃ (Table 4, entries 5–7). Remarkably, most of the phosphine was regenerated at the end of the reaction and only traces of catalyst decomposition were seen in the ³¹P{¹H} NMR spectrum (Figure 25).

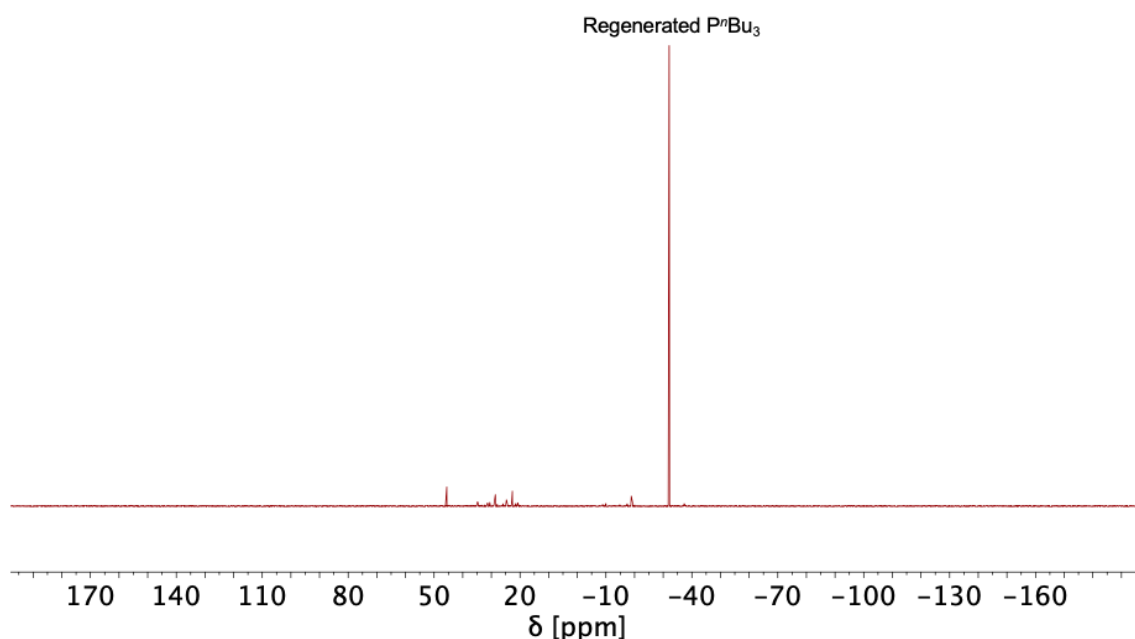


Figure 25 ³¹P{¹H} NMR spectrum (243 MHz, CD₃CN) of the reaction mixture of **Py-F₅** (1 equiv.), Ph₂SiH₂ (1 equiv.) and PⁿBu₃ (10 mol%) after 20 minutes at 20 °C.

Since PⁿBu₃ and PⁱPr₃ are both similarly strong electron-donors, we supposed that the difference in catalytic efficiency lay in the greater steric hindrance of PⁱPr₃ compared to PⁿBu₃. PMe₃ was omitted from this catalytic investigation, as it is more reactive and thus harder to handle, which was against the aim of optimising towards a simple, cheap and easy to handle catalyst system. When tested as a catalyst with **Py-F₅** and PhSiH₃, the system lacked selectivity, leading to the formation of several unidentified F-containing species as observed through ¹⁹F NMR analysis.

The combination of PⁿBu₃ and Ph₂SiH₂ provided optimal reaction conditions allowing selective HDF of **Py-F₅** to give **Py-F₄** in excellent yield (93%) (Figure 26), after only 20 minutes at 20 °C (Table 4, entry 6). This performance stands among the best reported for catalytic aromatic HDF by a main-group-element catalyst.^{214,299,300,312} Moreover, this phosphine-silane combination proved to be most economical (list prices from Merck August 2023: PⁿBu₃ £0.87/g (100 g quantity), PhSiH₃

£7.92/g (25 g quantity), PhSiH₂ £2.43/g (25 g quantity), Ph₃SiH £3.09/g (25 g quantity). List price from Fischer Scientific August 2023: PⁱPr₃ £29.6/g (10 g quantity)) and readily available among those tested. Additionally, PⁿBu₃ and Ph₂SiH₂ exhibited excellent selectivity for **Py-F₄** under these conditions, with no other HDF products observed, such as different regioisomers or multiple HDFs (Figure 26).

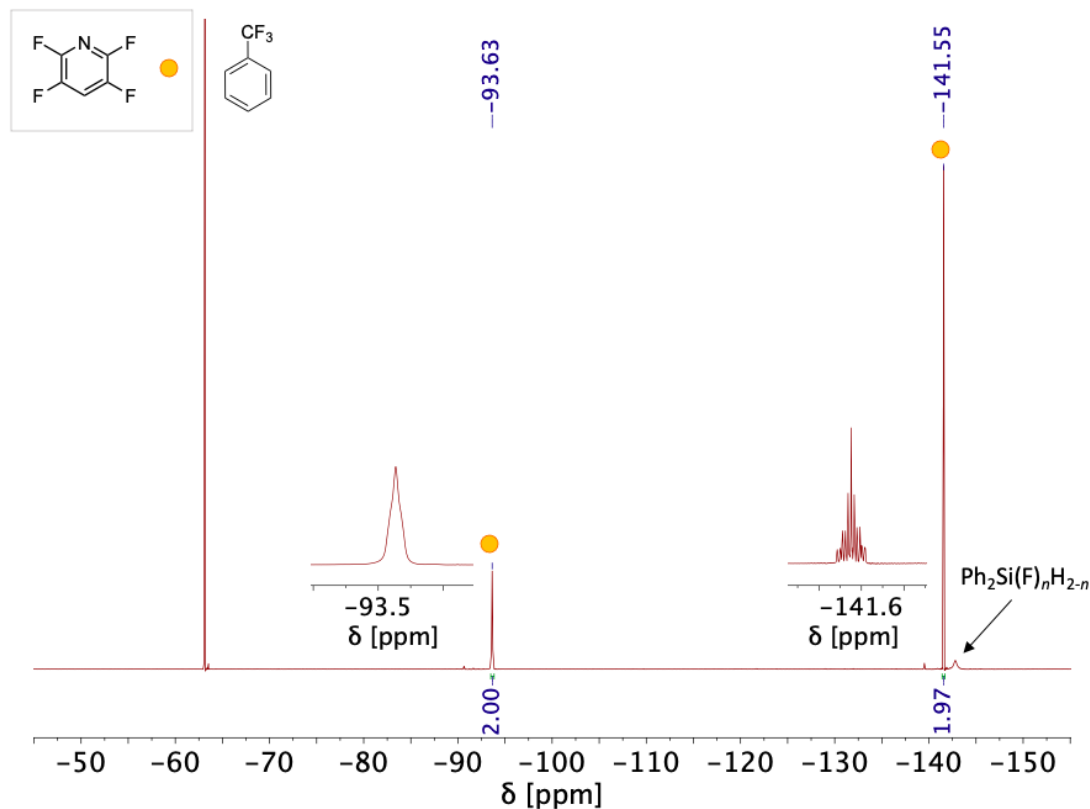


Figure 26: ¹⁹F NMR spectrum (565 MHz, CD₃CN) of the reaction mixture of **Py-F₅** (1 equiv.), Ph₂SiH₂ (1 equiv.) and PⁿBu₃ (10 mol%) after 20 minutes at 20 °C. Magnifications of the signals of **Py-F₄** are shown.

Experiments aiming to reduce the silane and phosphine loadings (Table 4, entries 8–10) showed that using a close to stoichiometric (in terms of hydride equivalents) amount of Ph₂SiH₂ still allowed good conversion to **Py-F₄** (87%), albeit at a slower rate and with a small amount of **15** formed (2%) (Table 4, entry 8). The almost complete regeneration of the phosphine (Figure 25) at the end of the reaction under optimal conditions (Table 4, entry 6) led to the exploration of the catalyst loading limits. Decreasing the phosphine loading to 5 mol% was still highly effective, although slower (93% of **Py-F₄** after 1 hour). At 1 mol% of PⁿBu₃, selective formation of **Py-F₄** was still possible, but with significantly longer reaction times (83% yield after 18 hours) and some unreacted **Py-F₅** (11%) was still present at this time. The reaction conditions outlined in entry 6 of Table 4 were selected for

further investigations, as these provided fast reactions without a substantial rise in cost, due to the cheap silane and phosphine used.

4.3.2 Substrate scope

The substrate scope for HDF was investigated, extending the studies to various fluoroarenes and heterocycles (Figure 27). Furthermore, preliminary aminodefluorination reactions were explored, resulting in products **24–27**, thus enabling C–F functionalisation to C–N.

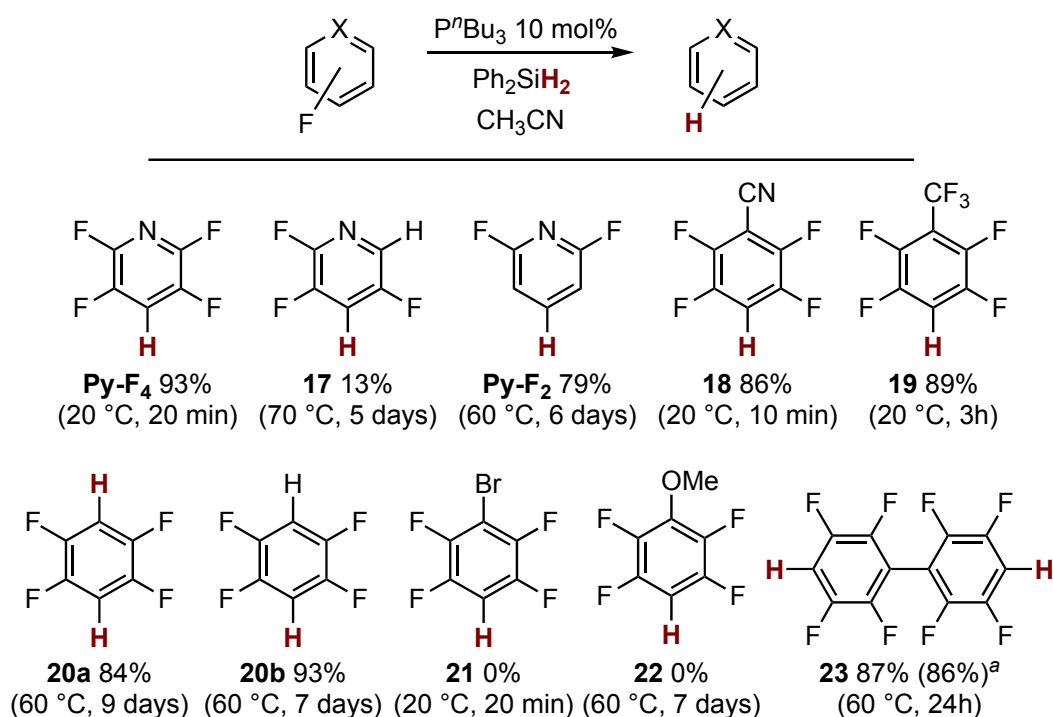


Figure 27 Results of substrate scope studies for the HDF reaction catalysed by P^nBu_3 . ^a Isolated yield after flash column chromatography shown in parentheses.

The impact that the degree of fluorination had on fluoropyridines and the regioselectivity of the HDF reaction were explored. **Py-F₄** led to the formation of **17**, albeit with a low 13% yield, requiring harsher conditions (5 days at 70 °C). The ¹⁹F NMR spectrum confirmed the presence of **17**, with the *ortho*-F signal at -92.3 ppm (*pseudo t*, $J_{FF} = 27.9$ Hz), the nearby *meta*-F at -129.0 ppm (ddd, $^3J_{FF} = 29.1$ Hz, $^3J_{FH} = 7.6$ Hz, $^4J_{FF} = 3.6$ Hz) and the remaining *meta*-F at -136.5 ppm (ddd, $^5J_{FF} = 26.3$ Hz, $^3J_{FH} = 9.2$ Hz, $^4J_{FF} = 3.7$ Hz) (Figure 29). A tentative assignment of the coupling constants is depicted in the Figure 28.

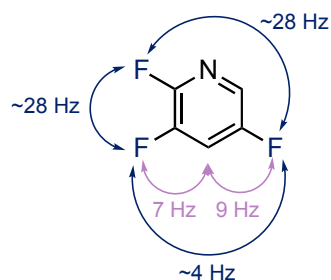


Figure 28 Assigned coupling constants for compound **17**.

The apparent triplet observed for the *ortho*-F may arise from the coupling with the other two F atoms, both displaying similar J_{FF} of 28 Hz. The ddd signals seen for the two *meta*-F result from their interaction with the other two fluorine atoms and a proton on the pyridine ring.

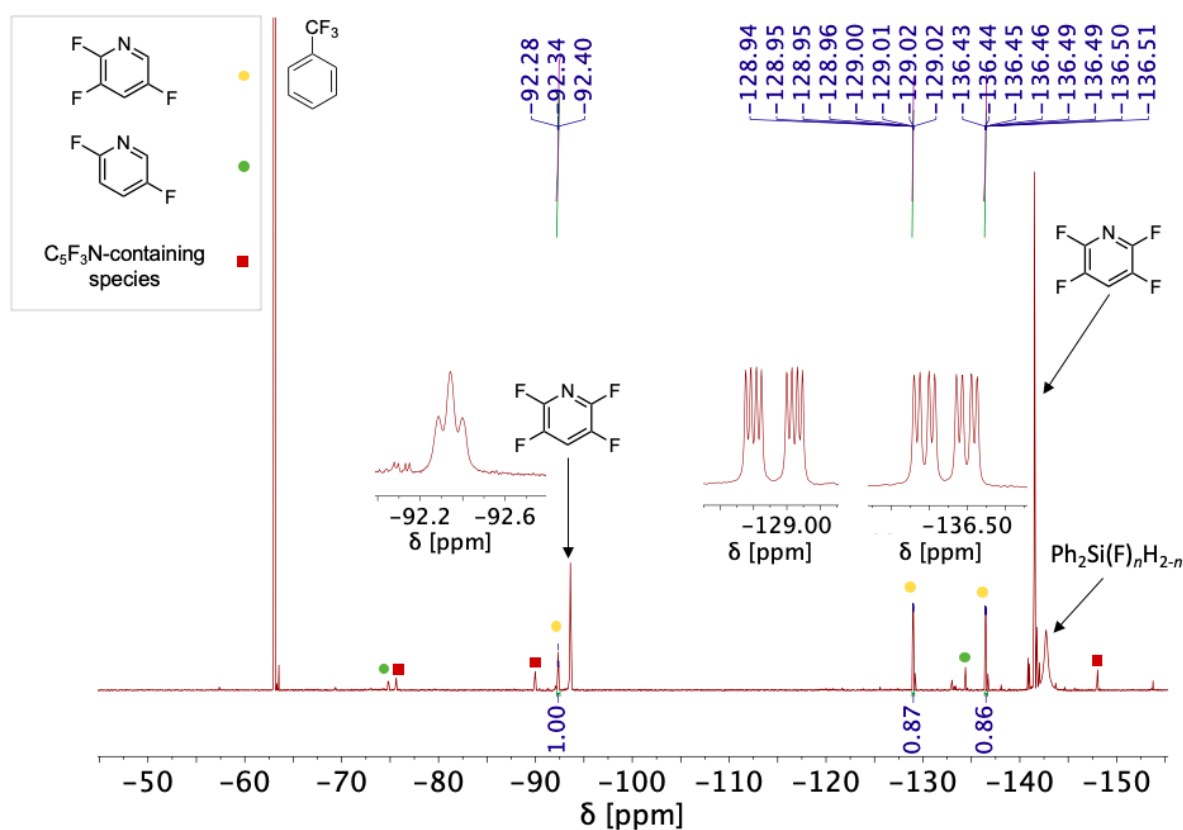


Figure 29 ^{19}F NMR spectrum (565 MHz, CD_3CN) of the reaction mixture of **Py-F₄** (1 equiv.), Ph_2SiH_2 (1 equiv.) and P^nBu_3 (10 mol%) after 5 days at 70 °C. Magnifications of the signals of **17** are given.

Unreacted **Py-F₄** (25%) was still present and other low-intensity signals were indicative of tri- and difluoropyridine isomers forming. In particular, one species was identified as 3,6-difluoropyridine according to the chemical shift of its signals and to the correlation evidenced by ^{19}F COSY NMR analysis. The corresponding peaks were a broad doublet at -74.8 ppm ($^5J_{FF} = 28.5$ Hz, *ortho*-F) and a doublet of doublets of doublets at -134.4 ppm ($^5J_{FF} = 27.5$ Hz, $^3J_{FH} = 7.4$ Hz, $^3J_{FH} = 3.4$ Hz, *meta*-

F).³¹⁵ The other main side product was proposed to be a trifluoropyridyl-derived species and it was characterised by two broad singlets at -75.6 and -90.0 ppm and a dddd at -148.0 ppm ($J = 26.8, 22.3, 8.5, 2.1$ Hz). Traces of other side products contained the $P^n\text{Bu}_3$ moiety, according to the ^1H - ^{19}F HMBC analysis.

This explains the selectivity of the HDF conditions in Table 4, entry 6, indicating a slower rate of the second HDF at the less activated *ortho*-position compared to the initial reaction at the *para*-position of **Py-F₅**. The presence of other tri- and difluoropyridines suggests that the rate of HDF at the *ortho*- and *meta*-positions was comparable and much slower than the rate of HDF at the *para*-position.

Reducing the degree of fluorination of the substrate while retaining a C-F bond at the *para*-position enabled the HDF and formation of **Py-F₂** (79% yield after 6 days at 60°C) from **Py-F₃**, although at a relatively slower rate (Figure 30).

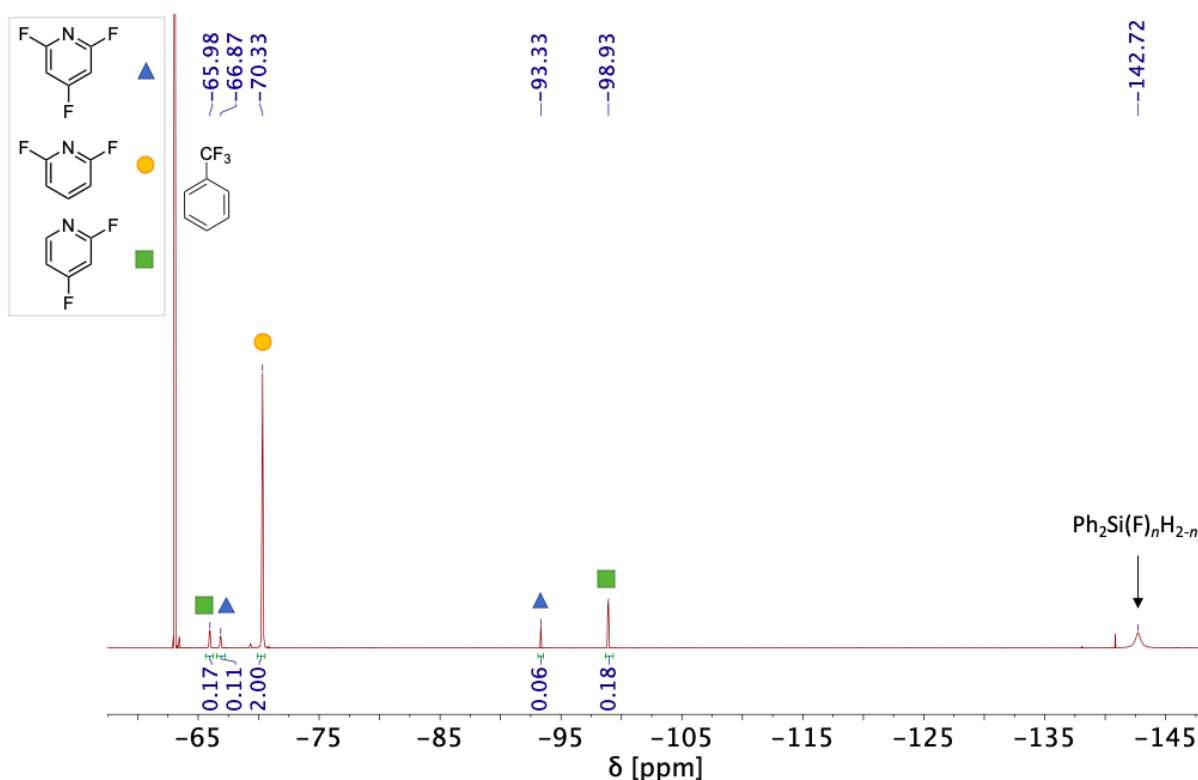


Figure 30 ^{19}F NMR spectrum (565 MHz, CD_3CN) of the reaction mixture of 2,4,6-trifluoropyridine (1 equiv.), Ph_2SiH_2 (1 equiv.) and $P^n\text{Bu}_3$ (10 mol%) after 6 days at 60°C .

Unreacted **Py-F₃** (5%) and some 2,4-difluoropyridine (14%) were observed after 6 days, indicating that more electron-poor heteroaromatics lead to faster reactions, aligning with the proposed mechanism (see Scheme 127).

The catalytic HDF reaction was extended beyond the scope of pyridines. Electron-poor aromatics like pentafluorobenzonitrile and perfluorotoluene rapidly underwent HDF, yielding **18** and **19** in

excellent yields (86 and 89% respectively). Simple fluorobenzenes exhibited similar reactivity to fluoropyridines. Hexafluorobenzene underwent double HDF, forming tetrafluorobenzene (Figure 27, **20a**). The formation of **20a** was detected after 2 hours, with the amount increasing after 18 hours. Interestingly, only trace amounts of pentafluorobenzene were seen in the ^{19}F NMR spectra at these time periods. It seems that the rate of HDF of hexa- and pentafluorobenzene were similar and overall significantly slower than perfluorotoluene. This was corroborated by direct HDF of pentafluorobenzene (Figure 27, **20b**), which occurred within a similar timescale to **20a** under comparable conditions. Both reactions yielded 1,2,4,5-tetrafluorobenzene in high yields (84% and 93%, respectively). Perfluorobiphenyl was effectively converted into the doubly hydrodefluorinated product **23**, yielding 87% after 24 hours at 60 °C. Throughout the reaction, the mono-hydrodefluorinated product was observed (39%) after 1 hour (^{19}F NMR signals at $\delta = -139.5, -152.6$ and -162.9 ppm), along with **23** (15%) and unreacted perfluorobiphenyl (42%) in the ^{19}F NMR spectrum.

The introduction of an electron-donating substituent in pentafluoroanisole was not tolerated in this system, yielding only traces of hydrodefluorinated products after 7 days at 60 °C, with most of the starting material remaining unreacted.

When bromopentafluorobenzene was employed as a substrate at 20 °C, no conversion to the hydrodefluorinated product **21** was observed within 20 minutes. However, a small amount of pentafluorobenzene (3%) was observed, accompanied by a new species detected in the ^{19}F NMR spectrum at $\delta = -128.4, -142.9$ and -158.3 ppm (11%) (yellow label in Figure 31). This was correlated with a signal in the ^{31}P NMR spectrum at 36.6 ppm, corresponding to the main phosphorus-containing product.

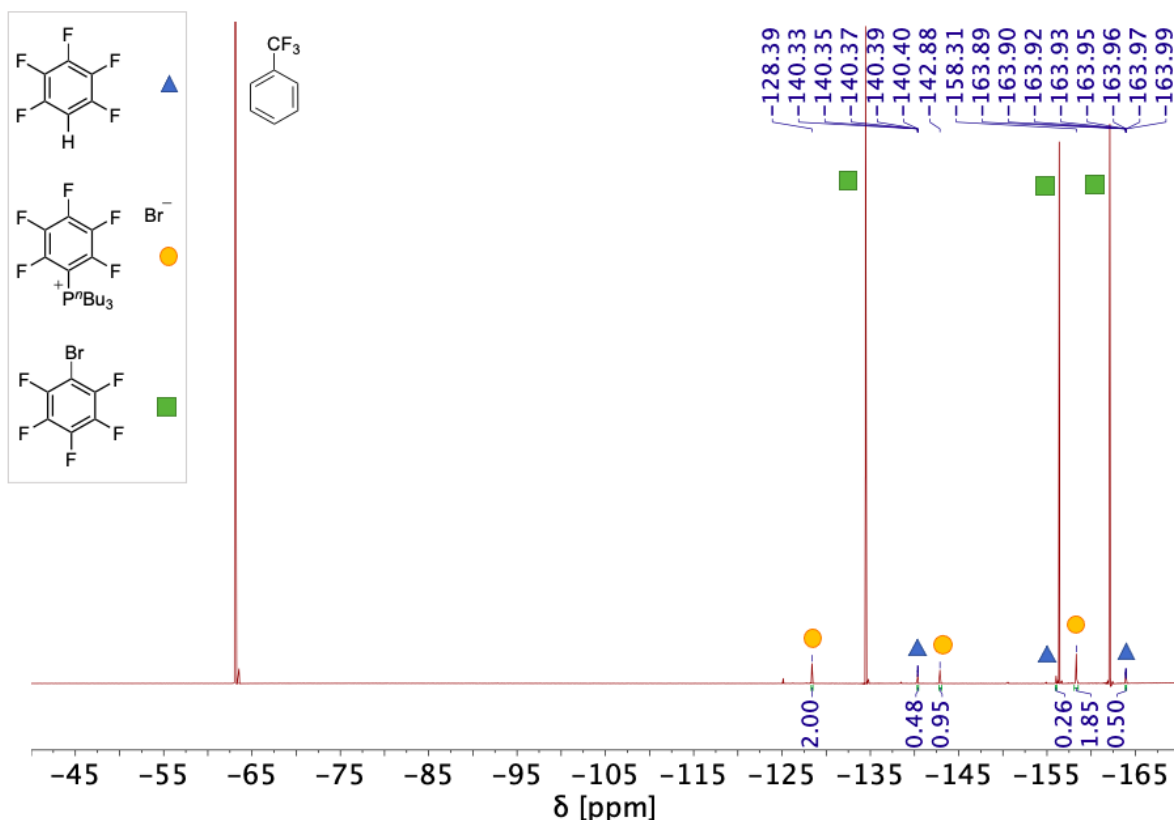


Figure 31 ^{19}F NMR spectrum (565 MHz, CD_3CN) of the reaction mixture of bromopentafluorobenzene (1 equiv.), Ph_2SiH_2 (1 equiv.) and P^nBu_3 (10 mol%) obtained after 20 minutes at 20°C .

The addition of further 0.9 equivalents of P^nBu_3 significantly intensified the signals of this species in both the ^{19}F and ^{31}P NMR spectra (recorded after 30 minutes at 20°C), together with the consumption of most of the bromopentafluorobenzene (more spectroscopic details are shown in the mechanistic studies section, chapter 4.3.4). This newly formed species was identified as the phosphonium salt $[\text{P}(\text{C}_6\text{F}_5)(^n\text{Bu})_3]\text{Br}$ (**[28]Br**), resulting from C–Br activation of the fluoroarene rather than C–F activation. At that stage, further production of pentafluorobenzene was observed (21%) and after 18 hours at 20°C this had increased slightly to 35%. For this substrate, hydrodebromination appeared to be favoured over HDF, although higher phosphine loadings were required as the system appeared to rest as the relatively unreactive salt **[28]Br**, which has implications in terms of the mechanistic proposal.

4.3.3 Catalytic aminodefluorination reaction

The potential of this catalytic methodology for other C–F functionalisations, such as the aminodefluorination reaction, was also explored. Aromatic amines are important intermediates in pharmaceuticals, agrochemicals and materials science industries.^{316–318} They are commonly prepared by reduction of the corresponding aromatic nitrocompound³¹⁹ or, in the case of more complex amines, through transition-metal-catalysed C(sp²)–N cross-coupling reactions involving aryl halides and nucleophilic amines (e.g., Ullmann,³²⁰ Buchwald-Hartwig^{321,322} and metallaphotoredox amination reactions).³²³ Transition-metal-free strategies usually involve S_NAr of Ar–F with aliphatic amines. Alkali metal salts of strong nucleophiles, such as LiHMDS,³²⁴ *n*BuLi,³²⁵ LiH,³²⁶ and KOtBu³²⁷ have been used in this context, although their high basicity makes it challenging to control the system selectivity. Furthermore, the use of other main-group elements like Mg,³²⁸ Al,²⁹⁰ Pb³²⁹ and Sn³³⁰ has shown to enable the C–F cleavage and the formation of new C–N bonds.

In the final part of this reactivity study, investigations were carried out to explore the C–F amination of **Py-F₅** using silylamides in the presence of catalytic P^{*n*}Bu₃.²¹⁴ The synthesis of Ph₂Si(Cl)(NEt₂) was conducted by adapting existing dialkylsilyldiamides R₂Si(N(R')₂)₂ (where R = Me, Et, vinylmethyl; R' = Me, Et) preparation procedures present in the literature.^{331,332} The reaction is reported in Scheme 117.



Scheme 117 Reaction of Ph₂SiCl₂ (1 equiv.) and dried Et₂NH (2 equiv.) in dried Et₂O under N₂ atmosphere resulted in the synthesis of Ph₂Si(Cl)(NEt₂) and precipitation of [Et₂NH₂]Cl.

However, contrary to the reported methods, in our case the reaction exhibited selectivity for only the monoamidation product. Both ¹H NMR spectroscopy (Figure 32) and mass analysis (MS-APCI: [C₁₆H₂₁ClNSi]⁺ 290.113336 *m/z*, 2.4 ppm deviation from theoretical mass) confirmed the identity of the product. This selectivity is likely attributed to the higher steric hindrance of the two aromatic rings on the silicon atom compared to the alkyl groups (Me and Et) employed in the literature.^{331,332}

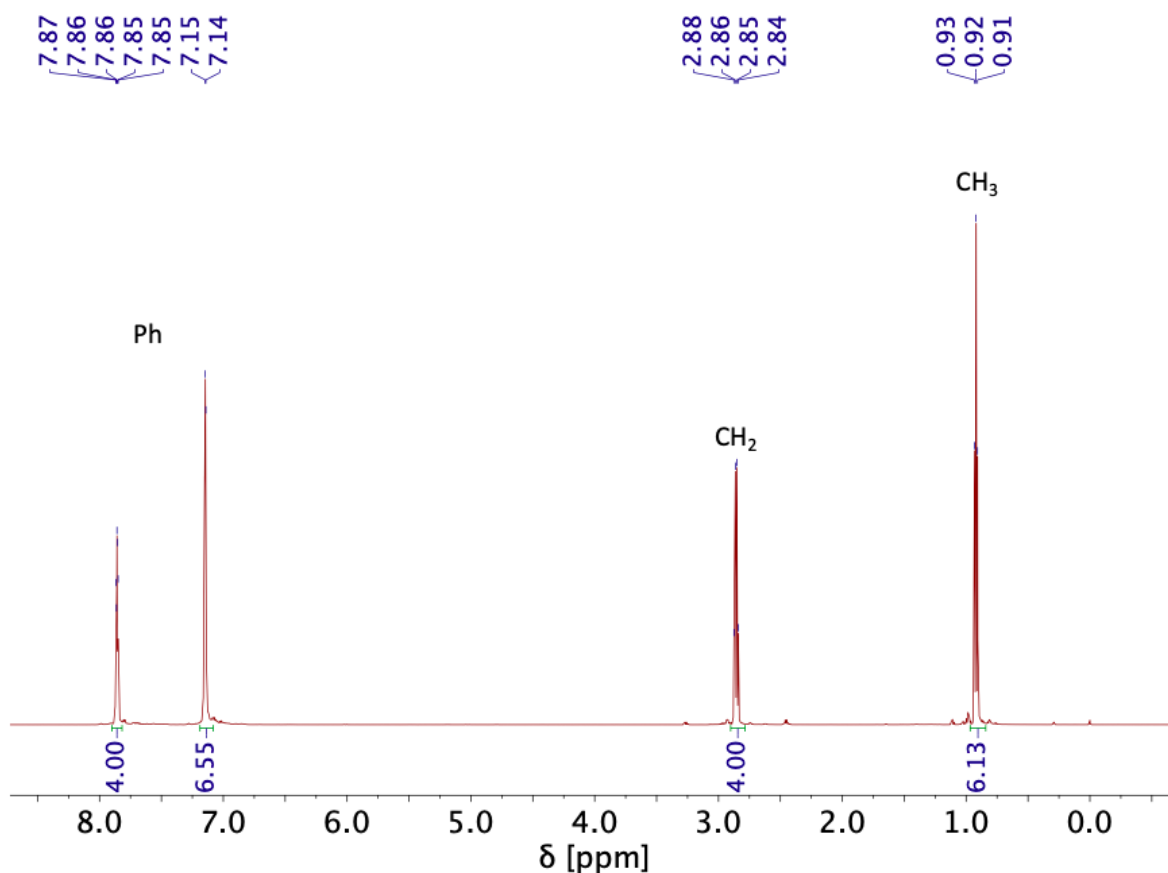
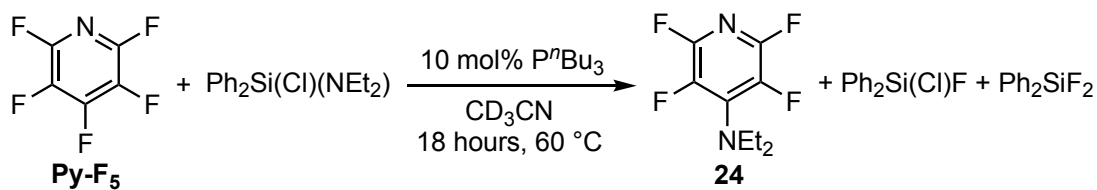


Figure 32 ^1H NMR spectrum (C_6D_6 , 600 MHz) of the isolated $\text{Ph}_2\text{Si}(\text{Cl})(\text{NEt}_2)$.

When **Py-F₅** was treated with a slight excess of $\text{Ph}_2\text{Si}(\text{Cl})(\text{NEt}_2)$ and 10 mol% of P^nBu_3 at 60 °C for 18 hours, a good yield (75%) of the aminated product **24** was achieved, accompanied by a small amount of unreacted **Py-F₅** (10%) (Scheme 118).



Scheme 118 Reaction of aminodefluorination of **Py-F₅** (1 equiv.) in the presence of $\text{Ph}_2\text{Si}(\text{Cl})(\text{NEt}_2)$ (1.1 equiv.) and P^nBu_3 (10 mol%).

Compound **24** was characterised by two multiplets in the ^{19}F NMR spectrum at $\delta = -96.7$ and -157.0 ppm (Figure 33), two signals in the ^1H NMR at $\delta = 3.43$ (qt, $^3J_{\text{HH}} = 7.1$ Hz, $^5J_{\text{HF}} = 1.6$ Hz, $-\text{CH}_2\text{CH}_3$) and 1.22 ppm (t, $^3J_{\text{HH}} = 7.1$ Hz, $-\text{CH}_2\text{CH}_3$) (Figure 34) and a molecular radical cation $[\text{M}]^+$ of 222.07810 m/z (2.85 ppm deviation from theoretical) in the GC(EI)-MS.

However, this reaction displayed a minor drawback. Unlike most HDF reactions reported previously, which were generally highly selective, under aminodefluorination conditions an additional product (**29**, in a 10% yield) was observed in the ^{19}F NMR spectrum at $\delta = -89.0$ (ddd, $^3J_{\text{FF}} = 33.0$ Hz, $^5J_{\text{FF}} = 27.5$ Hz, $^4J_{\text{FP}} = 6.3$ Hz), -125.2 (dd, $^3J_{\text{FF}} = 32.3$, $^4J_{\text{FF}} = 10.8$ Hz) and -151.3 ppm (*pseudo* dt, $^5J_{\text{FF}} = 26.9$, $^4J_{\text{FF}} \cong ^3J_{\text{FP}} \cong 10$ Hz) (green label in Figure 33) and in the $^{31}\text{P}\{^1\text{H}\}$ NMR spectrum at $\delta = 36.4$ ppm (Figure 35).

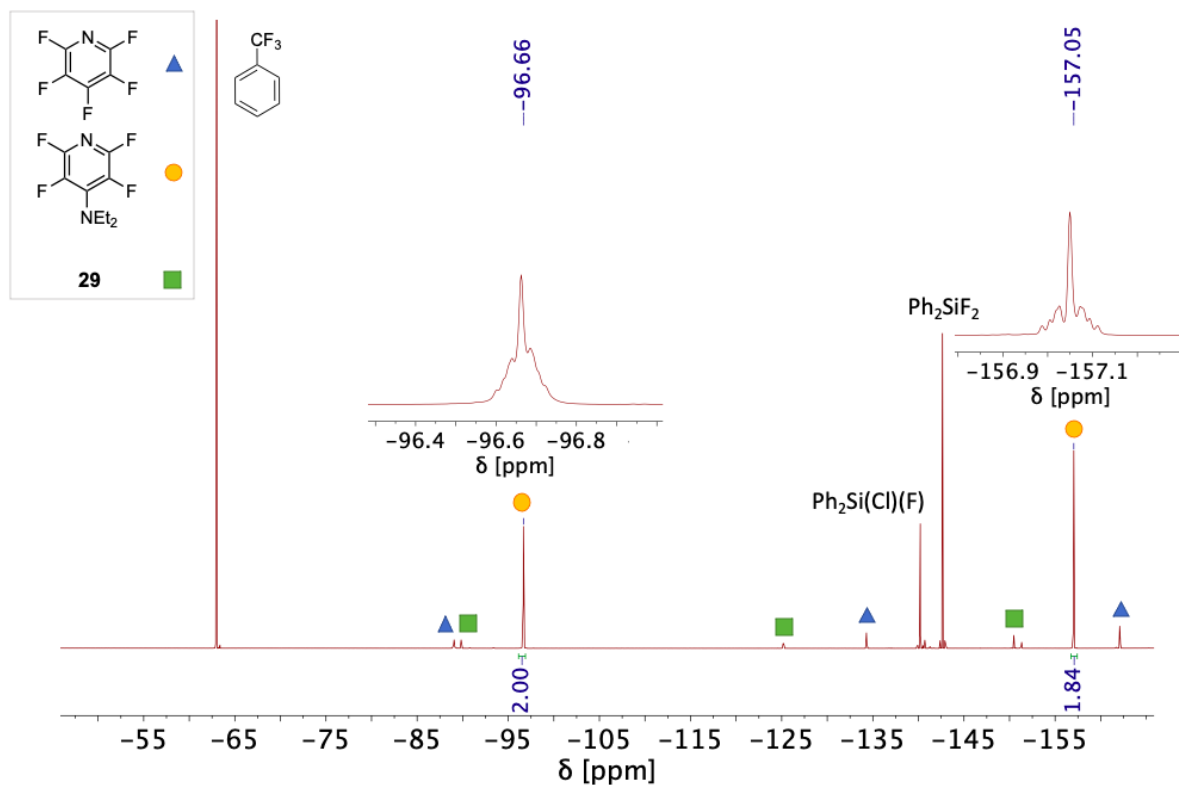


Figure 33 ^{19}F NMR spectrum (565 MHz, CD_3CN) of the reaction mixture of **Py-F₅** (1 equiv.), $\text{Ph}_2\text{Si}(\text{Cl})(\text{NEt}_2)$ (1.1 equiv.) and P^nBu_3 (10 mol%) obtained after 18 hours at 60 °C. Magnifications of the signals of **24** are given.

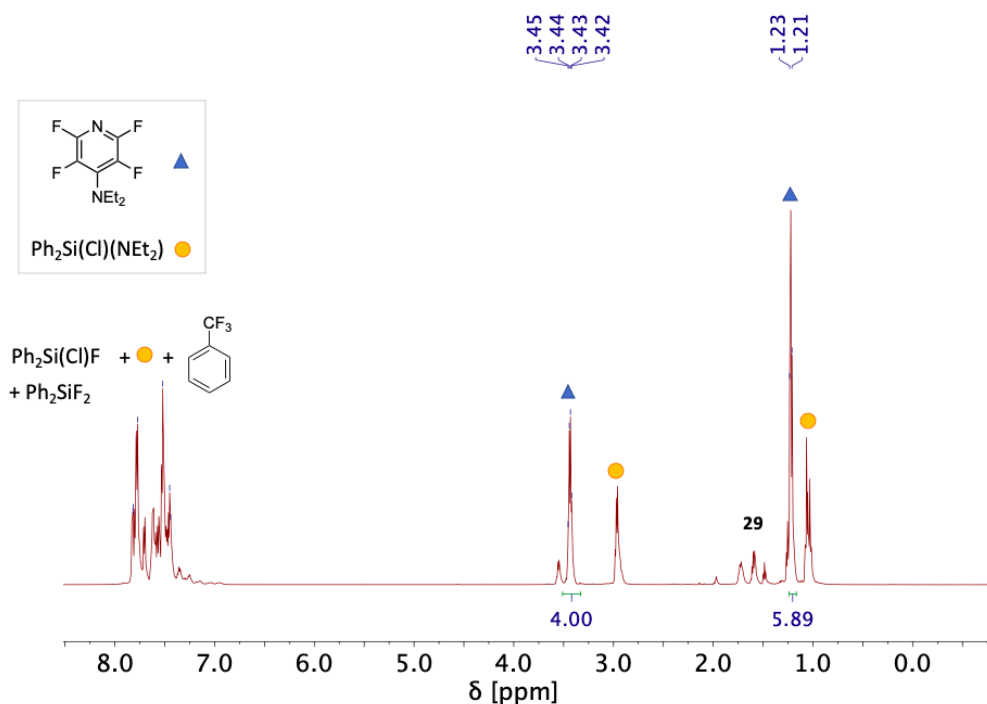


Figure 34 ^1H NMR spectrum (600 MHz, CD_3CN) of the reaction mixture of **Py-F₅** (1 equiv.), $\text{Ph}_2\text{Si}(\text{Cl})(\text{NEt}_2)$ (1.1 equiv.) and P^nBu_3 (10 mol%) obtained after 18 hours at 60 °C.

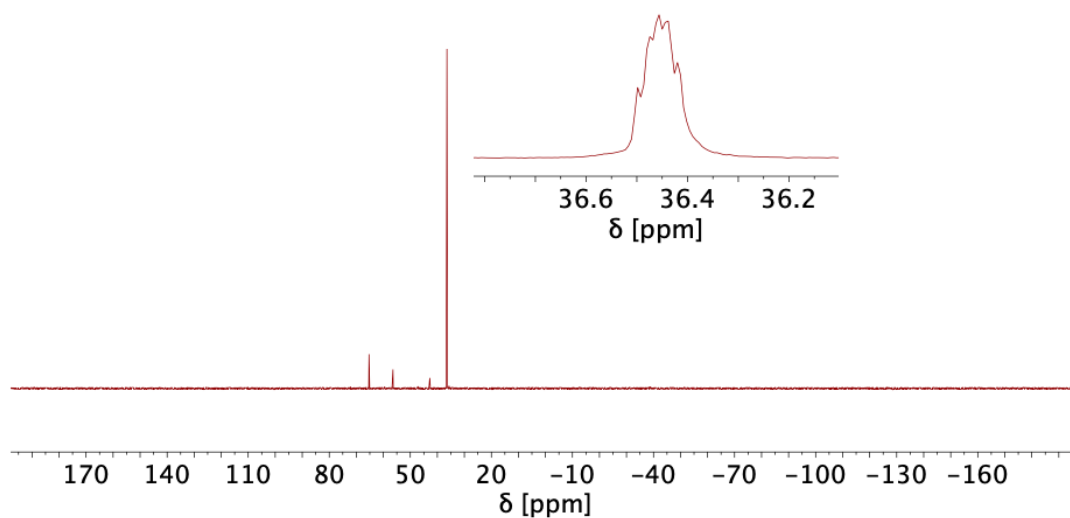


Figure 35 $^{31}\text{P}\{^1\text{H}\}$ NMR spectrum (243 MHz, CD_3CN) of the reaction mixture of **Py-F₅** (1 equiv.), $\text{Ph}_2\text{Si}(\text{Cl})(\text{NEt}_2)$ (1.1 equiv.) and P^nBu_3 (10 mol%) obtained after 18 hours at 60 °C. A magnification of the signal of **29** is given.

Species **29** did not form in the stoichiometric version of the reaction, making it challenging to isolate and analyse it effectively using NMR and MS techniques. However, the presence of three different ^{19}F NMR signals with an integral ratio of 1:1:1 (Figure 33) and the multiplet in the $^{31}\text{P}\{^1\text{H}\}$ NMR

spectrum (Figure 35) suggested the formation of a trifluoropyridyl-substituted phosphonium salt. A possible structure is proposed in Figure 36.

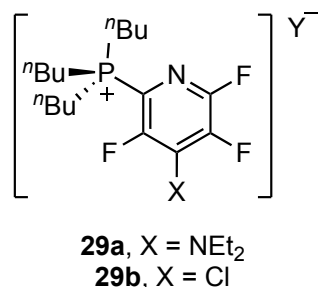
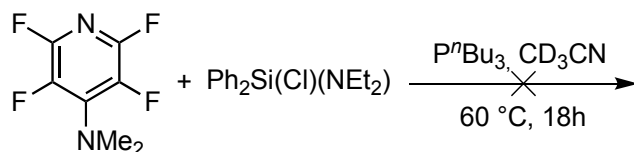


Figure 36 Possible structure of the unidentified species **29**.

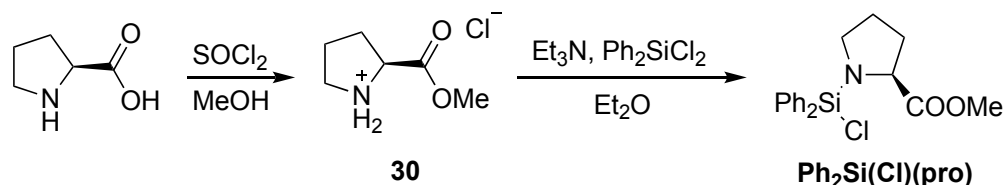
The substituent X could be a chloride or amino-group and Y a chloride or a silicate anion. To investigate whether the proposed species with a *para*-NEt₂ substitution (**29a**), which would derive from the *ortho*-C–F activation of the monoaminodefluorination product **24**, was formed, the commercially available 4-dimethylamino-tetrafluoropyridine was reacted with one equivalent of PⁿBu₃ in the presence of one equivalent of Ph₂Si(Cl)(NEt₂) for 18 hours at 60 °C (Scheme 119).



Scheme 119 Reaction test between 4-dimethylamino-tetrafluoropyridine (1 equiv.), PⁿBu₃ (1 equiv.) and Ph₂Si(Cl)(NEt₂) (1 equiv.) carried out in CD₃CN for 18 hours at 60 °C.

The NMR analyses showed no reactivity of the system. This led to the rejection of the hypothesis that species **29a** corresponds to the unidentified phosphonium. This observation makes the formation of species **29b** (where X = Cl) more probable, derived from the *ortho*-C–F activation of the chlorodefluorination product. Nevertheless, this hypothesis also has some potential challenges, as the mechanistic studies section (chapter 4.3.4) demonstrates that, in the presence of other halogens in the *para*-position of the pyridine, the cleavage of the *para*-C–halogen bond is favoured over the *ortho*-C–F bond. Additional studies will be conducted to enhance our understanding of the unknown species **29** and increase this reaction selectivity.

The extension of this reaction to more complex amines also proved possible. Ph₂Si(Cl)(pro) (where pro is *L*-proline methyl ester) was synthesised through the esterification of *L*-proline, followed by the monoamidation of Ph₂SiCl₂ (Scheme 120).



Scheme 120 Synthesis of $\text{Ph}_2\text{Si}(\text{Cl})(\text{pro})$ via esterification of L-proline to form the L-proline methyl ester hydrochloride (**30**) and amidation of Ph_2SiCl_2 .

In the initial step of the reaction, standard conditions for esterification were employed: MeOH reacted with SOCl_2 to provide anhydrous HCl which led to the acid-catalysed esterification of L-proline (similar to the Fischer esterification)³³³ forming the L-proline methyl ester hydrochloride **30**. Subsequently, a procedure similar to that used to prepare $\text{Ph}_2\text{Si}(\text{Cl})(\text{NEt}_2)$ was applied. Two equivalents of NEt_3 were used to doubly deprotonate the hydrochloride salt **30** in the presence of one equivalent of Ph_2SiCl_2 , resulting in the liberation of the desired product $\text{Ph}_2\text{Si}(\text{Cl})(\text{pro})$ and the precipitation of two equivalents of $[\text{HNEt}_3]\text{Cl}$. In a practical view, though, this reaction lacked selectivity. The formation of the desired compound $\text{Ph}_2\text{Si}(\text{Cl})(\text{pro})$ as the main product was confirmed through mass spectrometry (MS-APCI: $[\text{C}_{18}\text{H}_{21}\text{ClNO}_2\text{Si}]^+$ 346.102908 m/z (1.3 ppm deviation from theoretical mass); $[\text{C}_{18}\text{H}_{20}\text{NO}_2\text{Si}]^+$ 310.126372 m/z (1.9 ppm deviation from theoretical mass)) and ^1H , ^{13}C and ^{29}Si NMR analyses. The ^1H NMR signals were distinctive of the proline ester moiety (Figure 38). Interestingly, the signal at $\delta = 3.94$ ppm, corresponding to the proton on the α -C to the carbonyl, is a doublet of doublets ($^3J_{\text{HH}'} = 8.6$ Hz, $^3J_{\text{HH}''} = 3.3$ Hz). This multiplicity arises from the coupling with the two diastereotopic protons in the β -position. In contrast, the signal for the two H_δ appeared as a triplet ($\delta = 6.21$ ppm, $^3J_{\text{HH}} = 6.5$ Hz) due to the coupling with the two H_γ protons (Figure 37). It is worth noting that due to the rapid proline interconversion between its *endo* and *exo* conformations (on the NMR timescale), the two H_γ appear to be magnetically equivalent.³³⁴

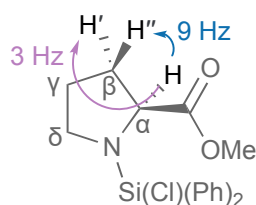


Figure 37 Proton coupling constants of $\text{Ph}_2\text{Si}(\text{Cl})(\text{pro})$.

Nevertheless, the synthesis was not completely selective because two additional sets of signals were observed in the ^1H NMR spectrum, indicating the presence of another diphenylsilyl-containing compound (Ph peaks in the aromatic region, labelled with a green square in Figure 38) and a

derivative of *L*-proline methyl ester (characterised by similar ^1H and ^{13}C NMR signals of $\text{Ph}_2\text{Si}(\text{Cl})(\text{pro})$, labelled with yellow circles in Figure 38).

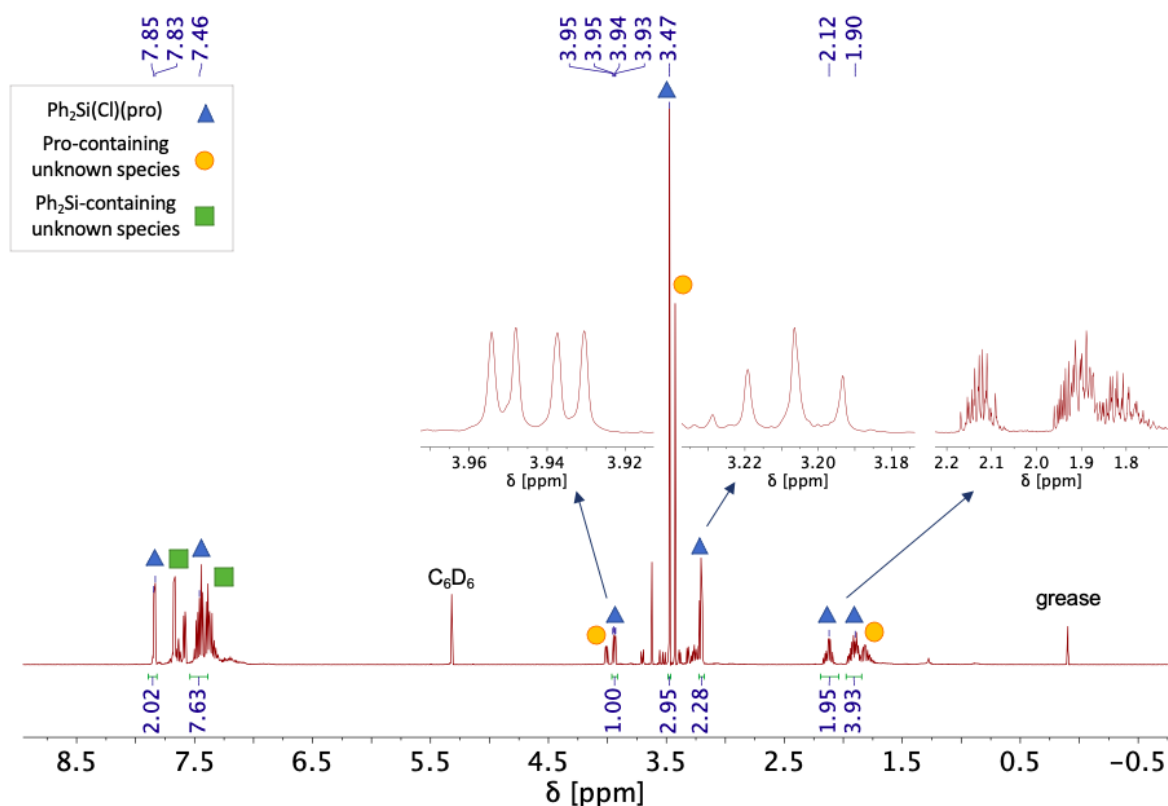


Figure 38 ^1H NMR spectrum (600 MHz, C_6D_6) of the reaction mixture obtained from the final step of Scheme 120, after filtration of the precipitated $[\text{HNEt}_3]\text{Cl}$ salt and extraction with pentane of the products.

While it is plausible that these signals could belong to the same compound, 2D-NMR spectra did not reveal any correlations between these resonances. Additionally, the mass analysis conducted failed to provide any pertinent information about this species. It is hypothesised that the unknown species might be a $\text{Ph}_2\text{Si}(\text{pro})$ -derivative; however, its precise identity remains elusive at this stage.

To enhance the selectivity of the reaction, initial tests on the silylation step (second step of Scheme 120) were conducted using the commercial salt **30**. While these tests showed an improved selectivity toward the desired product, challenges arose, due to the lower solubility of the commercial **30** than the synthesised one. This limited the reaction going to completion as the starting material, Ph_2SiCl_2 , remained unreacted even after 72 hours in acetonitrile at 20°C .

Nevertheless, the possibility of performing the catalytic aminodefluorination reaction of **Py-F₅** with the mixture analysed in Figure 38 was investigated. Remarkably, the reaction gave a very good yield of **25** (88%) alongside a minor amount of unreacted **Py-F₅** and a 7% yield of an unknown pyridine-

containing phosphonium salt — displaying similar spectroscopic features as **29**. The ^{19}F NMR spectrum of **25** closely resembled that of **24**, displaying ^{19}F NMR signals at $\delta = -97.0$ and -160.1 ppm (Figure 39). The ^1H NMR spectrum indicated the retention of the proline methyl ester moiety (Figure 40).

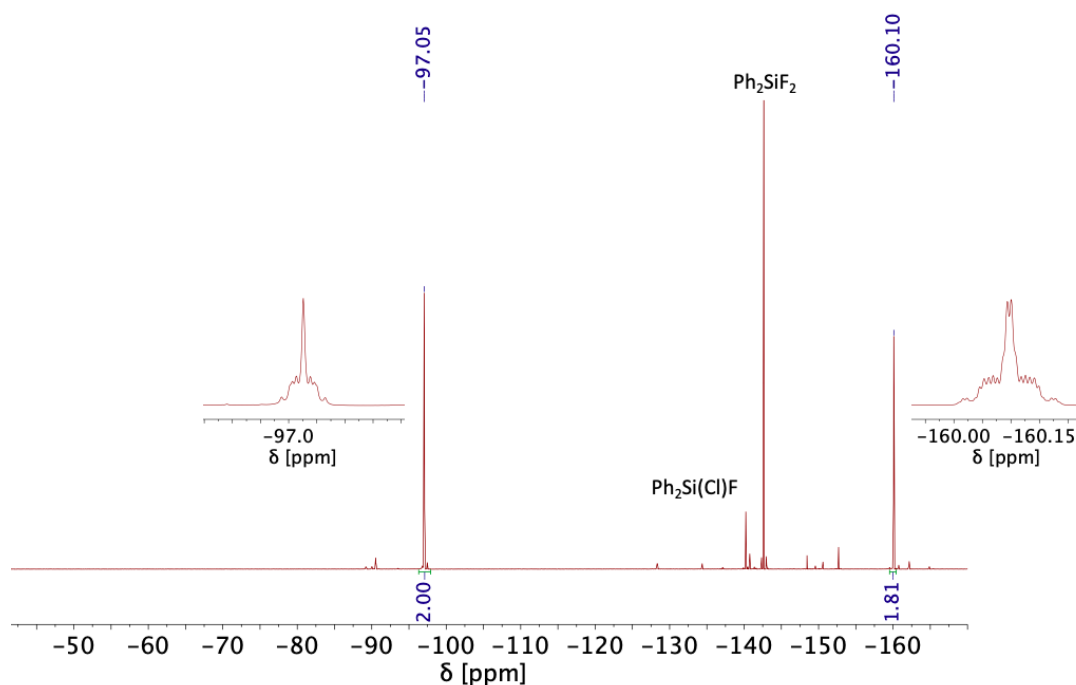


Figure 39 ^{19}F NMR spectrum (565 MHz, CD_3CN) of the reaction mixture of **Py-F₅** (1 equiv.), $\text{Ph}_2\text{Si}(\text{Cl})(\text{pro})$ (1.1 equiv.) and P^nBu_3 (10 mol%) obtained after 18 hours at 60 °C. Magnifications of the signals of product **25** are given.

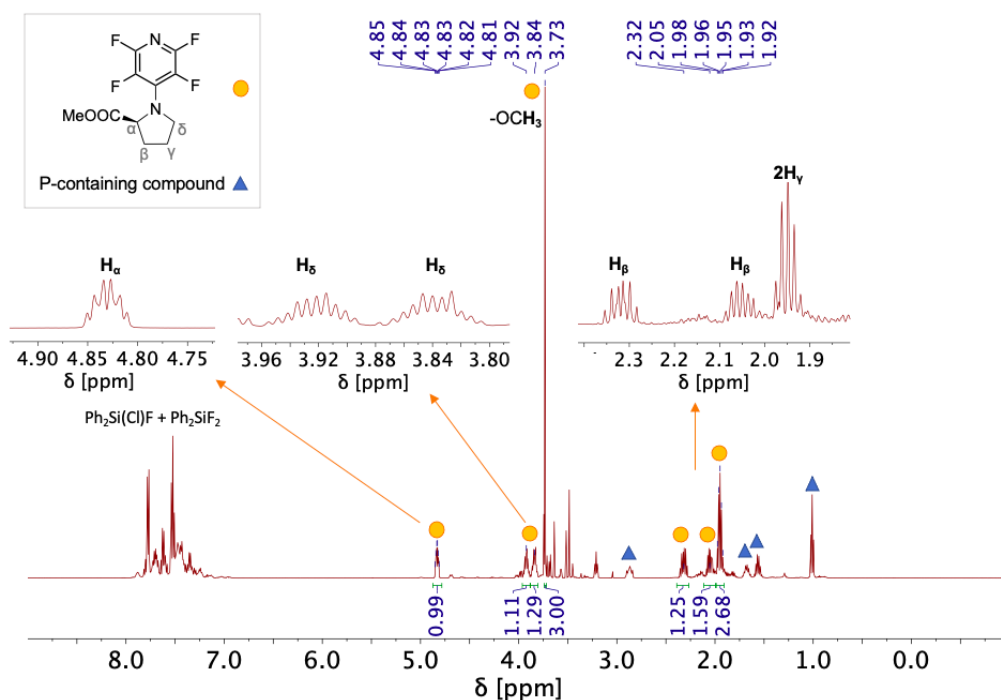


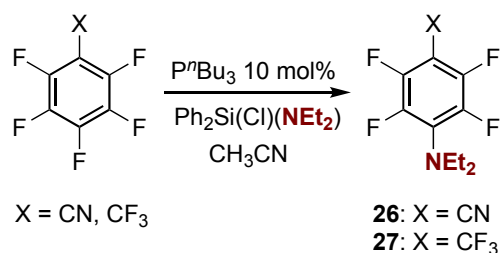
Figure 40 ^1H NMR spectrum (600 MHz, C_6D_6) of the reaction mixture of **Py-F₅** (1 equiv.), $\text{Ph}_2\text{Si}(\text{Cl})(\text{pro})$ (1.1 equiv.) and P^nBu_3 (10 mol%) obtained after 18 hours at 60 °C. Magnifications of the signals of product **25** are given.

Through ^1H , ^{13}C and related 2D-NMR analyses, signals corresponding to the desired product **25** were successfully identified. In the ^1H NMR spectrum (Figure 40), the number of the peaks and the complexity of their multiplicity increased due to the coupling with the pyridine F-atoms and the system's enhanced rigidity, limiting the *endo-exo* interconversion of the proline ring.³³⁴ This resulted in six distinct signals for the ring protons. For instance, H_α at $\delta = 4.83$ ppm appears as an apparent dq, where the doublet ($^3J_{\text{HH}} = 8.2$ Hz) derives from the coupling with H^1_β and the *pseudo* quartet ($J = 3.5$ Hz) from the interaction with H''_β and the two pyridine *meta*-F atoms. Similarly, the two signals for H_δ at 3.92 and 3.36 ppm are pure dtt: they couple with the other geminal proton ($^2J_{\text{HH}} \approx 10$ Hz), the two H_γ ($^3J_{\text{HH}} \approx 7$ Hz) and the two *meta*-F atoms ($^5J_{\text{HF}} \approx 3$ Hz). The two H_β signals at 2.32 and 2.06 ppm exhibit an apparent dq pattern. The doublet arises from the coupling with the geminal proton ($^2J_{\text{HH}} \approx 12$ Hz), the *pseudo* quartet from the two H_γ and H_α , all with similar J around 7 Hz. Lastly, the apparent pentet ($J = 6.8$ Hz) at 1.95 ppm represents the H_γ , coupling with the two H_β and the two H_δ .

Moreover, the GC-MS(EI) confirmed the accurate mass of the molecular radical cation $[\text{C}_{11}\text{H}_{10}\text{N}_2\text{O}_2\text{F}_4]^+$ at 278.06880 m/z (5.41 ppm deviation from theoretical). Other fragments were also associated with the loss of the -COOMe moiety ($[\text{C}_9\text{H}_7\text{N}_2\text{F}_4]^+$ 219.05493 m/z) and a further loss of part of the pyrrolidine ring ($[\text{C}_6\text{HN}_2\text{F}_4]^+$ 177.00778 m/z).

Confirmation of the retention of the configuration of the stereogenic centre was achieved through specific rotation measurements. Optical rotation studies typically measure the angle by which the plane of polarisation rotates when polarised light passes through a liquid. The specific optical rotation, denoted as $[\alpha]_D^T$, of a sample solution is directly proportional to the observed rotation angle, divided by the pathlength of the sample in millimetres and the mass (in g) of the analysed substance in 100 mL of the solution.³³⁵ In this analysis, a solution of *L*-proline showed an average value of $[\alpha]_D^{20} = -79$ (*c* 1.0, CH₃OH). A solution of Ph₂Si(Cl)(pro) exhibited $[\alpha]_D^{20} = -25$ (*c* 0.5, CH₂Cl₂) and the reaction mixture containing product **25** displayed $[\alpha]_D^{20} = -65$ (*c* 2.5, CH₂Cl₂), both indicating the rotation of polarised light. It is important to note that the latter two solutions contained impurities, which might affect the accuracy of the measurements. Despite this, the results still provide an indication that the Ph₂Si(Cl)(pro) and product **25** solutions are optically active, suggesting that no or little racemisation occurred during these reactions.

Extending the fluoroarene substrates beyond **Py-F₅** also proved possible, with both pentafluorobenzonitrile and perfluorotoluene reacting with Ph₂Si(Cl)(NEt₂) in the presence of 10 mol% P^{*n*}Bu₃ to give **26** (in 82% NMR yield after four days at 60 °C and one day at 80 °C) and **27** (in 50% NMR yield after four days at 60 °C and six days at 80 °C) (Scheme 121).



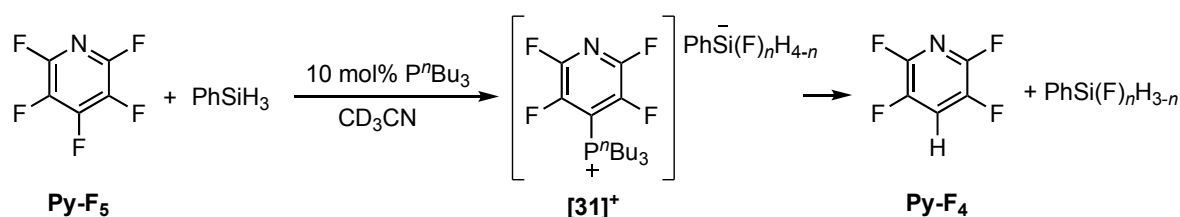
Scheme 121 Catalytic aminodefluorination of pentafluorobenzonitrile and perfluorotoluene using P^{*n*}Bu₃ as catalyst.

However, these substrates proved more sluggish under the reaction conditions optimised for HDF. Further optimisation is required in future studies to extend the aminodefluorination reactions.

This investigation demonstrated that potentially sensitive functional groups were tolerated by this catalytic aminodefluorination reaction and that it may find application in the preparation of functionalised, fluorinated amines (e.g. in pharmaceutical or agrochemical synthesis).

4.3.4 Mechanistic studies

Experimental and computational mechanistic studies were conducted to further investigate the pathways involved in the HDF reaction. Under the optimised conditions for HDF of **Py-F₅** (Table 4, entry 6), the reaction was too fast to detect any intermediates. However, in slower reactions at room temperature, some insights were gained by observing the phosphorus-containing intermediates. When **Py-F₅** was treated with PhSiH₃ and 10 mol% of PⁿBu₃ in CD₃CN at 20 °C (Scheme 122), the quantitative conversion of PⁿBu₃ into a new species displaying an apparent septet resonance at $\delta = 38.1$ ppm ($J \approx 5$ Hz) was observed in the ³¹P{¹H} NMR spectrum after 1 hour (Figure 42). This chemical shift is distinctive for a phosphonium cation.²²⁷ At the same time, new complex multiplets in the ¹⁹F NMR spectrum at $\delta = -88.5$ and -130.3 ppm appeared. The only other species detected by the ¹⁹F NMR analysis were unreacted **Py-F₅**, **Py-F₄** and the fluorosilane produced by H/F exchange (Figure 41). Based on these results, the newly formed species was assigned to the ion [(C₅F₄N)PⁿBu₃]⁺, [**31**]⁺.



Scheme 122 HDF reaction of **Py-F₅** (1 equiv.) with PhSiH₃ (1 equiv.) and PⁿBu₃ (10 mol%) in CD₃CN at 20 °C.

At the end of the catalytic reaction, when **Py-F₅** was fully consumed, the signal for [**31**]⁺ disappeared from both the ³¹P and ¹⁹F NMR spectra and free phosphine was regenerated in the reaction mixture ($\delta(^{31}\text{P}\{^1\text{H}\}) = -32.1$ ppm), suggesting its role as a resting state (Figure 42).

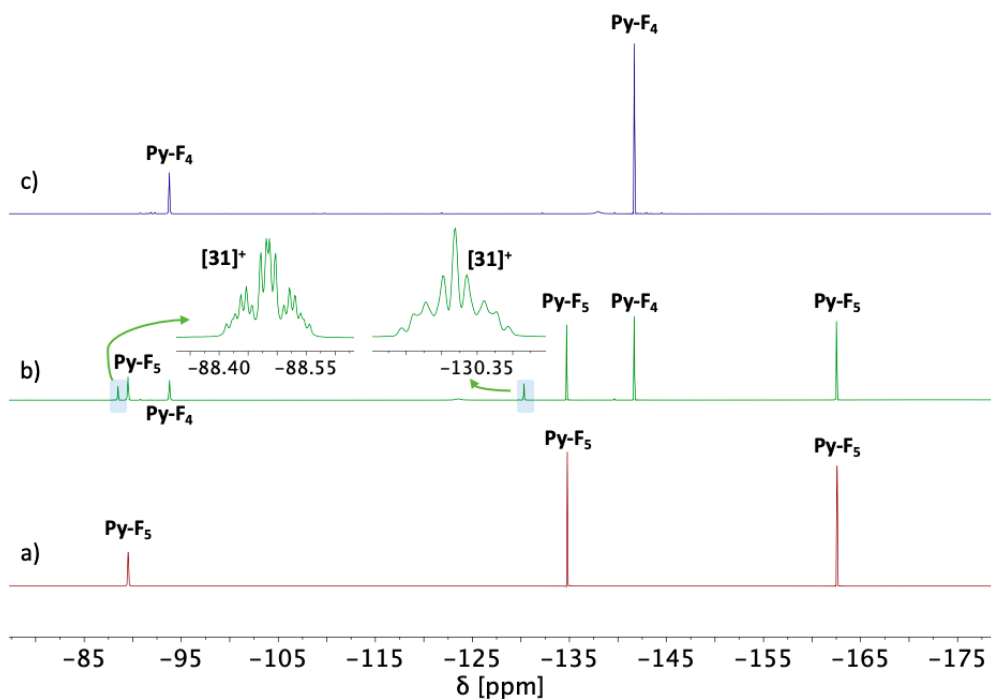


Figure 41 ^{19}F NMR spectrum (565 MHz, CD_3CN) of the mixture of HDF reaction of **Py-F₅** (1 equiv.) with PhSiH_3 (1 equiv.) and P^nBu_3 (10 mol%) in CD_3CN at 20 °C after $t = 0$ (spectrum a)), 1 hour (spectrum b)) and 2 hours at 60 °C (spectrum c)).

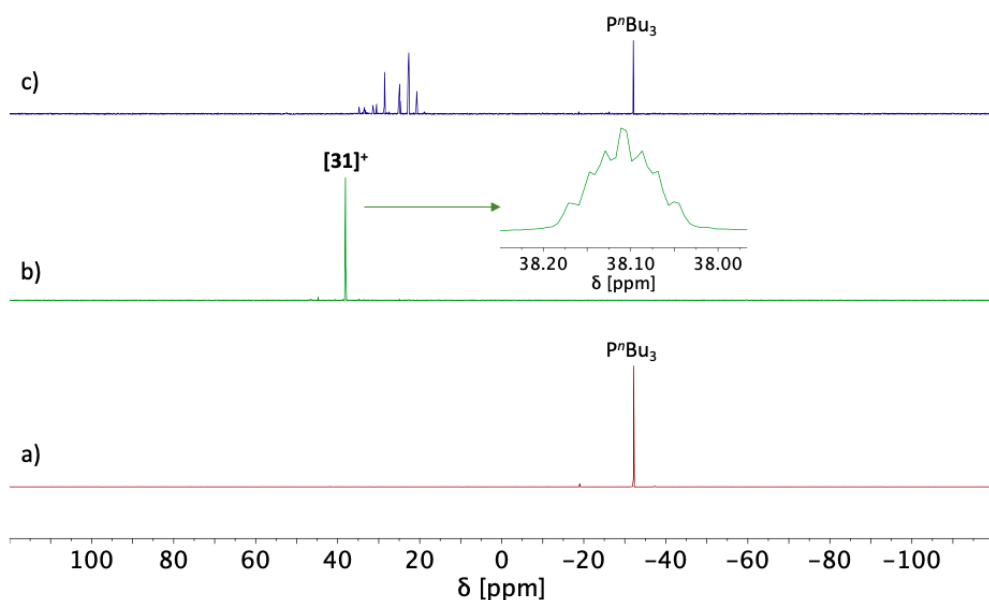
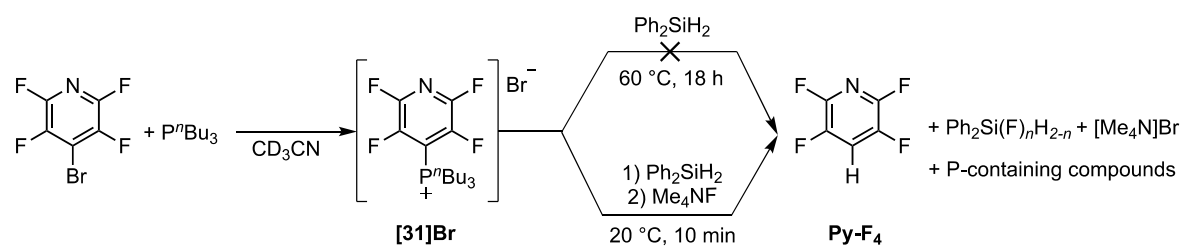


Figure 42 $^{31}\text{P}\{^1\text{H}\}$ NMR spectrum (243 MHz, CD_3CN) of the mixture of HDF reaction of **Py-F₅** (1 equiv.) with PhSiH_3 (1 equiv.) and P^nBu_3 (10 mol%) in CD_3CN at 20 °C after $t = 0$ (spectrum a)), 1 hour (spectrum b)) and 2 hours at 60 °C (spectrum c)).

Inspired by the work of Markus and Anders,³³⁶ who prepared phosphonium salts by reacting phosphines (such as PPh₃) with activated pyridines (i.e. *N*-trifluoromethanesulfonylpyridinium salts), the independent preparation of [(C₅F₄N)PⁿBu₃]Br (**[31]Br**) was carried out to confirm the identity of **[31]**⁺. The treatment of PⁿBu₃ with 4-bromo-2,3,5,6-tetrafluoropyridine (Scheme 123) resulted in a species with virtually identical spectroscopic resonances ($\delta(^{31}\text{P}\{^1\text{H}\}) = 37.9$ ppm, $\delta(^{19}\text{F}) = -89.2$ and -130.3 ppm) and coupling patterns to those observed for **[31]**⁺.



Scheme 123: Preparation of **[31]Br** and its reactivity towards silanes in the presence, and absence, of a fluoride source.

In addition, phosphonium salts derived from fluoroalkanes have been formed by FLP systems through aliphatic C–F activation by a strong Lewis acid (e.g. B(C₆F₅)₃), followed by trapping of the resulting carbocation by PR₃.^{210,337} Related fluorinated phosphonium salts, e.g. [(C₆F₅)₃PF][B(C₆F₅)₄], have also been used in the catalytic HDF of fluoroalkanes.^{198,200,338} However, these species are significantly more Lewis acidic than ions such as **[31]**⁺ and directly abstract fluoride from aliphatic C–F bonds, which is very different to the role of the phosphonium salts described here (see below).

To assess the relevance of **[31]**⁺ as a catalytic intermediate, Ph₂SiH₂ was added to the independently prepared sample of **[31]Br** in CD₃CN (Scheme 123). No changes were noticeable in the ³¹P and ¹⁹F NMR spectra after 10 minutes at 20 °C. The mixture was heated to 40 °C overnight and no reaction occurred between **[31]Br** and the silane. Remarkably, after 10 minutes from the addition of one equivalent of anhydrous [Me₄N]F at 20 °C, the formation of **Py-F₄**, fluorosilane Ph₂Si(F)_nH_{2-n} and some unreacted **[31]**⁺ was observed (Figure 43). The increase in the concentration of **Py-F₄** over time, in combination with the decrease in that of **[31]**⁺, suggested that **[31]**⁺ was an intermediate in the catalytic cycle but that it does not react directly with the silane to form the HDF product.

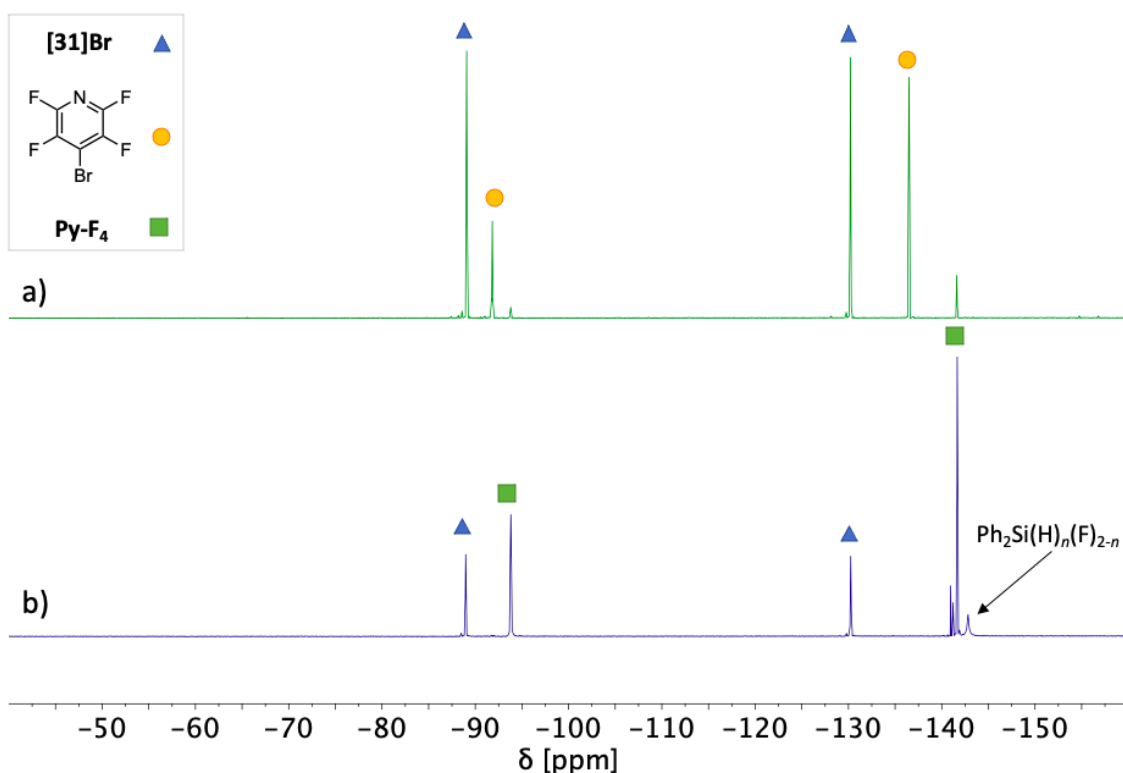
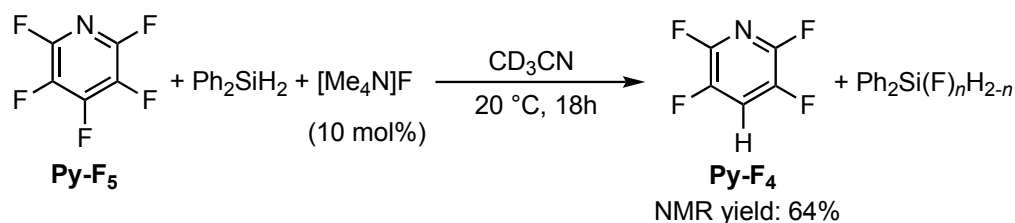


Figure 43 ^{19}F NMR spectrum (565 MHz, CD_3CN) of the reaction mixture of Scheme 123 after 18 hours at 40 °C from the addition of Ph_2SiH_2 (spectrum a)) and after 10 minutes at 20 °C from the addition of $[\text{Me}_4\text{N}]\text{F}$ (spectrum b)).

It is proposed that the formation of a silicate anion, e.g. $[\text{Ph}_2\text{Si}(\text{F})\text{H}_2]^-$, obtained upon addition of the fluoride to Ph_2SiH_2 , promotes the hydride transfer and the release of the HDF product.

The necessity of the silicate formation for the hydride transfer is reminiscent of the work reported by Ogoshi and coworkers²⁹⁹ already described in the introduction chapter 4.1.3 (Scheme 110). The authors presented the HDF reaction catalysed by TBAT and proposed that the fluoride transfer from TBAT to silanes, such as Ph_3SiH , generates hydrofluorosilicate ions. Through ligand redistribution, these proceed to form transient dihydrosilicates that ultimately perform the HDF of fluoroarenes. In our study, it is currently unclear whether mono- or dihydrosilicate ions are involved in the hydride transfer step to phosphonium ions like $[\mathbf{31}]^+$.

In order to rule out the possibility that the hydride transfer in this catalytic system occurs as in Ogoshi's system, *i.e.* it comes directly from a hydrosilicate anion $[\text{Ph}_2\text{Si}(\text{F})_n\text{H}_{3-n}]^-$ to Py-F_5 bypassing the phosphine-induced HDF, a control reaction was performed. Py-F_5 was treated with Ph_2SiH_2 and 10 mol% of $[\text{NMe}_4]\text{F}$ in CD_3CN at 20 °C and the reaction mixture was monitored over time by ^{19}F NMR spectroscopy (Scheme 124).



Scheme 124 Reaction of **Py-F₅** (1 equiv.) with Ph_2SiH_2 (1 equiv.) and $[\text{Me}_4\text{N}]\text{F}$ (10 mol%) in CD_3CN at $20\text{ }^\circ\text{C}$ to test the catalytic ability of $[\text{Ph}_2\text{Si}(\text{F})_n\text{H}_{3-n}]^-$ in absence of the phosphine.

After 20 minutes of reaction time a 19% yield of the HDF product **Py-F₄** was observed and **Py-F₅** was mainly unreacted. After 18 hours, **Py-F₄** was present in only 64% yield. This is in sharp contrast to the reactivity mediated by P^nBu_3 (Table 4, entry 6), where 93% of **Py-F₄** was formed under similar conditions after only 20 minutes. Therefore, it can be deduced that, although the direct HDF of **Py-F₅** via catalytic hydrosilicate anions generated *in situ* through the reaction of **Py-F₅** with P^nBu_3 is feasible, it occurs at a considerably lower rate than HDF through a phosphine-mediated pathway for this substrate and so is not the dominant pathway.

An additional possibility that was explored to explain the need for fluoride to be present to initiate a reaction between **[31]⁺** and Ph_2SiH_2 was fluoride addition to **[31]⁺** to form a fluorophosphorane, which could aid Ph_2SiH_2 activation through an FLP-type mechanism similar to that proposed by Piers for Si–H activation (Figure 44).^{339,340} This would involve activation of the silane by the fluorophosphorane, acting as a Lewis bases and donating a fluoride to the silane, alongside **[31]⁺** acting as a LA to abstract a hydride from the silane, in a concerted manner.

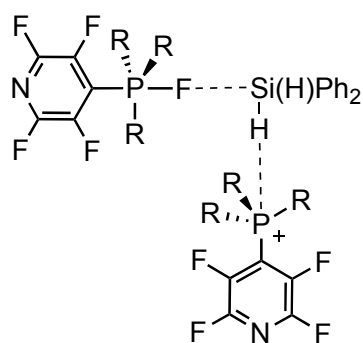
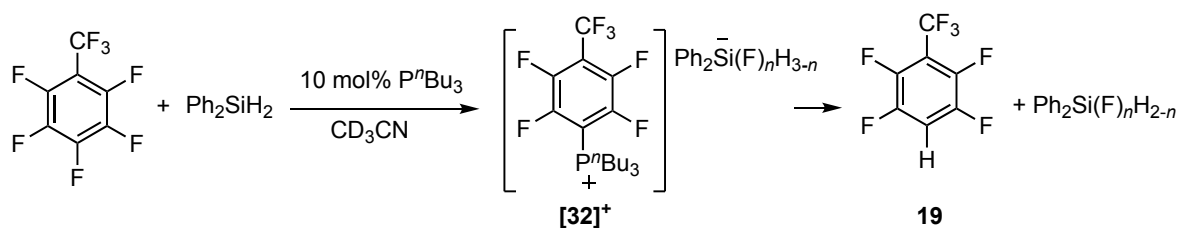


Figure 44 Considered activation mode of the silane according to a FLP-type mechanism.

DFT studies performed by Prof. J. Lynam and Dr. J. Slattery explored this suggestion, but a transition state associated with a concerted P–H/Si–F bond formation mechanism was not found. Instead, a two-step pathway, where initially a fluoride transfers to Si to form a fluorosilicate anion, followed by hydride transfer to a phosphonium ion, was seen. Thus, from these computational studies and

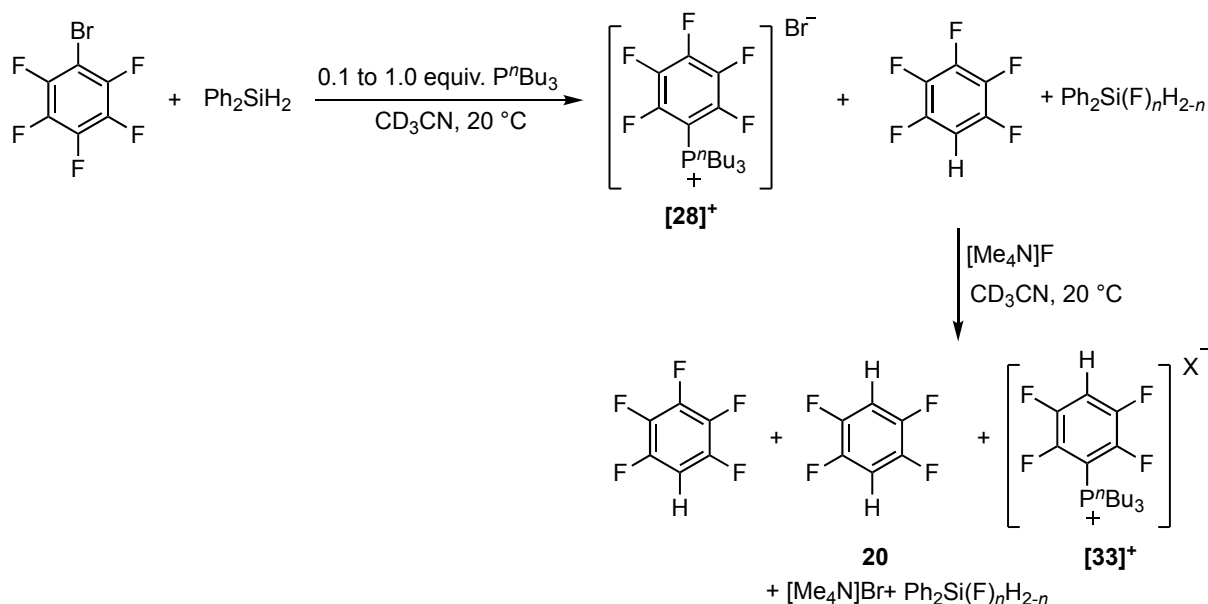
the fact that cations such as **[31]**⁺ are seen as intermediates in the ³¹P NMR spectra, it is possible to conclude that fluorosilicate anion formation is a key step in the catalytic reaction mechanism.

Further evidence of the formation of the phosphonium ion during the HDF reaction was observed for other substrates. The reaction of perfluorotoluene with Ph₂SiH₂ and PⁿBu₃ as the catalyst (10 mol%) in CD₃CN led to the formation of a phosphonium ion, which was identified as [(C₆F₅CF₃)PⁿBu₃]⁺ (**[32]**⁺), after 10 minutes at 20 °C (δ(³¹P{¹H}) = -38.1 ppm, apparent septet, *J* is approximately 4 Hz; δ(¹⁹F) = -58.0 (t, ⁴J_{FF} = 18 Hz), -126.8 (m) and -137.3 ppm (m)) (Scheme 125).



Scheme 125 Reaction of perfluorotoluene (1 equiv.) with Ph₂SiH₂ (1 equiv.) and PⁿBu₃ (10 mol%) in CD₃CN at 20 °C showed the formation of the intermediate phosphonium **[32]**⁺.

Moreover, when bromopentafluorobenzene was used as a substrate, it reacted stoichiometrically with the phosphine forming the phosphonium salt [(C₆F₅)PⁿBu₃]Br (**[28]**Br) (Scheme 126, first step).



Scheme 126 Mono- and dihydrodehalogenation of bromopentafluorobenzene (1 equiv.) with Ph₂SiH₂ (1 equiv.) and PⁿBu₃ (1 equiv.) in CD₃CN at 20 °C *via* the phosphonium intermediate **[28]**⁺ formation.

It was then possible to increase its concentration by addition of an extra 0.9 equivalents of P^nBu_3 , as shown in Scheme 126. Some pentafluorobenzene was formed (35%) after 18 hours in these conditions as a result of hydrodebromination, but the reaction was sluggish, due to the slow reactivity of **[28]Br** with the silane. Addition of one equivalent of $[NMe_4]F$ to this solution (Scheme 126, second step) resulted in the complete consumption of **[28]Br** after 10 minutes at 20 °C and an increase in the amount of pentafluorobenzene (43%), along with the formation of some tetrafluorobenzene **20** (16%) (Figure 45). In addition, a new phosphonium ion was formed, assigned as $[(C_6F_4H)P^nBu_3]^+$ (**[33]**⁺) and characterised by NMR signals at $\delta(^{31}P\{^1H\}) = 36.3$ ppm (tt, $^3J_{PF} = 8.4$ Hz, $^4J_{PF} = 4.8$ Hz) (Figure 46) and $\delta(^{19}F) = -129.7$ and -135.7 ppm (Figure 45, labelled in red). This represented the 43% of the fluoroarene-derived species and resulted from the C–F activation by the phosphine of the formed pentafluorobenzene.

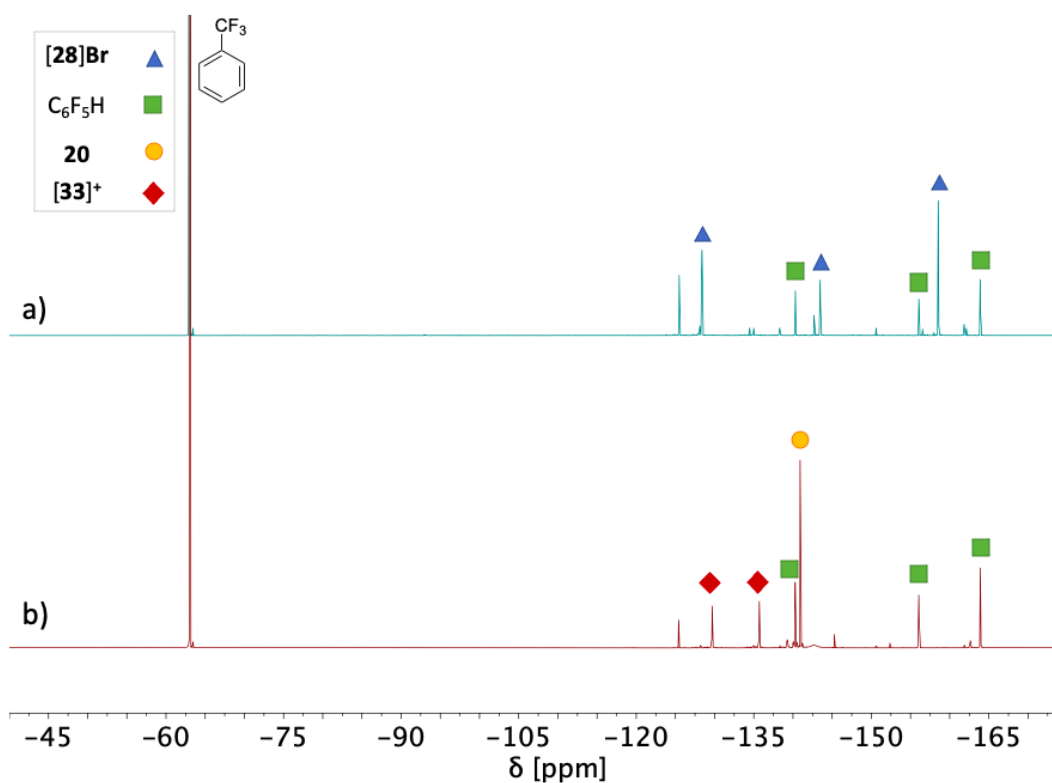


Figure 45 ^{19}F NMR (471 MHz, CD_3CN) spectra of the system described in Scheme 126 after 18 hours at 20 °C from the further addition of 0.9 equivalents of P^nBu_3 (spectrum a)) and after 10 minutes at 20 °C from the addition of $[Me_4N]F$ (spectrum b)).

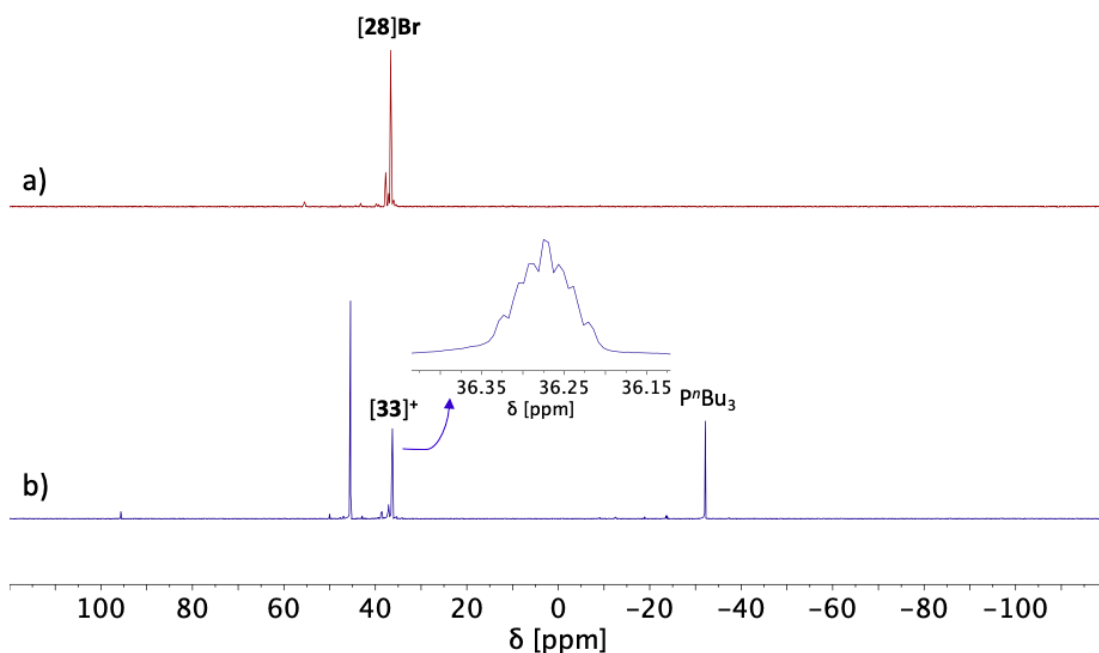


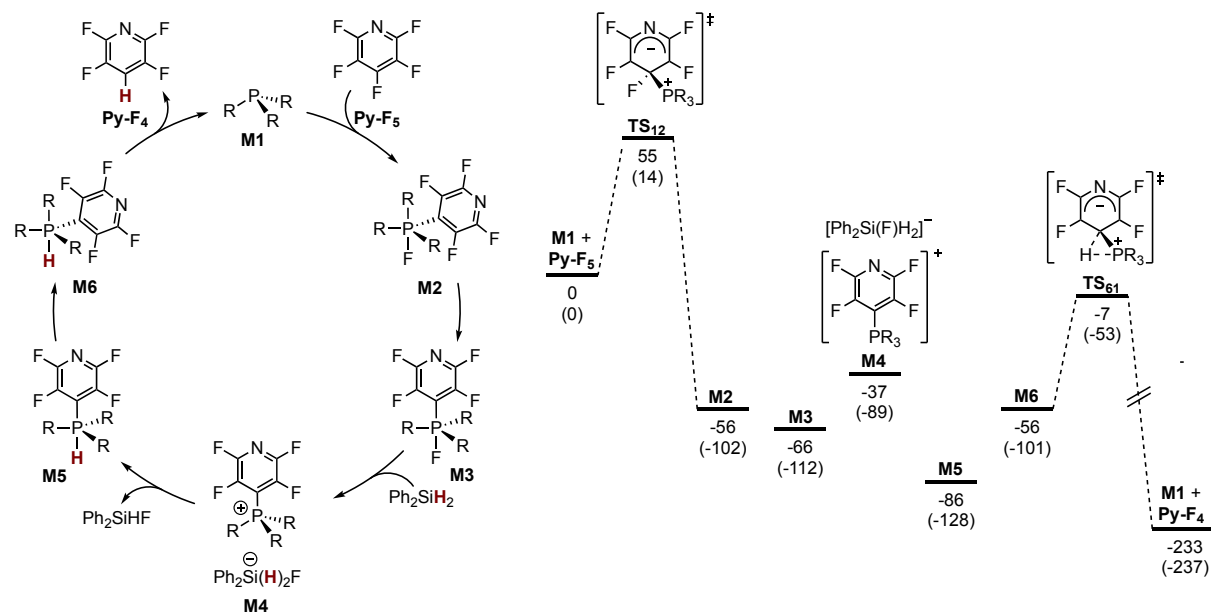
Figure 46 $^{31}\text{P}\{^1\text{H}\}$ NMR (202 MHz, CD_3CN) spectra of the system described in Scheme 126 after 18 hours at 20 °C from the further addition of 0.9 equivalents of P^nBu_3 (spectrum a)) and after 10 minutes at 20 °C from the addition of $[\text{Me}_4\text{N}]\text{F}$ (spectrum b)).

After 18 hours at 20 °C, a slightly reduced amount of pentafluorobenzene (41%), increased quantity of **20** (23%) and a similar concentration of the phosphonium ion **[33]⁺** (41%) were detected.

The addition of the fluoride source to the system seems to significantly increase the rate of hydrodebromination, which was then followed by HDF of the formed pentafluorobenzene (Figure 27, **20**). This further supports the proposed importance of the silicates in this catalytic system. Reaction of **[28]Br** with Ph_2SiH_2 to form $[\text{Ph}_2\text{Si}(\text{Br})\text{H}_2]^-$ would be considerably less favourable than fluoride transfer to the silane to form $[\text{Ph}_2\text{Si}(\text{F})\text{H}_2]^-$, therefore the concentration of the hydrosilicate ions would remain limited and hydrodebromination was slow until a source of fluoride was added to the system. At this point, the silicate ion concentration would increase and thus the hydride transfer was promoted.

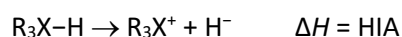
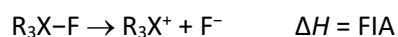
In addition, as described in chapter 3.3.2, the stoichiometric reaction of PR_3 with **Py-F₅** in CD_3CN led to the fast formation of the reductive coupling product **15**, together with the simple difluorophosphorane $\text{P}(\text{R})_3\text{F}_2$ product. Dobrovetsky and coworkers observed a similar reactivity when a geometrically constrained tetrafluoropyridyl-substituted fluorophosphorane was heated to 110 °C for 10 hours in *o*-DFB. Specifically, they observed the formation of **15** and the corresponding difluorophosphorane.²¹⁴ In our system, a related phosphorane $\text{R}_3\text{P}(\text{C}_5\text{F}_4\text{N})\text{F}$ is not observed as the reaction to form **15** is rapid at room temperature. However, the observation of **15** in both systems

suggests that a fluorophosphorane resulting from OA of **Py-F₅** to PR₃ is also a likely intermediate in the catalytic HDF reaction promoted by PR₃.



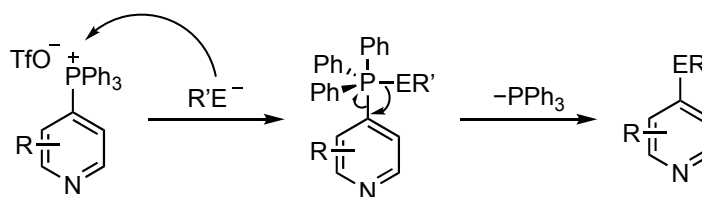
Scheme 127 Proposed catalytic cycle and computed potential energy surface (PES) for R = Me. All energies at the PBE0/def2-TZVP//BP86/SV(P) level in CH₃CN. Relative Gibbs energies (in kJ/mol at 298 K) shown outside brackets and relative enthalpies (in kJ/mol at 298 K) shown in brackets.

Based on the obtained experimental results, a mechanism for the catalytic cycle was proposed (Scheme 127). The initial step involves the nucleophilic attack of the phosphine on the fluoroarene/heteroarene, leading to the fluoride transfer to the phosphorus centre and the formation of the corresponding fluorophosphorane, such as the fluorophosphorane P(F)(ⁿBu)₃(C₅F₄N) represented by compound **M2**. This reactivity is very similar to the addition of phosphines to the fluoroarene rings of B(C₆F₅)₃, which is also followed by fluoride transfer to a Lewis acid to form a phosphonium borate salt.³⁴¹ Subsequently, the isomerisation of **M2** to **M3** takes place. Following this, the silane acts as a Lewis acid, abstracting a fluoride ion from the phosphorane to form a phosphonium salt, for example, [(C₅F₄N)PⁿBu₃][Ph₂Si(F)H₂] (intermediate **M4**). The hydrosilicate anion then transfers a hydride to the phosphonium ion, generating a hydrophosphorane, which then eliminates the hydrodefluorinated product and regenerates the phosphine. This exchange of H/F between phosphorus and silicon is driven by differences in the fluoride ion (FIA) and hydride ion affinities (HIA) of the phosphorane and the silane. FIA and HIA are defined by the following equations:



These parameters have been extensively studied in the case of silanes and a general linear relationship between them has been established.²⁷⁹ The reported FIA values for $R_n(H)_{3-n}Si^+$ ions range from 840 to 1090 kJ/mol in the gas phase, depending on the R-substituents present, with corresponding HIA values generally slightly smaller. In contrast, there are no correlation tables for these parameters in the case of phosphoranes. However, it is known that PF_5 has one of the highest FIAs among phosphoranes (363 kJ/mol).²⁴⁵ The presence of electron-donating substituents, such as nBu or iPr , on the phosphorane effectively reduces its fluoride ion affinity, making it more prone to transfer F^- to strong fluoride-acceptors like boranes, silanes or arsenates, leading to the formation of phosphonium salts.^{342,343}

Another example of pyridine functionalisation assisted by P^{III}/P^V redox cycling was reported by McNally and coworkers.^{344–346} They described the stoichiometric reactivity of non-fluorinated pyridylphosphonium salts with nucleophiles (such as ROH, RSH, R_2NH , RSeH). These processes are proposed to occur *via* phosphorane intermediates and lead to the formation of substituted pyridines (Scheme 128). This reactivity is underpinned by the facile redox cycling between the P^{III} and P^V oxidation states, a feature that is notable to see in simple trialkylphosphines.



Scheme 128 Synthetic strategy for pyridine functionalisation *via* the formation of a phosphorane intermediate proposed by McNally *et al.*³⁴⁵

DFT calculations were performed by Dr J. M. Slattery and Prof J. M. Lynam to support the experimental mechanistic studies. These calculations showed that the initial reaction step consists of the phosphine attack at the *para*-position of $Py-F_5$ *via* a Meisenheimer-like transition state (Scheme 127, TS_{12}) to form a fluorophosphorane (**M2**) in a manner akin to the mechanism proposed by García and coworkers for reaction of $Py-F_5$ with PEt_3 (Scheme 78).^{155,347} This process is associated with a low barrier of 55 kJ/mol.

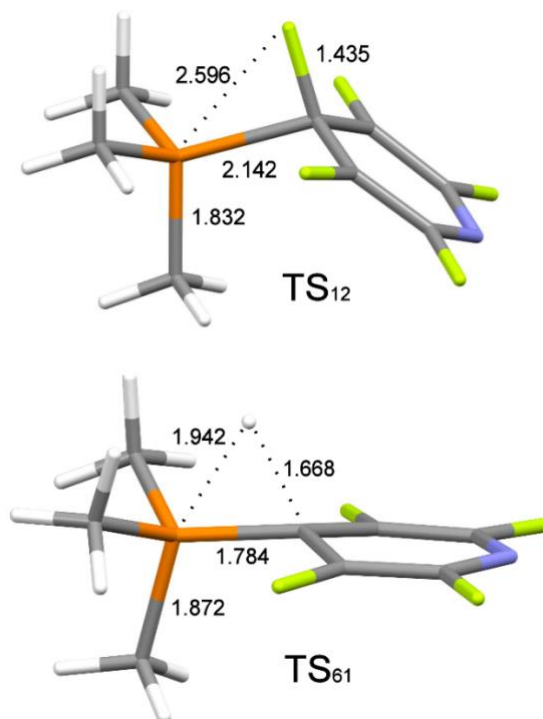


Figure 47 Transition states for addition of PMe_3 to Py-F_5 (TS_{12}) and elimination of Py-F_4 from phosphorane **M6** (TS_{61}). Hydrogen is shown in white, carbon in grey, phosphorus in orange, nitrogen in blue and fluorine in green. Selected distances (in Å) are shown.

The structure of TS_{12} (Figure 47) shows the early nature of this transition state, where P–C bond formation and C–F bond elongation precedes fluorine transfer to phosphorus to form the phosphorane **M2**. This step is effectively initiated by a nucleophilic addition of the trialkylphosphine to Py-F_5 . This rationalises the preference for electron-poor arenes/heteroarenes in this reaction, where this is promoted. Consequently, switching from pentafluoropyridine to less electron-poor substrates, like 2,4,6-trifluoropyridine and 2,6-difluoropyridine, results in a slower reaction rate. In the presence of electron-donating substituents such as anisole, the HDF reaction does not take place because the addition of the phosphine to the arene is no longer favoured (Figure 27). No additional intermediates or transition states for fluorine transfer to phosphorus were identified. The addition of Py-F_5 to the phosphine leads to a formal oxidation state change from P^{III} to P^{V} and so can be characterised as an OA process, albeit one that is highly asynchronous in terms of C–F bond cleavage and reminiscent of concerted $\text{S}_{\text{N}}\text{Ar}$ mechanisms.³⁴⁸ The key structural parameters of TS_{12} are almost identical to those calculated by Dobrovetsky and coworkers for addition of Py-F_5 to a geometrically constrained $\sigma^3\text{-P}$ compound, suggesting a similar activation process, despite the very different structural frameworks involved.²¹⁴

The fluorophosphorane that is initially formed (**M2**) can undergo isomerisation to a lower energy isomer (**M3**) with fluorine *trans* to the tetrafluoropyridyl group, both in the apical positions. Fluoride transfer to Ph_2SiH_2 results in the formation of the observed phosphonium ion [**31**]⁺, in this case as the salt **M4**. Moving between neutral and ionic manifolds in this way will be strongly influenced by solvation effects. This leads to a small mismatch between the computed energies and the experimental observations, where **M4** is higher in energy than the phosphoranes, although phosphonium ions and not the phosphoranes are observed experimentally. This is likely due to limitations in using a dielectric continuum solvation model, which under-solvates the ions and raises their energies relative to neutral species. The neutral/ionic manifold switch may help to explain the solvent effect seen in this system, where moving from *o*-DFB (ϵ 13.4 = at 25 °C) to the more polar CH_3CN (ϵ = 35.9 at 25 °C) led to an increase in the catalytic rate.^{349,350} It is well known that more polar solvents like CH_3CN promote the formation of ionic species from phosphoranes and this would facilitate the formation of **M4** (this phenomenon has already been discussed in chapter 3.3.3).³⁵¹

Hydride transfer from the silicate anion then leads to phosphorane **M5**, which can isomerise to form **M6**. This is very different from the mechanistic proposal of Dobrovetsky for HDF by geometrically constrained $\sigma^3\text{-P}$ systems,²¹⁴ where it was suggested that PhSiH_3 reacts directly with the fluorophosphorane through a transition state that involves concerted hydride transfer to P and fluoride transfer to Si. The experiments described above showed that for simple trialkylphosphines, phosphonium ions are relevant intermediates and these do not react directly with the neutral silanes. It may be that the positive charge on Dobrovetsky's constrained $\sigma^3\text{-P}$ systems disfavors this pathway and leads to this divergence in mechanistic behaviour.

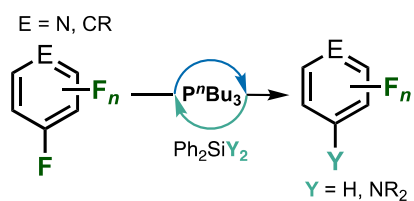
The final step involves RE of **Py-F₄** from **M6** via **TS₆₁** (Figure 47). This transition state is more concerted than **TS₁₂**, although still somewhat asynchronous, presumably because direct concerted RE from the axial and equatorial positions of a phosphorane is symmetry forbidden.³⁵² **TS₆₁** is again Meisenheimer-like, although less than in the constrained $\sigma^3\text{-P}$ systems of Radosevich,²¹³ where the C–H bond length of a related RE transition state is 1.33 Å, and Dobrovetsky where it is 1.53 Å.²¹⁴ It seems as though the substituents and geometric environment around phosphorus have a significant impact on the RE process. These final steps give rise to the energetic span for the reaction, which is defined by the turnover-determining intermediate (TDI) **M5** and transition state (TDTS) **TS₆₁**, and give an overall barrier for the catalytic reaction of 79 kJ/mol. This low barrier is consistent with the observed fast reaction between **Py-F₅** and Ph_2SiH_2 when a sterically relatively small phosphine like P^nBu_3 is used as the catalyst (full conversion in 20 minutes at 20 °C in CH_3CN). The calculated energetic span for HDF of **Py-F₅** by a constrained $\sigma^3\text{-P}$ system was significantly larger (140 kJ/mol), which is consistent with the slower reactions observed in that study.²¹⁴

In conclusion, it was demonstrated that using only a simple and readily commercially available phosphine as the catalyst enables both hydrodefluorination and aminodefluorination for a wide range of substrates. The product yields and reaction times are some of the bests reported for main-group catalysts with highly electron-poor fluoroarenes. Remarkably, the performance of this system often exceeds that of related geometrically constrained P^{III}/P^V systems, although the silane/solvent combination used here is different. This suggests that geometric constraints are not essential for achieving effective reactivity.

4.4 Summary, conclusions and perspectives

In recent years, there has been a significant interest in the activation and functionalisation of small molecules and strong bonds by main-group element compounds that mimic the reactivity of transition metals. An essential concept driving this research is metallomimetic behaviour, where main-group elements can be induced to exhibit reactivity similar to that of transition metals.³⁵³ One of the peculiar reactivity of TMs is to undergo reversible two-electron redox processes, such as OA and RE. Nevertheless, redox cycles with main-group elements are relatively rare. Among these elements, the pnictogens stand out, as they often provide access to stable species in various oxidation states.²⁷⁶ A crucial structural feature that seems to enable the observation of redox cycling in Pn-containing systems involves the introduction of geometric constraints around pnictogen atoms.³⁰⁹ Recent studies in this field described how geometrically constrained pnictogens can effectively hydrodefluorinate perfluorinated aromatics, both stoichiometrically and catalytically.^{213,214,312} These works highlight the crucial role of this structural design in accessing the Pn^{III}/Pn^V redox cycle, enabling the specific reactivity desired for this transformation.

The results reported in this chapter demonstrate that complex molecular architectures are not required for P^{III} systems to act as catalysts for HDF or aminodefluorination of highly fluorinated arenes and heterocycles. Simple trialkylphosphines were found to be fast and effective catalysts for these reactions with a range of substrates, but especially for highly electron-poor ones (Scheme 129). This is an important observation, as some trialkylphosphines, particularly the P^tBu_3 used here, are cheap, readily available from commercial suppliers and easy to handle.



Scheme 129 Representative scheme of our system for the catalytic reaction of HDF and hydroamination.

Experimental and computational mechanistic studies have shown that the catalytic HDF reactions in this system are supported by remarkable metallomimetic behaviour for such simple phosphines. The ease of $\text{P}^{\text{III}}/\text{P}^{\text{V}}$ redox cycle allows the phosphine catalyst to undergo OA of the fluorinated substrate and RE of the hydrodefluorinated product. Phosphonium ions, such as $[(\text{C}_5\text{F}_4\text{N})\text{P}^{\text{V}}\text{Bu}_3]^+$ (**[31]**⁺), have been identified as key intermediates during catalysis. It is proposed that these cations undergo hydride transfer from their hydrosilicate counterions, as part of a transmetalation step similar to that of transition metals, prior to the product RE. This helps to explain the solvent and silane dependence of the observed reactions, where more polar solvents favour the formation of phosphonium salts and specific substituents on the silane favour the formation of hydrosilicate anions.

Future work in this field includes optimising the catalytic aminodefluorination system, studying its mechanism and exploring the use of more complex silylamides than those employed in this investigation. Additionally, other types of functionalisations, such as defluorinative borylation and oxodefluorination, will be investigated.

Chapter 5 – Experimental Section

5.1 General considerations

Unless otherwise indicated, the reactions were performed in flame- or oven-dried glassware with rigorous exclusion of air and moisture, using a nitrogen-filled *MBraun* glove box ($O_2 < 1$ ppm, $H_2O < 1$ ppm) or regular Schlenk-line techniques.³⁵⁴ Anhydrous Et_2O , CH_2Cl_2 , pentane and toluene were pre-dried by passing through a Puresolv MD 7 solvent purification machine. When phosphines were involved in the reactions, the solvents were also degassed by three freeze-pump-thaw cycles before use. THF, deuterated-THF, deuterated toluene and C_6D_6 were dried over metallic sodium, purified by trap-to-trap transfer and degassed by freeze-pump-thaw. CD_2Cl_2 and CD_3CN were dried over calcium hydride for three days, purified by trap-to-trap transfer and degassed by freeze-pump-thaw. Cyclohexane and deuterated cyclohexane were dried over molecular sieves prior to use. Reagents were purchased from commercial suppliers and purity was confirmed by NMR spectroscopy. Et_2NH and Et_3N were dried over KOH and distilled before use. Tetramethylammonium fluoride was purchased from Sigma-Aldrich and dried at $100^\circ C$ for 48 hours under hi-vac (10^{-3} mbar) prior to use. MeOH was purchased from Honeywell and dried over molecular sieves prior to use. The fluorinated aromatics and silanes (Ph_3SiH , Ph_2SiH_2 and $PhSiH_3$) were purchased from Sigma Aldrich, Fluorochem and Apollo Scientific, dried over molecular sieves and degassed by freeze-pump-thaw cycles prior to use.

All NMR spectra were obtained using J. S. Young's NMR tubes sealed under argon or nitrogen. 1H , $^{13}C\{^1H\}$, ^{29}Si , ^{19}F and $^{31}P\{^1H\}$ NMR spectra were recorded on Bruker Avance II 400 MHz, Avance III HD 400 MHz, Bruker AVIHD 500 MHz and Avance Neo 600 MHz spectrometers. Chemical shifts are in parts per million (ppm) downfield from tetramethylsilane and are referenced to the residual solvent resonances as the internal standard (CHD_2CN : δ reported = 1.94 ppm; C_6HD_5 : δ reported = 7.16 ppm; $CHDCl_2$: δ reported = 5.32 ppm; C_6HD_{11} = 1.38 ppm; C_4HD_7O = 3.58 ppm; C_7HD_{12} = 2.09 ppm for 1H NMR). $^{13}C\{^1H\}$ NMR spectra were calibrated according to the IUPAC recommendation using a unified chemical shift scale based on the proton resonance of tetramethylsilane as primary reference.^{355,356} ^{19}F and $^{19}F\{^1H\}$ NMR chemical shift δ are reported in ppm, relative to the resonance shift of an external solvent $CFCl_3$, at δ 0.0 ppm. $^{31}P\{^1H\}$ and ^{31}P NMR chemical shifts reported in ppm, relative to the resonance shift of an external solvent H_3PO_4 at δ 0.0 ppm. Data are reported as follows: chemical shift, multiplicity (br = broad, s = singlet, d = doublet, t = triplet, q = quartet, p =

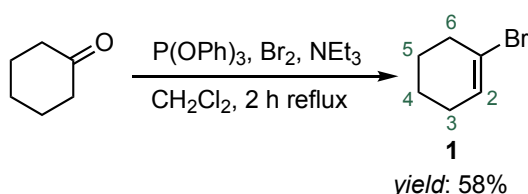
quintet, sext = sextet, hept = heptet, m = multiplet), coupling constant (Hz) and integration. ^1H and $^{13}\text{C}\{^1\text{H}\}$ resonance signals were attributed by means of 2D ^1H COSY, ^1H - ^{13}C HSQC, ^1H - ^{13}C HMBC, ^1H - ^{31}P HMBC and ^1H - ^{19}F HMBC experiments.

Elemental analyses were performed in the facility available in Laboratoire de Chimie de Coordination (CNRS) using PerkinElmer 2400 Series Analyser. HR-MS ESI-MS and APCI spectra were measured using a Bruker Daltronics micrOTOF MS, Agilent series 1260LC with electrospray ionization (ESI), liquid injection field desorption ionization (LIFDI) or atmospheric pressure chemical ionization (APCI) ionization.

Single-crystals diffraction data were collected using a Bruker Kappa APEX II diffractometer at 100 – 115 K using Mo K α radiation ($\lambda = 0.71073 \text{ \AA}$) filtered through a graphite monochromator.

5.2 Chapter 2 – C–F bond functionalisation promoted by a zirconium-cyclohexyne complex

5.2.1 Synthesis of 1-bromocyclohexene (1)

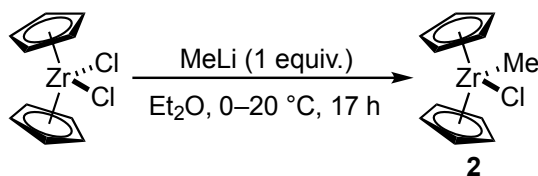


1-Bromocyclohexene was prepared according to a reported procedure.³⁵⁷ To a cold solution of triphenyl phosphite (9.25 mL, 35.0 mmol, 1.1 equiv.) in anhydrous CH_2Cl_2 (100 mL) maintained at $-60 \text{ }^\circ\text{C}$ under Ar flow, bromine (2.00 mL, 38.5 mmol, 1.2 equiv.) was added dropwise. Anhydrous triethylamine (6.00 mL, 42.0 mmol, 1.3 equiv.) and cyclohexanone (3.14 g, 32.0 mmol, 1.0 equiv.) were added to the resulting pale orange solution. The reaction mixture was stirred for 18 hours, while warming to room temperature, and then heated to reflux for a further 2 hours. Purification by chromatography column (pentane) of crude ($R_f = 0.7$, pentane) and by trap-to-trap transfer yielded a colourless liquid (2.98 g, 18.5 mmol, 58% yield).

^1H NMR (400 MHz, CDCl_3): δ 6.36 – 5.74 (m, 1H, 2-H), 2.38 (m, 2H, 6-H), 2.05 (m, 2H, 3-H), 1.70 (m, 2H, 5-H), 1.58 (m, 2H, 4-H). The NMR analysis is in agreement with that reported in the literature.³⁵⁷

5.2.2 Synthesis of methylzirconocene chloride (2)

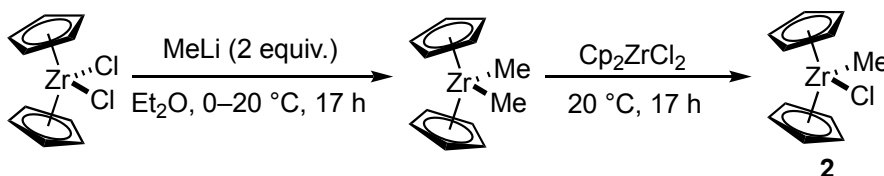
5.2.2.1 Via reaction between zirconocene dichloride and 1 equivalent of MeLi:



Complex **2** was synthesised following a reported procedure.³⁵⁸ Cp₂ZrCl₂ (2.00 g, 6.8 mmol, 1.0 equiv.) was suspended in 16 mL of diethyl ether and MeLi (4.52 mL of a 1.5 M solution in diethyl ether, 6.7 mmol, 1.0 equiv.) was added at 0 °C. After 3 hours at 0 °C, the reaction mixture was stirred at room temperature overnight, then the solvent was removed in vacuo. The residue was treated with 8 mL of toluene and stirred at 80 °C for 24 h, then cooled to room temperature and the LiCl was filtered off.

¹H NMR (400 MHz, C₆D₆): δ 6.24 (s, 10H, Cp), 0.32 (s, 3H, CH₃). The NMR analysis is in agreement with that reported in the literature.³⁵⁸ However, the system was not selective as Cp₂ZrMe₂ was also detected by ¹H NMR analysis.

5.2.2.2 Via reaction between zirconocene dichloride and 2 equivalents of MeLi:



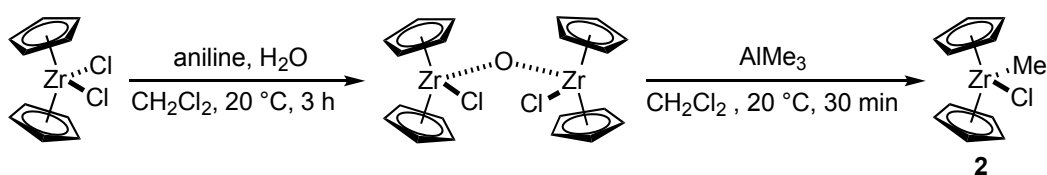
*First step: synthesis of Cp₂ZrMe₂.*³⁵⁹

To a stirred suspension of Cp₂ZrCl₂ (2.00 g, 6.8 mmol, 1.0 equiv.) in diethyl ether (11 mL) at 0 °C was added MeLi solution (9.20 mL of 1.5 M solution in diethyl ether, 13.7 mmol, 2.0 equiv.) over 1 hour. After stirring overnight at 20 °C, the mixture was filtered under argon and the filtrate was evaporated to dryness under reduced pressure to afford a white solid.

¹H NMR (400 MHz, C₆D₆): δ 5.72 (s, 10H, Cp), –0.12 (s, 9H, CH₃). The NMR analysis is in agreement with that reported in the literature.³⁵⁹

However, the system was not selective as complex **2** was also detected by ¹H NMR analysis. Attempted purification by crystallisation or sublimation were not successful.

5.2.2.3 Via $[(\text{Cp}_2\text{ZrCl})_2(\mu\text{-O})]$:



5.2.2.3.1 First step: synthesis of $[(\text{Cp}_2\text{ZrCl})_2(\mu\text{-O})]$

Complex **2** was synthesised following a reported procedure.³⁶⁰ A 250 mL Schlenk flask was charged with Cp_2ZrCl_2 (10.00 g, 34.2 mmol, 1.0 equiv.), CH_2Cl_2 (80 mL) followed by aniline (3.4 mL, 37.2 mmol, 1.1 equiv.). After stirring for 5 minutes, distilled water (0.43 mL, 23.8 mmol, 0.7 equiv.) was added and a white solid of aniline hydrochloride salt was observed instantly. Stirring was continued for about 3 hours at $20\text{ }^\circ\text{C}$. The flask was placed in the fridge ($+4\text{ }^\circ\text{C}$) for 15 hours. Cold filtration under argon of the resulting mixture afforded a clear yellowish filtrate. The solid filtered was washed once with cold ($0\text{ }^\circ\text{C}$) CH_2Cl_2 (10 mL) and the combined CH_2Cl_2 layers were concentrated to a yellowish solid. Dry pentane (11 mL) was added and stirred for 20 minutes. The white solid in suspension was filtered, washed once with dry pentane (11 mL) and dried under high vacuum for 1 hour to afford the zirconium bridged oxide $[(\text{Cp}_2\text{ZrCl})_2(\mu\text{-O})]$ (7.04 g, 13.3 mmol, 78% yield) as a pale pink solid.

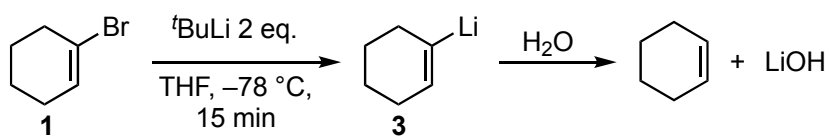
$^1\text{H NMR}$ (400 MHz, C_6D_6): δ 6.02 (s, Cp).

5.2.2.3.2 Second step: synthesis of **2**

To a 100 mL Schlenk flask containing a suspension of $[(\text{Cp}_2\text{ZrCl})_2(\mu\text{-O})]$ (7.04 g, 13.3 mmol, 1.0 equiv.) in dry CH_2Cl_2 (65 mL) was added a trimethylaluminium solution (2M in hexane, 16.7 mL, 33.3 mmol, 2.5 equiv.) at $20\text{ }^\circ\text{C}$. After a few seconds the mixture became a homogenous yellowish solution, no exotherm was observed. After 30 minutes, dry Et_2O (26 mL) was added, stirring was stopped after 2 minutes. The solvent was slowly evaporated until the first yellow solids started to precipitate (about 3–5 mL left in the flask). Stirring on, dry pentane (26 mL) was added. After 10 minutes stirring, the white solid obtained was filtered under argon and washed twice with dry pentane (17 mL each) and finally dried under vacuum for 3 hours to afford **2** (4.47 g, 16.5 mmol, 62%) as a white to off-white solid.

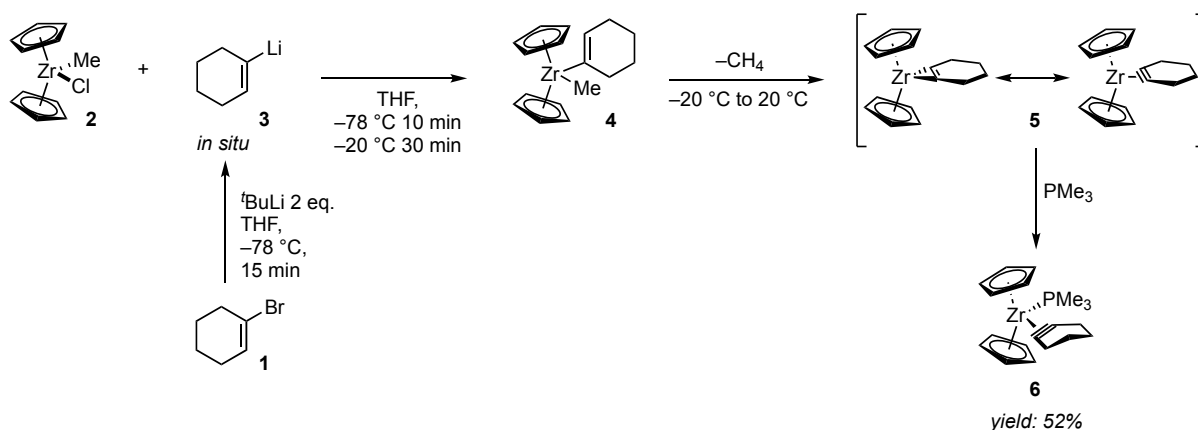
$^1\text{H NMR}$ (400 MHz, C_6D_6): δ 5.74 (s, 10H, Cp), 0.45 (s, 3H, CH_3). The NMR analysis is in agreement with that reported in the literature.³⁶⁰

5.2.3 Li/Br exchange test



To a Schlenk flask under argon was added dry THF (11 mL) and cooled to $-78\text{ }^\circ\text{C}$. $t\text{BuLi}$ in pentane 1.72 M (3.19 mL, 5.5 mmol, 2.0 equiv.) was added under stirring. 1-Bromocyclohexene (0.44 g, 2.7 mmol, 1.0 equiv.) was added to the solution dropwise *via* syringe and the yellow reaction mixture was allowed to stir at $-78\text{ }^\circ\text{C}$. After 15 minutes and after 2 hours, an aliquot of 0.1 mL was taken from the mixture, it was quenched with distilled water and analysed by ^1H NMR spectroscopy. The NMR analysis of the cyclohexene formed is in agreement with that reported in the literature.³⁶¹

5.2.4 Synthesis of complex 6



Complex **6** was prepared according to a reported procedure.³⁶² To a Schlenk flask under argon was added dry THF (21 mL), which was cooled to $-78\text{ }^{\circ}\text{C}$. ^tBuLi in pentane 1.72 M (5.8 mL, 10.7 mmol, 2.1 equiv.) was added with stirring. 1-Bromocyclohexene (0.86 g, 5.4 mmol, 1.1 equiv.) was added to the solution dropwise, *via* syringe and the yellow reaction mixture was allowed to stir at $-78\text{ }^{\circ}\text{C}$ for 15 minutes. The 1-lithiocyclohexene, so formed, was added dropwise *via* cannula to a $-78\text{ }^{\circ}\text{C}$ solution of **2** (1.44 g, 5.1 mmol, 1.0 equiv.) in THF (28 mL). The reaction mixture was stirred for 10 minutes at $-78\text{ }^{\circ}\text{C}$ and was then warmed to $-20\text{ }^{\circ}\text{C}$ and stirred for an additional 10 min. At this point, trimethylsilyl chloride (0.05 mL, 0.3 mmol, 0.1 equiv.) was added *via* syringe (to destroy excess alkenyllithium) and the brown reaction mixture was stirred at $-20\text{ }^{\circ}\text{C}$ for additional 10 minutes. Trimethylphosphine (0.81 mL, 8.0 mmol, 1.6 equiv.) was added *via* syringe and the deep red reaction mixture was allowed to stir at $20\text{ }^{\circ}\text{C}$ for 16 hours. The resulting mixture was concentrated *in vacuo* and the solid residue was extracted with toluene (7 mL) and filtered under argon. The remaining lithium salts were washed with five portions of toluene (10 mL each) and the toluene solution was concentrated to dryness to afford **6** (1.00 g, 2.7 mmol, 52%) as a dark red solid.

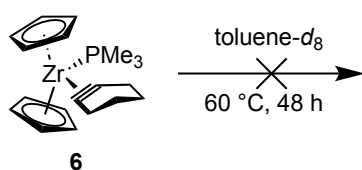


¹H NMR (400 MHz, C₆D₆): δ 5.25 (d, $J_{\text{HP}} = 5.8\text{ Hz}$, 10H, Cp), 2.85 (t, $^3J_{\text{HH}} = 5.9\text{ Hz}$, 2H, 1-*H*), 2.28 (tm, $^3J_{\text{HH}} = 5.8\text{ Hz}$, 2H, 1-*H*), 1.77 – 1.62 (m, 4H, 2-*H*), 0.96 (d, $^2J_{\text{HP}} = 5.8\text{ Hz}$, 9H, PCH₃).

³¹P NMR (243 MHz, C₆D₆): δ -2.22 (bs).

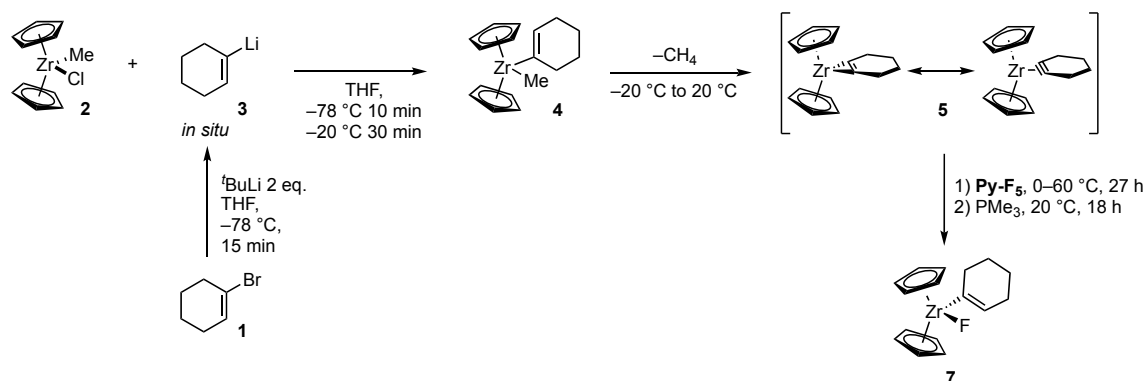
The NMR analysis is in agreement with that reported in the literature.³⁶²

5.2.5 Stability test of complex 6



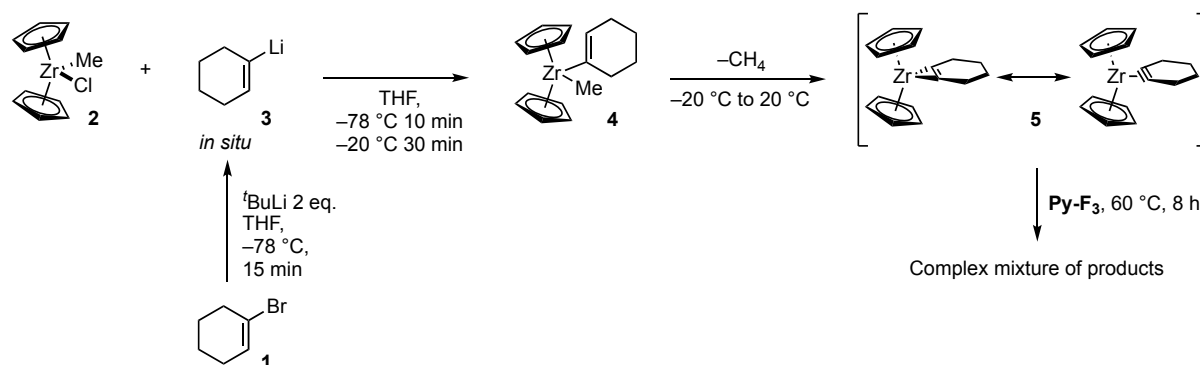
The following manipulation was carried out in an Ar-filled glovebox. Complex **6** (15.0 mg, 0.04 mmol) was dissolved in toluene-*d*₈ (0.7 mL) in an NMR tube equipped with a J. S. Young's valve. The mixture was heated up to 60 °C for 48 hours and analysed by ¹H and ³¹P NMR spectroscopy, which showed that no decomposition occurred.

5.2.6 Study of the reactivity of complex 5 with Py-F₅



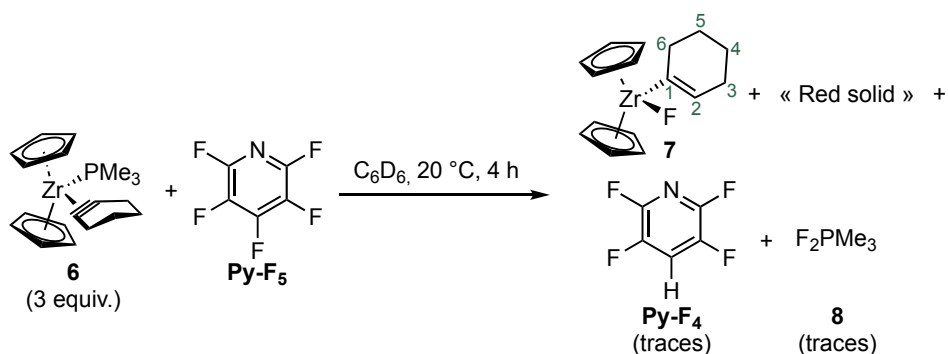
To a Schlenk flask under argon was added dry THF (5 mL) and cooled to -78 °C. ^tBuLi in pentane 1.72 M (1.6 mL, 2.7 mmol, 2.1 equiv.) was added under stirring. 1-Bromocyclohexene (0.22 g, 1.4 mmol, 1.1 equiv.) was added to the solution dropwise, *via* syringe and the yellow reaction mixture was allowed to stir at -78 °C for 15 minutes. The 1-lithiocyclohexene, so formed, was added dropwise *via* cannula to a -78 °C solution of **2** (0.35 g, 1.31 mmol, 1.0 equiv.) in THF (7 mL). The reaction mixture was stirred for 10 minutes at -78 °C and was then warmed to -20 °C and stirred for an additional 10 min. **Py-F₅** (0.2 mL, 2.0 mmol, 1.5 equiv.) was added into the solution. The system was heated up to 60 °C for 27 hours and monitored by ¹⁹F NMR spectroscopy. As no substantial change was observed in the ¹⁹F NMR spectra over time, 1.6 equivalents of PMe₃ (0.81 mL, 8.0 mmol, 1.6 equiv.) were added and the system was kept at 20 °C for 18 hours. The progress of the reaction was monitored by ¹⁹F and ³¹P NMR. After this time, the formation of a dark red solid was observed. The ¹⁹F NMR spectrum displayed a singlet at 51.0 ppm corresponding to complex **7** and many signals in the area of the *ortho*- and *meta*-F of the pyridine ring. The ³¹P NMR spectrum displayed only traces of F₂PET₃ and other difluorophosphoranes that could not be unambiguously identified.

5.2.7 Reactivity of complex 5 with Py-F₃



Dry THF (11 mL) was added to a Schlenk flask under argon which was then cooled to -78 °C. ^tBuLi in pentane 1.63 M (3.43 mL, 5.5 mmol, 2.1 equiv.) was added with stirring. 1-Bromocyclohexene (0.44 g, 2.7 mmol, 1.1 equiv.) was added to the solution dropwise, *via* syringe and the yellow reaction mixture was allowed to stir at -78 °C for 15 minutes. The 1-lithiocyclohexene, so formed, was added dropwise *via* cannula to a -78 °C solution of 2 (0.71 g, 2.6 mmol, 1.0 equiv.) in THF (14 mL). The reaction mixture was stirred for 10 minutes at -78 °C and was then warmed to -20 °C and stirred for an additional 10 min. 2.0 equivalents of the **Py-F₃** (0.47 mL, 5.2 mmol) were added into the solution. The system was heated up to 60 °C for 8 hours and the progress of the reaction was monitored by ¹⁹F NMR over time. The system remained mostly unchanged after this period and no signal indicative of a Zr-F bond appeared in the ¹⁹F NMR spectrum.

5.2.8 Synthesis of 1-cyclohexenylzirconocene fluoride (7)



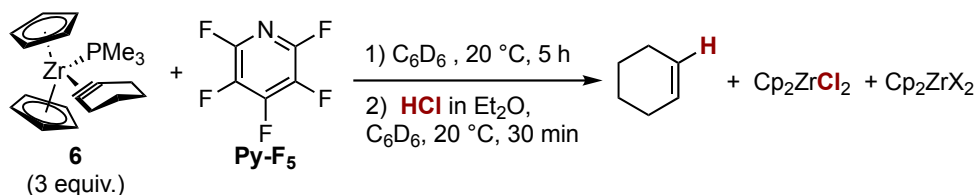
The following manipulation was carried out in an Ar-filled glovebox. Complex **6** (15.0 mg, 0.04 mmol, 3.0 equiv.) was dissolved in cyclohexane (0.7 mL) in an NMR tube equipped with a J. S. Young's valve. Pentafluoropyridine (31.1 μ L of a 0.43 M in cyclohexane, 0.01 mmol, 1.0 equiv.) was added and the mixture was kept at 20 °C for 5 hours. The dark red solid was filtered, the filtrate was dried under reduced pressure to afford **7** as a dark brown solid.

¹H NMR (400 MHz, C₆D₆): 6.09 – 5.92 (m, 1H, 2-H), 5.86 (s, 10H, Cp), 2.19 – 2.02 (m, 4H, 3-H, 6-H), 1.68 – 1.55 (m, 4H, 4-H, 5-H).

¹⁹F NMR (377 MHz, C₆D₆): 51.0 (s, Zr-F).

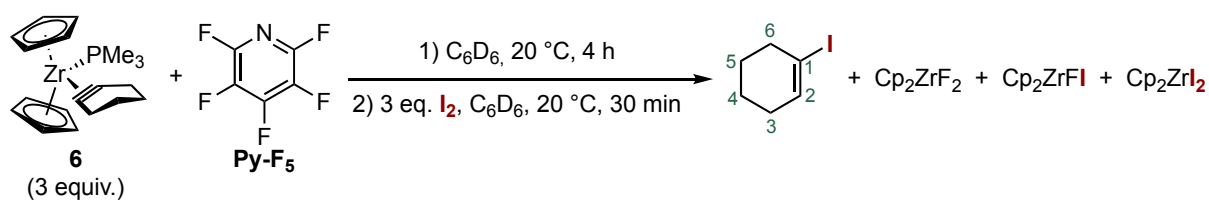
¹³C{¹H} NMR (101 MHz, C₆D₆): 185 (s, 1-C), 126 (s, 2-C), 113 (s, Cp), 35.1 (s, 3-C), 28.3 (s, 6-C), 25.5 (s, 5-C), 23.8 (s, 4-C).

5.2.9 Addition of HCl to 7



Complex **6** (15.0 mg, 0.04 mmol, 3.0 equiv.) was dissolved in cyclohexane (0.7 mL) in an NMR tube equipped with a J. S. Young's valve. Pentafluoropyridine (31.1 μ L of a 0.43 M in cyclohexane, 0.01 mmol, 1.0 equiv.) was added and the mixture was kept at 20 °C for 5 hours. HCl (2M in Et₂O, 0.02 mL, 0.04 mmol, 3.0 equiv.) was added into the mixture. After 30 minutes at 20 °C, the disappearance of 1-cyclohexenylzirconocene fluoride and the formation of cyclohexene, Cp₂ZrCl₂ and other Cp₂ZrX₂ that could not be unambiguously identified were detected by ¹⁹F and ¹H NMR spectroscopy.³⁶¹

5.2.10 Synthesis of 1-iodocyclohexene



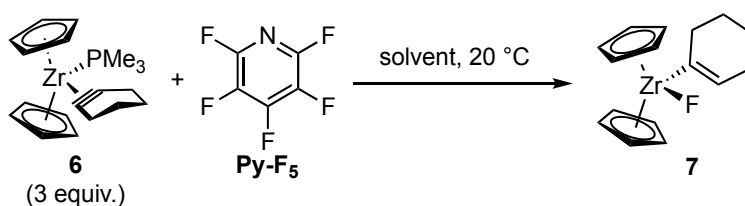
The following manipulation was carried out in an Ar-filled glovebox. Complex **6** (15.0 mg, 0.04 mmol, 3.0 equiv.) was dissolved in cyclohexane (0.7 mL) in an NMR tube equipped with a J. S. Young's valve. Pentafluoropyridine (31.1 μL of a 0.43 M in cyclohexane, 0.01 mmol, 1.0 equiv.) was added and the mixture was kept at $20\text{ }^\circ\text{C}$ for 4 hours. The dark red solid was filtered, the filtrate was dried under reduced pressure and dissolved in 0.6 mL of C_6D_6 . I_2 (10.0 mg, 0.04 mmol, 3.0 equiv.) was added to get a mixture of 1-iodocyclohexene, Cp_2ZrF_2 , Cp_2ZrFI , Cp_2ZrI_2 after 30 min reaction time at $20\text{ }^\circ\text{C}$.

$^1\text{H NMR}$ (400 MHz, C_6D_6): 6.35 – 6.05 (m, 1H, 2-H), 2.37 – 2.21 (m, 2H, 3-H), 1.73 – 1.53 (m, 2H, 3-H), 1.32 – 1.13 (m, 4H, 4-H).

$^{13}\text{C}\{^1\text{H}\}$ NMR (101 MHz, C_6D_6): 138.1 (s, 2-C), 97.0 (s, 1-C), 39.6 (s, 3-C), 29.0 (s, 2-C), 25.3 (s, 4-C), 20.9 (s, 4-C).

The NMR analysis is in agreement with that reported in the literature.³⁶³

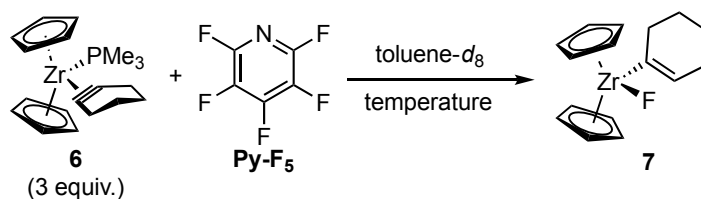
5.2.11 Solvent effect investigation in the reaction of complex 6 with Py-F₅



The following manipulation was carried out in an Ar-filled glovebox. Complex **6** (15.0 mg, 0.04 mmol, 3.0 equiv.) was dissolved in 0.7 mL of the tested solvent (i.e., C_6D_6 , toluene- d_8 , cyclohexane, THF- d_8) in an NMR tube equipped with a J. S. Young's valve. Pentafluoropyridine (31.1 μL of a 0.43 M in cyclohexane, 0.01 mmol, 1.0 equiv.) was added and the mixture was monitored over time by ^1H , ^{31}P and ^{19}F NMR spectroscopy.

5.2.12 Temperature effect investigation for the reaction of complex 6 and

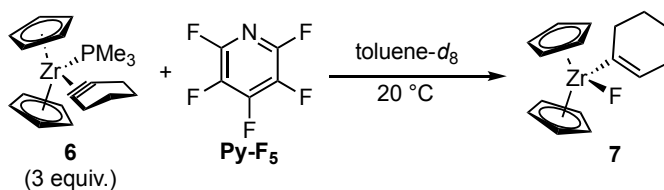
Py-F₅



The following manipulation was carried out in an Ar-filled glovebox. Complex 6 (15.0 mg, 0.04 mmol, 3.0 equiv.) was dissolved in 0.7 mL of toluene-*d*₈ in an NMR tube equipped with a J. S. Young's valve. Pentafluoropyridine (31.1 μ L of a 0.43 M in cyclohexane, 0.01 mmol, 1.0 equiv.) was added and the mixture was kept at variable temperatures (-40 $^{\circ}$ C, 0 $^{\circ}$ C) and monitored over time by 1 H, 31 P and 19 F NMR spectroscopy.

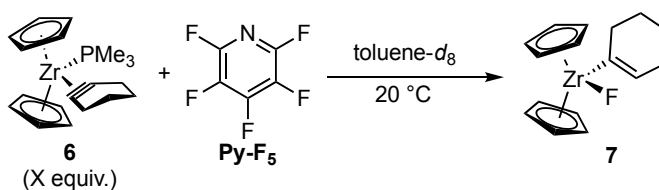
5.2.13 Concentration effect investigation for the reaction of complex 6 and

Py-F₅



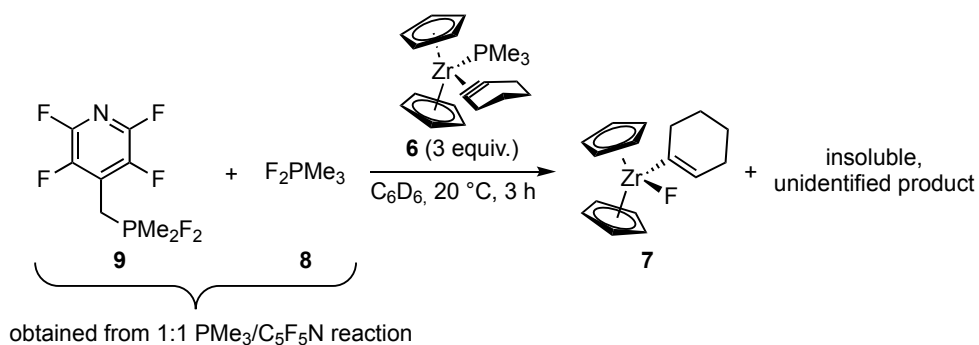
The following manipulation was carried out in an Ar-filled glovebox. Complex 6 (0.1 M, 0.3 M) was dissolved in 0.7 mL of toluene-*d*₈ in an NMR tube equipped with a J. S. Young's valve. Pentafluoropyridine (0.03 M, 0.1 M) was added and the mixture was monitored over time by 1 H, 31 P and 19 F NMR spectroscopy.

5.2.14 Reagent ratio study for the reaction of complex **6** and Py-F₅



The following manipulation was carried out in an Ar-filled glovebox. Different ratios of complex **6** and pentafluoropyridine (1:1, 3:1, 1:3, 5:1) were dissolved in 0.7 mL of toluene-*d*₈ in an NMR tube equipped with a J. S. Young's valve. The mixture was monitored over time by ¹H, ³¹P and ¹⁹F NMR spectroscopy.

5.2.15 Mechanistic investigation on the formation of **7**



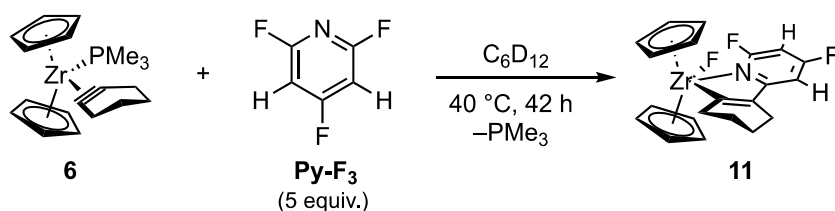
In an Ar-filled glovebox, PMe₃ (4.0 μL, 0.04 mmol, 1.0 equiv.) was added using a Hamilton[®] micro-syringe to C₆D₆ (0.6 mL) in an NMR tube equipped with a J. S. Young's valve. Pentafluoropyridine (4.2 μL, 0.04 mmol, 1.0 equiv.) was added using a Hamilton[®] micro-syringe into the solution which became instantly orange. After 1 hour at 20 °C, complex **6** (45.2 mg, 0.12 mmol, 3.0 equiv.) was added. 3.0 equiv. of **6** were needed to completely consume **9** and **8** by ¹⁹F NMR spectroscopy. The formation of a dark red solid was observed. **7** and unreacted Py-F₄ were identified by ¹H and ¹⁹F NMR analysis.

2,3,5,6-tetrafluoropyridine (Py-F₄):³⁶⁴

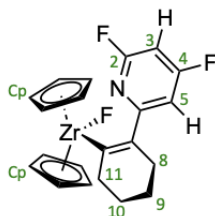
¹H NMR (600 MHz, C₆D₆): δ 6.51 (tt, ³J_{HF} = 7.0 Hz, ⁴J_{HF} = 7.7 Hz, CH).

¹⁹F NMR (564 MHz, C₆D₆): δ -90.5 to -92.6 (m, 2F, *ortho*-F), -139.9 to -141.2 (m, 2F, *meta*-F).

5.2.16 Synthesis of complex **11**



The following manipulation was carried out in an Ar-filled glovebox. Complex **6** (62.0 mg, 0.16 mmol, 1.0 equiv.) was dissolved in cyclohexane-*d*₁₂ (0.7 mL) in an NMR tube equipped with a J. S. Young's valve. 2,4,6-trifluoropyridine (68.2 μL, 0.82 mmol, 5.0 equiv.) was added and the mixture was kept at 40 °C for 42 hours. The product was dried under reduced pressure to afford **11** as a dark red solid (isolated yield 71%). 50 mg of the solid were dissolved in toluene and set for crystallisation by vapor diffusion with tetramethylsilane as antisolvent. The obtained crystals were suitable for X-ray diffraction analysis.

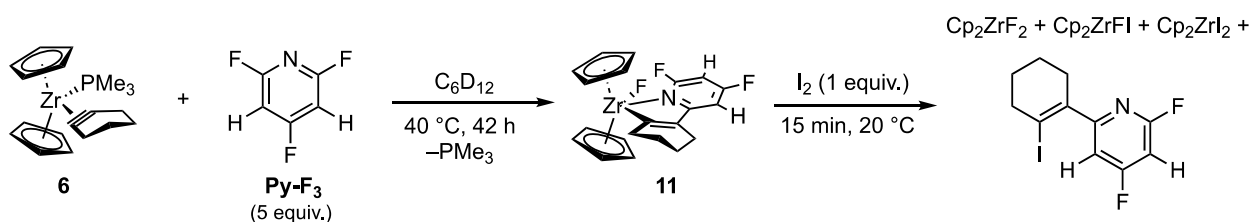


¹H NMR (400 MHz, C₆D₆): 6.35 (dd, 1H, ³J_{HF} = 9.7 Hz, ⁴J_{HH} = 2.3 Hz, 3-*H*), 5.96 (s, 10H, Cp), 5.58 (m, 1H, 5-*H*), 2.96 (m, 2H, 11-*H*), 1.94 (m, 2H, 8-*H*), 1.66 (m, 4H, 9-*H*, 10-*H*).

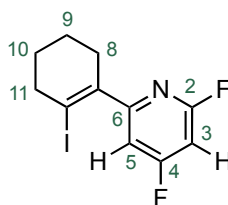
¹⁹F NMR (377 MHz, C₆D₆): 35.4 (s, 1F, F-Zr), -60.1 to -61.3 (m, 1F, 6-*F*), -93.9 to -95.2 (m, 1F, 4-*F*).

¹³C{¹H} NMR (101 MHz, C₆D₆): 215 (d, ²J_{CF} = 3.7 Hz, 12-*C*), 185 (s, 7-*C*), 172.23 (dd, ¹J_{CF} = 264.1 Hz, ³J_{CF} = 15.1 Hz, 6-*C*), 163 (dd, ¹J_{CF} = 246.2 Hz, ³J_{CF} = 15.1 Hz, 4-*C*), 138 (d, ³J_{CF} = 3.1 Hz, 2-*C*), 111 (s, Cp), 102 (dd, ²J_{CF} = 19.4 Hz, ⁴J_{CF} = 3.4 Hz, 3-*C*), 92.4 (dd, ²J_{CF} = 38.6 Hz, ²J_{CF} = 24.4 Hz, 5-*C*), 38.3 (d, ³J_{CF} = 14.3 Hz, 11-*C*), 27.6 (s, 10-*C*), 24.4 (d, ⁴J_{CF} = 3.6 Hz, 8-*C*), 23.5 (s, 9-*C*).

5.2.17 Synthesis of 2,4-difluoro-6-(2-iodocyclohexen-1-yl)-pyridine



The following manipulation was carried out in an Ar-filled glovebox. Complex **6** (62.0 mg, 0.16 mmol, 1.0 equiv.) was dissolved in cyclohexane-*d*₁₂ (0.7 mL) in an NMR tube equipped with a J. S. Young's valve. 2,4,6-trifluoropyridine (68.2 μL , 0.82 mmol, 5.0 equiv.) was added and the mixture was kept at 40 °C for 42 hours. The dark solid was filtered, the filtrate was dried under reduced pressure and dissolved in 0.6 mL of C₆D₆. I₂ (40.0 mg, 0.16 mmol, 1.0 equiv.) was added to get a mixture of 2,4-difluoro-6-(2-iodocyclohexen-1-yl)-pyridine, Cp₂ZrF₂, Cp₂ZrFI, Cp₂ZrI₂ after 30 min reaction time at 20 °C.



2,4-difluoro-6-(2-iodocyclohexen-1-yl)-pyridine:

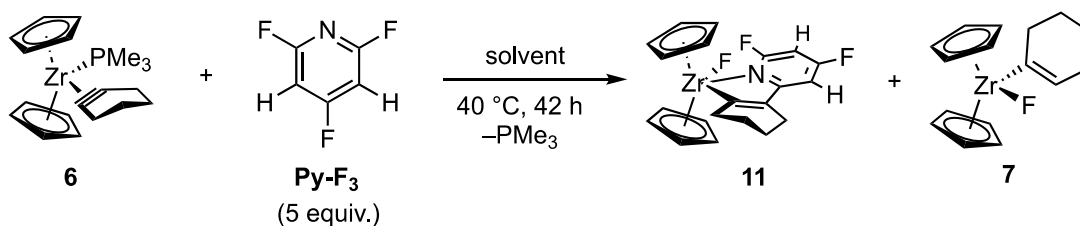
¹H NMR (400 MHz, C₆D₆): 6.63 (ddd, ³J_{HF} = 8.5 Hz, J_{HH} = 1.9 Hz, ⁵J_{HF} = 0.7 Hz, 1H, 5-*H*), 5.98 – 5.77 (m, 1H, 3-*H*), 2.56 – 2.37 (m, 2H, 11-*H*), 2.31 – 2.19 (m, 2H, 8-*H*), 1.40 – 1.28 (m, 1H, 10-*H*), 1.30 – 1.15 (m, 2H, 9-*H*).

¹⁹F NMR (377 MHz, C₆D₆): –63.3 (d, ³J_{HF} = 22.6 Hz, 1F, 2-*F*), –97.2 to –97.9 (m, 1F, 4-*F*).

¹³C{¹H} NMR (101 MHz, C₆D₆): 174.2 (d, ¹J_{CF} = 290.1 Hz, 2-*C*), 165.1 (d, ¹J_{CF} = 192.2 Hz, 4-*C*), 142.4 (d, ³J_{CF} = 3.4 Hz, 6-*C*), 110.1 (dd, J_{CF} = 18.9 Hz, J_{CF} = 5.5 Hz, 5-*C*), 100.3 (s, 7-*C*), 96.1 (dd, J_{CF} = 42.5 Hz, J_{CF} = 22.3 Hz, 3-*C*), 41.6 (s, 8-*C*), 31.6 (s, 11-*C*), 25.0 (s, 10-*C*), 21.9 (s, 9-*C*).

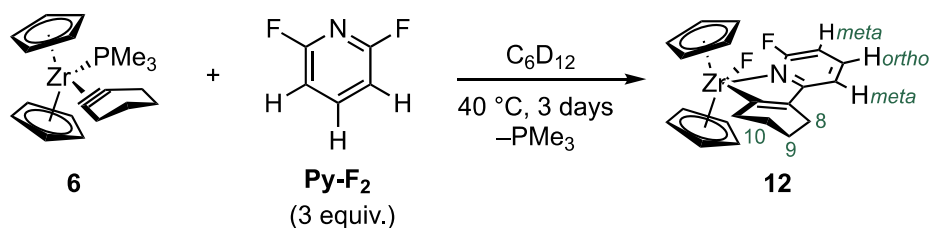
GC(EI)-MS: [C₁₁H₁₀F₂IN]⁺ 321, [C₁₁H₁₀F₂N]⁺ 194 *m/z*.

5.2.18 Investigation on the solvent effect in the synthesis of complex 11

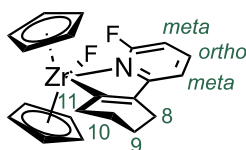


The following manipulation was carried out in an Ar-filled glovebox. Complex **6** (62.0 mg, 0.16 mmol, 1.0 equiv.) was dissolved in 0.7 mL of the tested solvent (i.e., C₆D₆, toluene-*d*₈, cyclohexane, chlorobenzene, Et₂O, THF-*d*₈) in an NMR tube equipped with a J. S. Young's valve. 2,4,6-trifluoropyridine (67.7 μL, 0.82 mmol, 5.0 equiv.) was added. The mixture was kept at 40 °C and monitored over time by ¹H, ³¹P and ¹⁹F NMR spectroscopy.

5.2.19 Synthesis of complex 12



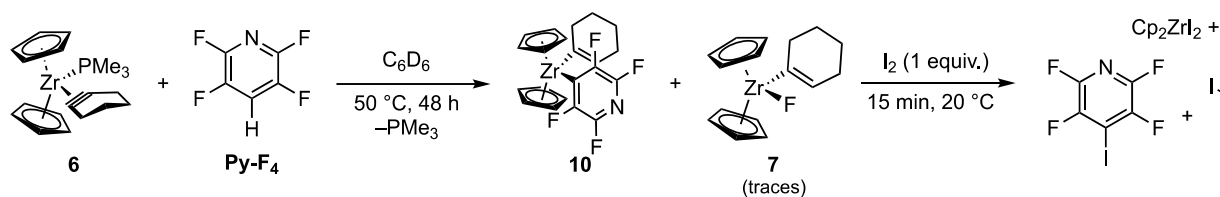
The following manipulation was carried out in an Ar-filled glovebox. Complex **6** (15.0 mg, 0.04 mmol, 1.0 equiv.) was dissolved in cyclohexane-*d*₁₂ (0.7 mL) in an NMR tube equipped with a J. S. Young's valve. 2,6-difluoropyridine (10.8 μL, 0.12 mmol, 3.0 equiv.) was added and the mixture was kept at 40 °C for 3 days. The reaction was monitored by ¹H, ³¹P and ¹⁹F NMR spectroscopy.



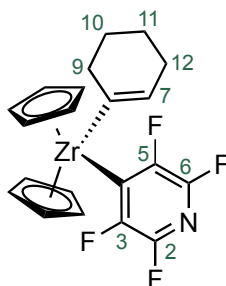
¹H NMR (500 MHz, C₆D₁₂): 8.33 (*pseudo q*, *J* = 7.9 Hz, 1H, *para-H*), 7.61 (*pseudo dt*, ³*J*_{HH} = 8.0 Hz, *J* = 1.2 Hz, 1H, *meta-H*), 7.16 (*pseudo dt*, ³*J*_{HH} = 8.0 Hz, *J* = 1.2 Hz, 1H, *meta-H*), 6.52 (s, 10H, Cp), 3.32 – 3.03 (m, 2H, 11-*H*), 2.86 (tt, ³*J*_{HH} = 6.4 Hz, ⁴*J*_{HH} = 2.2 Hz, 2H, 8-*H*), 2.54 – 2.12 (m, 2H, 9-*H*), 2.31 – 1.96 (m, 2H, 10-*H*).

¹⁹F NMR (471 MHz, C₆D₁₂): 34.6 (s, 1F, F–Zr), –64.3 (d, *J* = 7.6 Hz, 1F, *ortho-F*).

5.2.20 Synthesis of complex 10 and its iodinolysis



The following manipulation was carried out in an Ar-filled glovebox. Complex **6** (15.0 mg, 0.04 mmol, 1.0 equiv.) was dissolved in cyclohexane (0.7 mL) in an NMR tube equipped with a J. S. Young's valve. 2,3,5,6-tetrafluoropyridine (4.2 μ L, 0.04 mmol, 1.0 equiv.) was added and the mixture was kept at 40 °C for 48 hours. The reaction was monitored by ^1H , ^{31}P and ^{19}F NMR. The dark solid was filtered, the filtrate was dried under reduced pressure to yield complex **10**. It was then dissolved in 0.6 mL of C_6D_6 and I_2 (9.6 mg, 0.04 mmol, 1 equiv.) was added to get a mixture of 2,4-difluoro-6-(2-iodocyclohexen-1-yl)pyridine and Cp_2ZrI_2 after 30 min reaction time at 20 °C.



^1H NMR (400 MHz, C_6D_6): δ 5.40 (s, 10H, Cp), 5.13 – 4.91 (m, 1H, 7-*H*), 2.48 – 2.26 (m, 2H, 9-*H*), 2.03 – 1.80 (m, 2H, 12-*H*), 1.55 – 1.32 (m, 4H, 10-*H*, 11-*H*).

^{19}F NMR (377 MHz, C_6D_6): –97.2 to –97.9 (m, 2F, *ortho*-F), –114.3 to –115.1 (m, 2F, *meta*-F).

1-iodocyclohexene:

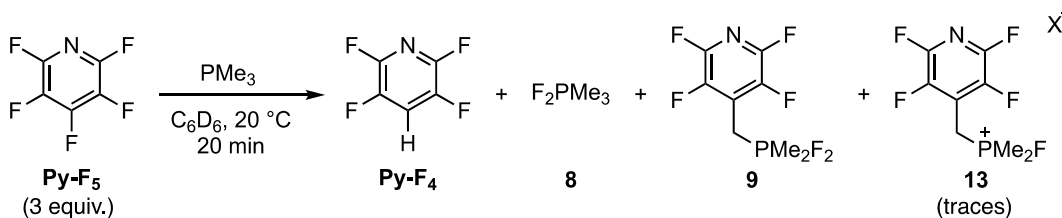
^1H NMR (400 MHz, C_6D_6): 6.28 – 6.04 (m, 1H, vinyl-*H*), 2.21 – 2.32 (m, 2H, CH_2), 1.58 – 1.68 (m, 2H, CH_2), 1.18 – 1.27 (m, 2H, CH_2).

2,3,5,6-tetrafluoro-4-iodopyridine:

^{19}F NMR (376 MHz, C_6D_6): –89.7 to –90.4 (m, 2F, *ortho*-F), –123.1 to –123.7 (m, 2F, *meta*-F).

5.3 Chapter 3 – Stoichiometric reactivity between trialkylphosphines and Py-F₅

5.3.1 Stoichiometric reactivity of PMe₃ and Py-F₅



The following manipulation was carried out in an Ar-filled glovebox. PMe₃ (20.3 μL, 0.20 mmol, 1.0 equiv.) was mixed with C₆D₆ (0.6 mL) in an NMR tube equipped with a J. S. Young's valve. Pentafluoropyridine (65.9 μL, 0.60 mmol, 3.0 equiv.) was added into the solution which became instantly orange at 20 °C. After 20 minutes at 20 °C, the formation of **Py-F₄**, **8**, **9** and **13** was observed by ¹H, ³¹P and ¹⁹F NMR spectroscopy.

Trimethyldifluorophosphorane (**8**):³⁶⁵

¹H NMR (400 MHz, C₆D₆): 1.42 (dt, ²J_{HP} = 17.3 Hz, ³J_{HF} = 12.3 Hz, 2H, CH₃).

¹⁹F NMR (377 MHz, C₆D₆): -5.5 (dm, ¹J_{PF} = 544.1 Hz, 2F, F₂P).

³¹P NMR (162 MHz, C₆D₆): -16.2 (tm, ¹J_{PF} = 544.0 Hz, 1P).

¹³C{¹H} NMR (101 MHz, C₆D₆): 18.7 (dt, ¹J_{PC} = 127.3 Hz, ²J_{FC} = 29.4 Hz, 2C, CH₃).

Compound 13:

¹H NMR (400 MHz, C₆D₆): δ 0.74 (ddt, ²J_{HP} = 14.6 Hz, ³J_{HF} = 4.6 Hz, ⁴J_{HF} = 1.0 Hz, 6H, CH₃), 3.14 (ddt, ²J_{HP} = 16.7 Hz, ³J_{HF} = 3.8 Hz, ⁴J_{HF} = 1.0 Hz, 2H, CH₂).

¹⁹F NMR (377 MHz, C₆D₆): δ -72.3 (dm, ¹J_{FP} = 1021.1 Hz, 1F, FP), -95.5 to -98.2 (m, 2F, *ortho*-F), -143.1 to -145.3 (m, 2F, *meta*-F).

³¹P NMR (162 MHz, C₆D₆): δ 76.2 (dm, 1021.4 Hz, 1P, FP).

4-methylenetetrafluoropyridine-substituted phosphorane (9)

^1H NMR (400 MHz, C_6D_6): δ 1.34 (dt, $^2J_{\text{HP}} = 17.3$ Hz, $^3J_{\text{HF}} = 12.5$ Hz, 6H, CH_3), 3.09 (dtt, $^2J_{\text{HP}} = 23.5$ Hz, $^3J_{\text{HF}} = 5.0$ Hz, $^4J_{\text{HF}} = 1.8$ Hz, 2H, CH_2).

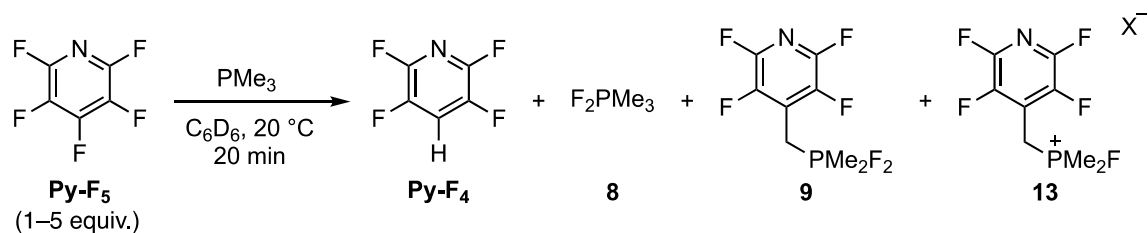
^{19}F NMR (377 MHz, C_6D_6): δ -9.7 (dm, $^1J_{\text{PF}} = 595.1$ Hz, 2F, F_2P), -92.1 to -94.2 (m, 2F, *ortho*-F), -143.6 to -145.3 (m, 2F, *meta*-F).

^{31}P NMR (162 MHz, C_6D_6): δ -20.5 (tm, $J_{\text{PF}} = 595.0$ Hz, PF_2).

$^{13}\text{C}\{^1\text{H}\}$ NMR (101 MHz, C_6D_6): δ 142.9 – 141.5 (m, 2C, CF), 140.1 – 138.7 (m, 2C, CF), 129.5 – 128.4 (m, 1C, $\text{C}(\text{sp}^2)\text{-CH}_2$), 27.9 (dt, $^1J_{\text{CP}} = 123.2$ Hz, $^2J_{\text{CF}} = 32.9$ Hz, 1C, CH_2), 18.7 (dt, $^1J_{\text{CP}} = 127.2$ Hz, $^2J_{\text{CF}} = 28.9$ Hz, 2C, CH_3).

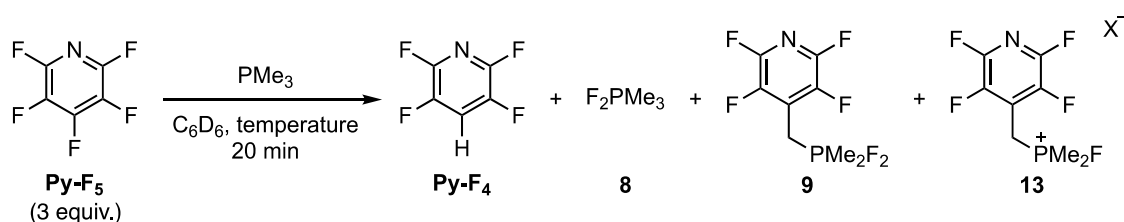
GC(EI)-MS: $[\text{C}_8\text{H}_8\text{F}_6\text{NP}]^{*+}$ 263.02817, $[\text{C}_8\text{H}_8\text{F}_6\text{NP}]^{*+}$ 248.00528, $[\text{C}_6\text{H}_2\text{F}_4\text{NP}]^{*+}$ 164.01269, $[\text{C}_2\text{H}_6\text{F}_2\text{P}]^{*+}$ 99.01827 m/z .

5.3.2 Reagent ratio study for the reaction of PMe_3 and Py-F_5



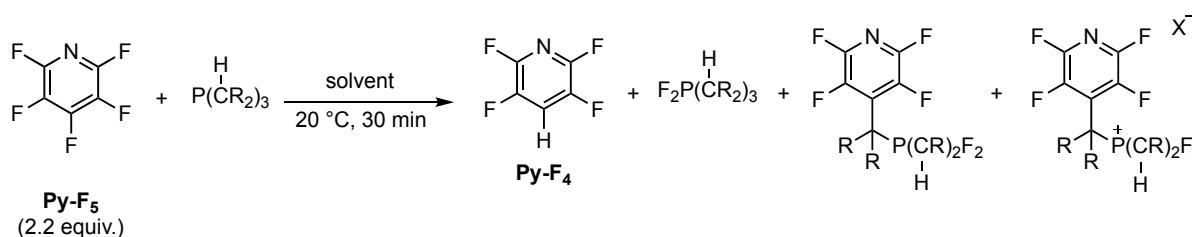
Different amounts of pentafluoropyridine (0.02 mmol, 0.06 mmol, 0.10 mmol) and PMe_3 (2.0 μL , 0.02 mmol, 1.0 equiv.) were dissolved in 0.6 mL of C_6D_6 and placed into an NMR tube equipped with a J. S. Young's valve. The mixture was monitored by ^{19}F and ^{31}P NMR spectroscopy.

5.3.3 Temperature study for the reaction of PMe_3 and Py-F_5

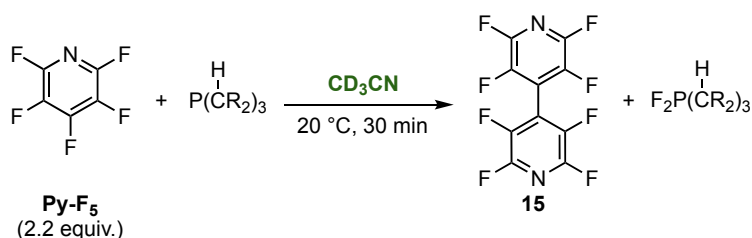


Pre-cooled (-40°C) reagents and solvent were used for these tests. Pentafluoropyridine (6.6 μL , 0.06 mmol, 3.0 equiv.) and PMe_3 (2.03 μL , 0.02 mmol, 1.0 equiv.) were dissolved in 0.6 mL of C_6D_6 and placed into an NMR tube equipped with a J. S. Young's valve. The mixture was kept at -40°C , 0°C and 20°C and monitored by ^{19}F and ^{31}P NMR spectroscopy.

5.3.4 Solvent study for the reaction of PR_3 and Py-F_5



solvent: toluene- d_8 , THF- d_8 and CD_2Cl_2
phosphine: PMe_3 , PCy_3 , P^iPr_3 , $\text{P}(\text{Me})_2\text{Ph}$

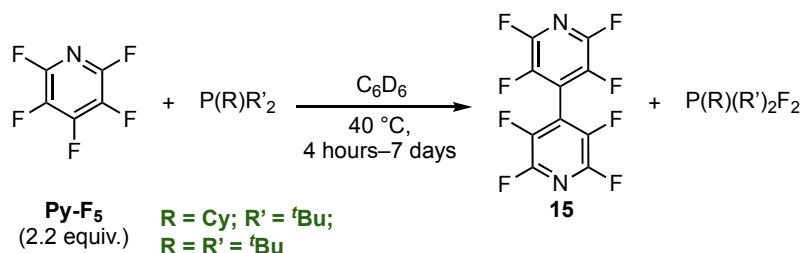
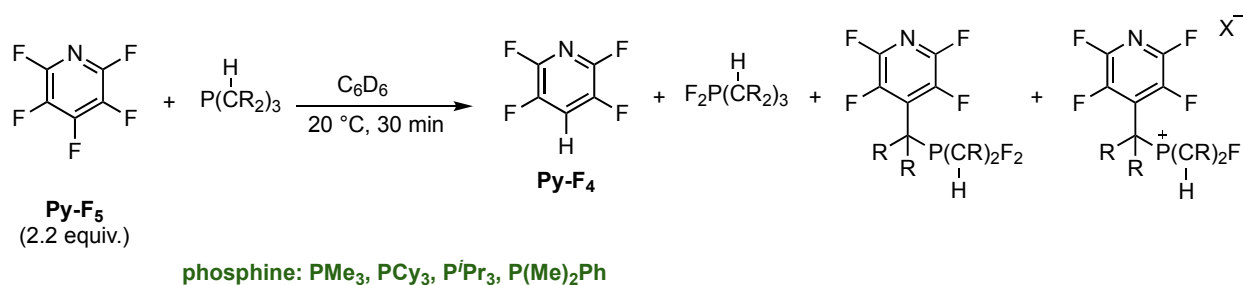


phosphine: PMe_3 , PCy_3 , P^iPr_3 , $\text{P}(\text{Me})_2\text{Ph}$

Pentafluoropyridine (4.8 μL , 0.04 mmol, 2.2 equiv.) and a range of phosphines (i.e., PMe_3 , PCy_3 , P^iPr_3 , $\text{P}(\text{Me})_2\text{Ph}$) (0.02 mmol, 1.0 equiv.) were dissolved in 0.6 mL of the tested solvent (i.e., C_6D_6 , toluene- d_8 , THF- d_8 , CD_2Cl_2 and CD_3CN) and placed into an NMR tube equipped with a J. S. Young's valve. The mixture was monitored by ^{19}F and ^{31}P NMR spectroscopy.

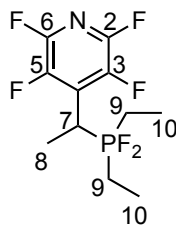
A comprehensive characterisation of the products was conducted in the PMe_3 experiment, including ^{13}C NMR and mass analyses (section 5.2.21). Given that the ^1H , ^{19}F and ^{31}P NMR analyses of such difluorophosphoranes are diagnostic when compared to PMe_3 data, the analysis of the same reaction with other phosphines was limited to these NMR spectra (see section 5.3.5.1).

5.3.5 Phosphine effect investigation on the reaction of PR₃ and Py-F₅



Pentafluoropyridine (4.8 μ L, 0.04 mmol, 2.2 equiv.) and PR₃ (i.e., PMe₃, PCy₃, PⁱPr₃, P(Me)₂Ph, P(Cy)^tBu₂, P^tBu₃) (0.02 mmol, 1.0 equiv.) were dissolved in 0.6 mL of C₆D₆ and placed into an NMR tube equipped with a J. S. Young's valve. The mixture was monitored by ¹⁹F and ³¹P NMR spectroscopy.

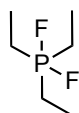
5.3.5.1 Spectroscopic data for the synthesised difluorophosphanes



¹H NMR (400 MHz, C₆D₆): δ 3.83 – 3.60 (m, 1H, 7-*H*), 1.88 – 1.62 (m, 4H, 9-*H*), 1.35 (ddt, ³J_{HP} = 20.1 Hz, ³J_{HH} = 7.6 Hz, ⁴J_{HF} = 1.6 Hz, 3H, 8-*H*), 0.89 (dtt, ³J_{HP} = 23.6 Hz, ³J_{HH} = 7.8 Hz, ⁴J_{HF} = 1.4 Hz, 9H, 10-*H*).

¹⁹F NMR (377 MHz, C₆D₆): δ –38.1 (dm, ¹J_{FP} = 643.1 Hz, 2F, PF₂), –91.0 to –93.1 (m, 2F, 2-*F*, 6-*F*), –142.3 (bs, 2F, 5-*F*, 3-*F*).

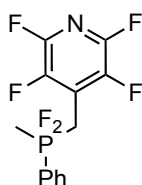
³¹P NMR (162 MHz, C₆D₆): δ –16.8 (tm, ¹J_{FP} = 643.5 Hz, 1P, PF₂).



^1H NMR (400 MHz, C_6D_6): δ 1.93 – 1.72 (m, 6H, CH_2), 1.06 (dtt, $^3J_{\text{HP}} = 22.8$ Hz, $^3J_{\text{HH}} = 7.7$ Hz, $^4J_{\text{HF}} = 1.0$ Hz, 9H, CH_3).

^{19}F NMR (377 MHz, C_6D_6): δ –39.0 (dm, $^1J_{\text{FP}} = 587.1$ Hz, 2F, PF_2).

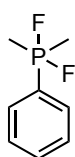
^{31}P NMR (162 MHz, C_6D_6): δ –12.1 (tm, $^1J_{\text{FP}} = 587.4$ Hz, 1P, PF_2).



^1H NMR (400 MHz, C_6D_6): δ 7.87 – 7.68 (m, 3H, Ph), 7.21 – 7.06 (m, 2H, Ph), 3.44 – 3.32 (m, 2H, CH_2), 1.72 – 1.55 (m, 3H, CH_3).

^{19}F NMR (565 MHz, C_6D_6): δ –23.0 (dm, $^1J_{\text{FP}} = 642.1$ Hz, 2F, PF_2).

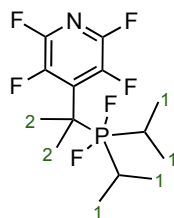
^{31}P NMR (243 MHz, C_6D_6): δ –36.2 (tm, $^1J_{\text{FP}} = 641.3$ Hz, 1P, PF_2).



^1H NMR (400 MHz, C_6D_6): δ 7.40 – 7.01 (m, 5H, Ph), 1.72 – 1.55 (m, 6H, CH_3).

^{19}F NMR (565 MHz, C_6D_6): δ –17.3 (dm, $^1J_{\text{FP}} = 590.1$ Hz, 2F, PF_2).

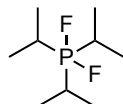
^{31}P NMR (243 MHz, C_6D_6): δ –29.6 (t, $^1J_{\text{FP}} = 590.0$ Hz, 1P, PF_2).



^1H NMR (600 MHz, toluene- d_8): δ 2.43 – 2.28 (m, 2H, CH), 1.59 (dm, $J = 17.8$ Hz, 6H, 2- CH_3), 1.06 (ddt, $^3J_{\text{HP}} = 20.5$ Hz, $^3J_{\text{HH}} = 7.3$ Hz, $^4J_{\text{HF}} = 2.3$ Hz, 12H, 1- CH_3).

^{19}F NMR (565 MHz, toluene- d_8): δ -51.0 (dm, $^1J_{\text{FP}} = 733.0$ Hz, 2F, PF_2), -93.4 (p, $J = 14.7$ Hz, 2F, *ortho*-F), -136.4 to -136.6 (m, 2F, *meta*-F).

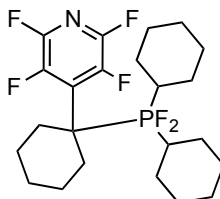
^{31}P NMR (243 MHz, toluene- d_8): δ -21.2 (tm, $^1J_{\text{FP}} = 733.6$ Hz, 1P, PF_2).



^1H NMR (400 MHz, CD_3CN): δ 2.47 – 2.21 (m, 3H, CH), 1.21 (ddt, $^3J_{\text{HP}} = 19.9$ Hz, $^3J_{\text{HH}} = 7.2$ Hz, $^4J_{\text{HF}} = 1.9$ Hz, 18H, CH_3).

^{19}F NMR (377 MHz, CD_3CN): δ -61.3 (dm, $^1J_{\text{FP}} = 646.4$ Hz, 2F, PF_2).

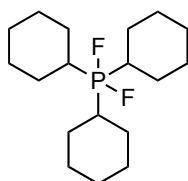
^{31}P NMR (162 MHz, CD_3CN): δ -14.6 (tm, $^1J_{\text{FP}} = 645.6$ Hz, 1P, PF_2).



^1H NMR (500 MHz, toluene- d_8): δ 3.36 – 2.93 (m, 2H, CH), 2.29 – 0.83 (m, 30H, CH_2).

^{19}F NMR (471 MHz, toluene- d_8): δ -57.5 (dm, $^1J_{\text{FP}} = 731.0$ Hz, 2F, PF_2), -94.3 (p, $J = 14.9$ Hz, 2F, *ortho*-F), -136.1 to -136.4 (m, 2F, *meta*-F).

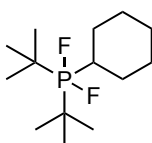
^{31}P NMR (202 MHz, toluene- d_8): δ -28.0 (tm, $^1J_{\text{FP}} = 733.7$ Hz, 1P, PF_2).



¹H NMR (500 MHz, CD₂Cl₂): δ 2.22 – 1.16 (m, 32H, CH₂ and CH).

¹⁹F NMR (471 MHz, CD₂Cl₂): δ –63.8 (dm, ¹J_{FP} = 639.9 Hz, 2F, PF₂).

³¹P NMR (202 MHz, CD₂Cl₂): δ –22.3 (tm, ¹J_{FP} = 645.2 Hz, 1P, PF₂).

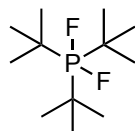


¹H NMR (500 MHz, toluene-*d*₈): δ 2.26 – 2.11 (m, 1H, CH), 1.77 – 1.35 (m, 10H, CH₂), 1.21 (dt, ³J_{HP} = 17.3 Hz, ⁴J_{HF} = 2.6 Hz, 27H, CH₃).

¹⁹F NMR (471 MHz, toluene-*d*₈): δ –61.4 (dm, ¹J_{FP} = 734.1 Hz, 2F, PF₂).

³¹P NMR (202 MHz, toluene-*d*₈): δ –22.5 (tm, ¹J_{FP} = 734.7 Hz, 1P, PF₂).

¹³C NMR (126 MHz, toluene-*d*₈): δ 47.1 (dt, ¹J_{CP} = 120.5 Hz, ²J_{CF} = 26.0 Hz, 1C, CH), 42.8 (dt, ¹J_{CP} = 114.4 Hz, ²J_{CF} = 21.3 Hz, 2C, quaternary C), 30.4 (td, ⁴J_{CF} = 7.5 Hz, ³J_{CP} = 4.0 Hz, 2C, CH₂), 29.2 (t, *J* = 5.7 Hz, 18C, CH₃), 28.1 (dt, ²J_{CP} = 17.0, ³J_{CF} = 1.5 Hz, 2C, CH₂), 26.5 (d, ⁴J_{CP} = 2.0 Hz, 1C, CH₂).



¹H NMR (400 MHz, toluene-*d*₈): δ 1.21 (dt, ³J_{HP} = 17.3 Hz, ⁴J_{HF} = 2.6 Hz, 27H, CH₃).

¹⁹F NMR (376 MHz, toluene-*d*₈): δ –61.4 (dm, ¹J_{FP} = 734.0 Hz, 2F, PF₂).

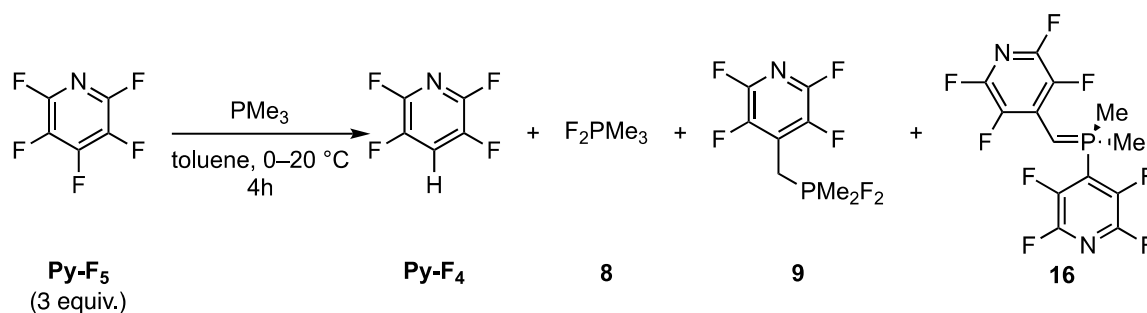
³¹P NMR (162 MHz, toluene-*d*₈): δ –22.5 (tm, ¹J_{FP} = 734.6 Hz, 1P, PF₂).

Perfluoro-4,4'-bipyridine (15):³⁶⁶

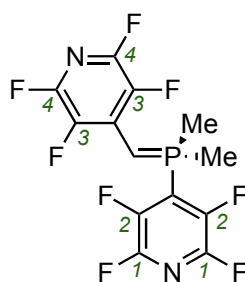
¹⁹F NMR (565 MHz, CD₃CN): δ -87.7 to -88.5 (m, 4F, CF), -138.0 to -139.2 (m, 4F, CF).

GC(EI)-MS [C₁₀N₂F₈]⁺ 299.99075 *m/z* (6.92 ppm deviation from theoretical mass).

5.3.6 Synthesis of ylide 16



The following manipulation was carried out under N₂ atmosphere. PMe₃ (0.34 mL, 3.4 mmol, 1.0 equiv.) was mixed with toluene (20 mL) in a Schlenk tube and the mixture was cooled down to 0 °C. Pentafluoropyridine (1.12 mL, 10.2 mmol, 3.0 equiv.) was added into the solution at 0 °C which was then heated up to 20 °C for 4 hours. ¹H, ¹⁹F and ³¹P NMR analyses showed the complete consumption of PMe₃ and the formation of **Py-F₄**, **8**, **9** and **16**. The solvent and the volatiles were removed under vacuum and crystals of **16** suitable for a single crystal X-ray diffraction (sc-XRD) analysis were grown after vapour diffusion of pentane into a concentrated toluene solution of the **9** and **16** at room temperature.



Compound 16:

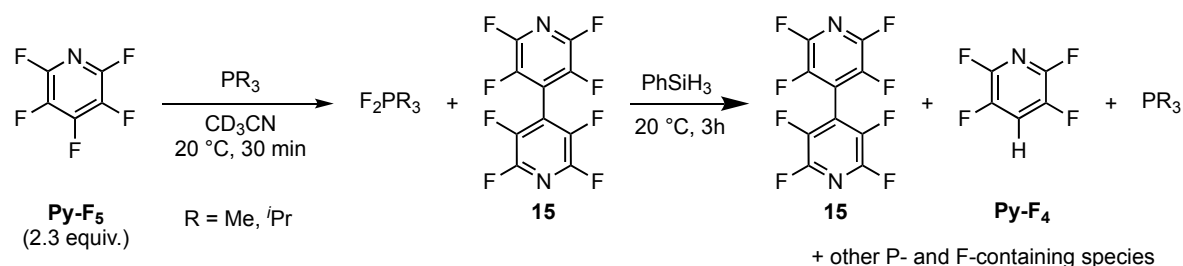
¹H NMR (500 MHz, C₆D₆): δ 2.71 (d, ²J_{HP} = 18.4 Hz, 1H, CH), 0.92 (d, ²J_{HP} = 13.8 Hz, 6H, CH₃).

¹⁹F NMR (471 MHz, C₆D₆): δ -88.1 to -88.4 (m, 2F, 1-F), -97.6 to -97.9 (m, 2F, 3-F), -134.8 to -135.3 (m, 2F, 2-F), -154.8 to -155.3 (m, 2F, 4-F).

³¹P NMR (243 MHz, C₆D₆): δ -1.5 to -1.9 (m, 1P).

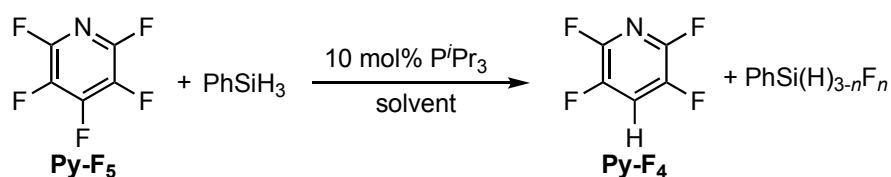
5.4 Chapter 4 – PⁿBu₃-catalysed hydro- and aminodefluorination of polyfluoroaromatics

5.4.1 Difluorination and reduction of difluorophosphanes by PhSiH₃



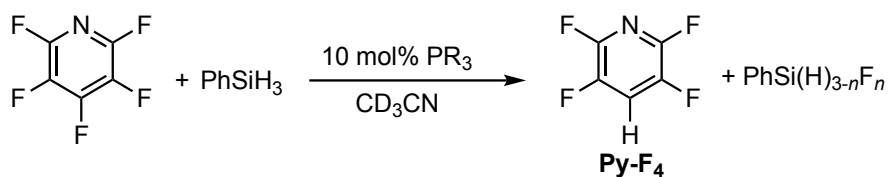
Pentafluoropyridine (24.1 μL , 0.22 mmol, 2.2 equiv.) and PR₃ (i.e., PMe₃, P^{*i*}Pr₃) (0.10 mmol, 1.0 equiv.) were dissolved in 0.6 mL of CD₃CN and placed into an NMR tube equipped with a J. S. Young's valve. After 30 minutes at 20 °C, the complete conversion of PR₃ into F₂PR₃, along with compound **15** and some unreacted **Py-F₅**, were detected by ¹⁹F and ³¹P NMR analysis. PhSiH₃ (12.3 μL , 0.10 mmol, 1.0 equiv.) was added into the solution. After 3 hours at 20 °C, the ¹⁹F and ³¹P NMR spectra proved that a significant amount of PR₃ was regenerated in solution, together with a small quantity of **Py-F₄** and other unidentified F- and P-containing species. Compound **15** remained untouched during the second step of the reaction. This test proved that PhSiH₃ is able to defluorinate and reduce difluorophosphanes into phosphines.

5.4.2 Procedure for the solvent optimisation in the catalytic HDF reaction



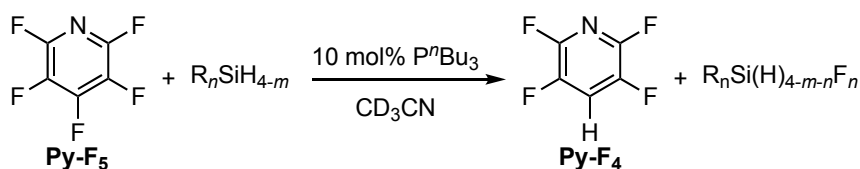
Pentafluoropyridine (43.9 μL , 0.40 mmol, 1.0 equiv.) and PhSiH₃ (49.2 μL , 0.40 mmol, 1.0 equiv.) were dissolved in 0.4 mL of the tested solvent and placed into a J. S. Young's NMR tube. P^{*i*}Pr₃ (7.6 μL , 0.04 mmol, 0.1 equiv.) was added and the tube was heated to monitor the progress of reaction (conditions specified in Table 4).

5.4.3 Procedure for catalyst optimisation in the catalytic HDF reaction



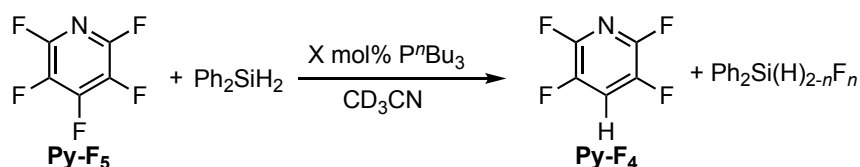
Pentafluoropyridine (43.9 μ L, 0.40 mmol, 1.0 equiv.) and PhSiH₃ (49.2 μ L, 0.40 mmol, 1.0 equiv.) were dissolved in 0.4 mL of CD₃CN and placed into a J. S. Young's NMR tube. The tested phosphine (0.04 mmol, 0.1 equiv.) was added and the tube was heated to monitor the progress of reaction (conditions specified in Table 4).

5.4.4 Procedure for silane optimisation in the catalytic hydrodefluorination reaction



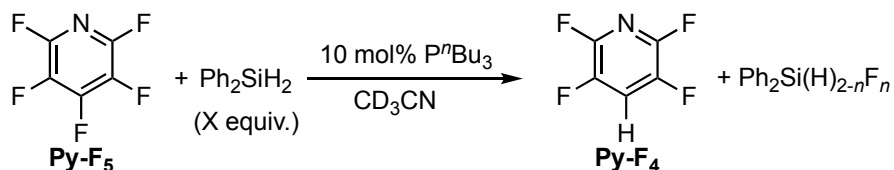
Pentafluoropyridine (43.9 μ L, 0.40 mmol, 1.0 equiv.) and the tested silane (0.40 mmol, 1.0 equiv.) were dissolved in 0.4 mL of CD₃CN and placed into a J. S. Young's NMR tube. PⁿBu₃ (10.0 μ L, 0.04 mmol, 0.1 equiv.) or PⁱPr₃ (7.6 μ L, 0.04 mmol, 0.1 equiv.) was added and the tube was heated to monitor the progress of reaction (conditions specified in Table 4).

5.4.5 Procedure for optimisation of the catalyst loading in the catalytic HDF reaction



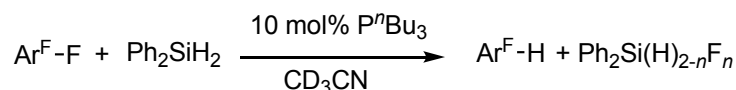
Pentafluoropyridine (43.9 μ L, 0.40 mmol, 1.0 equiv.) and Ph₂SiH₂ (74.2 μ L, 0.40 mmol, 1.0 equiv.) were dissolved in 0.4 mL of CD₃CN and placed into a J. S. Young's NMR tube. Different amounts of PⁿBu₃ were added (10 mol%, 5 mol% or 1 mol%) and the progress of reaction was monitored (conditions specified in Table 4).

5.4.6 Procedure for optimisation of the silane loading in the catalytic HDF reaction



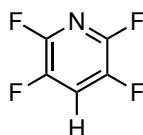
Pentafluoropyridine (43.9 μ L, 0.40 mmol, 1.0 equiv.) and different amounts of Ph₂SiH₂ (1.0 equiv. and 0.55 equiv.) were dissolved in 0.4 mL of CD₃CN and placed into a J. S. Young's NMR tube. PⁿBu₃ (10.0 μ L, 0.04 mmol, 0.1 equiv.) was added and the progress of reaction was monitored (conditions specified in Table 4).

5.4.7 General procedure for the catalytic HDF



The Ar-F (0.40 mmol, 1.0 equiv.) and Ph₂SiH₂ (74.2 μ L, 0.40 mmol, 1.0 equiv.) were dissolved in 0.4 mL of CD₃CN and placed into a J. S. Young's NMR tube. PⁿBu₃ (10.0 μ L, 0.1 equiv.) was added and the progress of reaction was monitored by ¹⁹F NMR spectroscopy. If the hydrodefluorination product is volatile, the reaction mixture was analysed by quantitative ¹⁹F NMR with trifluorotoluene used as internal standard. The NMR yield was calculated from the ratio of the integrals of the trifluorotoluene and Ar-F signals (blank) and the ratio of the trifluorotoluene and Ar-H signals at the end of the reaction. In the case of decafluorobiphenyl, after completion of the reaction the solution was evaporated and fully dried. The residue was dissolved in *n*-hexane and the resulting mixture was purified by chromatography column. Hexane was then evaporated and the product thoroughly dried.

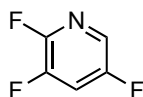
5.4.7.1 Spectroscopic data for the hydrodefluorinated products:



2,3,5,6-tetrafluoropyridine (Py-F₄):³⁶⁷ NMR yield of 93%.

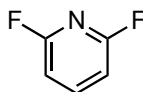
¹H NMR (600 MHz, CD₃CN): δ 7.88 (tt, ³J_{HF} = 7.9 Hz, ⁴J_{HF} = 7.1 Hz, 1H, CH).

¹⁹F NMR (565 MHz, CD₃CN): δ -93.4 to -93.7 (m, 2F, *ortho*-F), -141.3 to -141.7 (m, 2F, *meta*-F).



3,5,6-trifluoropyridine (17):¹⁸⁷ NMR yield of 13%. ¹H NMR peaks have not been identified due to the low conversion and the overlapping of Ph₂SiH₂, 2,3,5,6-tetrafluoropyridine and trifluorotoluene signals.

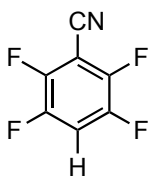
¹⁹F NMR (565 MHz, CD₃CN): δ -92.3 (t, ³J_{FF} = 27.9 Hz, 1F, 6-CF), -129.0 (ddd, ⁵J_{FF} = 29.1 Hz, ³J_{FH} = 7.6 Hz, ³J_{FF} = 3.6 Hz, 1F, 5-CF), -136.5 (ddd, ³J_{FH} = 26.3 Hz, ³J_{FH} = 9.2 Hz, ³J_{FF} = 3.7 Hz, 1F, 3-CF).



2,6-difluoropyridine (Py-F₂):³⁶⁸ NMR yield of 79%.

¹H NMR (600 MHz, CD₃CN): δ 8.12 – 7.78 (m, 1H, *para*-H), 6.93 (d, J = 8.0 Hz, 2H, *meta*-H).

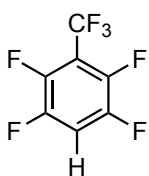
¹⁹F NMR (565 MHz, CD₃CN): δ -70.3 (bs, 2F, CF).



2,3,5,6-tetrafluorobenzonitrile (18):³⁶⁷ NMR yield of 86%.

¹H NMR (600 MHz, CD₃CN): δ 7.53 – 7.78 (m, 1H, CH).

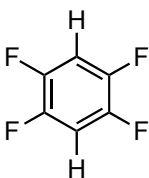
¹⁹F NMR (471 MHz, CD₃CN): δ –134.4 to –135.2 (m, 2F, CF), –136.9 to –137.9 (m, 2F, CF).



1,2,4,5-tetrafluoro-3-(trifluoromethyl)benzene (19):³⁶⁷ NMR yield of 89%.

¹H NMR (600 MHz, CD₃CN): δ 7.52 – 7.71 (m, 1H, CH).

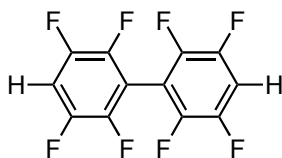
¹⁹F NMR (565 MHz, CD₃CN): δ –57.3 (t, ⁴J_{FF} = 22.3 Hz, 3F, CF₃), –137.7 to –138.8 (m, 2F, CF), –142.0 to –143.2 (m, 2F, CF).



1,2,4,5-tetrafluorobenzene (20):³⁶⁹ NMR yield of 84% when Ar–F is C₆F₆, 93% when Ar–F is C₆F₅H.

¹H NMR (500 MHz, CD₃CN): δ 7.26 (p, J = 8.9 Hz, 2H, CH).

¹⁹F NMR (471 MHz, CD₃CN): δ –141.0 (t, J = 8.9 Hz, 4F, CF).

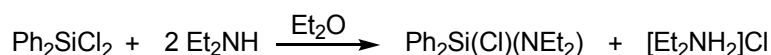


2,2',3,3',5,5',6,6'-octafluoro-1,1'-biphenyl (23):³⁶⁷ NMR yield of 87%. An isolated yield of 86% (1.026 g) was obtained when octafluorobiphenyl (1.34 g, 4.00 mmol, 1.0 equiv.), Ph₂SiH₂ (0.74 mL, 4.00 mmol, 1.0 equiv.) and PⁿBu₃ (0.10 mL, 0.1 equiv.) were dissolved in 4 mL of CH₃CN and heated up to 60 °C for 24 hours. The solvent was evaporated under reduced pressure, the residue was dissolved in *n*-hexane and the resulting mixture was purified by chromatography column. Hexane was then evaporated and the product thoroughly dried.

¹H NMR (600 MHz, CD₂Cl₂): δ 4.87 – 5.61 (m, 2H, CH).

¹⁹F NMR (565 MHz, CD₃CN): δ –138.9 to –139.8 (m, 2F, CF), –138.8 to –140.6 (m, 2F, CF).

5.4.8 Preparation of Ph₂Si(Cl)(NEt₂)



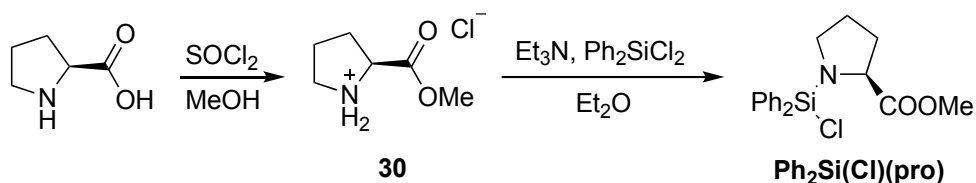
This product was prepared according to a literature method.³⁷⁰ A Schlenk tube was charged with 1.2 mL (5.9 mmol, 1.0 equiv.) of diphenyldichlorosilane and 13 mL of ether. The solution was cooled to –78°C in a dry-ice/acetone bath and treated with a solution of 2.4 mL (23.7 mmol, 4.0 equiv.) of diethylamine in 4 mL of ether over a 30 min period, causing formation of a voluminous precipitate of diethylamine hydrochloride. Filter under a positive pressure of nitrogen with a filter-stick, wash the solid with ether, combine the ether layers, dry the product under vacuum. N.B. the product may fume in contact with air. A yellow oil was obtained in 78% yield.

¹H NMR (C₆D₆, 600 MHz): δ 8.23 – 7.71 (m, 4H, Ph), 7.34 – 7.01 (m, 6H, Ph), 2.86 (q, ³J_{HH} = 7.1 Hz, 4H, CH₂), 0.92 (t, ³J_{HH} = 7.3 Hz, 6H, CH₃).

²⁹Si NMR (C₆D₆, 119 MHz): δ –6.56 (s, 1Si).

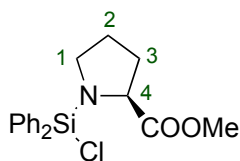
MS-APCI: [C₁₆H₂₁ClNSi]⁺ 290.113336 *m/z* (2.4 ppm deviation from theoretical mass).

5.4.9 Preparation of Ph₂Si(Cl)(pro)



L-Proline methyl ester hydrochloride (**30**) was prepared according to a literature method.³⁷¹ Thionyl chloride (0.72 mL, 10.1 mmol, 1.2 equiv.) was added dropwise to anhydrous methanol (42 mL) at 0 °C. The solution was stirred at 0 °C for 30 min and *L*-Proline (0.93 g, 8.3 mmol, 1.0 equiv.) was added. The reaction mixture was refluxed for 5 hours and TLC (CH₃Cl/MeOH, 9/1) indicated complete disappearance of *L*-Proline. The reaction mixture was evaporated under reduced pressure and a yellow oil was obtained.

Ph₂Si(Cl)(pro) was then prepared following a modified literature procedure.³⁷⁰ The obtained hydrochloride salt **30**, (1.62 g, 10.0 mmol, 1.2 equiv.) was dissolved in 11 mL of ether and Et₃N (2.79 mL, 20.0 mmol, 2.4 equiv.) was added in the solution to obtain the *L*-Proline methyl ester. 1.05 mL (5.0 mmol, 0.6 equiv.) of diphenyldichlorosilane and 4 mL of ether were placed in another Schlenk tube. The solution was cooled to -78 °C in a dry-ice/acetone bath and treated with the solution of *L*-Proline methyl ester over a 30 min period, causing formation of a voluminous precipitate. Filtration under a positive pressure of nitrogen with a filter-stick, washing the solid with ether, combination of the ether layers and drying the product under vacuum followed. The desired product was extracted with pentane (2 × 10 mL). A yellow oil was obtained in 43% yield.



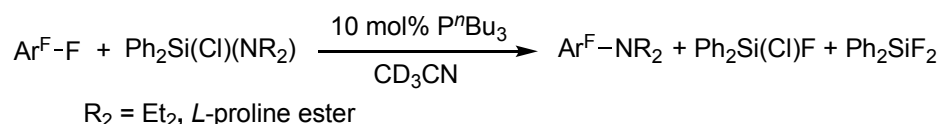
¹H NMR (500 MHz, DCM-*d*₂): δ 8.01 – 7.85 (m, 2H, Ph), 7.66 – 7.23 (m, 8H, Ph), 3.94 (dd, ³J_{HH} = 8.6 Hz, ³J_{HH} = 3.3 Hz, 1H, 4-CH), 3.47 (s, 3H, OCH₃), 2.25 – 2.01 (m, 2H, CH₂), 1.98 – 1.82 (m, 4H, CH₂).

²⁹Si NMR (C₆D₆, 119 MHz): δ -8.90 (s, 1Si).

¹³C{¹H} NMR (151 MHz, DCM-*d*₂): δ 175.6 (s, 1C, COOCH₃), 135.0 (s, 4C, Ph, CH), 130.7 (s, 4C, Ph, CH), 128.1 (s, 2C, Ph, CH), 60.6 (s, 1C, 4-CH), 51.4 (s, 1C, OCH₃), 47.6 (s, 1C, 1-CH), 31.7 (s, 1C, 2-CH), 25.9 (s, 1C, 3-CH).

MS-APCI: [C₁₈H₂₀NO₂Si]⁺ 310.126372 *m/z* (1.9 ppm deviation from theoretical mass); [C₁₈H₂₁ClNO₂Si]⁺ 346.102908 *m/z* (1.3 ppm deviation from theoretical mass).

5.4.10 Procedure for the catalytic aminodefluorination reaction



The Ar–F (0.40 mmol, 1.0 equiv.) and Ph₂Si(Cl)(NR₂) (0.44 mmol, 1.1 equiv.) were dissolved in 0.4 mL of CD₃CN and placed into a J. S. Young's NMR tube. PⁿBu₃ (10.0 μL, 0.04 mmol, 0.1 equiv.) was added and the system was heated at 60 °C for the synthesis of **24** and **25**, 60 °C for 4 days and 80 °C for the synthesis of **26** and **27**. The reaction mixture was analysed by quantitative ¹⁹F NMR with trifluorotoluene (25.1 μL, 0.20 mmol, 0.5 equiv.) used as an internal standard.

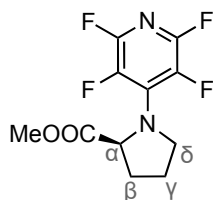


N,N-diethyl-2,3,5,6-tetrafluoropyridin-4-amine (24):²¹⁴ NMR yield of 75%.

¹H NMR (600 MHz, CD₃CN): δ 3.43 (qt, ³J_{HH} = 7.1 Hz, ⁵J_{HF} = 1.6 Hz, 4H, CH₂), 1.22 (t, ³J_{HH} = 7.1 Hz, 6H, CH₃).

¹⁹F NMR (565 MHz, CD₃CN): δ –95.9 to –96.8 (m, 2F, *ortho*-F), –156.3 to –157.6 (m, 2F, *meta*-F).

GC(EI)-MS [C₉H₁₀N₂F₄]⁺⁺ 222.07810 (2.85 ppm deviation from theoretical mass), [C₈H₇F₄N₂]⁺⁺ 207.05472, [C₇H₅F₄N₂]⁺⁺ 193.03912 *m/z*.



Methyl-2,3,5,6-tetrafluoropyrid-4-ylpyrrolidine-2-carboxylate (25): NMR yield of 88%.

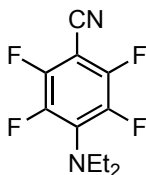
¹H NMR (500 MHz, CD₃CN): δ 4.83 (dq, *J* = 8.2, 3.5 Hz, 1H, CH_α), 3.92 (dt, *J* = 10.1, 6.7, 3.3 Hz, 1H, CH_δ), 3.88 – 3.84 (m, 1H, CH_δ), 3.73 (s, 3H, OCH₃), 2.32 (dq, *J* = 12.9, 7.6 Hz, 1H, CH_β), 2.06 (dq, *J* = 12.2, 6.1 Hz, 1H, CH_β), 1.95 (p, *J* = 6.8 Hz, 2H, CH_γ).

¹⁹F NMR (565 MHz, CD₃CN): δ –96.6 to –97.4 (m, 2F, *ortho*-F), –159.2 to –160.9 (m, 2F, *meta*-F).

¹³C{¹H} (151 MHz, CD₃CN): δ 62.9 (t, *J* = 5.4 Hz, CH), 52.2 (t, *J* = 6.6 Hz, CH₂), 52.1 (s, CH₃), 30.3 (bs, CH₂), 23.6 (t, *J* = 2.0 Hz, CH₂).

GC(EI)-MS [C₁₁H₁₀N₂O₂F₄]⁺ 278.06880 (5.41 ppm deviation from theoretical mass), [C₉H₇N₂F₄]⁺ 219.05493, [C₆HN₂F₄]⁺ 177.00778 *m/z*.

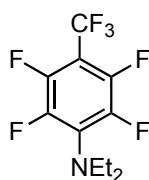
[α]_D²⁰ –65 (c 2.5, CH₂Cl₂).



4-(diethylamino)-2,3,5,6-tetrafluorobenzonitrile (26):²¹⁴ NMR yield of 82%.

¹H NMR (600 MHz, CD₃CN): δ 3.37 (qt, ³*J*_{HH} = 7.1 Hz, ⁵*J*_{HF} = 1.4 Hz, 4H, CH₂), 1.15 (t, ³*J*_{HH} = 7.1 Hz, 6H, CH₃).

¹⁹F NMR (565 MHz, CD₃CN): δ –136.9 to –138.7 (m, 2F, CF), –150.9 to –151.8 (m, 2F, CF).

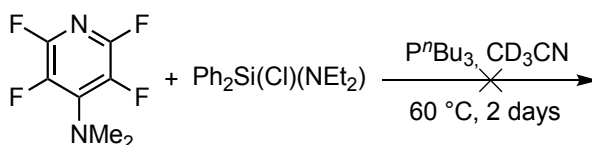


N,N-diethyl-2,3,5,6-tetrafluoro-4-(trifluoromethyl)aniline (27):²¹⁴ NMR yield of 50%.

¹H NMR (600 MHz, CD₃CN): δ 3.33 (qt, ³J_{HH} = 7.1 Hz, ⁵J_{HF} = 1.1 Hz, 4H, CH₂), 1.13 (t, ³J_{HH} = 7.1 Hz, 6H, CH₃).

¹⁹F NMR (565 MHz, CD₃CN): δ -56.0 (t, J = 21.1 Hz, CF₃), -144.8 to -146.1 (m, 2F, CF), -150.6 to -152.0 (m, 2F, CF).

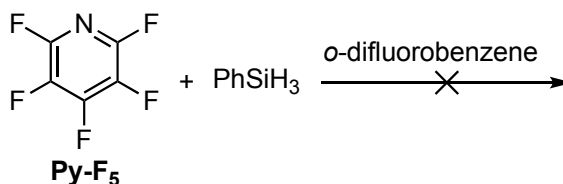
5.4.11 Reactivity test of 4-dimethylamino-tetrafluoropyridine and Ph₂Si(Cl)(NEt₂)



4-dimethylamino-tetrafluoropyridine (13.8 μL, 0.10 mmol, 1.0 equiv.) and PⁿBu₃ (25.0 μL, 0.10 mmol, 1.0 equiv.) were dissolved in 0.4 mL of CD₃CN and placed into a J. S. Young's NMR tube. The system was heated at 60 °C for two days and monitored by ¹⁹F and ³¹P NMR spectroscopy, which demonstrated that no reaction occurred.

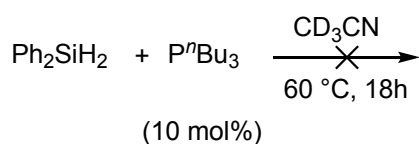
5.4.12 Mechanistic studies for the catalytic HDF reaction

5.4.12.1 Reactivity test of PhSiH₃ and pentafluoropyridine



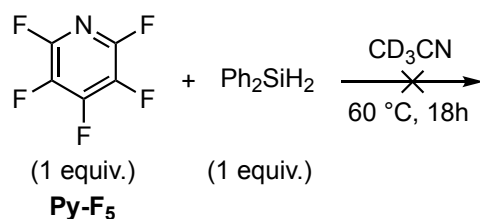
Pentafluoropyridine (43.9 μL, 0.40 mmol, 1.0 equiv.) and PhSiH₃ (49.2 μL, 0.40 mmol, 1.0 equiv.) were dissolved in 0.4 mL of *o*-difluorobenzene and placed into a J. S. Young's NMR tube. The mixture was heated at 60 °C for 18 hours and monitored by ¹⁹F NMR spectroscopy, which demonstrated that no reaction occurred.

5.4.12.2 Reactivity test of Ph₂SiH₂ and PⁿBu₃



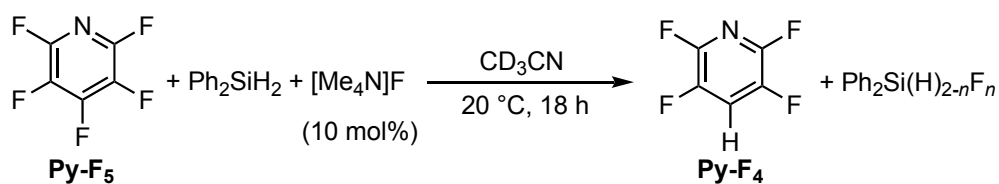
PⁿBu₃ (10.0 μL, 0.04 mmol, 0.1 equiv.) and Ph₂SiH₂ (43.9 μL, 0.40 mmol, 1.0 equiv.) were dissolved in 0.4 mL of CD₃CN and placed into a J. S. Young's NMR tube. The mixture was heated at 60 °C for 18 hours and monitored by ¹H and ³¹P NMR spectroscopy, which demonstrated that no reaction occurred.

5.4.12.3 Reactivity test of Ph₂SiH₂ and pentafluoropyridine



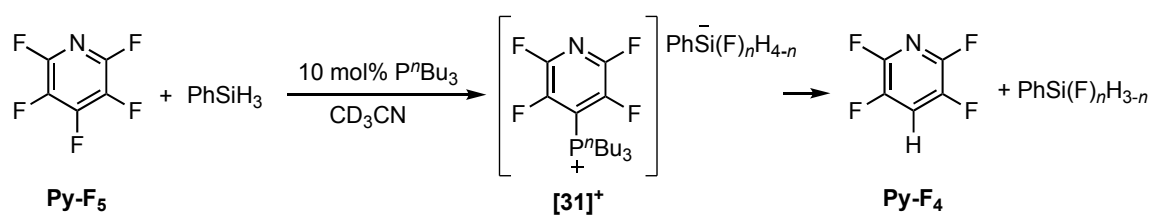
Pentafluoropyridine (43.9 μL, 0.40 mmol, 1.0 equiv.) and Ph₂SiH₂ (74.2 μL, 0.40 mmol, 1.0 equiv.) were dissolved in 0.4 mL of CD₃CN and placed into a J. S. Young's NMR tube. The mixture was heated at 60 °C for 18 hours and monitored by ¹H and ¹⁹F NMR spectroscopy, which demonstrated that no reaction occurred.

5.4.12.4 Reactivity test of Ph₂SiH₂ and pentafluoropyridine in the presence of [Me₄N]F



Pentafluoropyridine (43.9 μL, 0.40 mmol, 1.0 equiv.), Ph₂SiH₂ (74.2 μL, 0.40 mmol, 1.0 equiv.) and anhydrous Me₄NF (3.7 mg, 0.04 mmol, 0.1 equiv.) were dissolved in 0.4 mL of CD₃CN and placed into a J. S. Young's NMR tube. The mixture was kept at 20 °C for 18 hours and monitored by ¹H and ¹⁹F NMR spectroscopy. The yields are lower (19% after 20 minutes, 64% after 18 hours) than those of the reaction in the presence of the PⁿBu₃ (Table 4, entry 6, yield 93% after 20 minutes at 20 °C). Hence, direct hydrodefluorination of **Py-F₅** by catalytic hydrosilicate anions, formed *in situ* by reaction of **Py-F₅** with PⁿBu₃, is possible, but significantly slower than hydrodefluorination through a phosphine-mediated pathway.

5.4.12.5 Characterisation of phosphonium salt **[31][Ph₂Si(H)₃F]**



Pentafluoropyridine (43.9 μL , 0.40 mmol, 1.0 equiv.) and PhSiH_3 (49.3 μL , 0.40 mmol, 1.0 equiv.) were dissolved in 0.4 mL of the tested solvent and placed into a J. S. Young's NMR tube. $P^n\text{Bu}_3$ (10.0 μL , 0.04 mmol, 0.1 equiv.) was added and the progress of the reaction was monitored after 1 hour at 20 °C and 2 hours at 60 °C. The reaction mixture was analysed by ^1H , ^{31}P and quantitative ^{19}F NMR with trifluorotoluene (25.1 μL , 0.20 mmol, 0.5 equiv.) used as an internal standard.

The ^{31}P NMR spectrum showed the clean conversion of $P^n\text{Bu}_3$ into a new species **[31]⁺** after 1 hour at 20 °C.

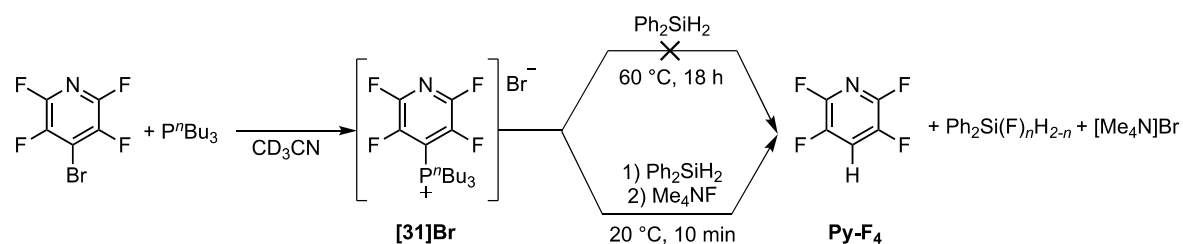
[31]⁺:

^1H NMR (600 MHz, CD_3CN): δ 2.68 (td, $J = 12.7, 8.4$ Hz, 6H, CH_2), 1.69 – 1.59 (m, 6H, CH_2), 1.54 (hept, $J = 7.1$ Hz, 6H, CH_2), 0.99 (t, $^3J_{\text{HH}} = 7.3$ Hz, 9H, CH_3).

$^{31}\text{P}\{^1\text{H}\}$ NMR (243 MHz, CD_3CN): δ 38.7 – 37.6 (m, 1P).

^{19}F NMR (565 MHz, CD_3CN): δ –87.7 to –88.8 (m, 2F, CF), –129.8 to –130.6 (m, 2F, CF).

5.4.12.6 Characterisation and reactivity of phosphonium salt [31]Br



4-bromo-2,3,5,6-tetrafluoropyridine (22.0 μL , 0.20 mmol, 1.0 equiv.) and P^nBu_3 (49.1 μL , 0.20 mmol, 1.0 equiv.) were dissolved in 0.4 mL of CD_3CN and placed into a J. S. Young's NMR tube. The mixture turned immediately brown and ^1H , ^{19}F and ^{31}P NMR analyses showed the formation of [31]Br. Heating the system at 40 $^\circ\text{C}$ for 18 hours did not make any change in the reaction mixture. Ph_2SiH_2 (37.1 μL , 0.20 mmol, 1.0 equiv.) was added and the system was heated at 40 $^\circ\text{C}$ for other 18 hours. ^1H , ^{19}F and ^{31}P NMR analyses demonstrated that no further reaction occurred. The addition of anhydrous $[\text{Me}_4\text{N}]\text{F}$ (20.2 mg, 0.20 mmol, 1.0 equiv.) induced the formation of a white solid corresponding to $[\text{Me}_4\text{N}]\text{Br}$, **Py-F₄**, fluorosilane $\text{Ph}_2\text{Si}(\text{H})_{2-n}\text{F}_n$ and some unreacted [31]Br.

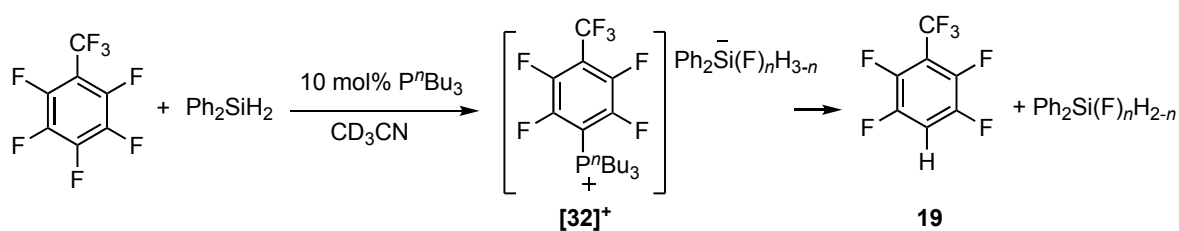
[31]Br:

^1H NMR (500 MHz, CD_3CN): δ 2.92 (td, $J = 13.0, 8.5$ Hz, 6H, CH_2), 1.66 (dq, $J = 16.5, 8.5$ Hz, 6H, CH_2), 1.52 (hept, $J = 7.3$ Hz, 6H, CH_2), 0.96 (t, $J = 7.3$ Hz, 9H, CH_3).

$^{31}\text{P}\{^1\text{H}\}$ NMR (202 MHz, CD_3CN): δ 38.9 – 36.9 (m, 1P).

^{19}F NMR (471 MHz, CD_3CN): δ -88.1 to -89.8 (m, 2F, *ortho*-F), -129.1 to -131.3 (m, 2F, *meta*-F).

5.4.12.7 Observation of the phosphonium salt [32][Ph₂Si(H)_{3-n}F_n]



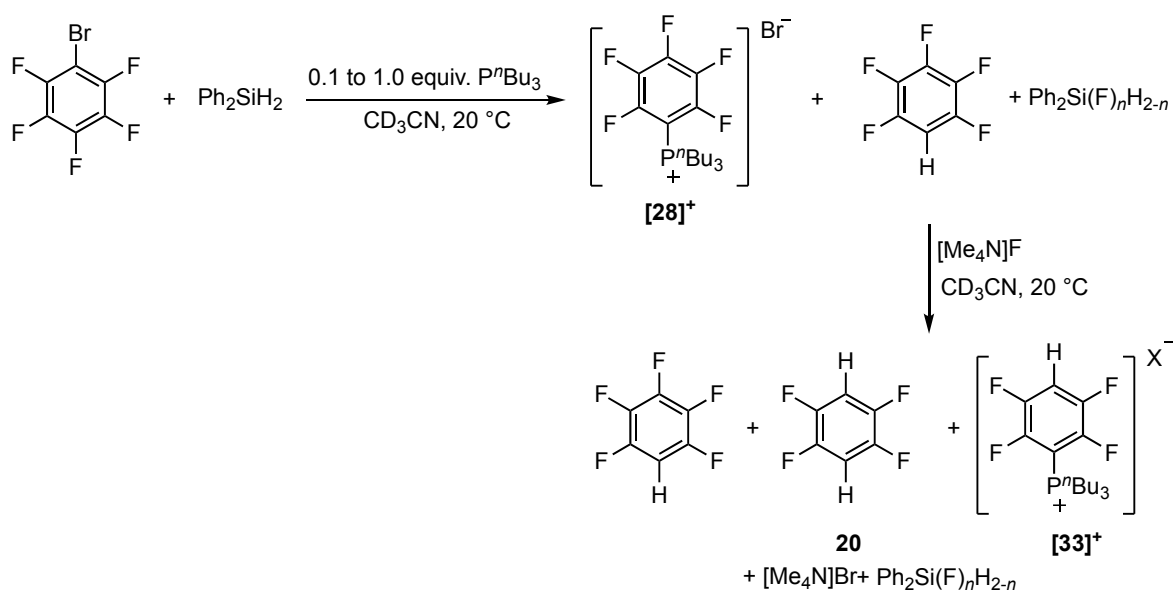
Perfluorotoluene (57.2 μ L, 0.40 mmol, 1.0 equiv.) and Ph₂SiH₂ (74.3 μ L, 0.40 mmol, 1.0 equiv.) were dissolved in 0.4 mL of CD₃CN and placed into a J. S. Young's NMR tube. PⁿBu₃ (10.0 μ L, 0.04 mmol, 0.1 equiv.) was added and the progress of reaction was monitored by ¹H, ³¹P and quantitative ¹⁹F NMR with trifluorotoluene (25.1 μ L, 0.20 mmol, 0.5 equiv.) used as an internal standard. After 10 minutes at 20 °C from the start of the reaction an apparent septet (coupling constant of *ca.* 4 Hz) was observed in the ³¹P NMR spectrum.

[32]⁺: ¹H signals of [32]⁺ were not identified due to their low intensity.

³¹P{¹H} NMR (202 MHz, CD₃CN): δ 37.1 – 38.9 ppm (m, 1P).

¹⁹F NMR (471 MHz, CD₃CN): δ -58.0 (t, ⁴J_{FF} = 18.1 Hz, 3F, CF₃), -125.7 to -127.9 (m, 2F, CF), -135.9 to -138.7 (m, 2F, CF).

5.4.12.8 Characterisation and reactivity of the phosphonium salt **[28]Br**



Bromopentafluorobenzene (51.1 μL , 0.40 mmol, 1.0 equiv.) and Ph_2SiH_2 (74.3 μL , 0.40 mmol, 1.0 equiv.) were dissolved in 0.4 mL of CD_3CN and placed into a J. S. Young's NMR tube. P^nBu_3 (10.0 μL , 0.04 mmol, 0.1 equiv.) was added and the reaction mixture was monitored by quantitative ^{19}F NMR with trifluorotoluene (25.1 μL , 0.20 mmol, 0.5 equiv.) used as an internal standard.

The formation of **[28]Br** (11% conversion) and pentafluorobenzene (3% conversion) was observed. More P^nBu_3 (90.2 μL , 0.36 mmol, 0.90 equiv.) was added in the mixture and the system was monitored over 18 hours at 20 $^\circ\text{C}$ by ^{31}P and ^{19}F NMR spectroscopy. The amount of **[28]Br** and pentafluorobenzene increased. The introduction of anhydrous $[\text{NMe}_4]\text{F}$ (37.1 mg, 0.40 mmol, 1.0 equiv.) in the mixture led to an increase in the amount of pentafluorobenzene, the formation of **20**, some **[33]⁺** and the precipitation of a white solid identified as $[\text{NMe}_4]\text{Br}$. The system was monitored over 18 hours at 20 $^\circ\text{C}$ by ^{31}P and ^{19}F NMR spectroscopy.

[28]Br:

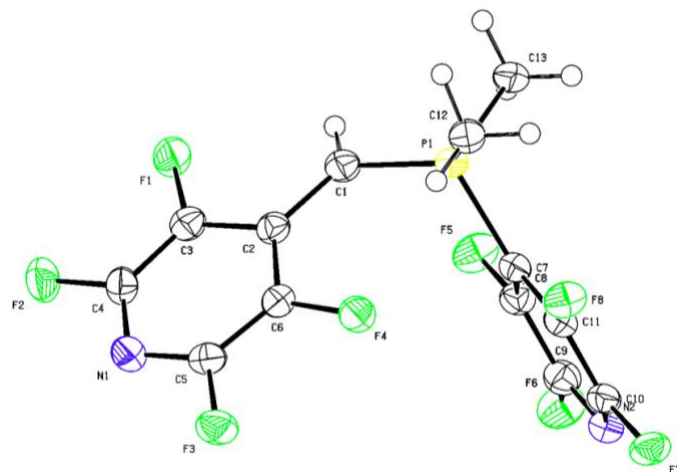
^1H NMR (500 MHz, CD_3CN): δ 2.93 (td, $J = 12.9, 8.6$ Hz, 6H, CH_2), 1.65 (dq, $J = 16.6, 8.6$ Hz, 6H, CH_2), 1.59 – 1.49 (m, 6H, CH_2), 0.95 (t, $^3J_{\text{HH}} = 7.4$ Hz, 9H, CH_3).

$^{31}\text{P}\{^1\text{H}\}$ NMR (202 MHz, CD_3CN): δ 36.9 – 36.1 (m, 1P).

^{19}F NMR (471 MHz, CD_3CN): δ -127.2 to -129.6 (m, 2F, CF), -142.3 to -144.6 (m, 1F, *para*-CF), -157.6 to -159.4 (m, 2F, CF).

5.5 Crystallographic data collection and structure determination

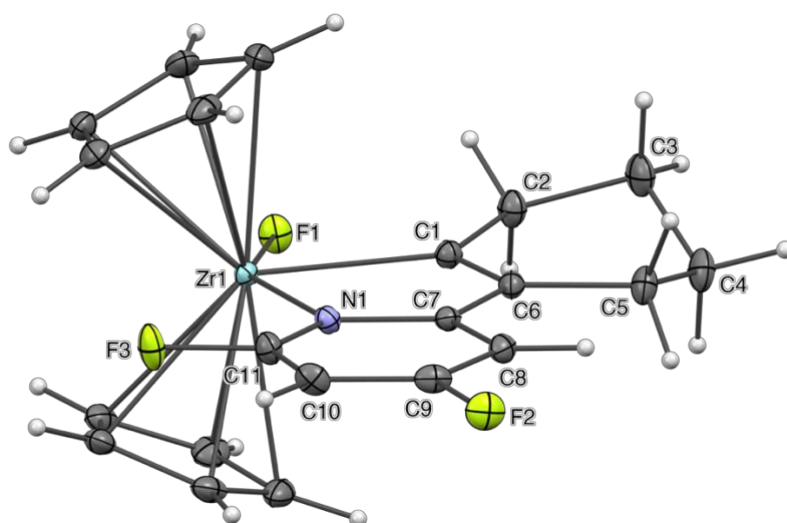
5.5.1 Molecular structure of 16



X-ray molecular structure of complex 16

Crystal data	
Chemical formula	C ₁₃ H ₇ F ₈ N ₂ P
<i>M_r</i>	374.18
Crystal system, space group	Monoclinic, <i>P</i> 2 ₁ / <i>c</i>
Temperature (K)	110
<i>a</i> , <i>b</i> , <i>c</i> (Å)	8.61890 (16), 9.85095 (18), 16.5708 (3)
β (°)	92.3006 (18)
<i>V</i> (Å ³)	1405.80 (5)
<i>Z</i>	4
Radiation type	Cu Kα
μ (mm ⁻¹)	2.67
Crystal size (mm)	0.20 × 0.14 × 0.09
Data collection	
Diffractometer	SuperNova
Absorption correction	Gaussian
<i>T_{min}</i> , <i>T_{max}</i>	0.649, 0.980
No. of measured, independent and observed [<i>I</i> > 2σ(<i>I</i>)] reflections	8545, 2504, 2316
<i>R_{int}</i>	0.034
(sin θ/λ) _{max} (Å ⁻¹)	0.597
Refinement	
<i>R</i> [<i>F</i> ² > 2σ(<i>F</i> ²)], <i>wR</i> (<i>F</i> ²), <i>S</i>	0.031, 0.086, 1.04
No. of reflection	2504
No. of parameters	245
H-atom treatment	All H-atom parameters refined
Δρ _{max} , Δρ _{min} (e Å ⁻³)	0.44, -0.31

5.5.2 Molecular structure of 11



X-ray molecular structure of complex 11

Crystal data	
Chemical formula	C ₂₁ H ₂₀ F ₃ NZr
<i>M_r</i>	434.60
Crystal system, space group	Monoclinic, <i>P2₁/n</i>
Temperature (K)	110
<i>a</i> , <i>b</i> , <i>c</i> (Å)	8.1766 (1), 15.5546 (2), 14.6671 (2)
β (°)	99.429 (1)
<i>V</i> (Å ³)	1840.21 (4)
<i>Z</i>	4
Radiation type	Cu Kα
μ (mm ⁻¹)	5.19
Crystal size (mm)	0.25 × 0.1 × 0.09
Data collection	
Diffractometer	SuperNova
Absorption correction	Gaussian
<i>T_{min}</i> , <i>T_{max}</i>	0.760, 1.000
No. of measured, independent and observed [<i>I</i> > 2σ(<i>I</i>)] reflections	12546, 3722, 3429
<i>R_{int}</i>	0.038
(sin θ/λ) _{max} (Å ⁻¹)	0.632
Refinement	
<i>R</i> [<i>F</i> ² > 2σ(<i>F</i> ²)], <i>wR</i> (<i>F</i> ²), <i>S</i>	0.025, 0.062, 1.10
No. of reflection	3722
No. of parameters	235
H-atom treatment	All H-atom parameters refined
Δρ _{max} , Δρ _{min} (e Å ⁻³)	0.32, -0.47

5.6 DFT Calculations

DFT calculations were performed by Dr. J. M. Slattery and Prof. J. M. Lynam. Initial optimisations were performed at the (RI-)BP86/SV(P) level, followed by frequency calculations at the same level. Transition states were located by initially performing a constrained minimisation (by freezing internal coordinates that change most during the reaction) of a structure close to the anticipated transition state. This was followed by a frequency calculation to identify the transition vector to follow during a subsequent transition-state optimisation. A final frequency calculation was then performed on the optimised transition-state structure. All minima were confirmed as such by the absence of imaginary frequencies and all transition states were identified by the presence of only one imaginary frequency.

Single-point calculations on the (RI-)BP86/SV(P) optimised geometries were performed using the hybrid PBE0 functional and the flexible def2-TZVPP basis set. The (RI-)PBE0/def2-TZVPP SCF energies were corrected for their zero-point energies, thermal energies and entropies (obtained from the (RI-)BP86/SV(P)-level frequency calculations). No symmetry constraints were applied during optimisations. All calculations were performed using the TURBOMOLE V6.40 package using the resolution of identity (RI) approximation.^{372–382} Solvation effects were modelled using the COSMO module of TURBOMOLE.³⁸³ The dielectric constant used was for CH₃CN ($\epsilon = 35.9$ at 25 °C).³⁸⁴ Both enthalpies and Gibbs energies at 298.15 K are shown on the PES'. Gibbs energy changes are discussed in chapter 4.3.4. The difficulty in assessing entropy changes in solution from gas-phase calculations is acknowledged.^{385–387} Single-point DFT-D3 corrections (on the (RI-)BP86/SV(P) geometries) have been applied at the PBE0-D3 level using Grimme's DFT-D3 V3.0 Rev 2 program (with BJ-damping)^{388,389} and data presented in chapter 4.3.4 include this correction. Both DFT-D3 and DFT data are presented below. Structures were visualised and modified using Facio,³⁹⁰ Jmol,³⁹¹ and gOpenMol.

5.7 Tabulated energies for mechanism presented in scheme 4

Table 5: Energies and corrections at the PBE0/def2-TZVPP//BP86/SV(P) level. As described above, vibrational frequencies and derived corrections were at the BP86/SV(P) level and electronic energies, both in the gas phase and COSMO solvation, in addition to DFT-D3 corrections were at the PBE0/def2-TZVPP level.

	SCF (a.u.)	DFT-D3 corr. (a.u.)	COSMO (MeCN) (a.u.)	ZPE (a.u.)	Chem. Pot. (kJ/mol)	Energy (kJ/mol)	Entropy (kJ/K/mol)	Entropy at 1 mol/dm ³ (kJ/K/mol)
Ph ₂ SiH ₂	-753.483828	-0.0272	-753.492017	0.193283	398.96	538.61	0.4767	0.4500
Ph ₂ SiHF	-852.752370	-0.0276	-852.762224	0.188550	386.01	528.26	0.4854	0.4587
[Ph ₂ SiH ₂ F] ⁻	-853.358399	-0.0279	-853.443879	0.194003	401.36	543.07	0.4836	0.4569
1	-744.021127	-0.0094	-744.026087	0.047281	34.67	146.81	0.3844	0.3577
M1	-460.870945	-0.0087	-460.876044	0.108851	208.40	303.74	0.3281	0.3014
TS₁₂	-1204.869012	-0.0257	-1204.889163	0.156088	292.08	453.44	0.5495	0.5228
M2	-1204.924023	-0.0264	-1204.934966	0.158689	302.77	459.48	0.5339	0.5072
M3	-1204.927511	-0.0265	-1204.939349	0.159287	304.61	460.72	0.5319	0.5052
M4	-1104.895087	-0.0247	-1104.978201	0.157190	304.30	451.77	0.5029	0.4762
M5	-1105.666078	-0.0259	-1105.676025	0.164088	314.91	472.54	0.5370	0.5103
M6	-1105.658139	-0.0258	-1105.665154	0.163477	316.35	470.38	0.5250	0.4983
TS₆₁	-1105.624638	-0.0265	-1105.642515	0.160201	307.65	461.22	0.5234	0.4967
2	-644.842167	-0.0091	-644.848657	0.055077	58.55	164.65	0.3642	0.3375

Table 6 Relative energies of different states in the gas phase, with COSMO solvation in MeCN and with both COSMO solvation and DFT-D3 corrections.

	Electronic E gas (kJ/mol)	Electronic E+D gas (kJ/mol)	Electronic E MeCN (kJ/mol)	Electronic E+D MeCN (kJ/mol)	Gas Phase 298.15 K			COSMO MeCN 298.15 K			DFT-D3 COSMO MeCN 298.15 K		
					Rel H (kJ/mol)	Rel S (J/K/mol)	Rel G (kJ/mol)	Rel H (kJ/mol)	Rel S (J/K/mol)	Rel G (kJ/mol)	Rel H (kJ/mol)	Rel S (J/K/mol)	Rel G (kJ/mol)
Ph ₂ SiH ₂													
Ph ₂ SiHF													
[Ph ₂ SiH ₂ F] ⁻													
1													
M1	0	0	0	0	0	0	0	0	0	0	0	0	0
TS₁₂	61	41	34	14	61	-163	110	34	-136	75	14	-136	55
M2	-84	-106	-86	-108	-77	-179	-24	-80	-152	-34	-102	-152	-56
M3	-93	-115	-98	-120	-85	-181	-32	-90	-154	-44	-112	-154	-66
M4	321	302	-73	-93	325	-203	385	-70	-176	-18	-89	-176	-37
M5	-112	-133	-116	-137	-103	-167	-53	-107	-140	-65	-128	-140	-86
M6	-91	-112	-87	-108	-84	-179	-31	-80	-152	-35	-101	-152	-56
TS₆₁	-3	-26	-28	-51	-5	-180	49	-30	-154	16	-53	-154	-7
2	-235	-236	-244	-244	-228	-12	-224	-236	-12	-233	-237	-12	-233

5.8 3-component alternative mechanism for Si-H activation (c.f. Piers' mechanism)

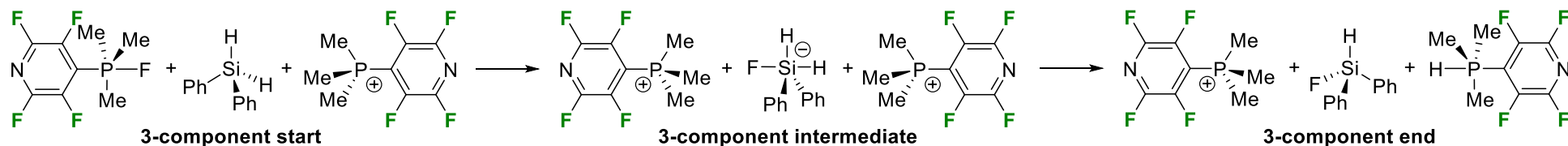


Table 7 Energies and corrections at the PBE0/def2-TZVPP//BP86/SV(P) level. As described above, vibrational frequencies and derived corrections were at the BP86/SV(P) level and electronic energies, both in the gas phase and COSMO solvation, in addition to DFT-D3 corrections were at the PBE0/def2-TZVPP level.

	SCF (a.u.)	DFT-D3 corr. (a.u.)	COSMO (MeCN) (a.u.)	ZPE (a.u.)	Chem. Pot. (kJ/mol)	Energy (kJ/mol)	Entropy (kJ/K/mol)	ln q(vib)	HOMO (eV)	LUMO (eV)	Entropy at 1 mol/dm ³ (kJ/K/mol)
Start	-3063.326992	-0.096063	-3063.403577	0.511531	1102.95	1467.39	1.2307	58.08	-9.1374	-5.6136	1.2040
TS1	-3063.316750	-0.098043	-3063.390751	0.510491	1105.55	1462.63	1.2060	55.99	-9.2997	-5.4042	1.1793
Intermediate	-3063.327427	-0.096175	-3063.404410	0.510482	1114.78	1460.32	1.1672	52.20	-8.5332	-5.0481	1.1405
TS2	-3063.323394	-0.096075	-3063.399502	0.510378	1106.89	1461.48	1.1976	55.27	-8.6778	-5.0141	1.1709
End	-3063.330657	-0.095090	-3063.409383	0.511033	1095.48	1466.34	1.2522	60.52	-8.7458	-5.6035	1.2255

Table 8 Relative energies of different states in the gas phase, with COSMO solvation in MeCN and with both COSMO solvation and DFT-D3 corrections.

	Electronic E gas (kJ/mol)	Electronic E+D gas (kJ/mol)	Electronic E MeCN (kJ/mol)	Electronic E+D MeCN (kJ/mol)	Gas Phase 298.15 K			COSMO MeCN 298.15 K			DFT-D3 COSMO MeCN 298.15 K		
					Rel H (kJ/mol)	Rel S (J/K/mol)	Rel G (kJ/mol)	Rel H (kJ/mol)	Rel S (J/K/mol)	Rel G (kJ/mol)	Rel H (kJ/mol)	Rel S (J/K/mol)	Rel G (kJ/mol)
Start	0	0	0	0	0	0	0	0	0	0	0	0	0
TS1	27	22	34	28	22	-25	29	29	-25	36	24	-25	31
Intermediate	-1	-1	-2	-2	-8	-63	11	-9	-63	10	-10	-63	9
TS2	9	9	11	11	4	-33	13	5	-33	15	5	-33	15
End	-10	-7	-15	-13	-11	22	-17	-16	22	-23	-14	22	-20

List of abbreviations

DIBAL	Diisobutylaluminium hydride
4-DPA-IPN	2,4,5,6-tetrakis(diphenylamino)isophthalonitrile
4-HTP	4-hydroxythiophenol
BDE	Bond dissociation energy
btmsa	Bis(trimethylsilyl)acetylene
CAAC	Cyclic alkyl amino carbene
CF ₃ Form	N,N'-bis(2-trifluoromethylphenyl) formamidine
cod	1,5-cyclooctadiene
Cy	Cyclohexyl
DBU	1,8-diazabicyclo(5.4.0)undec-7-ene
DFT	Density functional theory
DIPEA	N,N-diisopropylethylenamine
DMF	Dimethylformamide
EA	Electron affinity
ebthi	1,2-ethylene-1,1'-bis(η^5 -tetrahydroindenyl)
EDG	Electron-donating group
ETM	Early transition metal
EWG	Electron withdrawing group
FIA	Fluoride ion affinity
FLP	Frustrated Lewis pair
HDF	Hydrodefluorination
HFC	Hydrofluorocarbons
HFO	Hydrofluoroolefins
HIA	Hydride ion affinity
IE ₁	First ionisation energy
ⁱ Pr ₂ Im	1,3-di(isopropyl)imidazole-2-ylidene
LA	Lewis acid
LDA	Lithium diisopropylamide
LG	Leaving group
LM	Ligand metathesis
LTM	Late transition metals

NHC	N-heterocyclic carbene
o-DFB	<i>Ortho</i> -difluorobenzene
OA	Oxidative addition
PES	Potential energy surface
Pn	Pnictogens
PNP	Bis(2-(diisopropylphosphino)-4-methylphenyl)amide
ppy	2-phenylpyridine
pro	L-proline methyl ester
py	Pyridine
Py-F₂	2,6-difluoropyridine
Py-F₃	2,4,6-trifluoropyridine
Py-F₄	2,3,5,6-tetrafluoropyridine
Py-F₅	Pentafluoropyridine
RE	Reductive elimination
r _{vdW}	Van der Waals atomic radius
SEM	Trimethylsilylethoxymethyl
SET	Single electron transfer
S _N Ar	Nucleophilic aromatic substitution
TBAT	Tetrabutylammonium difluorotriphenylsilicate
TCICA	Trichloroisocyanuric acid
TDI	Turnover-determining intermediate
TDTS	Turnover-determining transition state
TM	Transition metal
TMG	1,1,3,3-tetramethylguanidine
TON	Turnover number
Tp*	Hydrotris(3,5-dimethylpyrazolyl)borate
TS	Transition state

References

1. Pauling, L. *J. Am. Chem. Soc.* **1932**, *54*, 3570–3582.
2. O'Hagan, D. *Chem. Soc. Rev.* **2008**, *37*, 308–319.
3. Smart, B. E. *The Chemistry of Functional Groups, Supplement D*; Wiley, 1983.
4. Kirsch, P. *Modern Fluoroorganic Chemistry*; Wiley, 2004.
5. Liang, T.; Neumann, C. N.; Ritter, T. *Angew. Chem. Int. Ed.* **2013**, *52*, 8214–8264.
6. Lück, E.; Lipinski, G. von R. *Ullmann's Encycl. Ind. Chem.*; Wiley, 2012; Vol. 10.
7. O'Hagan, D.; Schaffrath, C.; Cobb, S. L.; Hamilton, J. T. G.; Murphy, C. D. *Nature* **2002**, *416*:6878, 279–279.
8. Villalba, G.; Ayres, R. U.; Schroder, H. *J. Ind. Ecol.* **2007**, *11*, 85–101.
9. Inoue, M.; Sumii, Y.; Shibata, N. *ACS Omega* **2020**, *5*, 10633–10640.
10. Chen, K.; Chen, X. *Semin. Oncol.* **2011**, *38*, 70–86.
11. Tsai, W. T. *Chemosphere* **2005**, *61*, 1539–1547.
12. Zaelke, D.; Borgford-Parnell, N. *J. Environ. Stud. Sci.* **2015**, *5*, 169–175.
13. Zhou, J.; Jin, C.; Su, W. *Org. Process Res. Dev.* **2014**, *18*, 928–933.
14. Milner, L. M.; Pridmore, N. E.; Whitwood, A. C.; Lynam, J. M.; Slattery, J. M. *J. Am. Chem. Soc.* **2015**, *137*, 10753–10759.
15. Hooker, L. V.; Bandar, J. S. *Angew. Chem. Int. Ed.* **2023**, *62*, e20230888
16. Perutz, R. N.; Braun, T. In *Comprehensive Organometallic Chemistry III*; Elsevier Ltd, 2007; pp. 725–758.
17. Ahrens, T.; Kohlmann, J.; Ahrens, M.; Braun, T. *Chem. Rev.* **2015**, *115*, 931–972.
18. Campbell, M. G.; Ritter, T. *Chem. Rev.* **2015**, *115*, 612–633.
19. Hollingworth, C.; Gouverneur, V. *Chem. Commun.* **2012**, *48*, 2929–2942.
20. Kuehnel, M. F.; Lentz, D.; Braun, T.; Lentz, D.; Braun, T.; Kuehnel, M. F. *Angew. Chem. Int. Ed.* **2013**, *52*, 3328–3348.
21. Meier, G.; Braun, T. *Angew. Chem. Int. Ed.* **2009**, *48*, 1546–1548.
22. Douvris, C.; Ozerov, O. V. *Science* **2008**, *321*, 1188–1190.
23. Urbano, F. J.; Marinas, J. M. *J. Mol. Catal. A Chem.* **2001**, *173*, 329–345.
24. Mazurek, U.; Schwarz, H. *Chem. Commun.* **2003**, *3*, 1321–1326.
25. Natarajan, R.; Azerad, R.; Badet, B.; Copin, E. *J. Fluor. Chem.* **2005**, *126*, 424–435.
26. Klahn, M.; Rosenthal, U. *Organometallics* **2012**, *31*, 1235–1244.
27. Kuehnel, M. F.; Holstein, P.; Kliche, M.; Krüger, J.; Matthies, S.; Nitsch, D.; Schutt, J.; Sparenberg, M.; Lentz, D. *Chem. Eur. J.* **2012**, *18*, 10701–10714.

28. Edelbach, B. L.; Rahman, A. K. F.; Lachicotte, R. J.; Jones, W. D. *Organometallics* **1999**, *18*, 3170–3177.
29. Kraft, B. M.; Lachicotte, R. J.; Jones, W. D. *J. Am. Chem. Soc.* **2001**, *123*, 10973–10979.
30. Kraft, B. M.; Jones, W. D. *J. Organomet. Chem.* **2002**, *658*, 132–140.
31. Rieth, R. D.; Brennessel, W. W.; Jones, W. D. *Eur. J. Inorg. Chem.* **2007**, 2839–2847.
32. Jäger-Fiedler, U.; Klahn, M.; Arndt, P.; Baumann, W.; Spannenberg, A.; Burlakov, V. V.; Rosenthal, U. *J. Mol. Catal. A Chem.* **2007**, *261*, 184–189.
33. Dunlop, D.; Pinkas, J.; Horáček, M.; Žilková, N.; Lamač, M. *Dalton Trans.* **2020**, *49*, 2771–2775.
34. Gianetti, T. L.; Bergman, R. G.; Arnold, J. *Chem. Sci.* **2014**, *5*, 2517–2524.
35. Guo, H.; Kong, F.; Kanno, K. I.; He, J.; Nakajima, K.; Takahashi, T. *Organometallics* **2006**, *25*, 2045–2048.
36. Kiplinger, J. L.; Richmond, T. G. *J. Am. Chem. Soc.* **1996**, *118*, 1805–1806.
37. Kraft, B. M.; Lachicotte, R. J.; Jones, W. D. *Organometallics* **2002**, *21*, 727–731.
38. Fujiwara, M.; Ichikawa, J.; Okauchi, T.; Minami, T. *Tetrahedron Lett.* **1999**, *40*, 7261–7265.
39. Janjetovic, M.; Träff, A. M.; Ankner, T.; Wettergren, J.; Hilmersson, G. *Chem. Commun.* **2013**, *49*, 1826–1828.
40. Stahl, T.; Klare, H. F. T.; Oestreich, M. *ACS Catal.* **2013**, *3*, 1578–1587.
41. Chen, W.; Bakewell, C.; Crimmin, M. R. *Synthesis (Stuttg.)* **2017**, *49*, 810–821.
42. Kira, M.; Becerra, R.; Walsh, R.; Trans, D.; West, R.; Percival, P. W.; Junold, K.; Burschka, C.; Bertermann, R.; Tacke, R.; Klare, H. F. T.; Oestreich, M. *Dalton Trans.* **2010**, *39*, 9176–9184.
43. Weaver, J.; Senaweera, S. *Tetrahedron* **2014**, *70*, 7413–7428.
44. Amii, H.; Uneyama, K. *Chem. Rev.* **2009**, *109*, 2119–2183.
45. Kiplinger, J. L.; Richmond, T. G.; Osterberg, C. E. *Chem. Rev.* **1994**, *94*, 373–431.
46. Steffen, A.; Sladek, M. I.; Braun, T.; Neumann, B.; Stammler, H.-G. *Organometallics* **2005**, *24*, 4057–4064.
47. Breyer, D.; Berger, J.; Braun, T.; Mebs, S. *J. Fluor. Chem.* **2012**, *143*, 263–271.
48. Braun, T.; Izundu, J.; Steffen, A.; Neumann, B.; Stammler, H.-G. *Dalton Trans.* **2006**, 5118–5123.
49. Braun, T.; Parsons, S.; Perutz, R. N.; Voith, M. *Organometallics* **1999**, *18*, 1710–1716.
50. Cui, B.; Jia, S.; Tokunaga, E.; Shibata, N. *Nat. Commun.* **2018**, *9*, 1–8.
51. Teltewskoi, M.; Panetier, J. A.; Macgregor, S. A.; Braun, T. *Angew. Chem. Int. Ed.* **2010**, *49*, 3947–3951.

52. Lindup, R. J.; Marder, T. B.; Perutz, R. N.; Whitwood, A. C. *Chem. Commun.* **2007**, 3664–3666.
53. Sun, Y.; Sun, H.; Jia, J.; Du, A.; Li, X. *Organometallics* **2014**, *33*, 1079–1081.
54. Lu, W.; Gao, J.; Yang, J. K.; Liu, L.; Zhao, Y.; Wu, H. C. *Chem. Sci.* **2014**, *5*, 1934–1939.
55. Cornago, P.; Escolástico, C.; Santa María, M. D.; Claramunt, R. M.; Fernández-Castaño, C.; Foces-Foces, C.; Fayet, J. P.; Elguero, J. *Tetrahedron* **1996**, *52*, 11075–11094.
56. Zhivetyeva, S. I.; Selivanova, G. A.; Goryunov, L. I.; Bagryanskaya, I. Y.; Shteingarts, V. D. *J. Fluor. Chem.* **2015**, *180*, 21–32.
57. Birchall, J. M.; Haszeldine, R. N. *J. Chem. Soc.* **1959**, 13–17.
58. Fu, L.; Chen, Q.; Nishihara, Y. *Chem. Rec.* **2021**, *21*, 3394–3410.
59. Liu, C.; Zhang, B. *Chem. Rec.* **2016**, *16*, 667–687.
60. Ma, R.; Hu, H.; Li, X.; Mao, G.; Song, Y.; Xin, S. *Catalysts* **2022**, *12*, 1665.
61. Sun, Y.; Sun, H.; Jia, J.; Du, A.; Li, X. *Organometallics* **2014**, *33*, 1079–1081.
62. Matsubara, K.; Ishibashi, T.; Koga, Y. *Org. Lett.* **2009**, *11*, 1765–1768.
63. Lu, F.; Sun, H.; Du, A.; Feng, L.; Li, X. *Org. Lett.* **2014**, *16*, 772–775.
64. Xiong, Y.; Wu, J.; Xiao, S.; Xiao, J.; Cao, S. *J. Org. Chem.* **2013**, *78*, 4599–4603.
65. Hatakeyama, T.; Ito, S.; Nakamura, M.; Nakamura, E. *J. Am. Chem. Soc.* **2005**, *127*, 14192–14193.
66. Birchall, J. M.; Haszeldine, R. N. *J. Chem. Soc.* **1961**, 3719–3727.
67. Birchall, J. M.; Clarke, T.; Haszeldine, R. N. *J. Chem. Soc.* **1962**, *73*, 4977–4986.
68. Alsop, D. J.; Burdon, J.; Tatlow, J. C. *J. Chem. Soc.* **1962**, 183, 1801–1805.
69. Coe, P. L.; Oldfield, D.; Tatlow, J. C. *J. Fluor. Chem.* **1985**, *29*, 341–347.
70. Chambers, R. D.; Lomas, D.; Musgrave, W. K. R. *J. Chem. Soc. C: Org.* **1968**, 625–629.
71. Banks, B. R. E.; Haszeldine, R. N.; Young, M.; Banks, R. E.; Field, D. S.; Burgess, J. E.; Cheng, W. M.; R E Banks, R. N.; Latham, J. T. V. *J. Chem. Soc. C: Org.* **1967**, 2089–2091.
72. Schlosser, M.; Guio, L.; Leroux, F. *J. Am. Chem. Soc.* **2001**, *123*, 3822–3823.
73. Harper, R. J.; Soloski, E. J.; Tamborski, C. *J. Org. Chem.* **1964**, *29*, 2385–2389.
74. Dua, S. S.; Howells, R. D.; Gilman, H. *J. Fluor. Chem.* **1974**, *4*, 381–386.
75. Respass, W. L.; Tamborski, C. *J. Organomet. Chem.* **1970**, *22*, 251–263.
76. Lu, F.; Sun, H.; Du, A.; Feng, L.; Li, X. *Org. Lett.* **2014**, *16*, 772–775.
77. Davin, L.; Mcllellan, R.; Kennedy, A. R.; Hevia, E. *Chem. Commun.* **2017**, *53*, 11650.
78. Judge, N. R.; Logallo, A.; Hevia, E. *Chem. Sci.* **2023**, *14*, 11617–11628.
79. Maji, J.; Murarka, M. S.; Studer, S.; Leadbeater, A.; Marco, N. E.; Tominack, M. *Org. Lett.* **2013**, *15*, 3114–3117.

80. Ji, X.; Huang, T.; Wu, W.; Liang, F.; Cao, S. *Org. Lett.* **2015**, *17*, 5096–5099.
81. Liu, C.; Zhao, H.; Zhao, H.; Wang, Z.; Zhang, B. *RSC Adv.* **2015**, *5*, 31993–31997.
82. Schaub, T.; Backes, M.; Radius, U. *J. Am. Chem. Soc.* **2006**, *128*, 15964–15965.
83. Schaub, T.; Fischer, P.; Steffen, A.; Braun, T.; Radius, U.; Mix, A. *J. Am. Chem. Soc.* **2008**, *130*, 9304–9317.
84. Ohashi, M.; Saijo, H.; Shibata, M.; Ogoshi, S. *Eur. J. Org. Chem.* **2013**, 443–447.
85. Saijo, H.; Sakaguchi, H.; Ohashi, M.; Ogoshi, S. *Organometallics* **2014**, *33*, 3669–3672.
86. Kuntze-Fechner, M. W.; Kerpen, C.; Schmidt, D.; Häring, M.; Radius, U. *Eur. J. Inorg. Chem.* **2019**, *2019*, 1767–1775.
87. Nakamura, Y.; Yoshikai, N.; Ilies, L.; Nakamura, E. *Org. Lett.* **2012**, *14*, 3316–3319.
88. Ackermann, L.; Wechsler, C.; Kapdi, A. R.; Althammer, A. *Synlett* **2010**, *2010*, 294–298.
89. Jin, Z.; Li, Y. J.; Ma, Y. Q.; Qiu, L. L.; Fang, J. X. *Chem. Eur. J.* **2012**, *18*, 446–450.
90. Saeki, T.; Takashima, Y.; Tamao, K. *Synlett* **2005**, *2005*, 1771–1774.
91. Volker, P. W. D.; Herrmann, W. A. *Angew. Chem. Int. Ed.* **2001**, *40*, 3387–3389.
92. Ohashi, M.; Doi, R.; Ogoshi, S. *Chem. Eur. J.* **2014**, *20*, 2040–2048.
93. He, J.; Yang, K.; Zhao, J.; Cao, S. *Org. Lett.* **2019**, *21*, 9714–9718.
94. Singh, A.; Kubik, J. J.; Weaver, J. D. *Chem. Sci.* **2015**, *6*, 7206–7212.
95. Crespo, M.; Martinez, M.; De Pablo, E. *J. Chem. Soc., Dalton Trans.* **1997**, *1*, 1231–1235.
96. Crespo, M.; Martinez, M.; Sales, J. J. *J. Chem. Soc., Chem. Commun.* **1992**, 822–823.
97. Wang, T.; Love, J. A. *Organometallics* **2008**, *27*, 3290–3296.
98. Weaver, J.; Senaweera, S. *Tetrahedron* **2014**, *70(41)*, 7413–7428.
99. Cronin, L.; Higgitt, C. L.; Karch, R.; Perutz, R. N. *Organometallics* **1997**, *16(22)*, 4920–4928.
100. Nova, A.; Reinhold, M.; Perutz, R. N.; MacGregor, S. A.; McGrady, J. E. *Organometallics* **2010**, *29*, 1824–1831.
101. Braun, T.; Parsons, S.; Perutz, R. N.; Voith, M. *Organometallics* **1999**, *18*, 1710–1716.
102. Braun, T.; Perutz, R. N. *Chem. Commun.* **2002**, *2*, 2749–2757.
103. Braun, T.; Perutz, R. N.; Sladek, M. I. *Chem. Commun.* **2001**, *1(21)*, 2254–2255.
104. Breyer, D.; Berger, J.; Braun, T.; Mebs, S. *J. Fluor. Chem.* **2012**, *143*, 263–271.
105. Raza, A. L.; Panetier, J. A.; Teltewskoi, M.; Macgregor, S. A.; Braun, T. *Organometallics* **2013**, *32*, 3795–3807.
106. Noveski, D.; Braun, T.; Neumann, B.; Stammli, A.; Stammli, H. G. *Dalton Trans.*

- 2004**, 4106–4119.
107. Breyer, D.; Braun, T.; Kläring, P. *Organometallics* **2012**, *31*, 1417–1424.
 108. Braun, T.; Izundu, J.; Steffen, A.; Neumann, B.; Stammler, H.-G. *Dalton Trans.* **2006**, 5118–5123.
 109. Jasim, N. A.; Perutz, R. N.; Whitwood, A. C.; Braun, T.; Izundu, J.; Neumann, B.; Rothfeld, S.; Stammler, H. G. *Organometallics* **2004**, *23*, 6140–6149.
 110. Weydert, M.; Andersen, R. A.; Bergman, R. G. *J. Am. Chem. Soc.* **2002**, *115*, 8837–8838.
 111. Träff, A. M.; Janjetovic, M.; Ta, L.; Hilmersson, G. *Angew. Chem. Int. Ed.* **2013**, *52*, 12073–12076.
 112. Janjetovic, M.; Träff, A. M.; Hilmersson, G. *Chem. Eur. J.* **2015**, *21*, 3772–3777.
 113. Deacon, G. B.; Junk, P. C.; Werner, D. *Eur. J. Inorg. Chem.* **2015**, *2015*, 1484–1489.
 114. Clark, C. L.; Lockhart, J. J.; Fanwick, P. E.; Bart, S. C. *Chem. Commun.* **2015**, *51*, 14084–14087.
 115. Guo, H.; Kong, F.; Kanno, K. I.; He, J.; Nakajima, K.; Takahashi, T. *Organometallics* **2006**, *25*, 2045–2048.
 116. Gianetti, T. L.; Bergman, R. G.; Arnold, J. *J. Am. Chem. Soc.* **2013**, *135*, 8145–8148.
 117. Fuchibe, K.; Akiyama, T. *J. Am. Chem. Soc.* **2006**, *128*, 1434–1435.
 118. Fuchibe, K.; Kaneko, T.; Mori, K.; Akiyama, T. *Angew. Chem. Int. Ed.* **2009**, *48*, 8070–8073.
 119. Fuchibe, K.; Atobe, K.; Fujita, Y.; Mori, K.; Akiyama, T. *Chem. Lett.* **2010**, *39*, 867–869.
 120. Saito, K.; Umi, T.; Yamada, T.; Suga, T.; Akiyama, T. *Org. Biomol. Chem.* **2017**, *15*, 1767–1770.
 121. Nguyen, T. T.; Bertke, J. A.; Gray, D. L.; Hull, K. L. *Organometallics* **2015**, *34*, 4190–4193.
 122. Santamaría, C.; Beckhaus, R.; Haase, D.; Saak, W.; Koch, R. *Chemistry* **2001**, *7*, 622–626.
 123. Lanzinger, D.; Höhle, I. M.; Weiß, S. B.; Rieger, B. *J. Organomet. Chem.* **2015**, *778*, 21–28.
 124. Beweries, T.; Panda, T. K.; Roberts, C. C.; Tsurugi, H. *Organometallics* **2023**, *42*, 1039–1042.
 125. Rosenthal, U. *ChemistryOpen* **2021**, *10*, 1234–1243.
 126. Rosenthal, U. *Angew. Chem. Int. Ed.* **2018**, *57*, 14718–14735.
 127. Piglosiewicz, I. M.; Kraft, S.; Beckhaus, R.; Haase, D.; Saak, W. *Eur. J. Inorg. Chem.* **2005**, *2005*, 938–945.

128. Jäger-Fiedler, U.; Arndt, P.; Baumann, W.; Spannenberg, A.; Burlakov, V. V.; Rosenthal, U. *Eur. J. Inorg. Chem.* **2005**, *2005*, 2842–2849.
129. Fan, H.; Fout, A. R.; Bailey, B. C.; Pink, M.; Baik, M. H.; Mindiola, D. J. *Dalton Trans.* **2013**, *42*, 4163–4174.
130. Hoyt, H. M.; Michael, F. E.; Bergman, R. G. *J. Am. Chem. Soc.* **2004**, *126*, 1018–1019.
131. Romero, N.; Dufrois, Q.; Crespo, N.; Pujol, A.; Vendier, L.; Etienne, M. *Organometallics* **2020**, *39*, 2245–2256.
132. Luo, Y. R. *Comprehensive Handbook of Chemical Bond Energies*, 1st Ed.; CRC Press, 2007.
133. Dhokale, R. A.; Mhaske, S. B. *RSC Adv.* **2018**, *8*, 1–16.
134. Bennett, M. A.; Schwemlein, H. P. *Angew. Chem. Int. Ed. Engl.* **1989**, *28*, 1296–1320.
135. Johnson, R. P.; Daoust, K. J. *J. Am. Chem. Soc.* **1995**, *117*, 362–367.
136. Rondan, N. G.; Domelsmith, L. N.; Houk, K. N.; Bowne, A. T.; Levin, R. H. *Tetrahedron Lett.* **1979**, *20*, 3237–3240.
137. Bhunia, A.; Yetra, S. R.; Biju, A. T. *Chem. Soc. Rev.* **2012**, *41*, 3140–3152.
138. Anthony, S. M.; Wonilowicz, L. G.; McVeigh, M. S.; Garg, N. K. *J. Am. Chem. Soc. Au* **2021**, *1*, 897–912.
139. Erker, G.; Kropp, K. *J. Am. Chem. Soc.* **1979**, *101*, 3659–3660.
140. Buchwald, S. L.; Nielsen, R. B. *Chem. Rev.* **1988**, *88*, 1047–1058.
141. Broene, R. D.; Buchwald, S. L. *Science* **1993**, *261*, 1696–1701.
142. Erker, G.; Mühlenbernd, T. *J. Organomet. Chem.* **1987**, *319*, 201–211.
143. Suleiman, M.; Taullaj, F.; Fekl, U. *Int. J. Quantum Chem.*, **2021**, *121*, e26638.
144. Yan, X.; Xi, C. *Coord. Chem. Rev.* **2017**, *350*, 275–284.
145. Buchwald, S. L. *J. Am. Chem. Soc.* **1986**, *108*, 7441–7442.
146. Spaggiari, A.; Vaccari, D.; Davoli, P.; Torre, G.; Prati, F. *J. Org. Chem.* **2007**, *72*, 2216–2219.
147. Stanetty, P.; Roller, H.; Mihovilovic, M. *J. Org. Chem.* **1992**, *57*, 6833–6837.
148. Stuhldreier, T. *Organometallics* **2000**, *19*, 5231–5234.
149. Wailes, P. C.; Weigold, H.; Bell, A. P. *J. Organomet. Chem.* **1972**, *34*, 155–164.
150. Garrec, K.; Fletcher, S. P. *Org. Lett.* **2016**, *18*, 3814–3817.
151. Haynes, W. *Handbook of Chemistry and Physics*; CRC Press, 2014.
152. Nova, A.; Erhardt, S.; Jasim, N. A.; Perutz, R. N.; Macgregor, S. A.; McGrady, J. E.; Whitwood, A. C. *J. Am. Chem. Soc.* **2008**, *130*, 15499–15511.
153. Clot, E.; Eisenstein, O.; Jasim, N.; MacGregor, S. A.; McGrady, J. E.; Perutz, R. N. *Acc. Chem. Res.* **2011**, *44*, 333–348.

154. Edelbach, B. L.; Kraft, B. M.; Jones, W. D. *J. Am. Chem. Soc.* **1999**, *121*, 10327–10331.
155. Facundo, A. A.; Arévalo, A.; Fundora-Galano, G.; Flores-Álamo, M.; Orgaz, E.; García, J. J. *New J. Chem.* **2019**, *43*, 6897–6908.
156. Arévalo, A.; Tlahuext-Aca, A.; Flores-Alamo, M.; García, J. J. *J. Am. Chem. Soc.* **2014**, *136*, 4634–4639.
157. Zhao, J.; Zhang, S.; Zhang, W. X.; Xi, Z. *Organometallics* **2012**, *31*, 8370–8374.
158. Zhao, J.; Zhang, S.; Zhang, W. X.; Xi, Z. *Organometallics* **2011**, *30*, 3464–3467.
159. Arndt, P.; Lefeber, C.; Kempe, R.; Rosenthal, U. *Chem. Ber.* **1996**, *129*, 207–211.
160. Binger, P.; Sandmeyer, F.; Krüger, C. *Organometallics* **1995**, *14*, 2969–2976.
161. Burlakov, V. V.; Becker, L.; Bogdanov, V. S.; Andreev, M. V.; Arndt, P.; Spannenberg, A.; Baumann, W.; Rosenthal, U. *Eur. J. Inorg. Chem.* **2014**, *2014*, 5304–5310.
162. Bender, G.; Kehr, G.; Daniliuc, C. G.; Wibbeling, B.; Erker, G. *Dalton Trans.* **2013**, *42*, 14673–14676.
163. Becker, L.; Strehler, F.; Korb, M.; Arndt, P.; Spannenberg, A.; Baumann, W.; Lang, H.; Rosenthal, U. *Chem. Eur. J.* **2014**, *20*, 3061–3068.
164. Eisenstein, O.; Milani, J.; Perutz, R. N. *Chem. Rev.* **2017**, *117*, 8710–8753.
165. Clot, E.; Mégret, C.; Eisenstein, O.; Perutz, R. N. *J. Am. Chem. Soc.* **2009**, *131*, 7817–7827.
166. Chen, X.; Hu, X.; Deng, Y.; Jiang, H.; Zeng, W. *Org. Lett.* **2016**, *18*, 4742–4745.
167. Wipf, P.; Nunes, R. L. *Tetrahedron* **2004**, *60*, 1269–1279.
168. Ai, Y.; Ye, N.; Wang, Q.; Yahata, K.; Kishi, Y. *Angew. Chem. Int. Ed.* **2017**, *56*, 10791–10795.
169. Johnson, D. G.; Lynam, J. M.; Mistry, N. S.; Slattery, J. M.; Thatcher, R. J.; Whitwood, A. C. *J. Am. Chem. Soc.* **2013**, *135*, 2222–2234.
170. Kirsch, P. *Modern Fluoroorganic Chemistry: Synthesis, Reactivity, Applications*, 2nd Ed.; Wiley, 2005; pp. 1–308.
171. Banks, R. E.; Smart, B. E.; Tatlow, J. C. *Organofluorine Chemistry*, **1994**, Springer US, Boston, MA.
172. Hewitt, C. D.; Silvester, M. J. *Aldrichimica Acta* **1988**, *21*, 1, 1–9.
173. Furin, G. G.; Grebenschikova, G. F.; Lvova, A. Ya.; Vlasov, V. M.; Yakobson, G. G. *Syntheses of Fluoroorganic Compounds*, **1985**, 109–232.
174. Banks, R. E.; Smart, B. E.; Tatlow, J. C. *Organofluorine Chemistry. Principles and Commercial Applications.*, **1994**, Springer New York, NY.
175. Sandford, G. *Halogenated Heterocycles*, **2011**, In: Iskra, J. (eds) Topics in Heterocyclic Chemistry, vol 27. Springer, Berlin, Heidelberg.

176. Kirsch, P. *Modern Fluoroorganic Chemistry: Synthesis, Reactivity, Applications*, 2nd Ed.; Wiley, 2005; pp. 1–308.
177. Lennox, A. J. J. *Angew. Chem. Int. Ed.* **2018**, *57*, 14686–14688.
178. Kwan, E. E.; Zeng, Y.; Besser, H. A.; Jacobsen, E. N. *Nat. Chem.* **2018**, *10*:9, 917–923.
179. Neumann, C. N.; Hooker, J. M.; Ritter, T. *Nature* **2016**, *534*:7607, 369–373.
180. Pietrasiak, E.; Lee, E. *Synlett* **2020**, *31*, 1349–1360.
181. Chambers, R. D.; Seabury, M. J.; Williams, D. L. H.; Hughes, N. *J. Chem. Soc. Perkin Trans. 1* **1988**, 255–257.
182. Brooke, G. M. *J. Fluor. Chem.* **1997**, *86*, 1–76.
183. Chambers, R. D.; Martin, P. A.; Sandford, G.; Lyn, D.; Williams, H. *J. Fluorine Chem.* **2008**, *129*, 10, 998–1002.
184. Kobrina, L.; Furin, G.; Yakobson, G. *Zh. Org. Khim.* **1970**, *6*, 512–520.
185. Revesz, L.; Di Padova, F. E.; Buhl, T.; Feifel, R.; Gram, H.; Hiestand, P.; Manning, U.; Wolf, R.; Zimmerlin, A. G. *Bioorg. Med. Chem. Lett.* **2002**, *12*, 16, 2109–2112.
186. Cheong, C. L.; Wakefield, B. J. *J. Chem. Soc. Perkin 1* **1988**, 3301–3305.
187. Chambers, R. D.; Hall, C. W.; Hutchinson, J.; Millar, R. W. *J. Chem. Soc., Perkin Trans. 1*, **1998**, 1705–1713.
188. Kuhn, N.; Fahl, J.; Boese, R.; Henkel, G. *Z. Naturforsch. B* **1998**, *53*, 881–886.
189. Mallah, E.; Kuhn, N.; Maichle-Mößmer, C.; Steimann, M.; Ströbele, M.; Zeller, K. P. *Z. Naturforsch. B* **2009**, *64*, 1176–1182.
190. Kundu, G.; Ajithkumar, V. S.; Bisai, M. K.; Tothadi, S.; Das, T.; Vanka, K.; Sen, S. S. *Chem. Commun.* **2021**, *57*, 4428–4431.
191. Paul, U. S. D.; Radius, U. *Chem. Eur. J.* **2017**, *23*, 3993–4009.
192. Dutta, T.; Woody, K. B.; Watson, M. D. *J. Am. Chem. Soc.* **2008**, *130*, 452–453.
193. Wang, Y.; Watson, M. D. *J. Am. Chem. Soc.* **2006**, *128*, 2536–2537.
194. Artamkina, G. A.; Tarasenko, E. A.; Lukashev, N. V.; Beletskaya, I. P. *Tetrahedron Lett.* **1998**, *39*, 901–904.
195. Day, J. I.; Weaver, J. D. *J. Org. Chem.* **2017**, *82*, 6801–6810.
196. Nova, A.; Mas-Ballesté, R.; Lledós, A. *Organometallics* **2012**, *31*, 1245–1256.
197. Holthausen, M. H.; Mehta, M.; Stephan, D. W. *Angew. Chem. Int. Ed.* **2014**, *53*, 6538–6541.
198. Zhu, J.; Pérez, M.; Stephan, D. W. *Angew. Chem. Int. Ed.* **2016**, *55*, 8448–8451.
199. Holthausen, M. H.; Hiranandani, R. R.; Stephan, D. W. *Chem. Sci.* **2015**, *6*, 2016–2021.
200. Caputo, C. B.; Hounjet, L. J.; Dobrovetsky, R.; Stephan, D. W. *Science* **2013**, *341*, 1374–1377.

201. Chitnis, S. S.; Krischer, F.; Stephan, D. W. *Chem. Eur. J.* **2018**, *24*, 6543–6546.
202. Chitnis, S. S.; Lafortune, J. H. W.; Cummings, H.; Liu, L. L.; Andrews, R.; Stephan, D. W. *Organometallics* **2018**, *37*, 4540–4544.
203. Bayne, J. M.; Stephan, D. W. *Chem. Eur. J.* **2019**, *25*, 9350–9357.
204. Sasaki, S.; Tanabe, Y.; Yoshifuji, M. *Bull. Chem. Soc. Jpn.* **1999**, *72*, 563–572.
205. Hogarth, G.; Norman, T. J. *Chem. Soc., Dalton Trans.* **1996**, 1077–1085.
206. Ireland, T.; Tappe, K.; Grossheimann, G.; Knochel, P. *Chem. Eur. J.* **2008**, *14*, 3509.
207. Goryuno, L. I.; Grobe, J.; Shteingarts, D.; Krebs, B.; Lindemann, A.; Würthwein, E. U.; Mück-Lichtenfeld, C. *Chem. Eur. J.* **2000**, *6*, 4612–4622.
208. Veits, Y. A.; Karlstedt, N. B.; Chuchuryukin, A. V.; Beletskaya, I. P. *ChemInform* **2001**, *32*, 6.
209. Caputo, C. B.; Stephan, D. W. *Organometallics* **2012**, *31*, 27–30.
210. Mandal, D.; Gupta, R.; Young, R. D. *J. Am. Chem. Soc.* **2018**, *140*, 10682–10686.
211. Burton, D. J.; Seiji, S.; Howells, R. D. *J. Am. Chem. Soc.* **1979**, *101*, 3689–3690.
212. Zhivetyeva, S. I.; Zakharova, O. D.; Ovchinnikova, L. P.; Baev, D. S.; Bagryanskaya, I. Y.; Shteingarts, V. D.; Tolstikova, T. G.; Nevinsky, G. A.; Tretyakov, E. V. *J. Fluor. Chem.* **2016**, *192*, 68–77.
213. Lim, S.; Radosevich, A. T. *J. Am. Chem. Soc.* **2020**, *142*, 16188–16193.
214. Chulsky, K.; Malahov, I.; Bawari, D.; Dobrovetsky, R. *J. Am. Chem. Soc.* **2023**, *145*, 3786–3794.
215. Furin, G. G. *Russ. Chem. Rev.* **1993**, *62*, 243–259.
216. Gutov, A. V.; Rusanov, E. B.; Ryabitskii, A. B.; Chernega, A. N. *J. Fluor. Chem.* **2010**, *131*, 278–281.
217. Bardin, V. V.; Pressman, L. S.; Rogoza, L. N.; Furin, G. G. *J. Fluor. Chem.* **1991**, *54*, 297.
218. Mehta, M.; Holthausen, M. H.; Mallov, I.; Pérez, M.; Qu, Z. W.; Grimme, S.; Stephan, D. W. *Angew. Chem. Int. Ed.* **2015**, *54*, 8250–8254.
219. Pérez, M.; Caputo, C. B.; Dobrovetsky, R.; Stephan, D. W. *Proc. Natl. Acad. Sci. U. S. A.* **2014**, *111*, 10917–10921.
220. Hounjet, L. J.; Caputo, C. B.; Stephan, D. W. *Angew. Chem.* **2012**, *124*, 4792–4795.
221. Goodenough, J. B.; Kim, Y. *Chem. Mater.* **2010**, *22*, 587–603.
222. Vekariya, R. L. *J. Mol. Liq.* **2017**, *227*, 44–60.
223. Kobayashi, Y.; Akashi, C.; Morinaga, K. *Chem. Pharm. Bull.* **1968**, *16*, 1784–1787.
224. Yang, Z.; Shen, X. *Fluorination*; Springer, 2018; pp. 297–304.
225. Vabre, B.; Chansaenpak, K.; Wang, M.; Wang, H.; Li, Z.; Gabbai, F. P. *Chem. Commun.* **2017**, *53*, 8657–8659.

226. Forster, A. M.; Downs, A. J. *Polyhedron* **1985**, *4*, 1625–1635.
227. Solyntjes, S.; Neumann, B.; Stammler, H. G.; Ignat'ev, N.; Hoge, B. *Eur. J. Inorg. Chem.* **2016**, *2016*, 3999–4010.
228. Schmidbaur, H.; Mitschke, K. -H.; Buchner, W.; Stühler, H.; Weidlein, J. *Chem. Ber.* **1973**, *106*, 1226–1237.
229. Gupta, O. D.; Shreeve, J. M. *J. Chem. Soc., Chem. Commun.* **1984**, 416–417.
230. Firth, W. C.; Frank, S.; Garber, M.; Wystrach, V. P. *Inorg. Chem.* **1965**, *4*, 765–766.
231. Banks, R. E.; Haszeldine, R. N.; Hatton, R. *Tetrahedron Lett.* **1967**, *8*, 3993–3996.
232. Lermontov, S. A.; Polivanova, A. G.; Shkavrov, S. B. *Russ. J. Gen. Chem.* **2010**, *80*, 1646–1651.
233. Frohn, H. J.; Maurer, H. J. *Fluor. Chem.* **1986**, *34*, 73–82.
234. Schmutzler, R. *Inorg. Chem.* **1964**, *3*, 410–415.
235. Tyree, S. Y. *Inorg. Syntheses*; Wiley, 1967; vol. 9, pp. 86–88.
236. Fluck, E.; Braun, R. *Phosphorus Sulfur Relat. Elem.* **1988**, *40*, 83–90.
237. Fujimoto, H.; Kusano, M.; Kodama, T.; Tobisu, M. *Org. Lett.* **2020**, *22*, 2293–2297.
238. Eljo, J.; Carle, M. S.; Murphy, G. K. *Synlett* **2017**, *28*, 2871–2875.
239. Bornemann, D.; Pitts, C. R.; Wettstein, L.; Brüning, F.; Küng, S.; Guan, L.; Trapp, N.; Grützmacher, H.; Togni, A. *Angew. Chem. Int. Ed.* **2020**, *59*, 22790–22795.
240. Bornemann, D.; Brüning, F.; Bartalucci, N.; Wettstein, L.; Pitts, C. R. *Helv. Chim. Acta* **2021**, *104*, e2000218.
241. Sawamura, T.; Takahashi, K.; Inagi, S.; Fuchigami, T. *Angew. Chem. Int. Ed.* **2012**, *51*, 4413–4416.
242. Ignat'ev, N.; Sartori, P. *J. Fluor. Chem.* **2000**, *103*, 57–61.
243. MouWang, C.; Mallouk, T. E. *J. Am. Chem. Soc.* **1990**, *112*, 2016–2018.
244. Rotering, P.; Mück-Lichtenfeld, C.; Dielmann, F. *Green Chem.* **2022**, *24*, 8054–8061.
245. Solyntjes, S.; Neumann, B.; Stammler, H. G.; Ignat'ev, N.; Hoge, B. *Eur. J. Inorg. Chem.* **2016**, *2016*, 3999–4010.
246. Reiter, D.; Frisch, P.; Szilvási, T.; Inoue, S. *J. Am. Chem. Soc.* **2019**, *141*, 16991–16996.
247. Rufanov, K. A.; Müller, B. H.; Spannenberg, A.; Rosenthal, U. *New J. Chem.* **2006**, *30*, 29–31.
248. Mitzel, N. W.; Brown, D. H.; Parsons, S.; Brain, P. T.; Pulham, C. R.; Rankin, D. W. H. *Angew. Chem. Int. Ed.* **1998**, *37*, 1670–1672.
249. Schmidbaur, H.; Schier, A.; Frazão, C. M. F.; Muller, G. *J. Am. Chem. Soc.* **1986**, *108*, 976–982.
250. Aitken, R. A.; Boubalouta, Y.; Chang, D.; Cleghorn, L. P.; Gray, I. P.; Karodia, N.; Reid,

- E. J.; Slawin, A. M. Z. *Tetrahedron* **2017**, *73*, 6275–6285.
251. Cronin, L.; Higgitt, C. L.; Karch, R.; Perutz, R. N. *Organometallics* **1997**, *16*, 4920–4928.
252. Burling, S.; Elliott, P. I. P.; Jasim, N. A.; Lindup, R. J.; McKenna, J.; Perutz, R. N.; Archibald, S. J.; Whitwood, A. C. *Dalton Trans.* **2005**, 3686–3695.
253. Yang, Z.; Shen, X. *Fluorination*; Springer, 2018; pp. 297–304.
254. Henderson, W. A.; Streuli, C. A. *J. Am. Chem. Soc.* **1960**, *82*, 5791–5794.
255. Abdur-Rashid, K.; Fong, T. P.; Greaves, B.; Gusev, D. G.; Hinman, J. G.; Landau, S. E.; Lough, A. J.; Morris, R. H. *J. Am. Chem. Soc.* **2000**, *122*, 9155–9171.
256. Streitwieser, A.; McKeown, A. E.; Hasanayn, F.; Davis, N. R. *Org. Lett.* **2005**, *7*, 1259–1262.
257. Haav, K.; Saame, J.; Kütt, A.; Leito, I. *Eur. J. Org. Chem.* **2012**, *2012*, 2167–2172.
258. Fluck, E.; Braun, R. *Phosphorus Sulfur Relat. Elem.* **1988**, *40*, 83–90.
259. Schmidbaur, H.; Mitschke, K.-H.; Weidlein, J. *Angew. Chem. Int. Ed. Engl.* **1972**, *11*, 144–145.
260. Kornath, A.; Neumann, F.; Oberhammer, H. *Inorg. Chem.* **2003**, *42*, 2894–2901.
261. Schmidbaur, H.; Mitschke, K.-H.; Buchner, W.; Stühler, H.; Weidlein, J. *Chem. Ber.* **1973**, *106*, 1226–1237.
262. Fujimoto, H.; Kodama, T.; Yamanaka, M.; Tobisu, M. *J. Am. Chem. Soc.* **2020**, *142*, 17323–17328.
263. Kolodiazhnyi, O. I.; Schmutzler, R. *Synlett.* **2001**, *2001*, 1065–1078.
264. Kolodiazhnyi, O. I.; Grishkun, V. E. *Heteroatom Chem.* **1998**, *9*, 659–664.
265. Zhang, X.; Nottingham, K. G.; Patel, C.; Alegre-Requena, J. V.; Levy, J. N.; Paton, R. S.; McNally, A. *Nature* **2021**, *594*, 217–222.
266. Hilton, M. C.; Zhang, X.; Boyle, B. T.; Alegre-Requena, J. V.; Paton, R. S.; McNally, A. *Science* **2018**, *362*, 799–804.
267. Boyle, B. T.; Hilton, M. C.; McNally, A. *J. Am. Chem. Soc.* **2019**, *141*, 15441–15449.
268. Middleton, W. J. *J. Org. Chem.* **1975**, *40*, 574–578.
269. Nielsen, M. K.; Ugaz, C. R.; Li, W.; Doyle, A. G. *J. Am. Chem. Soc.* **2015**, *137*, 9571–9574.
270. Sladojevich, F.; Arlow, S. I.; Tang, P.; Ritter, T. *J. Am. Chem. Soc.* **2013**, *135*, 2470–2473.
271. Li, L.; Ni, C.; Wang, F.; Hu, J. *Nat. Commun.* **2016**, *7*, 1–11.
272. Ahrens, T.; Kohlmann, J.; Ahrens, M.; Braun, T. *Chem. Rev.* **2015**, *115*, 931–972.
273. Ai, H. J.; Ma, X.; Song, Q.; Wu, X. F. *Sci. China Chem.* **2021**, *64*, 1630–1659.

274. Power, P. P. *Nature* **2010**, *463*, 171–177.
275. Chu, T.; Nikonov, G. I. *Chem. Rev.* **2018**, *118*, 3608–3680.
276. Lipshultz, J. M.; Li, G.; Radosevich, A. T. *J. Am. Chem. Soc.* **2021**, *143*, 1699–1721.
277. Luo, Y. R. *Comprehensive Handbook of Chemical Bond Energies*, 1st Ed.; CRC Press, 2007.
278. Stahl, T.; Klare, H. F. T.; Oestreich, M. *ACS Catal.* **2013**, *3*, 1578–1587.
279. Gusev, D. G.; Ozerov, O. V. *Chem. Eur. J.* **2011**, *17*, 634–640.
280. Krause, J. R.; Lampe, F. W. *J. Phys. Chem.* **1977**, *81*, 281–286.
281. McLafferty, F. W. *Science*. **1981**, *214*, 280–287.
282. Scott, V. J.; Çelenligil-Çetin, R.; Ozerov, O. V. *J. Am. Chem. Soc.* **2005**, *127*, 2852–2853.
283. Panisch, R.; Bolte, M.; Müller, T. *J. Am. Chem. Soc.* **2006**, *128*, 9676–9682.
284. Caputo, C. B.; Stephan, D. W. *Organometallics*. **2012**, *31*, 27–30.
285. Chitnis, S. S.; Krischer, F.; Stephan, D. W. *Chem. Eur. J.* **2018**, *24*, 6543–6546.
286. Ahrens, M.; Scholz, G.; Braun, T.; Kemnitz, E. *Angew. Chem. Int. Ed.* **2013**, *52*, 5328–5332.
287. Stahl, T.; Klare, H. F. T.; Oestreich, M. *J. Am. Chem. Soc.* **2013**, *135*, 1248–1251.
288. Nicolaou, K. C.; Dolle, R. E.; Chucholowski, A.; Randall, J. L. *J. Chem. Soc. Chem. Commun.* **1984**, 1153–1154.
289. Klahn, M.; Fischer, C.; Spannenberg, A.; Rosenthal, U.; Krossing, I. *Tetrahedron Lett.* **2007**, *48*, 8900–8903.
290. Terao, J.; Begum, S. A.; Shinohara, Y.; Tomita, M.; Naitoh, Y.; Kambe, N. *Chem. Commun.* **2007**, 855–857.
291. Stephan, D. W. *J. Am. Chem. Soc.* **2015**, *137*, 10018–10032.
292. Meißner, G.; Kretschmar, K.; Braun, T.; Kemnitz, E. *Angew. Chem. Int. Ed.* **2017**, *56*, 16338–16341.
293. Hayatifar, A.; Borrego, A.; Bosek, D.; Czarnecki, M.; Derocher, G.; Kuplicki, A.; Lytle, E.; Padilla, J.; Paroly, C.; Tubay, G.; Vyletel, J.; Weinert, C. S. *Chem. Commun.* **2019**, *55*, 10852–10855.
294. Yan, G. *Chem. Eur. J.* **2022**, *28*, e202200231.
295. Lu, J.; Khetrpal, N. S.; Johnson, J. A.; Zeng, X. C.; Zhang, J. *J. Am. Chem. Soc.* **2016**, *138*, 15805–15808.
296. Sap, J. B. I.; Straathof, N. J. W.; Knauber, T.; Meyer, C. F.; Médebielle, M.; Buglioni, L.; Genicot, C.; Trabanco, A. A.; Noël, T.; Am Ende, C. W.; Gouverneur, V. *J. Am. Chem. Soc.* **2020**, *142*, 9181–9187.

297. Phillips, N. A.; White, A. J. P.; Crimmin, M. R. *Adv. Synth. Catal.* **2019**, *361*, 3351–3358.
298. Schoch, T. D.; Mondal, M.; Weaver, J. D. *Org. Lett.* **2021**, *23*, 1588–1593.
299. Kikushima, K.; Grellier, M.; Ohashi, M.; Ogoshi, S. *Angew. Chem. Int. Ed.* **2017**, *56*, 16191–16196.
300. Zhang, J.; Zhao, X.; Yang, J. D.; Cheng, J. P. *J. Org. Chem.* **2022**, *87*, 294–300.
301. Légaré, M. A.; Pranckevicius, C.; Braunschweig, H. *Chem. Rev.* **2019**, *119*, 8231–8261.
302. Chu, T.; Korobkov, I.; Nikonov, G. I. *J. Am. Chem. Soc.* **2014**, *136*, 9195–9202.
303. Crimmin, M. R.; Butler, M. J.; White, A. J. P. *Chem. Commun.* **2015**, *51*, 15994–15996.
304. Chu, T.; Boyko, Y.; Korobkov, I.; Nikonov, G. I. *Organometallics* **2015**, *34*, 5363–5365.
305. Jana, A.; Samuel, P. P.; Tavčar, G.; Roesky, H. W.; Schulzke, C. *J. Am. Chem. Soc.* **2010**, *132*, 10164–10170.
306. Crivello, J. V. *J. Polym. Sci. A Polym. Chem.* **2009**, *47*, 5639–5651.
307. Sagae, T.; Ogawa, S.; Furukawa, N. *Tetrahedron Lett.* **1993**, *34*, 4043–4046.
308. Moon, H. W.; Cornella, J. *ACS Catal.* **2022**, *12*, 1382–1393.
309. Abbenseth, J.; Goicoechea, J. M. *Chem. Sci.* **2020**, *11*, 9728–9740.
310. Lee, K.; Blake, A. V.; Tanushi, A.; McCarthy, S. M.; Kim, D.; Loria, S. M.; Donahue, C. M.; Spielvogel, K. D.; Keith, J. M.; Daly, S. R.; Radosevich, A. T. *Angew. Chem. Int. Ed.* **2019**, *58*, 6993–6998.
311. Zeng, G.; Maeda, S.; Taketsugu, T.; Sakaki, S. *Angew. Chem. Int. Ed.* **2014**, *53*, 4633–4637.
312. Pang, Y.; Leutzsch, M.; Nöthling, N.; Katzenburg, F.; Cornella, J. *J. Am. Chem. Soc.* **2021**, *143*, 12487–12493.
313. Zhao, W.; McCarthy, S. M.; Lai, T. Y.; Yennawar, H. P.; Radosevich, A. T. *J. Am. Chem. Soc.* **2014**, *136*, 17634–17644.
314. Bonfante, S.; Lorber, C.; Lynam, J. M.; Simonneau, A.; Slattery, J. M. *J. Am. Chem. Soc.* **2024**, *146*, 2005–2014.
315. Dolbier, W. R. *Guide to Fluorine NMR for Organic Chemists*; Wiley, 2016.
316. Hili, R.; Yudin, A. K. *Nat. Chem. Biol.* **2006**, *2*, 284–287.
317. Evano, G.; Blanchard, N.; Toumi, M. *Chem. Rev.* **2008**, *108*, 3054–3131.
318. Walzer, K.; Männig, B.; Pfeiffer, M.; Leo, K. *Chem. Rev.* **2007**, *107*, 1233–1271.
319. Roberts, J. D.; Caserio, M. C. *Basic Principles of Organic Chemistry*, 2nd Ed.; W. A. Benjamin, 1977.
320. Sambigiato, C.; Marsden, S. P.; Blacker, A. J.; McGowan, P. C. *Chem. Soc. Rev.* **2014**, *43*, 3525–3550.

321. Park, N. H.; Teverovskiy, G.; Buchwald, S. L. *Org. Lett.* **2014**, *16*, 220–223.
322. Hartwig, J. F. *Acc. Chem. Res.* **2008**, *41*, 1534–1544.
323. Chan, A. Y.; Perry, I. B.; Bissonnette, N. B.; Buksh, B. F.; Edwards, G. A.; Frye, L. I.; Garry, O. L.; Lavagnino, M. N.; Li, B. X.; Liang, Y.; Mao, E.; Millet, A.; Oakley, J. V.; Reed, N. L.; Sakai, H. A.; Seath, C. P.; MacMillan, D. W. C. *Chem. Rev.* **2022**, *122*, 1485–1542.
324. Jacobsen, C. B.; Meldal, M.; Diness, F. *Chem. Eur. J.* **2017**, *23*, 846–851.
325. Lin, Y.; Li, M.; Ji, X.; Wu, J.; Cao, S. *Tetrahedron.* **2017**, *73*, 1466–1472.
326. Chen, J.; Huang, D.; Ding, Y. *Eur. J. Org. Chem.* **2017**, *2017*, 4300–4304.
327. Kong, X.; Zhang, H.; Xiao, Y.; Cao, C.; Shi, Y.; Pang, G. *RSC Adv.* **2014**, *5*, 7035–7048.
328. Bole, L. J.; Davin, L.; Kennedy, A. R.; McLellan, R.; Hevia, E. *Chem. Commun.* **2019**, *55*, 4339–4342.
329. Jana, A.; Pillai Sarish, S.; Roesky, H. W.; Leusser, D.; Objartel, I.; Stalke, D. *Chem. Commun.* **2011**, *47*, 5434–5436.
330. Samuel, P. P.; Singh, A. P.; Sarish, S. P.; Matussek, J.; Objartel, I.; Roesky, H. W.; Stalke, D. *Inorg. Chem.* **2013**, *52*, 1544–1549.
331. Pacl, Z.; Jakoubková, M.; Papoušková, Z.; Chvalovský, V. *Collect. Czech. Chem. Commun.* **1971**, *36*, 1588–1597.
332. Yoshida, H.; Minabe, T.; Ohshita, J.; Kunai, A. *Chem. Commun.* **2005**, 3454–3456.
333. Clayden, J.; Warren, S.; Greeves, N. *Organic Chemistry*, 2nd Ed.; University Press, 2012.
334. Pogliani, L.; Ellenberger, M.; Valat, J. *Org. Magn. Resonance* **1975**, *7*, 61–71.
335. Polavarapu, P. L. *Chirality* **2002**, *14*, 768–781.
336. Anders, E.; Markus, F. *Tetrahedron Lett.* **1987**, *28*, 2675–2676.
337. Mandal, D.; Gupta, R.; Jaiswal, A. K.; Young, R. D. *J. Am. Chem. Soc.* **2020**, *142*, 2572–2578.
338. Zhu, J.; Pérez, M.; Caputo, C. B.; Stephan, D. W. *Angew. Chem. Int. Ed. Engl.* **2016**, *55*, 1417–1421.
339. Parks, D. J.; Blackwell, J. M.; Piers, W. E. *J. Org. Chem.* **2000**, *65*, 3090–3098.
340. Parks, D. J.; Piers, W. E. *J. Am. Chem. Soc.* **1996**, *118*, 9440–9441.
341. Welch, G. C.; San Juan, R. R.; Masuda, J. D.; Stephan, D. W. *Science* **2006**, *314*, 1124–1126.
342. Seel, F.; Bassler, H.-J. *Z. Anorg. Allg. Chem.* **1975**, *418*, 263–272.
343. Brownstein, M.; Schmutzler, R. *J. Chem. Soc. Chem. Commun.* **1975**, 278–278.
344. Anderson, R. G.; Jett, B. M.; McNally, A. *Angew. Chem. Int. Ed.* **2018**, *57*, 12514–

- 12518.
345. Hilton, M. C.; Dolewski, R. D.; McNally, A. *J. Am. Chem. Soc.* **2016**, *138*, 13806–13809.
346. Anderson, R. G.; Jett, B. M.; McNally, A. *Tetrahedron.* **2018**, *74*, 3129–3136.
347. Bardin, V. V. *Russ. Chem. Bull.* **1997**, *46*, 1434–1436.
348. Kwan, E. E.; Zeng, Y.; Besser, H. A.; Jacobsen, E. N. *Nat. Chem.* **2018**, *10*, 917–923.
349. Côté, J. F.; Brouillette, D.; Desnoyers, J. E.; Rouleau, J. F.; St-Arnaud, J. M.; Perron, G. *J. Solution Chem.* **1996**, *25*, 1163–1173.
350. Pike, S. D.; Crimmin, M. R.; Chaplin, A. B. *Chem. Commun.* **2017**, *53*, 3615–3633.
351. Kornath, A.; Neumann, F.; Oberhammer, H. *Inorg. Chem.* **2003**, *42*, 2894–2901.
352. Hoffmann, R.; Howell, J. M.; Muetterties, E. L. *J. Am. Chem. Soc.* **1972**, *94*, 3047–3058.
353. Braunschweig, H.; Krummenacher, I.; Légaré, M. A.; Matler, A.; Radacki, K.; Ye, Q. *J. Am. Chem. Soc.* **2017**, *139*, 1802–1805.
354. Borys, A. M. *Organometallics* **2023**, *42*, 182–196.
355. Harris, R. K.; Becker, E. D.; de Menezes, S. M. C.; Granger, P.; Goodfellow, R. *Pure Appl. Chem.* **2001**, *73*, 1795–1818.
356. Harris, R. K.; Becker, E. D.; de Menezes, S. M. C.; Granger, P.; Hoffman, R. E.; Zilm, K. W. *Pure Appl. Chem.* **2008**, *80*, 59–84.
357. Spaggiari, A.; Vaccari, D.; Davoli, P.; Torre, G.; Prati, F. *J. Org. Chem.* **2007**, *72*, 2216–2219.
358. Stuhldreier, T.; Keul, H.; Höcker, H. *Organometallics* **2000**, *19*, 5231–5234.
359. Wailes, P. C.; Weigold, H.; Bell, A. P. *J. Organomet. Chem.* **1972**, *34*, 155–164.
360. Garrec, K.; Fletcher, S. P. *Org. Lett.* **2016**, *18*, 3814–3817.
361. Bauer, H.; Alonso, M.; Fischer, C.; Rösch, B.; Elsen, H.; Harder, S. *Angew. Chem. Int. Ed.* **2018**, *57*, 15177–15182.
362. Buchwald, S. L.; Lum, R. T.; Dewan, J. C. *J. Am. Chem. Soc.* **1986**, *108*, 7441–7442.
363. Skotnitzki, J.; Kremsmair, A.; Keefer, D.; Gong, Y.; de Vivie-Riedle, R.; Knochel, P. *Angew. Chem. Int. Ed.* **2020**, *59*, 320–324.
364. Wiesemann, M.; Stammler, H.-G.; Neumann, B.; Hoge, B. *Eur. J. Inorg. Chem.* **2017**, *2017*, 4733–4743.
365. Doxsee, K. M.; Hanawalt, E. M.; Weakley, T. J. R. *Inorg. Chem.* **2002**, *31*, 4420–4421.
366. Gutov, A. V.; Rusanov, E. B.; Ryabitskii, A. B.; Chernega, A. N. *J. Fluorine Chem.* **2010**, *131*, 278–281.
367. Chulsky, K.; Malahov, I.; Bawari, D.; Dobrovetsky, R. *J. Am. Chem. Soc.* **2023**, *145*, 3794.

368. Xu, P.; López-Rojas, P.; Ritter, T. *J. Am. Chem. Soc.* **2021**, *143*, 5349–5354.
369. Zhang, J.; Zhao, X.; Yang, J.-D.; Cheng, J.-P. *J. Org. Chem.* **2021**, *2022*, 300.
370. Yoshida, H.; Minabe, T.; Ohshita, J.; Kunai, A. *Chem. Commun.* **2005**, 3454–3456.
371. Lin, X.; Haimov, E.; Redko, B.; Vigalok, A. *Angew. Chem. Int. Ed.* **2022**, *61*, e202205368.
372. Császár, P.; Pulay, P. *J. Mol. Struct.* **1984**, *114*, 31–34.
373. Ahlrichs, R.; Bär, M.; Häser, M.; Horn, H.; Kölmel, C. *Chem. Phys. Lett.* **1989**, *162*, 165–169.
374. Treutler, O.; Ahlrichs, R. *J. Chem. Phys.* **1995**, *102*, 346–354.
375. Eichkorn, K.; Weigend, F.; Treutler, O.; Ahlrichs, R. *Theor. Chem. Acc.* **1997**, *97*, 119–124.
376. Von Arnim, M.; Ahlrichs, R. *J. Chem. Phys.* **1999**, *111*, 9183–9190.
377. Deglmann, P.; Furche, F.; Ahlrichs, R. *Chem. Phys. Lett.* **2002**, *362*, 511–518.
378. Deglmann, P.; May, K.; Furche, F.; Ahlrichs, R. *Chem. Phys. Lett.* **2004**, *384*, 103–107.
379. Baldes, A.; Weigend, F. *Mol. Phys.* **2013**, *111*, 2617–2624.
380. Furche, F.; Ahlrichs, R.; Hättig, C.; Klopper, W.; Sierka, M.; Weigend, F. *Wiley Interdiscip. Rev. Comput. Mol. Sci.* **2014**, *4*, 91–100.
381. Deglmann, P.; Furche, F. *J. Chem. Phys.* **2002**, *117*, 9535–9538.
382. Eichkorn, K.; Treutler, O.; Öhm, H.; Häser, M.; Ahlrichs, R. *Chem. Phys. Lett.* **1995**, *240*, 283–290.
383. Schäfer, A.; Klamt, A.; Sattel, D.; Lohrenz, J. C. W.; Eckert, F. *Phys. Chem. Chem. Phys.* **2000**, *2*, 2187–2193.
384. Côté, J. F.; Brouillette, D.; Desnoyers, J. E.; Rouleau, J. F.; St-Arnaud, J. M.; Perron, G. *J. Solution Chem.* **1996**, *25*, 1163–1173.
385. Ardura, D.; López, R.; Sordo, T. L. *J. Phys. Chem. B.* **2005**, *109*, 23618–23623.
386. Dub, P. A.; Poli, R. *J. Mol. Catal. A Chem.* **2010**, *324*, 89–96.
387. Leung, B. O.; Reid, D. L.; Armstrong, D. A.; Rauk, A. *J. Phys. Chem. A* **2004**, *108*, 2720–2725.
388. Grimme, S.; Antony, J.; Ehrlich, S.; Krieg, H. *J. Chem. Phys.* **2010**, *132*, 154104.
389. Grimme, S.; Ehrlich, S.; Goerigk, L. *J. Comput. Chem.* **2011**, *32*, 1456–1465.
390. Suenaga, M. *J. Comput. Chem. Jpn.* **2005**, *4*, 25–32.
391. Jmol: an open-source Java viewer for chemical structures in 3D, <https://jmol.sourceforge.net/>, (accessed 21 September 2023).